DECLARATION OF OWNERSHIP

JOHN VAN GEEST CANCER RESEARCH CENTRE

Nottingham Trent University

Development of a prostatic acid phosphatase-derived vaccine for the treatment of advanced prostate cancer

Jubini Elsa Thomas

A thesis submitted in partial fulfilment of the requirements of Nottingham Trent University for the degree of Doctor of Philosophy

Supervisors: Dr. Stephanie E.B McArdle

Dr. Jaykumar Vadakekolathu

Dr. Gabriel Kristian Pedersen

August 2024

DECLARATION OF OWNERSHIP

I declare that all data presented in this thesis have been generated by myself, except for the data shown in Figure 4.1, which was performed by Dr. Pauline Le Vu. Any other data not directly generated by me has been acknowledged accordingly. All assistance and advice received, other than that provided by my supervisors, has been appropriately acknowledged. The primary and secondary sources of information used in this thesis have been duly attributed. Should this declaration be found to be false, I understand that the Board of Examiners may recommend actions in accordance with the University's regulations on assessment, as outlined in the Handbook.

COPYRIGHT STATEMENT

ACKNOWLEDGEMENTS

I would like to express my sincere gratitude to my director of studies, Dr. Stephanie McArdle, for her valuable guidance and support over the past four years. I am particularly thankful for the opportunities provided, enabling me to present my research at an international congress abroad and within the UK during the second and third years of my studies as well as providing the opportunity to publish articles. I would also like to extend my heartfelt thanks to my second supervisor, Dr. Jaykumar Vadakekolathu, for his significant involvement and immense help throughout my PhD journey and for his dedication in teaching me the necessary lab techniques which had been crucial to my progress. I am grateful to Dr. Gabriel Kristian Pedersen for his advice and for providing CAF®09b adjuvant.

Thanks to Professor Sergio Rutella and everyone at JvGCRC. Appreciate Steve and Michael for their daily assistance with equipment operations and reagent purchasing. Special thanks to Dr. Murrium Ahmed for her management towards animal work and the acquisition of patient samples. I am also very thankful to the entire team in the animal unit—Andy, Adam, Joe, and Louise—for their excellent work on the *in vivo* experiments. I appreciate Clare and Cathy for their ongoing support in managing various lab tasks. Thanks to Massod Khan, consultant urological surgeon, at Leicester Hospital for giving access to patient samples for this research. I extend my sincere thanks to Dr. David Boocock for his assistance with mass spectrometry experiments. I feel fortunate to have been surrounded by amazing PhD colleagues throughout my journey, with special thanks to Carlos, Ikpo, Immanuel, Niky, and Josh, who made the lab a friendly environment and filled it with cherished memories.

Finally, I want to express my heartfelt appreciation to my family for their unwavering support. Above all, I give thanks to God Almighty for His greatness in my life, to whom I give all honor and glory.

TABLE OF CONTENT

TABLE OF CONTENT

TABLE OF CONTENT

TABLE OF CONTENT

TABLE OF CONTENT

TABLE OF CONTENT

TABLE OF CONTENT

TABLE OF CONTENT

TABLE OF CONTENT

LIST OF ABREVIATIONS

5-HT	**5-hydroxytryptamine**
AA	Amino acid
Ab	Antibody
APC	Antigen presenting cells
APC (conjugated)	Allophycocyanin conjugated
ADT	Androgen deprivation therapy
AF	AlexaFluor
AR	Androgen receptor
β2M	β2-microglobulin
BCR	B cell receptor
BCG	Bacillus Calmette-Guérin
biLSTM	Bidirectional Long Short-Term Memory Deep Neural Network
BPH	Benign prostatic hyperplasia
BSA	Bovine serum albumin
BV	Brilliant violet
CAF	Cancer-associated fibroblasts
CAF®09b	Cationinc adjuvant formulation
CCL2	CC chemokine ligand 2
CCK- 8	Cell counting kit-8
CCR2	CC chemokine receptor type 2
CCR7	C-C chemokine receptor type 7
CD	Cluster of Differentiation
CLIP	Class II-associated invariant chain peptide
CMP	Common myeloid progenitor cells
CpG-ODN	deoxycytidine-deoxyguanosine dinucleotides
CRISPR	Clustered regularly interspaced short palindromic repeats
CRPC	Castration-resistant prostate cancer

LIST OF ABREVIATIONS

CRP	C-Reactive Protein
CTA	Cancer testis antigen
CTLA-4	Cytotoxic T-lymphocyte antigen-4
CTL	cytotoxic T-lymphocyte
CO_2	Carbon dioxide
CX3CL1	C-X3-C motif chemokine ligand 1
DC	Dendritic cell
DDA	dimethyl-dioctadecyl ammonium
DHT	dihydrotestosterone
DMEM	Dulbecco's modified eagle medium
DMSO	Dimethyl sulfoxide
DNA	Deoxyribonucleic acid
DRE	Digital Rectal Examination
EBV	Epstein-Barr virus
ECL	Enhanced chemiluminescence
EDTA	Ethylenediamine tetra acetic acid
ELISA	Enzyme linked immunosorbent assay
ELISpot	Enzyme linked immunosorbent spot
EMT	Epithelial-mesenchymal transition
FABP2	Fatty acid binding protein 2
FBS/FCS	Fetal Bovine/Calf Serum
FDA	Food and Drug Administration
FITC	Fluorescein isothiocyanate
FoxP3	Forkhead box P3
FSC-(H/A)	Forward scatter- (height/area)
G418	Geneticin
GAPDH	Glyceraldehyde 3-phosphate dehydrogenase

LIST OF ABREVIATIONS

G-CSF	Granulocyte colony-stimulating factor
GITR	Glucocorticoid-induced tumour necrosis factor related protein
GM-CSF	Granulocyte -macrophage colony-stimulating factor
G-MDSC	Granulocytic MDSC
GnRH	Gonadotropin-releasing hormone
HLA	Human leucocyte antigen
HIV	Human immunodeficiency virus
HPV	Human papillomavirus
HRP	Horseradish peroxidase
IEDB	Immune Epitope Database
IFA	Incomplete Freund's adjuvant
IFN	Interferon
IL	Interleukin
iNOS	inducible nitric oxide synthase
Ki67	Antigen Kiel 67
LAG-3	Lymphocyte-activation gene 3
LH	luteinizing hormone
LN	Lymph node
LPS	Lipopolysaccharides
mAbs	Monoclonal antibodies
M-CSF	Macrophage colony-stimulating factor
mCRPC	Metastatic castration-resistant prostate cancer
MDSC	Myeloid-derived suppressor cells
MHC	Major Histocompatibility complex
MRI	Magnetic resonance imaging
mp-MRI	Multiparametric magnetic resonance imaging
M-MDSC-	Monocytic MDSC
mRNA	Messenger Ribonucleic acid

LIST OF ABREVIATIONS

n	Number of replicates
NK cells	Natural killer cells
NO	Nitric oxide
NOD-SCID	Nonobese diabetic mice and severe combined immunodeficiency
PAP	Prostatic acid phosphatase
PBS	Phosphate-buffered saline
PBMC	Peripheral blood mononuclear cell
PCa	Prostate cancer
pDCs	plasmacytoid DCs
(q/RT) PCR	(Quantitative /real-time) Polymerase chain reaction
PD-1	Programmed cell death 1
PD-L1	Programmed cell death ligand 1
PerCP	Peridinin Chlorophyll protein complex
PE	Phycoerythrin
PIA	Proliferative inflammatory atrophy
PIN	Prostatic intraepithelial neoplasia
PMN-MDSC	Polymorphonuclear MDSC
PNI	Perineural invasion
PRR	pattern-recognition receptors
PSA	Prostate-specific antigen
PSAD	Prostate-specific antigen density
PSMA	Prostate-specific membrane antigen
PTEN	Phosphatase and Tensin homolog deleted on chromosome 10
RAG	Recombination -activating gene
RNA	Ribonucleic acid
ROS	Reactive oxygen species
rpm	Rotation per minute

LIST OF ABREVIATIONS

SCC	Side scatter
SD	Standard deviation
SDS	Sodium dodecyl sulfate
SDS- PAGE	Sodium dodecyl sulfate-polyacrylamide gel
SE	Standard error
sgRNA	Synthetic guide Ribonucleic acid
shRNA	Short hairpin Ribonucleic acid
SV40	Simian virus
TAA	Tumour-associated antigens
TAM	Tumour-associated macrophage
TANs	Tumor-associated neutrophils
TCR	T cell receptor
T_{CM}	Central-memory T-cells
T_{EM}	Effector-memory T-cells
TEMRA	Terminally Differentiated Effector Memory Cells
TGFβ	Transforming growth factor beta
TILs	Tumour infiltrating lymphocytes
TIM-3	T-cell immunoglobulin domain and mucin domain protein 3
TLR	Toll-like receptors
TME	Tumour microenvironment
TNF	Tumour necrosis factor
TPH	Tryptophan hydroxylase
TRAMP	Transgenic adenocarcinoma mouse prostate
Treg	Regulatory T cells
TRUS	Tans-rectal ultrasound
TRP	Tryptophan
TSA	Tumour specific antigens

LIST OF ABREVIATIONS

VDJ	Variable -diversity- joining rearrangement
VEGF	Vascular endothelial growth factor
WST -8	Water soluble tetrazolium 8
WT	Wild type
Units	
cc	Cubic centimetres
L	Litre
µL	Microlitre
µg	Microgram
mL	Millilitre
mg	Milligram
ng	Nanogram
Greek alphabet	
α	Alpha
β	Beta
γ	Gamma
δ	Delta
ζ	Zeta

LIST OF FIGURES

LIST OF FIGURES

LIST OF FIGURES

LIST OF FIGURES

LIST OF TABLES

LIST OF TABLES

LIST OF PUBLICATIONS AND PRESENTATIONS

Publications (Journal articles)

1. Puig-Saenz, C., Pearson, J.R.D., Thomas, J.E., McArdle, S.E.B. (June 2023). " A Holistic Approach to Hard-to-Treat Cancers: The Future of Immunotherapy for Glioblastoma, Triple Negative Breast Cancer, and Advanced Prostate Cancer." *Biomedicines*. 11(8). DOI: 10.3390/biomedicines11082100.
2. Pearson, J., Puig Saenz, C., Thomas, J.E., McArdle, S.E.B. (July 2024). "TRP-2 / gp100 DNA vaccine and PD-1 checkpoint blockade combination for the treatment of intracranial tumors." *Cancer Immunology and Immunotherapy*, 73(9), DOI: 10.1007/s00262-024-03770-x.

Publication (Conference Paper)

1. Thomas, J.E., McArdle, S.E.B., Christensen, D., LeVu, P. (September 2022). "A mutated prostatic acid phosphatase (PAP) peptide-based vaccine induces PAP-specific CD8+ T cells with ex vivo cytotoxic capacities in HHDII/DR1 transgenic mice." *Journal for ImmunoTherapy of Cancer*, 10(1). DOI: 10.1136/jitc-2022-ITOC9.30 Presented at iTOC9 – 9th Immunotherapy of Cancer Conference, September 22–24, 2022, Munich, Germany.

Presentation (Poster presentation)

1. The 9th Immunotherapy of Cancer Conference (September 2022), Munich Germany. Poster Title: A mutated prostatic acid phosphatase (PAP) peptide-based vaccine induces PAP-specific CD8+ T cells with ex vivo cytotoxic capacities in HHDII/DR1 transgenic mice.
2. British Society for Immunology conference (December 2022), Liverpool UK. Poster Title: Development of an effective PAP-derived vaccine for advanced prostate cancer
3. British Society for Immunology, Midlands Immunology group Symposium (June 2023), Leicester UK. Poster Title: Development of an effective PAP-derived vaccine for advanced prostate cancer

Presentation (PowerPoint presentation)

1. STAR conference, Nottingham Trent University (June 2022).

ABSTRACT

Background: Current treatments for castrate-resistant prostate cancer (CRPC) remain limited, with a median survival from diagnosis of 23 months, the PAP-specific Sipuleucel-T vaccine, which was approved by the FDA in 2010, increases the Overall Survival by 4.1 months but is extremely expensive. Previous work in our laboratory has demonstrated that a 15mer PAP-derived peptide delayed TRAMP-C1 prostate tumours, yet this vaccine only targeted HLA A2 haplotype patients. Thereby the sequence was elongated to 42mer with an amino acid substitution to include epitopes predicted to bind to additional HLA haplotypes. The MutPAP42mer +CAF®09b vaccine has improved secretory IFNγ and PAP-specific splenic T-cells in HHDII DR mouse models, however, no CD4+ T-cell mediated responses were demonstrated. To improve the anti-tumour efficacy of MutPAP42mer by improving CD4+ T-cell mediated responses, a novel 15-mer PAP peptide was identified. MutPAP42mer with PAP15mer CPR immunogenicity was assessed using CpG ODN1826/2395+IFA and CAF®09b adjuvant. **Methods:** HHDII DR/DP4 and C57BL/6J mice were immunised with MutPAP42mer+CPR or hPAP42mer WT respectively with CAF®09b or CpG ODN1826/2395+IFA adjuvants. Vaccine-induced immune responses and cytotoxic capabilities were measured by assessing the proportion and functionality of splenic PAP-specific T-cells *in vitro*. **Results:** PAP peptide/s adjuvanted with CAF®09b was shown to have improved secretory IFN-γ and $CD4^+$/$CD8^+$ specific immune response in HHDII and C57BL/6J models. Moreover, the *in vivo* analysis of hPAP42mer WT +CAF®09b vaccine increased the percentage of IFN-γ-releasing CD8+ T-cells when applied with androgen ablation in TRAMP C2 prostate tumour bearing C57BL/6J models. However, the vaccine had no effect in reducing the tumour growth was reported to be due to the elevated levels of MDSC in the PCa tumours. Immunophenotyping of blood samples also revealed increased expression of M-MDSCs and G-MDSCs, with G-MDSCs being more prevalent in both PCa and benign patients. **Conclusions:** The preclinical analysis of the PAP peptide-based vaccine concludes that administering the vaccine in conjunction with androgen deprivation and strategies to reduce MDSC-mediated suppression, will enhance the therapeutic efficacy of the vaccination. Future studies should investigate the link between MDSCs and vaccine efficacy, particularly in humanized models, to develop more effective immunotherapy strategies for CRPC.

Chapter 1: INTRODUCTION

1. Introduction

1.1. Overview of Prostate Cancer

Prostate cancer (PCa) is the abnormal proliferation of cells in the prostate gland which is located directly below the bladder and encircles the proximal urethra in the lesser pelvis, mainly functioning to produce seminal fluid along with seminal vesicles to nourish and transport sperm (Singh and Bolla, 2023; Sekhoacha *et al*. 2022). Different from benign prostatic hyperplasia which primarily develops in the transitional zone, PCa usually manifests as an adenocarcinoma, with 75% of cases occurring in the peripheral zone of the prostate gland (Singh and Bolla, 2023). Symptoms of PCa include difficulty urinating and increased urination frequency due to difficulty in emptying the bladder. These symptoms are often mistaken as benign hyperplasia, however proper diagnostic measures are needed to confirm the cancerous growth. At the advanced stage, PCa cells metastasise from their primary site to the surrounding organs such as the bladder or travel through the bloodstream to get to various body parts. Although bone metastases account for 85-90% of cases, they can also spread to the liver, lymph nodes, lungs, and brain (Sekhoacha *et al*. 2022; Yu, Hwang, and Aragon-Ching, 2023).

1.1.1. Pathophysiology

The human prostate is a glandular organ located below the bladder composed of an epithelial bilayer; basal (40%) and columnar secretory luminal cells (60%), surrounded by fibromuscular stroma. The human prostate is divided into the anterior fibromuscular zone and three glandular zones (central, transition, and peripheral) (Henry *et al*. 2018). The central zone of the prostate contains the ductal tube from the seminal vesicle adjoining the descending urethra. Adjacent to the bladder, the transitional zone encircles the transitional urethra. The peripheral zone is located at the posterior of the gland and is where most neoplastic changes arise (Packer and Maitland, 2016). In contrast, Benign prostatic hyperplasia (BPH) occurs mostly in the transition zone (Henry *et al*. 2018).

Chapter 1: INTRODUCTION

The prostate gland comprises ducts and acini embedded in the stroma. The epithelial luminal cells, coat the internal surface of prostatic ducts, express androgen receptors, and secrete prostatic fluid and the glycoprotein called 'Prostate Specific Antigen' (PSA). The luminal cells are surrounded by basal cells, which generate proteins needed for fluid production and the arrangement of the acinar basement membrane which splits prostatic stroma from the epithelial acini (Murray, 2021). Three main cell subtypes are found in the basal layer: basal cells, transit-amplifying cells, and stem cells (Packer and Maitland, 2016). Luminal and basal cells have interspersed neuroendocrine cells. Neuroendocrine and basal cell types lack androgen receptors and thus are not testosterone dependent. Fibroblasts, smooth muscle, and infiltrating immunological cells together form prostate stroma (Murray, 2021; Rebello *et al*. 2021).

PCa is primarily of epithelium and is thus a carcinoma, about which 90-95% of prostate cancers are acinar adenocarcinomas that arise from the peripheral prostatic gland. The transformation of pre-existing benign epithelial cells into malignant phenotype is called prostatic intraepithelial neoplasia (PIN). PIN is a multicentric condition and is defined as the "neoplastic growth within the pre-existing benign epithelium of the acini or ducts" (Murray, 2021). High-grade PIN exhibits similar cytologic features to PCa and is recognised as a progenitor to most prostatic adenocarcinomas. However, in contrast to carcinoma in the peripheral zone, benign prostatic hyperplasia tends to occur in the transition zone, where the incidence of high-grade PIN is only 2% to 3%. A positive correlation has been observed between the volume of PIN and the pathologic stage and the Gleason grade of PCa (Brawer, 2005).

Most solid tumours develop from a single cell that acquires neoplastic growth abilities through the genomic and heritable epigenetic mutations which alter the cellular phenotype known as tumour clonality. A wide range of lesions, from small-scale mutations such as insertions/deletions (indels) and single-nucleotide variants to large-scale chromosomal abnormalities like translocations or gene fusions, can be found in tumour cells. Tumour clonality is the fundamental characteristic of cancer, however, cancer development is a multi-step process including an iterative process of clonal expansion, clonal selection, and genetic variation with the cumulative capability of proliferation, persistence, invasion, and metastasis

(Mateusz Kciuk *et al*. 2023; Cooper, 2020). The tumour initiates when the progenitor cell leads to an unusual proliferation leading to the outgrowth of a population of clonally derived cells. The driver gene alterations are shared between all daughter cells arising from the progenitor cell, giving rise to clonal expansion. Tumours progress as the clonally derived cells continue to obtain additional mutations resulting in a genetic and phenotypic diverse sub-clonal population. The subclones evolved can demonstrate rapid proliferation and enhanced survival, consequently becoming dominant within the tumour population. This process is known as the clonal selection, which is maintained throughout the tumour progression, thus tumours constantly become more aggressively growing (Haffner *et al*. 2020; Cooper, 2020).

1.1.2. Epidemiology

PCa is the second most frequent malignancy and the fifth leading cause of cancer-related death in men worldwide. The Global Cancer Observatory (GLOBOCAN)- 2022 report estimates 1,466,680 new cases of PCa causing 396,792 deaths which account for 4.1% of deaths caused by all cancers. Lung cancer was the most diagnosed cancer in 2022, accounting for roughly 2.5 million new cases, estimated as 12.4% of all cancer burden worldwide. PCa accounts for 7.3% of all cancers worldwide. In two-thirds of the world's countries (118 countries) PCa is the most common type of cancer diagnosed among men. In the past, there was a rapidly increasing PCa incidence rate reported in Southern and Eastern African countries from 1995 to 2018 and a 3% per annum average increase in the United States, from 2014 to 2019. However, a decrease in the mortality rates reported in countries including Northern America, Oceania, and Northern and Western Europe, in the early 21st century likely reflects the improvements in the earlier detection through increased testing of high-risk men. According to the GOBCAN 2022 reports, the incidence rate varies by region; Northern Europe, Northern America, Australia/New Zealand, and the Caribbean have the highest rates (6.4 to 82.8 per 100,000), while several Asian and African regions have the lowest rates. Furthermore, PCa is the leading cause of cancer-related death among men in 52 countries, with the highest mortality rate found in the Caribbean and sub-Saharan Africa (Bray *et al*. 2024).

Chapter 1: INTRODUCTION

According to the statistical analysis from 2016-2018 in the United Kingdom (UK), PCa was the most diagnosed cancer in men. There were around 52,300 new PCa diagnoses every year which accounts for 27% of all new cancer diagnoses in males in the UK. The incidence rates were highest in males aged 75 to 79. Statistics show that from 2017-2019, there were around, 12,000 PCa deaths in the UK every year which is accounting for 14% of all cancer deaths in males in the UK (https://www.cancerresearchuk.org/health-professional/cancer-statistics/statistics-by-cancer-type/prostate-cancer/incidence).

1.1.3. Risk factors (Aetiology)

The exact aetiology of PCa is unknown, however, genetic, social, environmental, and increasing age have been contributing factors to the development of PCa (Rawla, 2019; Belkahla *et al*. 2022). Risk factors can be explained as modifiable (environmental/ lifestyle) and nonmodifiable risk factors (age, race, and family history).

1.1.3.1. Non-modifiable risk factors

1.1.3.1.1. Age

The risks of developing PCa increase with age; 6 out of 10 cases of PCa are diagnosed in men over the age of 65. PCa associated with advanced ageing is seen in both developing and developed countries (Ng, 2021; Rawla, 2019). Older men are more likely to be diagnosed with high-risk PCa, with decreased overall survival. According to recent cancer statistics in the United States, the possibility of developing PCa is 1.8% in men aged 60-69 years while the risk is increased up to 9.0% in men aged 70 years (Al-Ghazawi *et al*. 2023). Approximately half of all PCa-related deaths occurred in patients older than 70 years (Belkahla *et al*. 2022).

1.1.3.1.2. Ethnicity and race

The incidence and mortality rate of prostate cancer exhibit geographical and ethnic variations. Black African descent has a higher rate of PCa incidence, severity, and death (Ng, 2021). PCa incidence rate is higher among African American men, often diagnosed at younger ages than Caucasian and Asian men and their PCa-related mortality rate is 2.4 times higher comparatively (Hinata and Fujisawa, 2022). The racial discrepancies may have multiple factors

including varying exposure to risk factors, genetic alterations, tumour biology, and circulating hormones (Gong *et al*. 2023; Zhen *et al*. 2018). The recent cancer statistics show lower PCa incidence and mortality rates among Asian, and American Indians or Alaskan natives (Al-Ghazawi *et al*. 2023).

1.1.3.1.3. Family history

Men with first-degree relatives such as a father or brother with PCa have a 2 to 4-fold increased risk of developing the disease (Zhen *et al*. 2018). According to Rawla, (2019), there is evidence linking genetic background to a 5-8% increased risk of disease. The Health Professional Follow-Up Study for 18 years (1986 to 2004) involving 3,695 patients confirmed a 2.3-fold increased risk of PCa with a family history of the disease (Belkahla *et al*. 2022). Furthermore, according to the Nordic Twin Study of Cancer, 57% of the variation in PCa risk between twins was ascribed to genetic factors. Monozygotic and dizygotic twins have demonstrated an increased risk of prostate cancer if a sibling is affected making prostate cancer one of the most heritable cancers (Ng, 2021). In addition to the family history of PCa, men in families with breast cancer history in the mother or sister also have a higher chance of developing PCa. According to a large prospective study conducted in the USA, involving 37002 men over 16 years recognised that those with a family history of breast cancer had a 21% greater risk of PCa overall (Ng, 2021). An explanation for the biological mechanism behind the familial clustering of prostate and breast cancer could be inherited BRCA mutation. There is a connection between BRCA1 and BRCA2 and breast cancer as well as evidence of an elevated prostate cancer risk among male BRCA carriers (Ng, 2021; Rawla, 2019; Hinata and Fujisawa, 2022).

1.1.3.2. Modifiable risk factor

1.1.3.2.1. Diet

An elevated risk of prostate, breast, and colon cancers has been associated with a Westernised diet which is heavy in processed foods and high in animal fat. Although the exact mechanism linking a high-fat diet to the risk of prostate cancer is unknown, it may be related to elevated basal metabolism and enhanced androgen-induced prostate carcinogenesis (Belkahla *et al*.

2022). Likewise, high-fat and high-calcium dairy products have been shown to promote the process of tumorigenesis. The elevated levels of calcium suppress the active form of vitamin D, calcitriol which functions to induce apoptosis and inhibit cell growth; higher calcium intake will reduce their vulnerability to apoptosis (Ng,2021).

1.1.3.2.2. Obesity

Obesity and increased body mass index have been associated with numerous cancers including PCa. Metabolic and hormonal imbalances, increased levels of insulin, insulin-like growth factor-1 (IGF-1), and leptin are sustained with adiposity raising the risk of disease development (Belkahla *et al*. 2022; Ng, 2021). Obesity is often associated with unfavourable disease progression, declined post-surgical outcomes, and mortality. Peri-prostatic adipose tissue expansion in the obesity-induced secretion of adipokines, chemokines, and cytokines from adipocytes and adipose stromal cells are significant factors in the development of PCa. Adipocytes are a source of lipids that are used by adjoining PCa cells. Adipose stromal cells in tumour stroma act as cancer-associated fibroblasts, which promote vascularisation, recruit immunosuppressive leukocytes to TME and induce mesenchymal transition (Saha, Kolonin and DiGiovanni, 2023).

1.1.3.2.3. Exposure to chemicals and smoking

Exposure to chemicals such as ‘Agent Orange’, pesticides, trace minerals and UV radiation increases the risk of developing various cancers including PCa. According to the International Agency for Research on Cancer, more than 60% of chemicals found in a cigarette are carcinogens. Polycyclic aromatic hydrocarbons in cigarettes have the potential to enhance cancer proliferation by inducing DNA mutations (Belkahla *et al*. 2022). A meta-analysis of 17 cohort studies revealed that smoking had a worse prognosis and higher risk of mortality in PCa patients. Smokers had a 42% higher risk of death from PCa compared to non-smokers with a relative risk of 1.42% (Al-Fayez and El-Metwally, 2023).

1.1.3.2.4. Inflammation

Persistent inflammation can induce oxidative stress and production of reactive oxygen radicals which can ultimately lead to mutation in the prostate cells. The stress induced by chronic inflammation could prompt epigenetic alterations which can accelerate the neoplastic transformation of prostate luminal epithelial cells. In PCa, inflammation is associated with developing atopic lesions or proliferative inflammatory atrophy (PIA), frequently observed in prostate biopsies. PIA has been proposed as a precursor lesion of PCa, directly or through the development of high-grade PIN (Al-Fayez and El-Metwally, 2023). These lesions share similar features with high-grade PIN and PCa; epithelial cells in the atrophic lesions resemble neoplastic cells morphologically, with increased nuclear size and loss of the nuclear-cytoplasmic ratio. Moreover, the genetic abnormalities found in the PIA lesions, such as gains in chromosomes and 8q24 gene – which contain risk regions for multiple epithelial cancers including PCa- are shared by high-grade PIN and PCa (A. Celma *et al*. 2014).

1.1.4. Screening and diagnostic

PCa is asymptomatic at the initial stage (Bratt *et al*. 2023). When cancer reaches the locally advanced stage, patients begin to experience symptoms such as trouble during urination, difficulty emptying the bladder, and persistent back, hip, or pelvic pain. PCa screening is usually done by PSA blood test and digital rectal examination (DRE). Patients with elevated PSA levels and abnormal DRE findings with hard mass or nodule are recommended to undertake prostate gland imaging and biopsy to confirm further the diagnosis of PCa (Bratt *et al*. 2023).

1.1.4.1. Prostate-specific antigen (PSA) blood test

PSA is a glycoprotein secreted by prostate epithelial cells and seminal vesicles, promoting seminal viscosity and sperm motility. A small amount of PSA is normally present in the bloodstream. The age-specific normal PSA range is 0 to 2.5 ng/mL for 40-49 years, 0 to 3.5 ng/mL for 50 to 59 years, 0 to 4.5 ng/mL for 60 to 69 years, and 0 to 6.5 ng/mL for 70 to 79 years. Elevated blood PSA levels are noticed in prostate malignancy; however, the PSA test alone is not a sufficient diagnostic measure for PCa. Increased PSA level is associated with benign

prostatic hyperplasia, prostatic inflammation or infection, perineal trauma, and PCa (Bratt *et al*. 2023; Jain and Sapra, 2020). Thus, for the screening of PCa, circulatory total PSA and free PSA levels are usually measured. In non-malignant prostate conditions, the free PSA is often higher whereas in PCa is lower. Thus, elevated total PSA (between 4-10ng/mL) and low free PSA percentage indicate a higher risk of PCa (Balk, Ko and Bubley, 2003; Jain and Sapra, 2020).

1.1.4.2. Digital rectal examination (DRE)

The nodularity, tissue consistency change, prostatic symmetry, and enlargement of the prostate gland are assessed by inserting a gloved lubricated finger through the anal passage. The abnormal findings of DRE include enlargement of the prostate gland, presence of nodules, hard consistency, and lobar asymmetry. Since the DRE examination has a 60% accuracy and sensitivity, it is used in conjunction with other PCa screening measures like PSA testing (Jain and Sapra, 2020).

1.1.4.3. Prostate imaging by Ultrasound or MRI Scan

Prostate biopsy is recommended for patients with abnormal DRE findings and higher PSA levels. Ultrasound imaging is carried out by inserting a lubricated ultrasound probe through the anal passage that generates sound waves to create an image of the prostate gland. Normal and abnormal tissue reflect different types of echoes, and their patterns are translated into a video image. Tans-rectal ultrasound (TRUS) guided biopsy, using these images as a guide to collect tissue samples by inserting a biopsy needle through the anal passage. Trans-perineal biopsies are also guided by TRUS scan, but the tissue samples are collected by inserting a biopsy needle into the prostate through the skin behind the perineum which is done under either general or local anaesthesia. However, TRUS biopsies are not targeted, which increases the possibility of over-diagnosing clinically indolent tumours while omitting PCa foci that are clinically significant (Carneiro *et al*. 2021). Magnetic resonance imaging (MRI) uses a magnetic field and computer-generated radio waves to create a detailed image of the prostate is more accurate than TRUS to estimate the prostate volume. Like TRUS-guided biopsy, MRI-guided biopsy also collects samples through the endorectal or transperineal approach. Multiparametric MRI (mp-

MRI) produces a more detailed three-dimensional image of the prostate by combining T2-weighted, diffusion-weighted, dynamic contrast-enhanced and magnetic resonance spectroscopy images. mp-MRI detects areas clinically suspicious for PCa and allows targeted biopsy sampling.

The biopsy samples are examined for histopathological changes under the microscopes to confirm the diagnosis of cancer. The degree of inflammation and aggressiveness of the cancer is determined by identifying how cancer cells look pathologically different from normal cells, which is crucial for determining the stage of the disease and planning the therapy (Streicher *et al*. 2019). Architectural and cytologic features of cells are examined under the microscope by staining the biopsy samples usually with Haematoxylin, eosin stain and specific studies such as immunohistochemistry for keratin 3βE12 (Mandel *et al*. 2021). Architectural features describe the spatial arrangement of prostatic acini. Most prostatic adenocarcinomas acini usually have an irregular arrangement, randomly dispersed in the stroma in clusters or individually. The cytologic features include prominent nucleoli, nuclear enlarged, and the absence of basal cells observed in most malignant cells (Magi-Galluzzi, 2018). The commonly used immunohistochemical markers in prostate pathology are PSA, PAP, and high-molecular-weight keratin 3βE12. Immunohistochemistry for basal cell-specific keratin is typically employed to differentiate adenocarcinoma from PIN, atrophy, or adenosis (Mandel *et al*. 2021).

1.1.5. Grading of PCa

PCa is graded according to a Gleason Score grading system (Figure 1.1), which was last modified in 2014 by the International Society of Urologic Pathology (ISUP). The aggressiveness of the adenocarcinoma is assessed based on the degree of differentiation in the histopathological evaluation of cancer cells (Murray, 2021).

Cancer cells are scored Gleason scores 2 to 10 depending on their appearance under the microscope compared to the normal cells. The larger the number, the more aggressive the cancer. A score up to 5 is considered normal and is no longer assigned. Score 6 is considered slightly abnormal and score 10 is highly abnormal. Grade (1 to 5) is further calculated from the scores by adding the most and second most common patterns (Table 1.1). For example, a

Chapter 1: INTRODUCTION

Gleason score of 7 can be characterised by mostly well-differentiated cancer with a less significant component of more poorly differentiated cancer (Gleason 3 + 4 = 7) or mostly poorly differentiated cancer with a lesser component of well-differentiated cancer (4 + 3 = 7). Prognostically, the two are different: the former (Gleason 3 + 4 = 7) is graded 2, and the latter (4 + 3 = 7) is grade 3 (Short, Warren and Varma, 2019; Epstein et al. 2016).

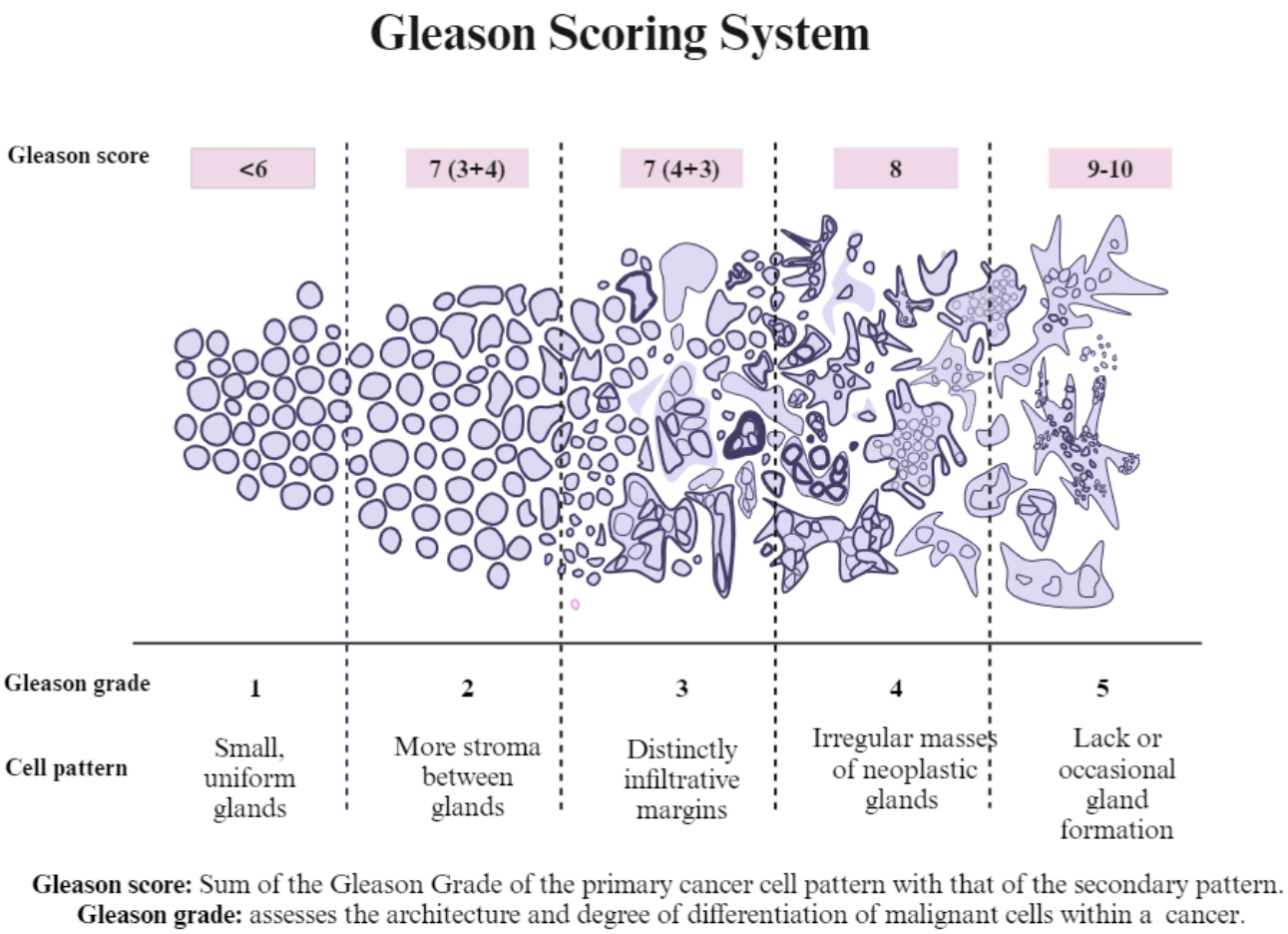

Figure 1.1. *2015 modified ISUP Gleason schematic diagram. Diagram re-created using https://www.biorender.com/.*

Risk of Progression D'Amico classification based on the tumour size, grade, and PSA level, PCa is classified as low, intermediate, and high risk. **At low risk –** the cancer is not aggressive, the tumour is confined to the prostate (T1-2), the PSA is ≤ 10ng/mL and the grade group is 1 (Gleason ≤ 6). **Intermediate risk –** the cancer is moderately aggressive, the tumour is confined

to the prostate (T2b), the PSA is between 10-20ng/mL, and the grade group is 2 or 3 (Gleason 7). H**igh risk –** the cancer is more aggressive, the tumour spreads outside the prostate (T 3-4), the PSA >20ng/mL, and or the grade group 4 or 5 (Gleason 8 to 10). The risk of progression category helps to guide the management and treatment of PCa (Frederik, 2015).

Grade Group	Gleason Score	Features
1	≤ 6	Only individual distinct well-formed glands,
2	3+4=7	Mainly well-formed glands with fewer components of poorly formed glands. Cancer is likely to grow slowly
3	4+3=7	Mainly poorly formed glands with fewer components of well-formed glands. Cancer is likely to grow at a moderate rate
4	4+4=8, 3+5=8 or 5+3=8	Mainly poorly formed glands with lesser components of well-formed glands. Cancer is likely to grow at a faster rate.
5	9 and 10	Lack of gland formation with or without poorly formed glands

Table1.1. *Gleason score grade groups for PCa (Murray, 2021).* Gleason grade refers to how abnormal the prostate cancer cells look under a microscope. The grading system ranges from 1 to 5: Grade 1: Cancer cells closely resemble normal prostate tissue (least aggressive). Grade 5: Cancer cells are highly abnormal and disorganised (most aggressive). The Gleason score is the sum of the two most common Gleason grades found in the biopsy sample, ranges from 6 to 10.

1.1.6. TNM staging of PCa

PCa is staged based on the size of the primary tumour (T), lymph node involvement (N), and metastases (M) (Murray,2021). The TNM system describes cancer using numbers and letters - The size of the tumour (T1 -4), lymph node (N 0- 1) and metastasis (M 0-1) -with the higher number indicating a larger spread. T1 and T2 tumours are confined to the prostate, with no involvement of nearby lymph nodes (N0) categorised as localised PCa (Francesco Saverio Guerra et al. 2023). T3 tumours are locally advanced PCa that typically involve pelvic regional lymph nodes (N1) but are not spread to other body parts (M0). Metastatic or advanced PCa spread outside of the pelvis (M1), most commonly to bone, lung, and liver which has lymph node involvement (N1), and tumour size T4 (Murray, 2021; Francesco Saverio Guerra *et al*. 2023).

Chapter 1: INTRODUCTION

1.2. Current treatments for PCa

Following PCa's diagnosis, the treatment is decided on several factors including the tumour risk group, prognosis of the disease, the patient's age, and preferences. The best course of action for patients who have low risk localised early cancer or those with short life expectancy is active surveillance also known as watchful waiting. This can benefit the patient by potentially avoiding unnecessary treatment and its associated side effects that can severely impact the quality of life. Treatment strategies for PCa are often associated with bowel dysfunction, urinary incontinence, and erectile dysfunction. Patients are closely monitored for the indication of cancer growth, without receiving any treatment may benefit patients to counteract the harm of overtreatment. During active surveillance, the progression of the cancer is monitored by regular PSA testing, DRE, medical imaging, and prostate biopsies, therefore definitive treatment is offered when the progression is evident (te Marvelde *et al*. 2020). (Shill *et al*. 2021) conducted a narrative review of 13 active surveillance cohorts to determine the safety and efficacy of active surveillance. Out of 13 studies included, 5 studies had included only low-risk patients while the other 8 studies had included intermediate-risk patients also. Their analysis revealed that most of the cohorts included in the review had reported a less than 0.5% risk of developing metastasis and death in 10 years. Half of the participants in most cohorts did not receive treatment for 5 to 10 years. Overall, the risk of developing PCa metastasis and PCA mortality ranged between 0.1 to 1.0% and 0 to 1.9% respectively at ten years. Taken together with the data collected from these cohorts, Shill et al. 2021 suggest that active surveillance is a safe approach for men with low-grade PCa and some patients with intermediate risk.

Treatment options for localised PCa include radical prostatectomy, radiation therapy and cryoablation. The advanced stage of the disease is treated with androgen deprivation therapy (ADT), chemotherapy or a combination of therapies. However, if the patient has developed metastatic castration resistant PCa (mCRPC), chemotherapy and radiation therapies are the only available options.

1.2.1. Radical prostatectomy

Radical prostatectomy – removal of the prostate gland through surgery- is a recommended therapeutic option for men with localised PCa. The prostate gland is surgically removed making an incision in the lower abdomen or perineum. Robort-assisted radical prostatectomy (RARP), a recent advancement in surgical approach has provided a reliable, and oncologically effective surgical option which allows surgeons to operate on the prostate with enhanced vision, control, and precision. RARP uses miniaturised robotic surgical instruments that are passed through various small keyhole incisions in the abdomen to remove the prostate gland and adjacent tissues (Tae Joo Shin and Yong Rok Lee, 2022). Radical prostatectomy is often associated with potential complications such as urinary incontinence and erectile dysfunction. Radical prostatectomy is usually discouraged in clinically advanced or high-risk PCa, due to the high-risk surgical margins and insufficient disease control. Moreover, surgically excising the prostate is pointless at this time, since cancer might have already metastasised (Sekhoacha *et al*. 2022). However, the survival outcomes of RARP for locally advanced PCa – clinical stage T2, and PSA > 20 ng/mL - have been studied by (Tae Joo Shin and Yong Rok Lee, 2022) including 188 patients who underwent RARP between July 2013 and May 2020. The study has reported a 100% biochemical recurrence-free and clinical recurrence-free during the 1 to 3-year follow-up of post-RARP (Tae Joo Shin and Yong Rok Lee, 2022).

1.2.2. Cryotherapy

Cryotherapy also known as cryoablation is the treatment option for localised, low and intermediate-risk PCa and is often recommended to patients with very large prostate glands. Cryoprobes are inserted into the prostate under ultrasound guidance, to destroy cancerous cells by freezing of prostate gland to a temperature between −100 °C to −200 °C for approximately 10 minutes. Cryotherapy-related side effects include rectal pain, erectile dysfunction, blood in the urine, urinary incontinence, and urine retention (Sekhoacha *et al*. 2022). This approach is not recommended for patients with localised high-risk PCa defined by PSA>20ng/mL, Gleason grade group 4 or 5 or clinical stage >T2. The role of prostate cryoablation for patients with high-risk PCa was investigated by (Chen, Tsai, and Pu, 2023)

including 191 patients with high-risk PCa who underwent primary total prostate cryoablation. Their findings show that prostate cryoablation provided an adequate 10-year cancer control in 50.8% of patients with high-risk disease, in terms of biochemical recurrence after a long-term follow-up duration.

1.2.3. Radiotherapy

Radiotherapy is a treatment option for all stages of PCa from localised to metastasis. Radiations are carried out as external beam therapy or brachytherapy. External beam therapy (EBT) uses a machine to direct high-energy waves like X-rays to kill cancerous cells. Brachytherapy is internal radiotherapy, where the radioactive seeds are placed inside the prostate to release radiation to destroy prostate cancer cells. For, low-risk PCa, EBT and low-dose brachytherapy are recommended. EBT, brachytherapy or a combination of both may be used to treat intermediate-risk patients. In high-risk patients, radiotherapy may be used in combination with other therapies such as ADT to improve survival outcomes. Recent advances in radiation techniques such as intensity-modulated radiation therapy (IMRT) and image-guided radiotherapy (IGRT) deliver a dose-escalated radiation therapy while minimizing treatment-associated morbidity and toxicities. IMRT uses computer-controlled radiation beams to irradiate specific areas with different radiation intensities. IGRT utilizes images, such as magnetic resonance imaging or computed tomography scans to direct the radiation delivery process which will allow a highly precise targeting of the tumour, leading to enhanced treatment outcomes (Kazuyuki Numakura *et al*. 2023). Dichloride radium-223, a radioactive form of the metal, is used for the treatment of painful bone metastases. This internal radiotherapy slows the progression of the disease and helps control pain by destroying cancer cells. A higher radiation dose targeting a large fraction of the prostate effectively controls tumour growth up to 91% in high-risk PCa, however high radiation dose may result in chronic tissue damage to the gland (Lee and Chung, 2022). A life expectancy of less than 5 years, distant metastasis, and recurrent haematuria are the other complications associated with brachytherapy. There was a 19-26% biochemical recurrence also noticed with radiotherapy within 12 years of treatment (Skowronek, 2013).

1.2.4. Hormonal therapy

The maintenance and survival of prostate luminal epithelial cells depend on the stimulation of the androgen receptor (AR), also referred to as NR3C4 (nuclear receptor subfamily 3, group C, member 4). Therefore, the initiation and progression of prostate cancer are reliant on the activation of AR. Testosterone, or its active metabolite dihydrotestosterone (DHT) predominantly binds to AR leading to its activation and nuclear translocation. The AR-DHT/testosterone complex regulates gene transcription which leads to cellular differentiation and proliferation. Androgenic blockade through its ligand binding domain, 5α-reductase (which converts testosterone to DHT) antagonists, and hypothalamic-pituitary-gonadal overstimulation *via* luteinizing hormone (LH) or gonadotropin-releasing hormone (GnRH) analogues can lead to epithelial cell apoptosis (Murray, 2021).

Androgen deprivation therapy (ADT) is universally accepted as a primary therapy for men with high-risk localized, or advanced PCa. Castration is achieved either via surgery or ADT drugs such as long-acting GnRH agonists (goserelin, histrelin, leuprolide, and triptorelin) or GnRH antagonists (degarelix). Patients who undergo castration therapy achieve reduced serum testosterone levels (< 50ng/dL) reduction in tumour burden and improved survival. However, despite attaining the castrate serum testosterone level, patients eventually develop clinical progression or new metastasis mostly to bone and lymph nodes. The risk of PCa-associated mortality is elevated in cases of castration-resistant prostate cancer (CRPC) (Desai, McManus, and Sharifi, 2021; Sekhoacha *et al*. 2022).

1.2.5. Chemotherapy

Chemotherapy uses anticancer drugs to lyse or restrain the growth of malignant cells. Taxane drug, Docetaxel has been proven to improve the clinical outcomes of patients with mCRPC. Taxanes induce apoptosis by inhibiting microtubule depolymerization, thereby suppressing mitotic cell division. Cabazitaxel is a novel antineoplastic semi-synthetic taxane used as second-line therapy to suppress docetaxel resistance. Increased upregulation of the P-glycoprotein-encoding multidrug resistance-1 gene has been linked to docetaxel resistance is

overcome by Cabazitaxel which has a low affinity for P-glycoprotein due to its additional methyl groups (Sekhoacha *et al*. 2022). Non-taxane chemotherapies used to treat PCa elicit non-specific cytotoxicity. Mitoxantrone is a type II topoisomerase inhibitor that interpolates into the DNA double helix, disrupting DNA synthesis and repair and inducing cell death (Quinn *et al*. 2017). Enzalutamide is an AR inhibitor that was accepted as one of the chemotherapeutic drugs for PCa in 2012. Enzalutamide targets the androgen pathway and induces apoptosis by; competitively inhibiting the binding of androgen to the AR, obstructing nuclear translocation and recruitment of cofactors, and hindering the binding of DNA with the activated AR (Sekhoacha *et al*. 2022).

1.3. Harnessing the immune system to treat PCa

The immune system has natural surveillance mechanisms to detect and eliminate the potential causes of infection and disease. Innate immune cells consist of NK cells, eosinophils, basophils, neutrophils, mast cells macrophages, dendritic cells (DCs), and monocytes generate the first line of defence whereas DCs further activate the adaptive immune system for antigen-specific prolonged immune defence. Adaptive immune system response initiates when the specialised phagocytic immature DC ingests a pathogen in the infected tissue. Uptake of foreign antigen activates/matures DCs, subsequently migrating to the lymph node (LN) via lymphatic vessels where they act as antigen-presenting cells (APC) to activate recirculating pathogen-specific naïve lymphocytes; B cells that generate humoral immune responses- and T-cells which are involved in cell-mediated immune responses. As a result, a more versatile means of defence is the complete removal of the pathogen, which also ensures increased protection against subsequent reinfection with the same pathogen. The immune system plays a crucial role in the surveillance against cancer (Zhang and Zhang, 2020; Rameshbabu *et al*. 2021).

1.3.1. Anti-tumour immune response

The cancer immunity cycle is a cascade of events which explains how the immune system recognises and lyses cancer cells. Neoantigens are released by oncogenesis which are taken

and processed by DCs simultaneously allowing DCs to mature by receiving suitable activation signals to redistribute the major histocompatibility complex (MHC) molecules to the cell surface from the intracellular endocytic compartment. The processed antigens are presented on MHC molecules, allowing DCs to migrate to the nearest lymphoid organs where naïve T-cells recognise the processed antigens, generating T-cell-mediated protective responses. T-cell activation and differentiation to perform different functions depend on many factors such as the interaction of T cell- APC surface receptors, involvement of co-stimulatory molecules, and the type of antigen presented (Mateusz Kciuk *et al*. 2023; Rameshbabu *et al*. 2021). Activated cytotoxic T-cells traffic and infiltrate into the tumour site by chemokine/cytokine gradients, interact with their cognate antigens and mediate direct tumour cell lysis. Lysed cancer cells subsequently release more antigens, starting a new round of the immune response cascade (Palaniyandi Muthukutty *et al*. 2023; Rameshbabu *et al*. 2021). A well-balanced cancer-immunity cycle, characterised by several stimulatory and inhibitory elements, modulates the immune response, and prevents the excessive response which could induce an autoimmune reaction.

Effective immune responses eradicate malignant cells, however, evolutionary changes in cancer cells developed multiple mechanisms to impede the effector function of immune cells and abrogate the antitumour immune responses. Those mechanisms include faulty antigen presentation, the upregulation of negative signalling pathways, and the recruitment of immunosuppressive cytokines and cell populations to the tumour site (Zhang and Zhang, 2020). Therefore, immunotherapy becomes less active in certain cancers due to the suppressive environment created by the tumour cells (Mateusz Kciuk *et al*. 2023). Immunotherapies that block immune checkpoints have shown unprecedented, sustained responses in certain cancers including melanoma and renal cancers. However, cancers like PCa, have shown limited responses against immunotherapy due to low tumour immunogenicity and other immune-suppressive factors present in the tumour microenvironment (TME). The immunosuppressive elements in TME allow tumour cells to evade the immune response and progress to an advanced stage of the disease. Thus, selecting the appropriate

immunotherapies will be aided by a better understanding of the complexity of PCa TME with its coexisting and interactive immune modulatory elements (Xu *et al*. 2022).

(A)

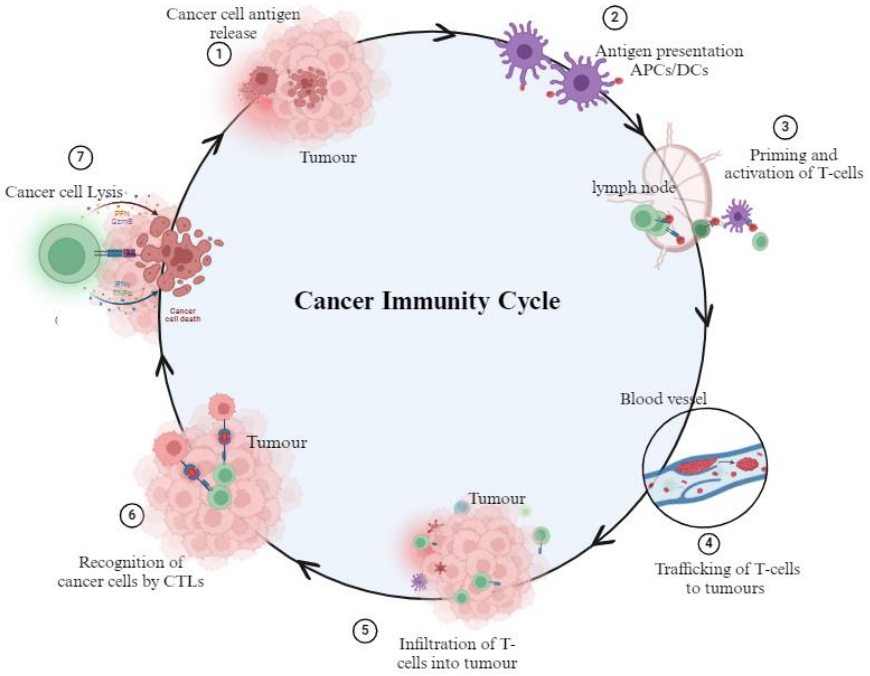

(B)

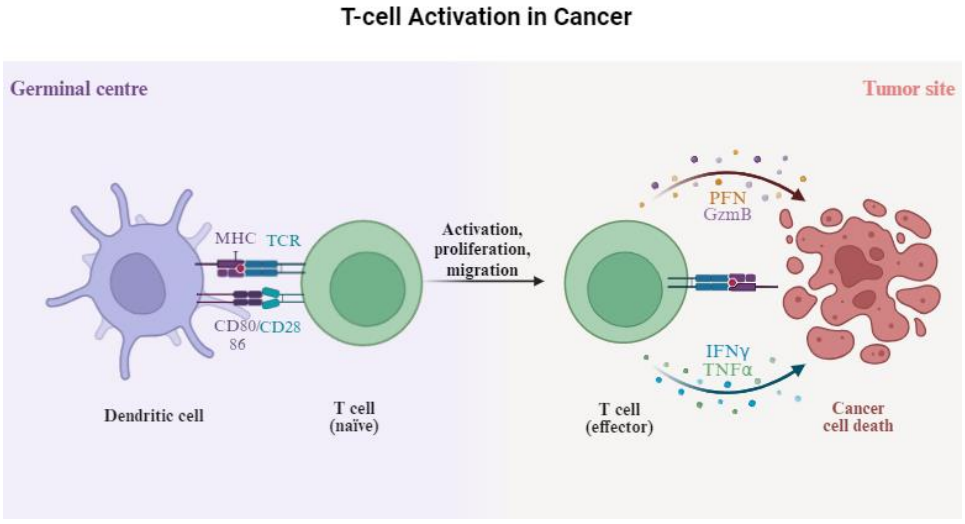

Figure1.2. (A) Cancer immunity cycle. (B) T-cell activation in cancer. *Dendritic cells present the antigen to be recognised by naïve T-cells leading to the activation of T-cells, which are then infiltrated into the tumour bed and interact with cognate antigens causing cancer cell lysis. More antigens are released by cancer cell lysis, initiating a new round of immune response cascade. The diagram is generated using biorender.com.*

1.3.2. PCa is a cold tumour.

Prostate cancer is immunologically considered a “cold” tumour with a low tumour mutation burden, low T-cell infiltration, and an immunosuppressive TME. In contrast to hot tumours, cold tumours are less likely to trigger an immune response or respond favourably to immunotherapy (Xu *et al.* 2022). Hot tumours have a high mutation load which causes them to generate specific molecules, neoantigens, on their cell surface. These neoantigens increase the tumour's susceptibility to being recognised by the immune system thereby eliciting a strong antitumour immune response. Most “hot" cancers react well to immunotherapy. Amongst the most common tumours are bladder cancer, non-small cell lung cancer, melanoma, liver cancer, kidney cancer, and head cancer. The immune properties of the tumour, the type and extent of immune cell infiltration into the TME and signalling pathways all influence how "hot" or "cold" the tumours are. The immune infiltration includes the presence of all immune cells within the TME but is not limited to T-cells, macrophages, bone marrow-derived suppressor cells (MDSCs), natural killer (NK) cells, mast cells, B cells, neutrophils, and DCs. Within the TME, some cell types may demonstrate pro-tumour and antitumour properties, for example, macrophages in the TME can differentiate into; M1 macrophages - which are linked to acute inflammatory and antitumour activity-, and M2 macrophages which are drawn in for pro-tumorous chronic inflammation. The TME of hot tumours is improved by a higher number of immune cells including T-cells, NK cells, and DCs, and fewer immunosuppressive factors. In contrast, immune cells like T-cells and NK cells are less prevalent in the TME of cold tumours. Most breast cancers, pancreatic cancer, ovarian cancer, glioblastomas, and PCa, are usually cold tumours (Wang *et al.* 2023; Wang *et al.* 2022).

1.3.3. Immune evasion in PCa

PCa evades destructive immune mechanisms by creating an immune-suppressive tumour microenvironment (Stultz and Fong, 2021) and a defective “cancer-immunity cycle” in the anti-tumour immune response. Any defect in the immunity cycle such as low expression of antigen-expressing molecules, low cytotoxic T-lymphocyte (CTL) recruitment and activation, impairment in antigen processing and presentation by APCs, or immunologic ignorance, due to

the lack of a danger signal may interfere with the antitumour responses generated (Bou-Dargham *et al*. 2020). The low mutational burden is associated with PCa, which could be the reason for developing reduced antigen expression. In addition to the low mutational burden, PCa is also associated with loss or reduction in the expression of MHC class I and II in antigen-presenting cells. Tumour infiltrating cytotoxic $CD8^+$ T-cells play a major role in recognising and lysing cancer cells; however, low levels of infiltrating T-cells are reported in PCa TME, which may contribute towards reduced T-cell mediated anticancer response (Xu *et al*. 2022). Moreover, most effector T-cells infiltrated have a dysfunctional phenotype or become exhausted due to the immunosuppressive signalling network within the TME. The immunosuppressive molecule indoleamine 2,3-dioxygenase (IDO), is produced by the malignant cells' constraint tryptophan accessibility and limits T-cell activity. The activation of immune checkpoint (For example: PD1, and CTLA-4) pathways ultimately inhibits the proliferation and activation of immune cells. The expression of suppressive ligand molecules has been associated with oncogenic mutations. Genomic abnormalities of the tumour suppressor gene Phosphatase and Tensin homolog deleted on chromosome 10 (*PTEN)* lead to loss of PTEN function ultimately leading to adverse oncological outcomes. In PCa, PTEN abnormalities are identified in ~20% of primary prostate tumours and as many as 50% in CRPC (Mateusz Kciuk *et al*. 2023). Other immunosuppressive factors like transforming growth factor beta (TGFβ), adenosine, IL-6, IL-8, IL-10, vascular endothelial growth factor (VEGF), and prostaglandin E2 in TME work together to evade the immune response in PCa (Stultz and Fong, 2021; Zhang *et al*. 2022).

1.3.4. The cellular component of PCa TME

PCa TME is composed of stromal cells such as cancer-associated fibroblasts (CAF), specialised mesenchymal cell types such as adipocytes and myogenic cells, mesenchymal stem cells, cancer cells, immune cells, neuronal cells, endothelial cells, extravasated blood cells and a variety of cytokines, growth factors, and extracellular matrix modulating agents (dos, Jerónimo and Correia, 2023). Stromal cells are phenotypically and genotypically altered with increased matrix remodelling to become reactive stroma which initiates during pre-malignant

prostatic intraepithelial neoplasia and co-evolves as cancer develops. CAFs are the main type of cells present in reactive stroma (Zhang *et al*. 2022). The immune compartment of the TME consists of tumour infiltrating lymphocytes (TILs) which include both positive regulatory immune cells such as DCs, T-cells, B-cells, and NK cells and negative regulatory immune cells such as tumour-associated macrophages (TAMs), regulatory T cells (Treg), MDSCs and tumour-associated neutrophils (TANs) (Wang *et al*. 2023; Messex and Liou, 2023).

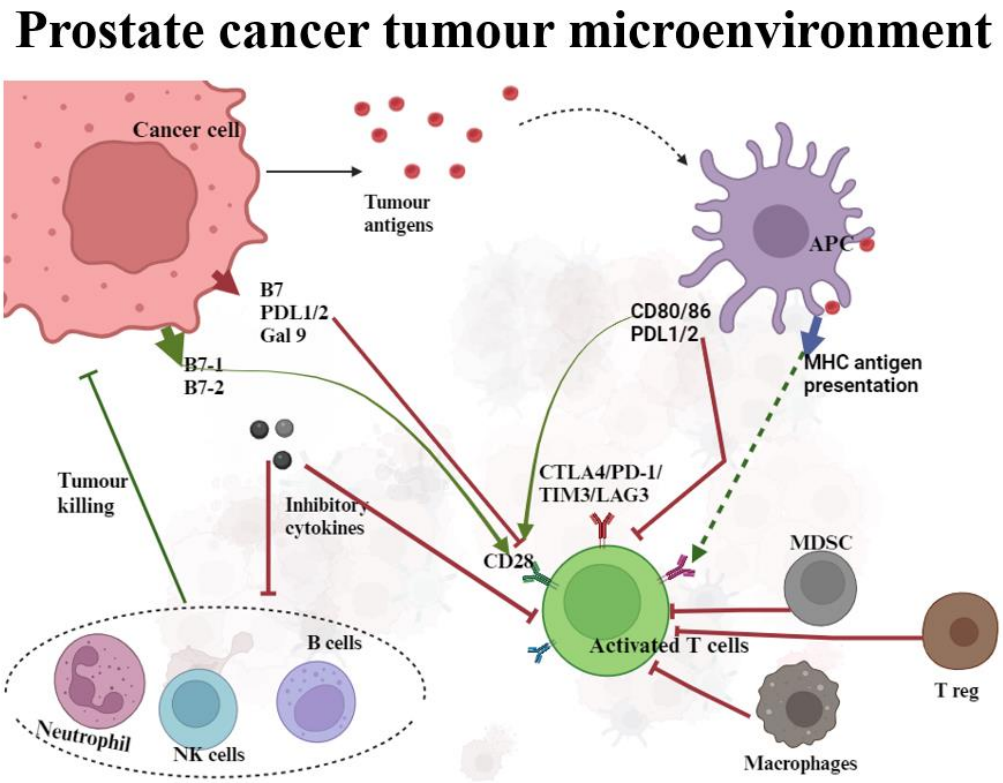

Figure 1.3. Cross-talks between immune and tumour cells in the tumour microenvironment. *Various anti-tumour immunities exist in the TME, including activated tumour-specific T-cells, NK cells, neutrophils, and B cells. Increased expression of immune checkpoint proteins on tumour cells (PDL1/2, B7-1/-2 and Gal9), the release of inhibitory cytokines, tumour-infiltrating Tregs, MDSCs and macrophages suppress the anti-tumour activity of cytotoxic T-lymphocytes. The Figure is created using https://www.biorender.com/.*

1.3.4.1. Immuno-stimulatory components of PCa TME

1.3.4.1.1. DCs

DCs are functional APCs critical for the initiation and orchestration of cellular and humoral immune response in an antigen-dependent manner, promote tolerance towards self-antigens, and maintain immunological homeostasis (dos, Jerónimo and Correia, 2023). DCs are divided into different subsets including monocyte derived DCs (moDCs), conventional DCs consisting of two subsets (cDC1 and cDC2), and plasmacytoid DCs(pDCs). cDC1s express the chemokine receptor XCR1 and the C-type lectin receptor and are specialised in the cross-presentation of exogenous antigens through MHC-I to $CD8^+$ T-cells. cDC2 express the signal regulatory protein CD172a and they present antigens via MHC-II to $CD4^+$ T-cells. pDCs are potent type I IFN producers and moDCs promote $CD4^+$ T cell polarization during inflammation. Though, each subset plays definite roles in antitumour immunity through activating different T-cell subsets and expressing costimulatory molecules and inflammatory cytokines cDCs1 employ potent anti-tumour functions through IL-12 induction and orchestrating $CD8^+$ T cell anti-tumour activity, by cross-presentation of antigen derived from necrotic and apoptotic tumour cells and induction of $CD4^+$ Th1 cells (Mateusz Kciuk *et al*. 2023). Nevertheless, these cells seemed to be fewer in number and immature or dysfunctional in PCa (Palano *et al*. 2022). The expression of chemokine receptor-7 (CCR7) is inhibited in PCa causing the impairment of chemotactic movement of DCs. Furthermore, PCa-derived exosomes induce CD73 expression on DCs, hindering Tumour Necrosis Factor (TNF)-α and IL-12 production, ultimately weakening $CD8^+$ T cell responses (dos, Jerónimo and Correia, 2023). It is also known that VEGF in PCa TME inhibits antigen presentation by DCs. Owing to the potential therapeutic applications of DCs, the FDA authorized Sipuleucel-T, the foremost DC therapy, in 2010 for the treatment of mCRPC (Palano *et al*. 2022).

1.3.4.1.2. Neutrophils

Neutrophils are the most prevalent circulating white blood cells and are involved in orchestrating the initial immune response at the site of inflammation. Owing to their short lifespan -less than 24 hours under physiological conditions-, they are constantly generated in

the bone marrow from granulocytes-monocytes progenitors. About 60% of bone marrow compartments are neutrophils and their precursors (Messex and Liou, 2023). The innate immune response of neutrophils against pathogens is released by producing reactive oxidative species (ROS), forming an extracellular trap, or releasing granules to engulf the pathogen. Besides the innate immune response, neutrophils also participate in the induction and regulation of adaptive immunity and act as APCs via direct interface with T and B cells. Freshly isolated human resting neutrophils have been found to express modest levels of MHC-II and co-stimulatory molecules and can present antigens to CD4 memory T-cells through HLA-DR (Li *et al*. 2019). There are mainly two subtypes of neutrophils: type 1 (N1) and type 2 (N2). The cytokines and chemokines released by neutrophil subtypes vary, which facilitates macrophage activation (Li *et al*. 2019). N1 subset promotes T-cell-mediated tumour elimination but pro-tumour N2-subsets function as immunosuppressive cells. Among the subtypes, the abundance of N2 neutrophils is associated with PCa TME. There is also evidence showing that the accumulation of pro-tumorigenic N2-neutrophils is driven by the increased levels of TGF-β at the tumour site. Conversely, in mouse models, the blockade of TGF-β has promoted the differentiation of N1 neutrophils with more chemokine/cytokine production and decreased arginine (Li *et al*. 2019). In PCa, the tumour-associated neutrophils influence angiogenesis which facilitates the tumour progression. Moreover, the neutrophil-induced strong expression of IL-6 and IL-6R in the PCa TME regulates STAT3 navigated immunosuppression (Messex and Liou, 2023; Palano *et al*. 2022).

Granulocytic MDSCs (G-MDSC) share many biological and clinical features associated with the N2-subset of neutrophils. Like G-MDSCs, N2-neutrophils are associated with different mechanisms involved in tumour progression by facilitating tumour angiogenesis, neoplastic endothelial to mesenchymal transition, and development of the pre-metastatic niche. Under chronic inflammation and stress conditions, suppressive monocytic Myeloid-Derived Suppressor Cells (M-MDSCs) can convert into suppressive neutrophil-like cells or G-MDSCs by the downregulation of tumour suppressor protein retinoblastoma-1. G-MDSCs can be differentiated from $Ly6G^+$ neutrophils by the lower expression of CD11b (CD11b is highly positive in $Ly6G^+$ neutrophils) and expression of CD115 as well as the CD244 markers.

Neutrophils are also phenotypically differentiated by the expression of intracellular markers such as LAMP2 and retinoblastoma-1 which are absent in G-MDSCs (Zilio and Serafini, 2016).

1.3.4.1.2. B cells

B cells are an important element of the adaptive immune system directly eliminating the pathogen by secreting antigen-specific antibodies to cover the outside of the pathogen, effectively neutralizing it (Messex and Liou, 2023). Naive B cells are activated through the interaction of antigens with B cell receptors and differentiate into follicular B cells, regulatory B cells, or memory B cells depending on the function they are entitled to (Zhang *et al.* 2023). The memory B cells generated will provide a rapid and effective antibody response against the same pathogen upon reinfection. Apart from the antibody-mediated immune response, B cells can act as antigen-presenting cells. Antigenic peptide-loaded B cells interact directly with CD4/CD8 T-cells to induce cell-mediated immune response. Additionally, B cells may encounter soluble antigens in the lymphatic fluid that travel to the follicles via the subcapsular sinus and then cross-present them to T cells (Rastogi *et al*. 2022). It has been revealed that B cell density was substantially higher in PCa than in the normal prostate areas. A study with the cohort analysis demonstrated that B cell infiltration in the prostate cancer region was more abundant with “improved recurrence-free survival” indicating the prognostic role of B cells in PCa (Messex and Liou, 2023). However, there was an increased population of IL-10-producing subset of B cells (regulatory B cells) has been identified in both murine and human cancers. Regulatory B cells in the TME suppress the T-cell mediated immunity by secreting cytokines such as IL-10 and IL-35 (Zhang *et al*. 2023) and can also differentiate CD4 T-cells to its immunosuppressive Treg subset which will result in poor prognosis (Rastogi *et al*. 2022).

1.3.4.1.4. Natural killer (NK) cells

Natural killer cells are large granular cytotoxic lymphocytes that are part of the innate immune system and can destroy malignant and virally infected cells. NK cells are non-antigen-specific innate immune cells. Unlike cytotoxic CD8 T-cells, NK cells do not require any antigen presentation by APCs and sufficient costimulatory molecules to prime their activity, rather they

induce pathogen apoptosis *via* exocytosis of cytolytic granules containing perforin and granzyme-B proteins. In addition to the first line of defence against pathogens, NK cells also contribute to the adaptive immune system by facilitating DC maturation through the production of cytokines such as interferon (IFN)-γ and Granulocyte-macrophage colony-stimulating factor (GM-CSF). They also release chemokines and effector cytokines such as IFN-γ and tumour necrosis factor (TNF)-α, needed for the recruitment of other immune cells (Wu, 2021). In PCa, the frequency of circulating NK cells is significantly lower than in healthy controls which is further reduced in metastatic disease PCa. The CD57 marker of NK cell maturation is expressed remarkably low on PCa-infiltrated NK cells compared to the circulating ones (Palano *et al*. 2022). A study reported that NK cells exposed to various PCa cell lines presented increased exhaustion markers Programmed cell death-1 (PD-1) and T-cell immunoglobulin and mucin domain 3 (TIM-3) expression, impaired degranulation capability, and decreased TNF-α, IFN-γ and Granzyme-B production (dos, Jerónimo, and Correia, 2023). Pasero *et al* (2015) found similar results while analysing the NK cell cytolytic capabilities and their surface receptors in 39 metastatic PCa patients compared to healthy individuals. The study has reported the high expression of NK-cell-activating receptors NKp46, NKG2D, and DNAM-1 on circulating NK cells. However, the NK cells infiltrated into the tumour site showed a loss of cytotoxic potential evidenced by the downregulation of activating receptor NKp46 and NKG2D, and high expression of the inhibitory surface receptor ILT2 (Pasero *et al*. 2015).

1.3.4.1.5. T-cells

T-lymphocytes are the major component of cell-mediated immunity. They originate from hematopoietic stem cells in the bone marrow and migrate to the thymus for maturation, selection, and succeeding exportation to the periphery. In the thymus, T-cells mature to express $CD4^+$ and $CD8^+$ co-receptors and undergo T-cell receptor (TCR) reorganisation to generate $CD4^+CD8^+$ double-positive thymocytes. Selection of double-positive cells results in $CD4^+$ or $CD8^+$ single-positive thymocytes, which eventually become naïve T-cells with $CD45RA^+CCR7^+$ phenotypes and emerge into the periphery and secondary lymphoid tissues-spleen and lung (Kumar, Connors, and Farber, 2018).

αβ T -cells and γδ T-cells are the two populations of T lymphocytes that are differentiated by the expression of αβ TCR or γδ TCR, respectively. Both αβ and γδ TCRs comprise two antigen-binding subunits either form the TCR-α/TCR-β heterodimer or the TCR-γ/TCR-δ heterodimer in addition to the proteins of the CD3 complex. CD4 and CD8 expression is absent in most γδ T-cells and thus does not recognise MHC molecules. Agonistic ligands for γδ TCRs include soluble proteins and small peptides, non-MHC cell surface molecules, and lipid-presenting/ stress-induced MHC-like molecules. On the other hand, foreign or mutated peptides displayed on MHC molecules function as ligands for αβ TCRs. Peptides presented by MHC class II are recognized by $CD4^+$ T cells, while peptides presented by MHC class I are recognized by $CD8^+$ T-cells. Invariant NK T-cells, a rare αβ TCR subset recognise lipids exhibited on the MHC-related CD1 molecule. γδ T-cells are less common in secondary lymphoid organs but are enriched in many peripheral tissues, such as the skin, intestines, and lungs, where they contribute to immune responses. IFNγ producing γδ T-cells and IL-17 producing γδ T (γδ17) cells are the two main subsets of γδ T-cells (Morath and Schamel, 2020).

T-cell activation through MHC-mediated antigen presentation

To produce T-cell-mediated immune defence, naïve T-cells must be activated via well-coordinated interactions between multiple molecules on the T cell and an APC. The TCR is composed of α and β chains and recognises the peptide antigen which is bound to an appropriate class I or class II MHC. TCR ligate with membrane protein complex CD3 (composed of γ-, δ-, ε-, and ζ-subunits), and transmits the intracellular signal for T-cell stimulation. The CD8 or CD4 co-receptor binds to MHC class I or class II on APC, further stabilises the interaction between the T-cell and APC and, undergoes membrane reorganization which facilitates the formation of the immunological synapse (Pennock *et al*. 2013; Koh *et al*. 2023). Co-stimulatory and /or adhesion molecules are recruited to the site of TCR- MHC interaction and a cascade of events including phosphorylation of CD3 component, ζ-chain-associated protein kinase-70 recruitment and ultimately leads to strong IL-2 production to enhance T-cell activation. T-cell stimulation with its cognate antigen alone doesn't fully activate T-cells

instead results in a T-cell hyporesponsive state known as anergy. Consequently, co-stimulatory molecules such as CD28 expressed on the T-cell surface provide co-stimulatory signals for further stimulation. T-cells also express inhibitory receptors including Cytotoxic T-lymphocyte antigen-4 (CTLA-4), programmed cell death-1, lymphocyte activation gene 3 (LAG-3), and V-domain Ig suppressor of T-cell activation, which act to both restrain costimulatory signalling as well as co-stimulatory molecule ligation (Koh *et al*. 2023).

T-cell differentiation

Antigen-stimulated T-cells are genetically programmed into a range of potential subsets that possess effector mechanisms suitable for eliminating the pathogen in response to the inflammatory cytokines generated by the interaction of pathogens and pattern recognition receptors (PRR). T-cell-based immune responses are categorised mainly as the generation of "helper" T-cells (CD4 T-cells) and the generation of "cytotoxic" T-cells (CD8 T-cells) (Jameson and Masopust, 2018). CD4 and CD8 T-cells differentiate into these by specific cytokines generated upon the pathogen-PRR interaction. For example, CD4 T-cell is differentiated into its subset Th-1 by IL-12 and IFN-γ and subset Th-2 by IL-4. Major T helper subsets are Th1, Th2, Th17, Th9, T22, Tfh, and Tregs. Each Th subset releases certain cytokines which may have pro- or anti-inflammatory, survival, or protective properties. For instance, Th1 releases IFN-γ and TNF-α while Th2 releases IL-4. Likewise, CD8 T-cell subsets include Tc1, Tc2 c, Tc9, Tc17, Tc22, Tfc, and suppressive Tregs (Koh *et al*. 2023). The subtypes of CD8 and CD4 T cells, and their functional cytokine released are illustrated in Figure 1.5.

As the name implies, CD4 T helper cells take a supportive role to activate neighbouring immune cells to perform their specific functions or recruit new immune cell subsets to sites of pathogen encounter by generating cytokines and chemokines (Jameson and Masopust, 2018). Cytolytic CD4 T-cells directly eliminate cancer cells expressing MHC class II molecules and improve anti-tumor immunity through cytokine production, which induces tumour cell senescence and tumor vasculature destruction (Oh and Fong, 2021; Cenerenti *et al*. 2022). While CD8 T-cells also generate cytokines, they function mainly to induce cytotoxicity for the elimination of

tumour cells. CD8 T-cells differentiate into cytotoxic T-cells when they identify their antigens in the presence of IFN-α/β and IL-12 cytokines. Cytotoxic T-cells exert their cytotoxicity by strong induction of IFN-γ and TNF-α. They also directly lyse the cells by generating large amounts of secretory vesicles which contain perforin and granzyme protein which is released near target cells (Golubovskaya and Wu, 2016; Koh *et al.* 2023).

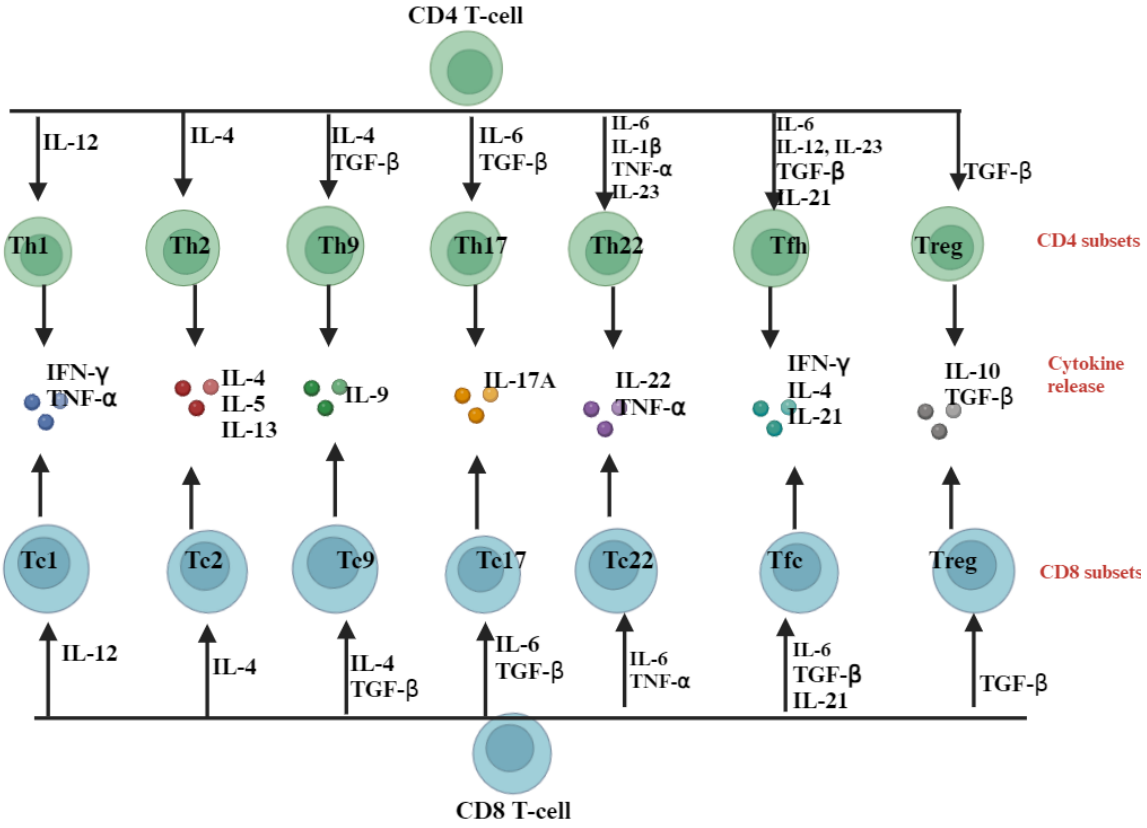

Figure 1.4. Subsets of CD4 and CD8 T-cells. *CD4/CD8 T-cells differentiate into each of its subsets under the influence of cytokines that are generated upon pathogen-PPR interaction. Each subsets release different cytokines to play diverse roles in diseases. For example, CD8 T-cells, differentiate into their subset Tc1 under the influence of IL-12 and subset Tc2 by IL-4. Tc1 cells release IFN-γ and TNF-α and are known for their cytotoxic capabilities against infected/malignant cells, while Tc2 is mainly involved in allergic diseases and they release IL-4, IL-5 and IL,13 (Koh et al. 2023). The Figure is generated using https://www.biorender.com/.*

T-Cell Memory

Complete activation of T-cells requires mainly three signals: interaction of antigenic peptide–MHC complex with TCR, costimulatory or co-inhibitory signal, and stimulation by extracellular

cytokines such as IL-2. The T-cell response usually reaches its maximum of approximately 7–15 days following the first antigen stimulation to eliminate the pathogen. Following days, 90-95% of them die off, leaving behind heterogeneous subsets of memory T-cells with a range of phenotypes, and self-renewal capabilities (Kumar, Connors, and Farber, 2018). Memory T-cells are activated *via* antigenic and co-stimulatory receptors on subsequent re-infection and generate a more rapid in situ response. There are mainly two subclasses of memory cells for both CD4 and CD8 T-cells: effector-memory (T_{EM}) and central-memory (T_{CM}) T-cells. T_{CM} cells are characterized by their high expression of the IL-7 receptor (CD127), high levels of adhesion markers such as CD44 and CD62L, low levels of the surface marker killer cell lectin-like receptor subfamily G member-1 (KLRG-1), and high levels of the chemokine/homing receptor C-C chemokine receptor type 7 (CCR7). These cells have enhanced potential for proliferation following antigen re-exposure. In contrast, T_{EM} cells express low levels of CD62L, low levels of CD127, high levels of KLRG-1, and are CCR7 deficient. T_{EM} cells exhibit swift effector function (granzyme B and IFN-γ production) but have limited proliferative capabilities.

T_{CM} cells localise in secondary lymphoid tissues, whereas T_{EM} cells localise in lymphoid and peripheral tissues. T_{EM} cells preferentially traffic through nonlymphoid tissues and they have enhanced cytolytic capacity, which makes them the first defence at the peripheral re-infection site. T_{EM} effector memory cells display an instantaneous, but not sustained, defence upon antigen re-exposure whereas, T_{CM} cells sustain the response by proliferating in the secondary lymphoid organs and creating a new round of effector T-cells, eventually endorsing the ultimate elimination of the pathogen. Subsets of memory cells are long-lived, have a half-life of approximately 8 to 15 years, and once formed, they can live for decades keeping the memory of the antigen encounter (Pennock *et al*. 2013).

Stem cell-like memory T-cells represent a newly identified subset of memory T cells, arise from asymmetric T lymphocyte division (Yi and Li, 2022) characterized by exceptional longevity, self-renewal capability, and rapid differentiation into T_{CM} and T_{EM} cells. These cells, which can persist for over a decade, play a crucial role in sustaining long-term immune memory and ensuring a rapid and efficient immune response to previously encountered pathogens or antigens (Wang, Cheng and Zheng, 2022; Wang *et al*. 2021). In humans, these cells are

identified by surface markers such as $CD45RA^+$, $CD62L^+$, $CCR7^+$, $CD95^+$, and while in mice, they are marked by $CD44^-$, $CD62L^+$ (Wang *et al*. 2021).

T-cell tolerance

Even though T-cells are the primary regulators of adaptive immune responses, immunopathology can result from persistent or exaggerated immune responses. To effectively eliminate foreign antigens and maintain immune tolerance to self-antigens to prevent autoimmunity, host immune systems typically regulate T-cell activation and tolerance. Immune tolerance is the condition of T-cell unresponsiveness of the immune system to self-antigens. Tolerance is primarily induced by the negative selection leading to the deletion of self-reactive T-cells in the thymus. Peripheral tolerance is maintained by anergy, apoptosis, or through the production of Tregs (Nurieva, Wang and Sahoo, 2013). Anergy is a functional inactive state where T-cells remain unresponsive after the antigen encounter due to the absence of co-stimulation. Nonetheless, Tregs, a regulatory subset of T-cells that inhibits a range of inflammatory processes, mediate dominant tolerance. Natural Tregs are generated through thymic selection, while induced Tregs are produced when they differentiate in response to peripheral stimuli like TGF-β and retinoic acid. Both natural and induced Tregs have suppressive activity through the expression of transcription factor forkhead box P3 (FoxP3) (Pennock *et al*. 2013).

In PCa, the TME aids T-cell tolerance, and the presence of Tregs promotes uncontrolled tumour growth. Moreover, it has been discovered that elevated expression of many negative co-stimulatory molecules which are either expressed by APCs, and tumour cells, such as PD-1 ligand 1, B7-S1 or B7-H3, or by activated T- cells, such as CTLA-4, PD-1, regulates immune tolerance and tumour evasion (Nurieva, Wang and Sahoo, 2013). The inhibitory immune checkpoint CTLA-4 is a CD28 homolog for B7-1(CD80) and B7-2 (CD86) molecules present on APC. CD28 binding to B7 molecules generates a co-stimulatory signal whereas the CTLA-4 to B7 generates an inhibitory signal. PD-1 suppress the T-cell activation by binding to its ligands PD-L1 and PD-L2. CTLA-4 inhibits T-cell proliferation primarily in the LN while PD-1 ligands are

expressed in peripheral tissues thus PD-1 interaction with PD-L1 and PD-L2 is thought to maintain the tolerance within the locally infiltrated tissues. Both PD1- and CLTA-4 inhibitory pathways inhibit IFN-γ, TNF-α, and IL-2 production (Stultz and Fong, 2021).

T-cell exhaustion

T-cells are the major type of lymphocyte that infiltrate into the tumour bed. Better clinical outcomes have been linked to higher numbers of infiltrating $CD8^+$ T-cells in the tumour epithelium; however, PCa is a cold tumour with insufficient T-cell infiltration (Zhang *et al*. 2022). The infiltrated T-cells are functionally inactivated due to being highly exhausted. T-cell exhaustion is a state of T-cell dysfunction in a chronic environment, usually occurring with malignancies or chronic infection which causes the immune system to stay active for a prolonged time. Consistent T-cell exposure to antigens, immune checkpoints and their ligands expression, and suppression of T-cell function by IL-10, TGF-β, and other inhibitory cytokines in the tumour site are the associated factors that lead to T-cell exhaustion. T-cell exhaustion in TME is also influenced by the synthesis of metabolites such as adenosine, prostaglandins, and lactic acid, as well as physiological changes in the TME such as hypoxia, low pH, and deprivation of nutrients like glucose or amino acids. Exhausted T-cells express high levels of inhibitory receptors, such as band T lymphocyte attenuator, PD-1, LAG-3, TIM-3, and CTLA-4. The loss of function of exhausted T-cells is described as the loss of IL-2 production and *ex vivo* killing ability at the early stage of exhaustion, loss of TNF-*α* production at the intermediate stage, and loss of IFN-*γ* and granzyme B production at the advanced stage of exhaustion (Jiang, Li, and Zhu, 2015). IL-2 is essential for T-cell survival and function, with Tregs being highly reliant on IL-2 for their activity. Tregs express high levels of the IL-2 receptor, which empowers them to compete with T-cells for IL-2, potentially limiting the expansion and survival of effector T-cells. This competition highlights the crucial role of IL-2 consumption by Tregs in their suppressive functions (Höfer, Krichevsky and Altan-Bonnet, 2012; Chinen *et al*. 2016).

Most T-cells in TME differentiate into exhausted T-cells expressing high levels of inhibitory receptors, producing fewer effector cytokines, and showing cytotoxic functional loss. Severely exhausted T-cells are cleared in the TME resulting in defective T-cell memory formation. Altered expression of transcriptional factors and surface expression markers are observed in

exhausted T-cells compared to the effector T-cells (Jiang, Li, and Zhu, 2015). T-cell antitumour activity and exhaustion are also regulated depending on their surface receptor interactive capabilities. The interaction of T-cell-specific surface glycoprotein CD28 with CD80/86 present on APCs will lead to the promotion of antitumour T-cell response. However, immune checkpoints on T-cells such as cytotoxic T-lymphocyte protein 4 (CTLA-4) interact with CD80/86 to suppress T-cell activation, proliferation, and cytokine synthesis. Likewise, PD-1 receptor on T cells interaction with programmed cell death ligand 1 (PD-L1) expressed on the surface of APCs, tumour cells, will lead to the suppression of T-cell activity and enhance the formation of Tregs (Mateusz Kciuk *et al*. 2023).

A study conducted by Ness et al. (2014) to evaluate the prognostic impact of adaptive immune cells residing in different tumour compartments in prostate cancer using tissue microarrays constructed from viable and representative tumour epithelial and stromal areas of primary PC tumours from 535 patients found out that, a high density of $CD8^+$ lymphocytes, especially in tumour epithelial areas, is an independent negative prognostic factor for biochemical failure-free survival. The failure of high levels of $CD8^+$ T-cells to reduce disease recurrence may be due to T-cell exhaustion, and associated expression of PD-1. Conversely, the study conducted by (Vicier *et al*. 2020) to determine the association between $CD8^+$ T-cells and PD-L1 expression in localised PCa, biochemical recurrence, and metastasis-free survival, has concluded that the presence of elevated $CD8^+$ T-cells and lower PDL-1 expression in prostatectomy was linked with low risk of biochemical relapse and metastatic disease. Ntala *et al* (2021) explored the tumour-infiltrating immune cells as a possible prognostic tool for regional LN metastasis and discovered that decreased T-cell infiltrates especially CD4 effector cells in the primary tumour are associated with a higher risk of LN metastasis.

1.3.4.2. Immunosuppressive elements on PCa TME

1.3.4.2.1. Cancer-associated fibroblasts (CAFs)

Fibroblasts are cells primarily derived from the mesenchyme and are the main component of extracellular matrix elements during normal development and physiology. CAFs are generated

from the local fibroblasts of the pre-neoplastic lesion and TME-recruited mesenchymal stem cells or adipocytes from bone marrow. CAFs share distinct properties from normal fibroblasts due to their involvement in tumorigenesis by creating a 'reactive stroma' (Bonollo et al. 2020). Smooth muscle cells and CAFs account for most of the stromal cell population in PCa and mCRPC (Li *et al*. 2023). CAFs are the most prevalent cell type within the stromal compartment of TME, and they are known to promote tumorigenesis and progression to mCRPC, mainly through crosstalk between fibroblasts and neighbouring PCa cells (Stultz and Fong, 2021). Crosstalk between cancer cells and stromal components is established by a variety of signalling factors, including growth factors, chemokines, and cytokines (Bonollo *et al*. 2020). Different from normal fibroblasts, CAFs upregulate, fibroblast activating protein, FN1, POSTN as well as C-X-C motif chemokine (CXCL)-12 which code for stromal proteins and are regarded as CAF markers. The platelet-derived growth factor receptor-β, fibroblast-specific protein-1, and α-smooth actin expressed by CAFs facilitate its function in tumorigenesis, invasion, and metastasis. CAFs release VEGF, IL-6, IL-8, TGFβ, fibroblast growth factors, matrix metalloproteinases, hepatocyte growth factor, and growth differentiation factor-15. CAFs remodel the extracellular matrix and promote tumour invasion by introducing epithelial-to-mesenchymal transition through the release of matrix metalloproteinases and extracellular vehicles. Enhanced IL-6 secretion by CAFs causes androgen-independent progression of PCa through the PI3K-AKT, STAT3, and MAPK/ERK pathways (Li *et al*. 2023; Stultz and Fong, 2021). *In vitro* and *in vivo* studies have shown that CAFs promote the growth of low tumorigenic prostate adenocarcinoma cells, castration resistance, and ultimately bone metastasis (Bonollo *et al*. 2020).

1.3.4.2.2. Regulatory T-cells (Tregs)

Tregs are regarded as one of the predominant cell types sensible for the generation and maintenance of an immunosuppressive TME (Stultz and Fong, 2021). The recruitment of Tregs in the TME is regulated by cytokines such as VEGF, TGF-β, and IL-10 (Zhang *et al*. 2022).

Tregs employ immunosuppressive effects through distinct mechanisms. They directly attenuate the immune response through the production of immunosuppressive cytokines such

as TGF-β and IL-10. They can induce immune cell apoptosis by secreting perforin/granzyme B or inhibit the proliferation of T cells and can induce T-cell lysis through Galectin-1. Tregs depend on IL-2 for their suppressive role, which is vital for T-cell survival and function. With high IL-2 receptor expression, Tregs compete with other T cells for IL-2, limiting effector T cell growth and maintaining immune tolerance (Höfer, Krichevsky and Altan-Bonnet, 2012; Chinen *et al*. 2016). Furthermore, CTLA-4 expressed on Tregs can bind to CD80 and CD86 on DCs and alter their antigen-presenting capabilities. Tregs promote tumour angiogenesis, downregulate NK cells and CTLs infiltration, and support MDSCs and M2 macrophages (Xu *et al*. 2022). The activation of Tregs attenuates antitumour immune responses via contact- and cytokine-dependent suppression of antitumour cytotoxic T-cells, NK cells, DCs, and neutrophils. Both $CD8^+$ and $CD4^+$ subsets of Tregs possess potent immunosuppressive properties, including suppression of CTL proliferation and activation (Stultz and Fong, 2021). There is an enhanced accumulation of FoxP3 together with inhibitory molecules such as PD-1, CTLA-4, LAG-3, and TIM-3 are identified with tumour-infiltrating Tregs which in turn promote tumorigenesis (Long et al. 2018). High levels of $FoxP3^+$ Tregs in PCa tumour and peripheral blood samples are associated with a higher risk of metastatic disease. Therapies targeting Tregs such as the combination of anti-CTLA-4 antibody and anti-CD25 antibody have been demonstrated to significantly inhibit tumour growth and progression *in vivo* (Xu *et al*. 2022).

1.3.4.2.3. MDSCs

MDSCs are a heterogeneous population of cells originating from bone marrow, phenotypically like monocytes and neutrophils, and are associated with chronic infection and malignancies. MDSCs are generated from common myeloid progenitors that arise under pathological conditions such as autoimmune diseases, chronic infection, excessive inflammation, and cancer. These heterogenous immature myeloid cells are phenotypically different – have alteration in the surface markers- and functionally different -Immunosuppressive in nature- from normal myeloid cells (Millrud, Bergenfelz and Leandersson, 2017). Granulocytic/polymorphonuclear MDSCs (G-MDSCs or PMN-MDSCs) and monocytic MDSCs (M-MDSCs) are the two main subgroups of MDSCs found in both humans and mice. These

subgroups are categorized based on whether they originated from the granulocytic or monocytic myeloid cell lineages, respectively. Human M-MDSCs are primarily identified as $CD11b^{+}CD14^{+}CD33^{+}HLA\text{-}DR^{low/neg,}$ while G-MDSCs are characterized as CD11b+ $CD15^{+}HLA\text{-}DR^{low}CD66b^{+}$. However, the mouse counterparts for M-MDSC and G-MDSC are described as $CD11b^{+}Ly6C^{+}$ and $CD11b+Ly6G^{+}$ $Ly6C^{low}$ respectively (Veglia, Sanseviero and Gabrilovich, 2021; Hegde, Leader and Mérad, 2021). MDSCs function to inhibit DC maturation, T-cells, B cells and NK cells mediated immune responses, and promote the expansion of Tregs in cancer (Koinis *et al*. 2022; Veglia, Sanseviero and Gabrilovich, 2021).

M-MDSCs and PMN-MDSCs mediated immune suppression often includes either one or more of the following mechanisms: upregulation of STAT3, induction of endoplasmic reticulum stress, and upregulation of arginase-1. PMN-MDSCs preferentially synthesise reactive oxygen species (ROS), peroxynitrite, arginase-1, and prostaglandin E_2, whereas M-MDSCs use nitric oxide, production of immunosuppressive cytokines such as IL-10 and TGFβ, and immune regulatory molecules like PD-L1 upregulation to mediate immune suppression (Veglia, Sanseviero and Gabrilovich, 2021). Upregulation of arginase-1 depletes arginine, which is essential for the expression of the TCR zeta-chain and the pairing of TCR-mediated antigen recognition to different signal transduction pathways (Cassetta *et al*. 2019). Like arginine, deprivation of other essential metabolites such as tryptophan and cysteine by MDSCs from the microenvironment induces T-cell suppressive mechanisms (Veglia, Sanseviero and Gabrilovich, 2021). Production of nitric oxide through activation of inducible nitric oxide synthase causes the nitration of T-cell receptors and chemokines which are important for T-cell migration. Increased PD-L1 ligand can interact with PD-1 leading to immune tolerance (Cassetta *et al*. 2019; Koinis *et al*. 2022).

MDSCs are recruited to the premetastatic niches primarily through the chemokine receptors CXCR2 and CXCR4 (Veglia, Sanseviero and Gabrilovich, 2021). The increased levels of MDSCs in the TME have been associated with disease progression and reduced prognosis in PCa (Xu *et al*. 2022). MDSCs induce immunosuppression and facilitate immune escape through upregulation of indoleamine 2,3-dioxygenase and arginase-1 which leads to the depletion of

tryptophan and arginine from the TME. Which ultimately leads to the suppression of T-cell, cell-cycle arrest, reduced T-cell receptor zeta chains expression, and downregulation of MHC class II molecules on APCs. A higher level of tumour infiltrating MDSCs was found in PCa tumour samples. Simultaneously, PCa progression in mouse models was markedly delayed by the inhibition of MDSC recruitment and its infiltration into PCa tumours (Stultz and Fong, 2021; Zhang *et al*. 2022).

1.3.4.2.4. Tumour-associated Macrophages (TAMs)

Macrophages are immunocytes, that perform a wide range of functions including defence against pathogens, tissue homeostasis modulation, and wound healing. These phagocytic cells ingest pathogens in a nonspecific manner and present exogenous antigens on their surface MHC-I molecules to direct a more definite response from other immune cells in the adaptive immune system. Although macrophages mediate immune responses, they also can cause cancer progression and metastasis in multiple ways including increased cellular migration, invasion, and epithelial-mesenchymal transition (EMT) (Messex and Liou, 2023). TAMs are the most abundant myeloid cells within the prostate TME. TAMs play a crucial role in the TME, influencing aspects such as tumour growth, angiogenesis, immune regulation, metastasis, and chemoresistance (Lin, Xu, and Lan, 2019). Macrophage recruitment and infiltration into PCa tumours are facilitated mainly through CC chemokine ligand 2 (CCL2) in response to tumour-derived parathyroid hormone-related protein. Compared to primary tumours, mCRPC, nodules have been found to have a higher proportion of TAMs. Besides, *in vitro,* and *in vivo* studies have demonstrated that CCL2-mediated signalling inhibition via antibodies significantly reduced the proportion of TAMs present in the TME and reduced the bone metastases development of localised PCa (Stultz and Fong, 2021). TAMs can be stratified into two distinct subpopulations, based on their phenotype: M1-like macrophages ($CD163^{-}CD206^{-}$) and M2-like macrophages ($CD163^{+}CD206^{+}$). M1-like macrophages are linked to increased tumour infiltration of cytotoxic and type-1 helper T-cells, as well as pro-inflammatory activities while M2-like macrophages demonstrate the lack of effective T-cell function and tumour progression (Wang *et al*. 2023; Stultz and Fong, 2021). Studies evidence the abundance of M2-like TAMs in both epithelial and stromal compartments, is associated

with tumour aggressiveness and insignificant patient outcomes (Stultz and Fong, 2021; Zhang *et al*. 2022). M2-like TAMs enhance bone metastasis by invoking NF-κB and STAT2 signals and inducing CXCL5 secretion (Li *et al*. 2023). Furthermore, PCa patients with higher Gleason scores, serum PSA and biochemical recurrence have demonstrated a higher M2-phenotyped TAM density (dos, Jerónimo and Correia, 2023).

1.3.4.2.5. Nerve cells

The prostate gland neural compartment originates from the sympathetic neurons of the hypogastric nerve and parasympathetic neurons from the pelvic nerve. The neuronal progenitors also travel through the bloodstream from the brain subventricular zone to the PCa TME, where they differentiate into new adrenergic neurons. Apart from their involvement in angiogenesis, nerve cells also function to transmit pro-inflammatory signals to the central nervous system, to generate neuromediators-influenced immune response primarily through the β-adrenergic pathway (Sejda *et al*. 2020). PCa cells spread along the nerve through a process known as perineural invasion (PNI) is an eminent mechanism for cancer progression. During the process of PNI, cancer cells closely interact with the nerve components in the TME and create the perineural niche, which comprises neurons, endothelial cells, chemoattractants, neurotransmitters, immune cells, and extracellular matrix. The perineural niche provides a supportive environment for the survival and invasion of malignant cells. PCa cells within the PNI lesions are associated with increased proliferative factors Ki-67, EGFR, and VEGF (Niu, Förster and Muders, 2022).

In contrast to the adrenergic fibers from the sympathetic system (β2- and β3-adrenergic receptors) involvement in PCa development, invasion, and metastasis of PCa cells are empowered by the influence of cholinergic fibers from the parasympathetic nervous system through the Chrm1 cholinergic receptor on cancer cells. A pre-clinical study by Magnon *et al* (2013) showed that involvement of the sympathetic adrenergic nerve was significant in the early phases of tumour development in mice bearing PC-3 PCa xenografts and double knockout of β2- and β3-adrenergic receptors in PCa mouse models significantly reduced the tumour development. Moreover, a quantitative confocal microscopy analysis of radical prostatectomy

samples from low-risk or high-risk PCa patients showed that high-risk tumours had higher overall nerve densities than low-risk tumours with infiltration of cholinergic fibers in the tumour tissues. High nerve densities were associated with increased preoperative levels of PSA and biochemical recurrence (Magnon *et al*. 2013). Furthermore, Helene Hartvedt Grytli *et al* (2014) assessed the association between β-blockers and PCa-specific mortality by gathering clinical information of 3561 high-risk PCa patients from the Cancer Registry of Norway and Norwegian Prescription Database between 2004 to 2011. This study reported that β-blocker consumption was linked with reduced PCa-specific mortality which correlates with the involvement of adrenergic fibers of the sympathetic nervous system in the PCa growth (Helene Hartvedt Grytli *et al*. 2014).

The neurons in PCa TME impact the tumour progression by modulating the immune system and reducing the anti-tumor response. PD-L1 expressed in PCa-associated nerves can negatively affect the $CD8^+$ tumor-associated lymphocytes. A study conducted by Mo *et al* (2019) to identify PD-L1-specific expression in prostatic stromal nerve cells and analyse the effect of response to anti-PD-L1/PD-1 immunotherapy in PCa patients, found that the expression of PD-L1 is prevalent in the nerve branches in the tumour associated stroma, which had an inhibitory effect on CTLs (Mo *et al*. 2019).

1.3.4.3. Immunosuppressive mediators in PCa TME

Immune checkpoints are inhibitory receptors expressed on immune cells, that function to prevent immune responses which creates an immune suppressive TME facilitating tumour growth. PD-1, CTLA-4, TIM-3, and LAG-3 are the primary checkpoints involved in TME. These proteins bind to their ligand molecules which are expressed on tumour cells and generate inhibitory signals to T-cells (Wang *et al*. 2023; Long *et al*. 2018).

1.3.4.3.1. CTLA-4

CTLA-4 is a prominent immune checkpoint in PCa which is, constitutively expressed on Tregs during homeostasis and on T-cells upon activation. CTLA-4 expression is also upregulated on T-cells that reach a state of exhaustion. The higher binding affinity of CTLA-4 for CD80 and CD86

on APCs than the co-stimulatory ligand CD28 leads to inhibition of PI3K-mediated activation of Akt, interrupting CD3-dependent T-cell stimulation and effector function, involving reduced secretion of cytokines like IL-2 and TNF-α, without causing T-cell apoptosis. Thus, PCa tumours would benefit directly from CTLA-4-mediated immunosuppression and indirectly *via* general anergy which enhance the PCa cells to evade immune surveillance and proliferate (Stultz and Fong, 2021).

1.3.4.3.2. PD-1

The PD-1, together with its complementary ligands PD-L1 and PD-L2, function as inhibitory co-receptor-ligand pairs for maintaining a balance between immune activation, T-cell anergy, and immunosuppression. PD-1 is expressed on Tregs, NK cells, and activated B cells. Conversely, PD-L1 is expressed on multiple tissues, including hepatocytes, placenta, pancreatic islet cells, epithelium, vascular endothelium, mesenchymal stem cells, and immune cells such as DCs, T-cells, mast cells B-cells, and macrophages. PD-L2 is expressed in, tumour cells, macrophages and DCs. PD-1 binds to its ligand PDL-I/PD-L2 and regulates immune tolerance by downregulating TCR-mediated lymphocyte proliferation and cytokine secretion. The enhanced expression of PD-L1 in PCa, enables prostate TME to activate and maintain Tregs as well as silence the anti-tumour immune responses of effector T cells. Several studies support that, the expression of PD-L1 in PCa has been substantially linked to poorer patient prognosis (Stultz and Fong, 2021). In a particular study, patients with PCa and confirmed LN metastasis were graded based on the PD-L1 expression and it was discovered that patients with high levels of PD-L1 expression experienced significantly reduced metastasis-free survival (Petitprez *et al*. 2019).

1.3.4.3.3. TGF-β

TGF-β is a pleiotropic cytokine, produced by stromal cells and several lineages of leukocytes. TGF-β regulates cell growth under homeostatic conditions, by acting as a tumour suppressor molecule and an effective cell cycle regulator (Stultz and Fong, 2021). TGF-β family plays a critical role in embryonic development and differentiation of mammary, salivary, sebaceous glands, and prostate epithelial cells. TGF-β plays a dual role in PCa; at the early stage of cancer,

it acts as an anti-proliferative factor, while in the advanced stage, TGF-β develops pro-metastatic properties. TGF-β secreted by the normal prostate stromal cells has an inhibitory proliferative effect on the epithelial cell. On the other hand, tumour cells in PCa develop resistance to the inhibitory action of TGF-β leading to uncontrolled cell proliferation. TGF-β facilitates PCa progression by inducing angiogenesis and epithelial-to-mesenchymal transition and through its inhibitory effects on immune cells (Thompson-Elliott, Johnson, and Khan, 2021). TGF-β receptor type-II signalling pathway inhibition enhances the cytotoxic capabilities of T-cells and NK cells. In the high-grade PIN murine model, inhibition of TGF-β receptors resulted in decreased cell proliferation, indicating that TGF-β acts as a tumour promoter rather than a tumour suppressor (Qin *et al*. 2016). Moreover, TGF-β acts as a mediator for the recruitment of immunosuppressive cells such as Tregs and secretion of cytokines such as IL-2 and IFN-γ in the TME. It has been revealed that TGF-β alone or in conjunction with epithelial growth factors can induce the transformation of CAFs. In addition to CAF-mediated fibrosis stimulation, TGF-β has also been demonstrated to be an essential signalling molecule in angiogenesis, metastasis, and immunosuppression (Stultz and Fong, 2021; Tang *et al*. 2023).

1.3.4.3.4. TIM-3

TIM-3 is expressed in immune cells, including $CD4^+$ and $CD8^+$ T-cells, Tregs, NK cells, macrophages, mast cells, and DCs. TIM-3 is a negative regulator for type -1 immunity which consists of IFN-γ-producing group 1 innate lymphoid cells such as NK cells, CD4 Th1 cells, and CD8 cytotoxic T-cells (Tc1) (Tang *et al*. 2023). The IgV domain of TIM-3 can interact with four different ligands which include galectin-9 (Gal-9), High mobility group box 1(HMGB1), carcinoembryonic antigen cell adhesion molecule (Ceacam-1), and phosphatidyl serine (PtdSer). By binding to its ligands, TIM-3 inhibits Th1 and Th17 responses and lowers $CD8^+$ lymphocyte proliferation and cytokine production. Interaction of TIM3 with Gal-9 (a plasma and nuclear glycoprotein implicated in the signal transduction pathways) induces peripheral tolerance by inhibiting Th1 and Th17 responses. Necrotic cells release HMGB1, a nuclear protein that binds to TIM-3 and TIM-3 expressed on DCs, preventing activation. HMGB1/TIM-3 complex can also directly inhibit effector T-cell proliferation, which in turn initiates inhibitory

pathways in the adaptive immune system (Tian and Li, 2021; Tang *et al*. 2023; Cazzato *et al*. 2021). CAM-1 expressed on activated T-lymphocytes is a negative regulator of the T-lymphocyte response. TIM-3 interaction with PtdSer which is exposed on the membranes of apoptotic cells promotes antigen cross-presentation by DCs and the clearance of apoptotic bodies (Cazzato *et al*. 2021).

TIM-3 expression is upregulated in the tumour infiltrating $CD8^+$ and $CD4^+$ lymphocytes causing the T-cells to respond less to antigenic stimulation. Together with other inhibitory molecules such as CTLA-4, PD-1, and LAG-3, it is also involved in T-cell exhaustion during chronic immune stimulation and, therefore used as an inhibitory marker for exhausted T-cells during malignancy. Research has demonstrated that PCa patients have significantly higher levels of TIM-3 expression on $CD4^+$ and $CD8^+$ T cells in their peripheral blood compared to patients with benign prostatic hyperplasia (Tang *et al*. 2023). Additionally, immunohistochemical results have demonstrated that TIM-3 is positively expressed in prostate tumours but nearly negative in benign tissues. It has been demonstrated that TIM-3 blockade inhibits Treg, MDSC-mediated immune suppression, which improves the immune response in cancer (Tang *et al*. 2023; Tian and Li, 2021).

1.3.4.3.5. Lymphocyte activation gene-3 (LAG-3)

LAG-3 (CD223) is a type I transmembrane protein associated with the CD3- TCR complex. Like other inhibitory immune checkpoints like PD-1, CTLA-4, and TIM-3, LAG-3 is not expressed on naive T-cells however, its expression can be induced on activated $CD4^+$ and $CD8^+$ T-cells upon antigen stimulation. The lymphocytes infiltrated to the TME, are constantly exposed to tumour-associated antigens and, therefore, express high levels of inhibitory co-receptors including LAG-3, which ultimately results in functional exhaustion (Maruhashi *et al*. 2020). Apart from CD4/CD8 T-cells, Tregs, NK cells, B cells, and DCs also express LAG-3. In the extracellular regions, LAG-3's structure is comparable to that of CD4, and it binds to MHC II on APCs with a significantly higher affinity than CD4. LAG-3 interacts with MHC II to prevent the MHC II binding with TCR and CD4, thereby directly hindering TCR signalling and impairing T-cell proliferation

and cytokine secretion (Long *et al*. 2018). LAG-3 signalling pathway down-regulates the proliferation of NK cells by arresting DNA replication in the cell cycle. LAG-3-mediated invariant NKT cell exhaustion also reduces IFN-γ production (Maruhashi *et al*. 2020). LAG-3 blockade advances CD8 effector T-cell function and upregulates IFN-γ production in self-tolerance models, indicating the role of LAG-3 in limiting self-tolerance (Maruhashi *et al*. 2020). LAG-3 expressed on the FoxP3$^+$LAG-3$^+$Tregs in TME causes higher secretion of immunosuppressive cytokines IL-10 and TGF-β to intensify the immunosuppressive activity of Tregs (Long *et al*. 2018). LAG-3 constitutively expresses on plasmacytoid DCs at a higher level than any other DC subset negatively regulates its proliferation (Long *et al*. 2018).

1.3.4.3.6. Adenosine

Adenosine is a nucleoside that acts primarily through the activation of the adenosine A2 receptor as an anti-inflammatory mediator to protect healthy tissues from inflammation-related damage under physiological conditions. Nonetheless, under pathological conditions, elevated levels of adenosine are implicated in anti-inflammatory immunity in the tissues and oppressive anti-tumour responses in various cancers. Within the TME adenosine binds to adenosine A2 and B2 receptors to facilitate immunosuppression. Adenosine plays a critical role in the development of tumours, as evidenced by most immune cells in TME expressing CD39/CD73 and/or adenosine receptors. Adenosine inhibits the maturation of NK cells and their transportation to tumour sites (Stultz and Fong, 2021). The differentiation, maturation, and antigen presentation properties of DCs are negatively regulated by adenosine in the TME. High tolerogenic factors such as IL-6, IL-8, IL-10, TGF-β, VEGF and COX-2 facilitate the differentiation of DC upon adenosine binding to myeloid DC in TME which favours the activation of suppressive CD4 Tregs (Xing, Zhang, and Wang, 2023). In TME, adenosine causes tumour reactive CD8$^+$ T cells to become dysfunctional. Research has demonstrated that high levels of A2AR, which are regulated by adenosine, are expressed by CD8+ T_{CM} in the TME, which leads to the functional exhaustion of CD8$^+$ T-cells (Mastelic-Gavillet *et al*. 2019). In addition, adenosine also promotes the proliferation of TAM. Studies demonstrate that adenosine binds to adenosine receptor A2 of TAMs, encouraging M2-like macrophage polarization and

proliferation through the activation of phosphatidylinositol-3-kinase (PI3K)/Akt and MEK/ERK pathways (Xing, Zhang, and Wang, 2023). One study highlighted the importance of the CD73-adenosinergic pathway in PCa immunosuppression, revealing the substantial correlation between CD73 levels and the interval of biochemical recurrence-free survival. This study has concluded that adenosine synthesis and CD73 activities have an immunosuppressive effect on the TME (Stultz and Fong, 2021).

1.3.4.4. Cytokines and signalling Molecules in PCa TME

An overabundance of cytokines present in the TME promotes tumorigenesis by regulating the immunosuppressive environment. Several cytokines including IL-2 and TGF-β function to maintain healthy immune balance and promote tumour invasiveness and metastasis because of their overexpression and repressed signalling pathways (Zhang *et al*. 2022). An increased level of immunosuppressive secretory factors such as IL-1a and β, IL-6, that allow prostate tumours to evade antitumour immune response are noticed in PCa. IL-6 is also used as a prognostic marker for PCa (Xu *et al*. 2022; Mao, Ding and Xu, 2021).

Cytokines in PCa TME	**Role**
Anti-tumour cytokines	
IL-12	Stimulating Th1 responses, IFN-γ production (Mao, Ding and Xu, 2021) (Long *et al*. 2018)
IL27	Anti-angiogenic effect (Mao, Ding and Xu, 2021)
IFN γ	Induce IL-6 and IL-8 release (Zhang *et al*. 2022; Zhang and Zhang, 2020)
GM-CSF	Stimulation of macrophages, DCs, NK T-cells, and granulocytes, increases tumour antigens presentation to effector T-cells and induces the production of CD4+ T cells (Mao, Ding and Xu, 2021)
Flt3-L	Infiltration of $CD4^+$ and $CD8^+$ T cells, NK-cells and DCs (Mao, Ding and Xu, 2021)
Cytokines that play a dual role in TME	
TNF α	Both apoptotic and survival impacts on tumour cells, increase the expression of PDL-1 (Mao, Ding and Xu, 2021)

IL-2	NK cell activation, induce Tregs and tumour growth and progression (Long *et al*. 2018)
IL-5	Induce locomotion and infiltration of T-cells into the TME and induce eosinophils and anti-tumour effects (Mao, Ding and Xu, 2021)
Pro-tumour and immunosuppressive cytokines	
IL-1	Cell proliferation, induces STAMP2 expression and IL-1α induces the immunosuppressive function of MDSCs (Xu *et al*. 2022)
IL-4	Increases the expression of androgens (Mao, Ding and Xu, 2021)
IL-6	Induces EMT, cancer metastasis, formation of premetastatic niche, TME remodelling, Alteration of the bone tissue, increases expression of AR and induces locomotion and infiltration of T-cells into the TME (Mao, Ding and Xu, 2021)
IL-7	Induces of EMT and Cancer metastasis (Mao, Ding and Xu, 2021; Long *et al*. 2018)
IL-8	Induces EMT, Induces locomotion and infiltration of T cells into the TME, Cancer metastasis and Angiogenesis (Mao, Ding and Xu, 2021)
IL-10	Inhibits anti-tumour responses, regulates the androgen response, increases expression of COX-2, Induction release of IL-6 and IL-8 and Th17 survival (Xu *et al*. 2022)
TGF- β	Induction of EMT, cancer metastasis (alteration of bone tissue), Inhibition of anti-tumour responses, reduce the expression of MHC-I, Angiogenesis via regulating IL-8 expression and formation of the premetastatic niche (Mao, Ding and Xu, 2021; Zhang *et al*. 2022)
EGF	Bone metastasis (Mao, Ding and Xu, 2021)
RANKL	Alteration of the bone tissue, Osteoclastogenesis and Formation of the premetastatic niche (Mao, Ding and Xu, 2021)
VEGF	Angiogenesis, Formation of premetastatic niche, TME remodelling, Mitogenic properties, Induce endothelial cell proliferation and Tumour invasion and metastasis (Mao, Ding and Xu, 2021)

Table 1.2. *Anti-tumour, pro tumour and immunosuppressive cytokines present in the PCa tumour microenvironment.*

Chapter 1: INTRODUCTION

1.4. Immunotherapies of PCa

Understanding the role and mechanisms of the immune system in combatting cancer led to the development of various immunotherapies for cancer over the years. Depending on their ability to activate the immune system against malignant cells immunotherapies are categorized into passive or active immunotherapies (Galluzzi *et al*. 2014). Passive immunotherapies known as target therapies induce a direct anti-cancer effect. This includes tumour-targeting monoclonal antibodies, and adoptive cell transfer. Conversely, active immunotherapies such as vaccines, immune checkpoint inhibitors, oncolytic virus therapies and immunostimulatory cytokines, aim at stimulating the host immune system to fight against cancer (Galluzzi *et al*. 2014; Bou-Dargham *et al*. 2020; Enokida, Moreira and Bhardwaj, 2021).

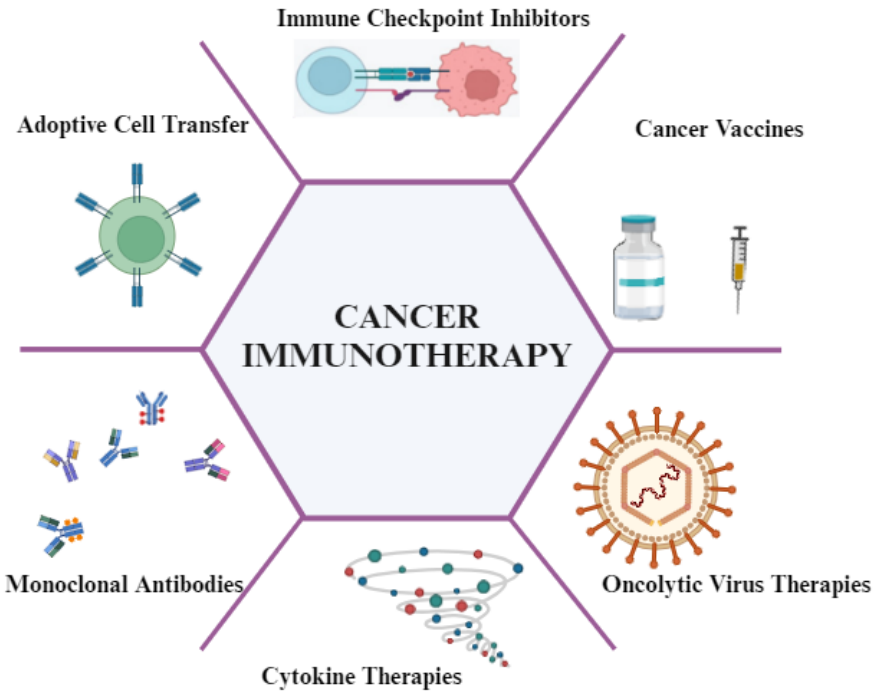

Figure 1.5. Different types of cancer immunotherapies. *Diagram created with https://www.biorender.com/*

Immunotherapies have offered significant benefits for several cancers, but only a marginal benefit for advanced PCa is reported due to the immunosuppressive TME. Therapeutic vaccine

Chapter 1: INTRODUCTION

Sipuleucel-T and immune checkpoint inhibitor pembrolizumab are the two FDA-approved treatments of advanced PCa. Ongoing clinical trials are investigating the implications of monotherapies, combinations of therapies, or immunotherapies combined with chemotherapy/ADT/ radiation to elucidate the promising avenues for the treatment of advanced PCa (Xu *et al*. 2022).

1.4.1. Immune checkpoint inhibitors (ICIs)

Immune checkpoints are molecules present on immune cells that function to maintain immune tolerance through co-inhibitory signalling pathways, yet their excessive expression on cancer cells aids cancer cells in evading immunosurveillance. ICI therapies also known as Antibodies Targeting Immune Cells- block the checkpoint proteins engaged to its ligand molecules, allowing immune cells to respond more strongly to cancer. The most widely used targets for ICIs are CTLA-4, PD-1, and PD-L1(Tang *et al*. 2023).

CTLA-4 expressed on T-cells negatively regulates T-cell activation, thus CTLA-4 blocking with antibodies could reverse the process and lead to tumour regression. Ipilimumab, a CTLA-4 antibody, is the first ICI approved for cancer treatment due to its ability to enhance T-cell activation. This drug has been approved for the treatment of metastatic colorectal cancer (Zhang and Zhang, 2020). PD-1 expressed on the surface of T-cells was originally thought to be involved in programmed cell death, yet, in cancer, it acts as a tumour promoter by binding to its ligand, PD-L1, excessively expressed on tumour cells. Research has shown that blocking PD-1 or PD-L1 pathway has achieved remarkable clinical outcomes (Zhang and Zhang, 2020). FDA has approved PD-1 inhibitors - pembrolizumab, nivolumab, and cemiplimab- and PD-L1 inhibitors - atezolizumab, avelumab, and durvalumab for the treatment of multiple cancers. Pembrolizumab, has been used to treat a selected subset of PCa patients who have mutations in mismatch repair genes and/or exhibit microsatellite instability in the tumour. However, this therapy has not benefited unselected PCa patients when combined with chemotherapy, thus its use in a wider population of metastatic PCa patients is still being assessed (Tsai *et al*. 2024) (Tang *et al*. 2023; Wang *et al*. 2022). In preclinical settings, the combination of Anti-PD-L1, such

as Atezolizumab with anti-angiogenic agent Cabozantinib was shown to increase neutrophil infiltration, reduce Treg infiltration and decrease intra-tumour $CD8^{+}PD1^{+}$T-cell and proportions. Atezolizumab in combination with Cabozantinib is being tested in phase 1b clinical trials (NCT03170960) (Esteban-Fabró *et al*. 2022).

Nivolumab a human IgG4 monoclonal antibody for blocking PD-1 when administered as a monotherapy, has shown to significantly increase the ratio of regulator effector T lymphocytes present in the TME. FDA approves nivolumab for the treatment of unresectable or metastatic urothelial carcinoma in combination with other anti-cancer therapies cisplatin and gemcitabine. However, in the phase II clinical trial, CheckMate 650 (NCT02985957) the combined effect of ipilimumab and nivolumab developed resistance to ADT and sizable adverse effects which resulted in less than 25% objective response in mCRPC patients (Wang *et al*. 2022).

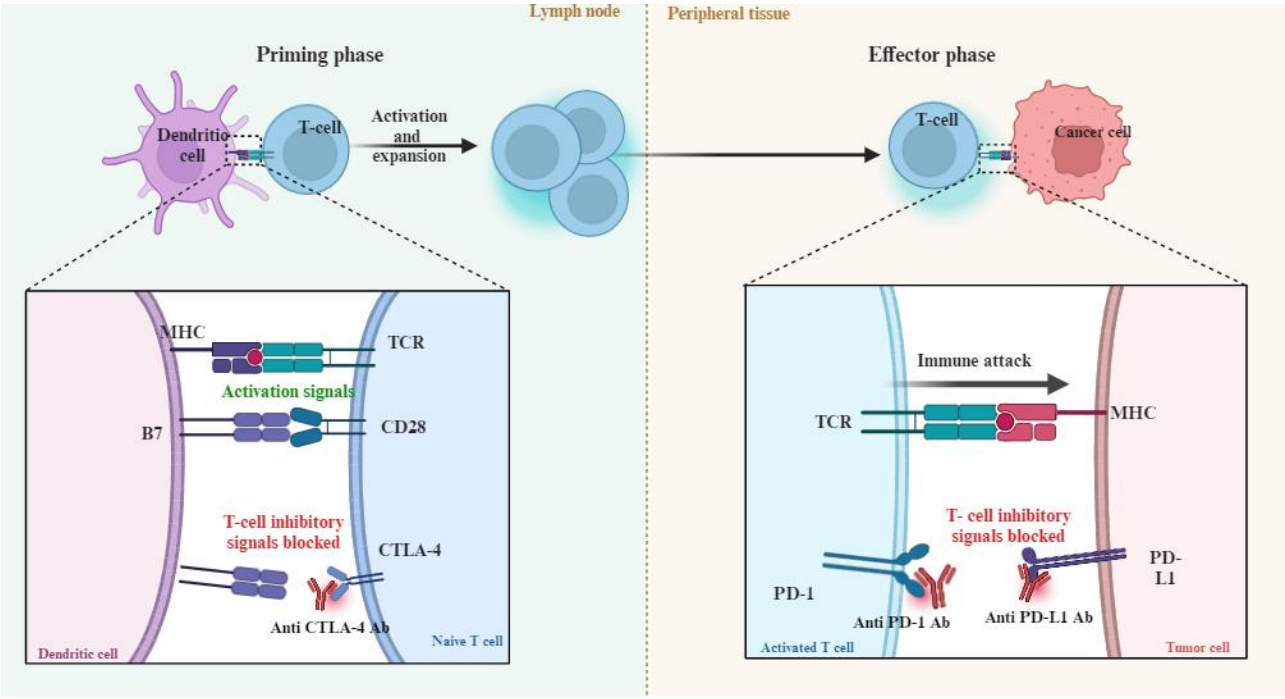

Figure 1.6. Schematic illustration of immune checkpoint and their inhibition*. CTLA binding to the B7 present on DCs generates inhibitory signals that are blocked by anti-CTLA-4 Ab, promoting the activation and expansion of T-cells in the LN. PD-1 is expressed on T-cells and its ligand PD-L1 on tumour cells is blocked by anti-PD-1 and anti-PD-L1 Ab to promote the tumour cell lysis.*

1.4.2. Adoptive cell transfer (ACT) therapy

In ACT therapy, malignant tumours are treated using adoptively transferred autologous immune cells, which are isolated, and *ex vivo* expanded, genetically engineered T-cells, chimeric antigen receptor (CAR)-T cells or T-cell receptor -engineered T cells (Zhang and Zhang, 2020). Depending on the type of modification performed or the type of immune cell used, ACT therapy can be categorised as tumour-infiltrating lymphocyte (TIL) therapy, engineered T-cell receptor therapy, chimeric antigen receptor therapy and Natural Killer Cell Therapy.

In TIL therapy, naturally, tumour-infiltrated T-cells are isolated from patients, activated, and expanded *ex vivo* and then re-infused back into patients with IL2 which is an effective cytokine for T-cell growth and survival. For the TIL therapy, fresh tumour tissues are collected through surgery. Tumour cells are then cultured in a complete growth medium with IL2 when the phenotypic selection of activated and tumour-reactive T-cells is made using surface or co-stimulatory markers. When enough of the initial TIL has been acquired, it is then instantly cryopreserved or used immediately for further expansion with IL2. TIL therapy has been proven to have remarkable clinical benefits against metastatic melanoma and other solid tumours such as cervical, colorectal, breast cancer, and non-small cell lung cancers (Zhao *et al*. 2022). Chandran *et al* (2017) describe that when TIL therapy was applied to 21 patients with rare stage-2 phase-2 uveal melanoma (clinical trial number NCT01814046) there was 4.5 % complete response, and 31.8% partial response was reported (Chandran *et al*. 2017). However, the process is time-consuming and complex due to the heterogenicity of the cellular population present in the TME and this approach was realistic only for tumours which can be resected where enough T-cells could be isolated.

Engineered T-cell receptor (eTCR) therapy involves isolated T-cells being equipped with a new T-cell receptor which facilitates them to target specific cancer antigens. CAR T-cell therapy involves genetically engineering isolated T-cells to express specifically designed synthetic chimeric antigen receptors which are capable of binding naturally occurring antigens on cancer cell surfaces directly without the need for antigen-presenting cells. Since TCR can recognise

both surface and intracellular antigens, the selection of targetable antigens for eTCR therapy is larger than for CAR-T cells where the target recognition is limited to surface antigens. However, the TCR-antigen binding is dependent upon the HLA allele, thus restricting the number of patients benefiting from eTCR therapy. CD19-targeting CAR T-cell for treating leukaemia and lymphoma and B cell maturation antigen (BCMA) targeting CAR T-cell for the treatment of advanced B-cell lymphoma has been approved by FDA (Wang *et al*. 2022). Currently, PSCA-CAR-T cells (NCT03873805), PSMA-CAR-T cells (NCT04429451 and NCT04249947) and CAR-T-PSMA-TGFβRDN69 cells (NCT03089203 and NCT04227275) are being tested for its safety and efficacy in phase I or phase II clinical trials (Messex and Liou, 2023). Adverse effects generally associated with currently approved ACT may include cytokine storm, acute kidney injury, heart arrhythmias and haemorrhages (Berraondo *et al*. 2019).

1.4.3. Cytokine based therapies.

Cytokines are small proteins sized between 10 to 80 kDa produced by immune and nonimmune cells in response to cellular stress including cancer. They act as mediators for the rapid propagation of immune signalling to generate effective and coordinated immune responses. Consequently, cytokines IL-2 and IFN-α have been approved FDA to treat several cancers. IFN-α was approved for the treatment of melanoma, lymphoma, hairy cells, and leukaemia whereas IL-2 was approved for the treatment of advanced renal cell carcinoma and metastatic melanoma (Mao, Ding, and Xu, 2021). IL-2, initially named T-cell growth stimulator, can expand T-cells *in vitro* and *in vivo* and thus exerts immune-stimulatory properties. Among the cytokines in the IFN family, IFN-α, a type-I IFN, is the significant determinant of antitumour immunity through the maturation of DCs and the enhancement of T-cell cytotoxicity (Zhang and Zhang, 2020). Despite clinical benefits, high toxicity linked with high doses and poor tolerability relegated their clinical application as monotherapies, nonetheless, cytokines are still being evaluated in combination with other immunotherapies (Zhang and Zhang, 2020; Berraondo *et al*. 2019).

GM-CSF stimulates macrophages, DCs, and NK cells, as well as improves tumour antigen presentation to effector T-cells, thus being used as an adjuvant in several cancer vaccine

formulations. In addition, GM-CSF-based vaccines have been demonstrated to induce $CD4^+$ T cell production (Zhang and Zhang, 2020). Recombinant GM-CSF is clinically used to promote myeloid reconstitution following bone marrow transplantation or with acute myelogenous leukaemia (Berraondo *et al*. 2019). It was also used, fused with PAP protein for the FDA-approved autologous DC vaccine called Sipuleucel-T to treat mCRPC. The Phase I clinical trial of pTVG-HP DNA vaccine, encoding PAP protein fused with GM-CSF in biochemical recurrent PCa patients, and the phase II study of PROSTVAC vaccine that contains PSA and GM-CSF in a group of men with mCRPC has proven the clinical safety and effective anti-tumour response of GM-CSF (Kantoff, Gulley and Pico-Navarro, 2017). In the Phase III clinical trial, PROSTVAC plus GMCSF was shown to be well tolerated however there were no effects in overall survival noticed in mCRPC patients (Gulley *et al*. 2019).

1.4.4. Oncolytic virus therapies

Oncolytic virus therapies, use replication-competent viruses to infect tumour cells, thereby generating a proinflammatory environment to enhance systemic anti-tumour immunity. Oncolytic viruses are either genetically engineered (adenovirus, herpes simplex virus type 1, vaccinia virus), or naturally attenuated (Newcastle disease virus). Oncolytic adenoviruses generally employ anti-tumour effects by direct tumour cell lysis by disrupting tumour vasculature. They also act as delivering vectors for certain genes with anti-tumour efficacy which enables the continuous expression of genes as the virus replicates enhancing the tumour cell lysis (Yang, Feng, and Luo, 2022). T-Vec, a genetically modified herpes simplex virus, has demonstrated impressive clinical benefits against advanced melanoma thus, has been approved for the management of unresectable metastatic melanoma (Zhang and Zhang, 2020).

A replication-competent oncolytic adenovirus Ad5-yCD/mutTKSR39rep-human IL-12 expressing cytosine deaminase -thymidine kinase (TK-from herpes simplex virus) and human IL-12 was tested for toxicity, and quantitation of proinflammatory cytokines IL-12, IFN-γ, and CXCL10 in a phase I study (NCT02555397), including 15 patients with localized recurrent prostate cancer. The Ad5-yCD/mutTKSR39rep-hIL-12) was well tolerated and the study

reported an increase in IL-12, IFN-γ, and CXCL10 production observed in 57%, 93%, and 79% patients, respectively (Shyam Nyati *et al*. 2023). ORCA-010 is a novel and improved oncolytic adenovirus based on the adenovirus serotype 5 genome designed to treat patients with localized PCa and is currently being tested in phase I/phase II clinical trial (NCT04097002) for its safety and tolerability (https://classic.clinicaltrials.gov/ct2/show/NCT04097002).

PROSTVAC is an active immunotherapy consisting of prime-boost immunisation using two live poxviral-based vectors: PROSTVAC-V, a recombinant vaccinia virus (rilimogene galvacirepvec), and PROSTVAC-F, a recombinant fowlpox virus (rilimogene glafolivec). Both vaccina and flowpox vectors comprise transgenes for PCa-associated antigen PSA and three costimulatory molecules for T-cells which are collectively referred to as TRICOM: intercellular adhesion molecule-1, B7.1 and leukocyte function-associated antigen-3. In a randomised blinded phase-II trial, PROSTVAC prolonged the median overall survival by 8.5 months compared to the placebo-treated group in mCRPC patients. The therapeutic benefits of PROSTVAC were further tested in mCRPC patients in a phase III, international, randomized, double-blinded, placebo-controlled study. This study observed that vaccine-induced T-cells were capable of infiltrating into tumours, however, no clinical progression or prolonged median overall survival was reported between treatment and control groups. Moreover, the adverse reactions fatigue, injection site reaction, and arrhythmia were similar for the treatment and the placebo groups (Gulley *et al*. 2019).

1.4.5. Monoclonal antibodies (mAbs)

mAbs are clonal versions of specific antibody isotypes designed to bind to antigens expressed selectively by tumour cells to achieve cancer cell detection and destruction; they induce tumour cell lysis by blocking the growth factor receptor signalling. For example, Targeted mAbs therapies like Herceptin (trastuzumab) for HER2-positive breast cancer are designed to directly bind to the HER2 receptors on the cancer cells, stopping cell proliferation and thereby reducing tumour progression. The mAbs such as cetuximab designed to bind to epidermal growth factor receptor (EGFR) which is overexpressed by various cancers, will inhibit tumour cell

proliferation and migration. Bevacizumab is an anti-vascular endothelial growth factor (VEGF), that decreases angiogenesis and enhances blood vessel penetration of chemotherapy drugs like taxanes when used in combination. Siltuximab, abituzumab, Cixutumumab and ramucirumab are other examples of mAbs which are designed to bind to interleukin-6, integrin alpha-V, insulin-like growth factor-1 receptor (IGF-1R) and VEGFR-2 respectively (Zahavi and Weiner, 2020).

Lu-TLX591 is a prostate-specific membrane antigen (PSMA) mAb aimed to treat advanced PCa or mCRPC. Its therapeutic benefit was proven in small trials (Abusalem *et al*. 2023). Larger studies are required and are currently in progress (NCT04786847; NCT05146973; NCT04876651) to evaluate its effectiveness amongst different PCa populations (Nguyen *et al*. 2024). Enoblituzumab is an IgG1-type mAb toward B7-H3 which is a cell surface immunomodulatory glycoprotein highly expressed in PCa but minimally in normal cells. The therapeutic applications of B7-H3 are being studied (NCT02923180) in a large PCa population (Shenderov *et al*. 2023). Though immunotherapies are proven to be effective in cancer treatments, some therapies like CAR T-cell therapy and mAb therapy may lead to an overreactive immune response which may lead to cytokine release syndrome due to the dysregulated production and release of inflammatory cytokines (Berraondo *et al*. 2019).

1.4.6. Cancer vaccines

Vaccines have proven effective in preventing infectious diseases caused by viruses and bacteria since the first vaccine was developed two centuries ago. However, the concept underlying vaccination goes beyond just prevention; therapeutic vaccines designed to treat infections have advanced to the final stage and have shown encouraging outcomes (Lin *et al*. 2022). Unlike bacteria and viruses, which appear foreign to the human immune system, cancer cells more closely resemble normal healthy cells therefore developing a vaccine for cancer is more complex. Moreover, tumour cells express unique antigens, which makes it difficult to create efficient cancer vaccines (Kaczmarek *et al*. 2023).

1.4.6.1. Preventive cancer vaccine

Viral infections are the cause of the development of certain cancers, such as cervical cancer and head and neck cancer, which can be caused by human papillomavirus (HPV), whereas hepatocellular carcinoma can be caused by hepatitis B (HBV). There are FDA-approved vaccines against HPV and HBV virus developed to prevent viral infections that can lead to cancer. Vaccination against these oncogenic viruses enhances the immune system to neutralize the oncogenic viruses by blocking virus-host cell interactions or stimulating CTLs to eliminate premalignant and residual cancer cells. Other oncogenic viruses, such as Epstein–Barr virus (EBV), human T cell leukaemia virus-1 (HTLV-1), hepatitis C virus (HCV), and polyomavirus, have recently seen revived efforts related to the impact on virus-associated malignancies (Enokida, Moreira, and Bhardwaj, 2021). Prophylactic vaccinations, however, cannot prevent every cancer because not all cancers are triggered by viruses. There is currently no preventive vaccine approved for use as a preventive measure against non-viral cancers.

1.4.6.2. Therapeutic cancer vaccines

Therapeutic cancer vaccines are developed to treat existing malignancies either on their own or in combination with other immunotherapies. They induce an anti-tumour response by targeting tumour antigens, including tumour-specific antigens (TSA) and tumour-associated antigens (TAA) (Elsheikh, Makram and Nguyen Tien Huy, 2023). Treating established malignancy with therapeutic vaccines activates the immune system to identify and eradicate tumour cells, thereby reducing tumour growth and preventing recurrence or metastasis (Kaczmarek *et al*. 2023). Following immunization, the tumour-related antigen is processed by APCs and presented via MHC class I/II complexes for recognition by T-cells, leading to T-cell priming and activation. Activated T-cells then infiltrate the tumour bed, guided by chemokine gradients for direct or chemokine-mediated tumour cell lysis (Fan *et al*. 2023). Depending on the existing platform, cancer vaccines can be divided into; cancer-associated membrane-bound carbohydrate vaccines, viral/bacterial vaccines, nucleic acid vaccines, cell-based vaccines, and peptide-based vaccines (Elsheikh, Makram and Nguyen Tien Huy, 2023).

1.4.6.2.1. Cancer-associated membrane-bound carbohydrate vaccine

Membrane-bound carbohydrate fractions including, globo H, Thompson–Friedenreich antigen and, mucin-1 are expressed preferentially on the surface of a variety of tumour cells including PCa, suggesting that these fractions might be immunotherapeutic targets for PCa (Rastogi, Muralidhar and McNeel, 2023). Slovin *et al* (2005) in phase-I vaccine trials including biochemically recurrent, non-metastatic PCa patients targeting Thompson–Friedenreich antigen which was conjugated to keyhole limpet haemocyanin- an immunogenic foreign protein- and delivered with a saponin-containing adjuvant QS-21. Before the trial, participants were screened by immunohistochemistry for the expression of Thompson–Friedenreich antigen and compared with tissues from healthy individuals. Two of five patients recorded a decrease in the PSA from pre-treatment to post-treatment, suggesting that immunisation targeting these antigens might reduce PCa progression. Consequently, this vaccine was tested in a phase-II trial including thirty patients with castration-sensitive non-metastatic PCa where the patients received 6 doses of carbohydrate antigens in QS-21 adjuvant over a year. Nonetheless, no variations in serum PSA slopes were observed and this strategy was not further developed (Slovin *et al*. 2005).

1.4.6.2.2. Viral or bacterial vaccines

Virus/bacteria-based vaccines comprise inactivated, live attenuated viruses/bacteria (Elsheikh, Makram and Nguyen Tien Huy, 2023) which are phagocytosed by APCs, particularly DCs, initiating an inflammatory response and the release of proinflammatory cytokines, chemokines, and other signalling molecules. These vaccine platforms aim to generate a memory response that can drive a rapid and robust immune response upon subsequent encounters with tumour cells expressing the same antigens (Kaczmarek *et al*. 2023). Herpes simplex virus and adenovirus are the two oncolytic viruses that are most frequently used for viral-based vaccines. Because of its adaptability, reproducibility, mucous membrane infectivity, and host cell tropism, adenovirus is considered revolutionary in developing a viral-based vaccine (Elsheikh, Makram and Nguyen Tien Huy, 2023). Likewise, certain bacterial species, such as Escherichia coli, Clostridium, Shigella, Lactococcus,

Bifidobacteria, Listeria, Salmonella, Vibrio, and Bifidobacteria, have extraordinary potential for cancer treatment. Bacillus Calmette-Guérin (BCG), a tuberculosis vaccine that uses weakened bacteria to stimulate the immune system, became the first immunotherapy approved by the FDA in 1990 and is still used for the treatment of early-stage bladder cancer (Rommasi, 2021).

1.4.6.2.3. Nucleic acid vaccine

Nucleic acid vaccines use genetic material -DNA or RNA - from a pathogen to introduce protective immunity against it. Different from other vaccines, these formulations deliver DNA or RNA encoding antigen to the body instructing the cells to produce antigen proteins through normal physiological activities that will trigger an immune response against tumour cells. Nucleic acid vaccines allow multiple antigens to be delivered in one formulation, have relatively low production costs, are safe to administer, and are more specific in eliciting both humoral and cellular immune responses against target antigens (Elsheikh, Makram and Nguyen Tien Huy, 2023; Liu *et al*. 2022). DNA molecules, cross the cell membrane of APCs to the cytoplasm and the nucleus to be transcribed to be mRNA and then translated into specific proteins in the cytoplasm and are presented by the APC cells to initiate host immune responses, while mRNA molecules enter the cytoplasm, translate to express antigen directly. Compared to DNA vaccines, mRNA vaccines generate efficient immune responses due to instantaneous antigen production without mRNA having to cross the nuclear membrane for transcription. However, RNA is less stable and degrades fast due to the catalytic activity of ribonucleases. DNA vaccines are more stable, and one DNA plasmid can generate multiple mRNA copies, producing more antigens, thus DNA vaccines have been studied the most compared to RNA vaccines (Liu *et al*. 2022). The efficacy of RNA vaccine also may affect due to its hindered delivery of the synthesised RNA by crossing the cell membrane and escaping from endosomes. Nonetheless, mRNA vaccines gained sizable attention, particularly in the context of recent achievements in developing the COVID-19 vaccine against the SARS-CoV-2 virus. Various approaches have been attempted to modify the structural elements of mRNA such as altering untranslated regions, coding regions and the addition of a 5’ cap poly(A) tail which has

enhanced the stability, safety, and efficiency of mRNA vaccines. In addition, using nanoscale lipid-based carriers to deliver mRNA intracellularly has also improved the translational efficacy of mRNA vaccines. Their lipid bilayer structure of nanoparticles effectively encapsulates synthetic mRNA and prevents endosome degradation. The lipid nanoparticles have been used as carriers in formulating FDA-approved SARS-CoV-2 mRNA vaccines Pfizer–BioNTech vaccine (BNT162b2) and the Moderna vaccine (mRNA-1273) (Wang Bolin *et al*. 2023).

The plasmid DNA vaccine, pTVG-HP which encodes PCa-associated antigen PAP has demonstrated potential immunostimulatory and antineoplastic activities against PCa. A randomized phase-II trial was conducted to evaluate the effect of this vaccine on cancer metastatic progression in patients with non-metastatic, castration-sensitive PCa. The vaccine was administered intradermally 6 times at 2-week intervals, with GM-CSF and compared against GM-CSF alone. A subset of patients treated with pTVG-HP improved metastasis-free survival by 12.0 months vs 6.1 months in patients who received GM-CSF alone. However, overall results suggest that the PAP DNA vaccine exhibited immunological activity but was not sufficient to delay disease progression thus vaccine was not pursued as a monotherapy. This has led to several other trials to evaluate the efficacy of vaccine with other immunostimulatory agents (McNeel *et al*. 2019). The efficacy of pTVG-HP vaccination in combination with PD1 blockade pembrolizumab was tested in mCRPC patients. Overall, 10 of 25 patients who received the combinational therapy, demonstrated decreased tumour volume, and 1 patient had a partial response. 32% of patients who remained on trial beyond 6 months showed no progression. Another trial was conducted to evaluate the safety and efficacy of the vaccination with PD-1 blockade, nivolumab in 19 patients with non-metastatic early recurrent PCa. Patients received 100µg pTVG-HP intradermally and 240 mg nivolumab intravenously every two weeks for three months followed by every 4 four weeks for a year followed by a year off treatment. 21% of patients had a PSA drop >50%. Overall, the study concluded that pTVG-HP vaccination was safe and immunologically active when administered together with nivolumab. The investigators proposed that additional treatments be added to this therapy to target resistance or that treatment should be continued indefinitely until the disease progresses (McNeel *et al*. 2023; Rastogi, Muralidhar and McNeel, 2023).

DOM-PSMA is a DNA vaccine encoded for the HLA-A2-binding epitope of the prostate-specific membrane antigen (PSMA) fused to a fragment of the tetanus toxin was investigated in a phase I/II dose-escalation trial. A high frequency of immunological responses was demonstrated with DOM-PSMA vaccination. An increased PSA doubling time has also been demonstrated from 11.97 months pre-treatment to 16.82 months throughout the 72-week follow-up (Chudley *et al*. 2012).

A mRNA vaccine approach CV9103 for the treatment of PCa has been developed with self-adjuvanted mRNA that encodes antigens for PSCA, prostate stem cell antigen, PSA, PSMA and STEAP-1. The immunogenicity and safety of vaccination were assessed in CRPC patients in the phase I/IIa trial. 26 out of 33 patients demonstrated an immune response to one or more antigens, and 15 out of 33 patients developed an immunogenicity to multiple antigens. Based on this evidence of immunogenicity, a second-generation vaccine, named CV9104 was further developed by including two additional antigens PAP and MUC1 to CV9103. CV9104 was evaluated in a randomised phase I/IIb trial comprising 197 mCRPC patients. No increase in overall survival was noticed in patients who received the vaccine (35.5 months) compared with the patients who received the placebo (33.7 months) (Stenzl *et al*. 2017).

1.4.6.2.4. Peptide-based vaccine

Peptide-based tumour vaccines consist of short (8-12 AA long) or long peptides (20 amino acids or more) of tumour-specific antigens that are engineered to induce specific anti-tumour immune responses. Peptide vaccines are formulated with suitable adjuvants such as Alum, oil in water emulsions or TLR agonists to enhance the immune response by preventing serum protease antigen degradation and improving the antigen uptake by APCs (Nelde, Rammensee and Walz, 2021). Compared to whole protein sequences or whole inactivated viruses, long peptides are immunodominant to produce focused immune responses against the long peptide-derived short epitopes (Liu *et al*. 2022). After being administered, peptide antigens are processed by APCs and presented by MHC molecules to be recognised by the T-cells to initiate antigen-specific immune responses. To generate efficient anti-tumour response, peptide vaccines must have $CD8^+$ T-cell epitopes to activate CTL via antigen cross-presentation

pathway and $CD4^+$ T-cell epitopes to sustain CTL effector functions by T helper cell activation (Melief *et al*. 2015). Therefore, the sequence length of the peptide used to formulate the vaccine is important for promoting a strong immunogenic response (Abd-Aziz and Poh, 2022). Short peptides tend to have a short half-life, are easily degraded in serum, and bind to MHC class-I groove even without further being processed by professional APCs. However, short-term induction of $CD8^+$ T cells, without simultaneous activation of $CD4^+$ helper T cells could result in tolerance (Buhrman and Slansky, 2013; Melief *et al*. 2015). Moreover, Short peptides are HLA restricted, preventing the diversity required for the high HLA polymorphisms in the general population. Synthetic long peptides (20 amino acids or more) are more stable and consist of MHC class I and MHC class II epitopes, which are capable of inducing $CD8^+$ CTLs activation, $CD4^+$ T-cells involved long-lasting antitumoral immune responses and antibody production by B cells (Abd-Aziz and Poh, 2022; Melief *et al*. 2015).

Personalized peptide vaccines, in which fourteen HLA-matched peptides derived from various PCa-associated antigens were used as a therapeutic approach in patients with mCRPC. Peptides for vaccine development were selected based on the patient's pre-existing immunity to specific antigens before vaccination. This treatment was shown to be safe in early-phase clinical trials. However, results from a phase III trial in which 310 HLA A24-positive patients with mCRPC who had previously received taxane chemotherapy were randomized to receive vaccination or placebo. Patients received up to 4 peptides for which they had pre-existing immunity. Some of the participants responded to the treatment and generated peptide-specific IgG. 41% of participants in both groups generated grade ≥3 adverse reactions, however, no difference in overall survival between the treatment and control groups was observed (Noguchi *et al*. 2021).

1.4.6.2.5. Cell-based vaccines

Therapeutic cell-based vaccines fall into two categories: Tumour cell and immune cell vaccines. Tumour cell vaccines are developed by using patients' tumour cells (autologous) or allogenic cell lines modified *ex vivo* through irradiating/lysing the cells or genetically modifying these *ex vivo* so that they encode cytokine genes such as IL-2, IL-12, or GM-CSF to promote

immune signals. Genetic modification through immunomodulatory cytokines, specifically GM-CSF, is applied to overcome low immunogenicity to activate both humoral and cellular immunity. Tumour cell vaccines are advantageous because they can present all tumour-specific mutated antigens; in particular, genetic modification can boost the immune response against tumour antigens. However, the production and administration of vaccines are difficult and time-consuming.

GVAX, containing autologous PCa cells expanded *ex vivo* with retrovirus to express GM-CSF was tested clinically. The approach of transfecting autologous cells as a vaccine was challenging due to the higher number of tumour cells needed, thus GVAX containing autologous tumour cells was not further pursued. In the following studies, allogeneic PCa cell lines were transfected to express GM-CSF and were evaluated in PCa patients at different stages in different phase I/II trials. The findings observed in the trials suggested the efficacy of GVAX vaccination in slowing down the progression of PCa (Rastogi, Muralidhar and McNeel, 2023). The efficacy of this vaccine was then tested in randomised phase-III trials, where GVAX was administered with or without docetaxel, a chemotherapy drug in mCRPC patients. No improvement in overall survival was observed in this study. Moreover, the combination therapy was found to cause a greater death rate in the patients, therefore the trial was terminated and the clinical development of GVAX for PCa was suspended (Ward and McNeel, 2007).

Immune cell vaccines are developed by the *in vitro* activation of intrinsic immune cells, including NK cells or dendritic cells, by viral peptides/genes, autologous tumour antigens, and/or immunomodulatory cytokines. DCs, as primary APCs, can cross-present and stimulate naive T-cells against specific antigens and establish efficient immunological memory. Many DC-based vaccines have been studied so far in which the target antigen was directly presented using DCs loaded with proteins, peptides, or nucleic acids. DCvax-Brain is an orphan drug developed to treat glioma by extracting DCs from PBMCs of patients and *ex-vivo* loading with autologous tumour antigens.

Autologous DCs cultured with HLA A2-specific epitopes from the PSMA protein were tested for efficacy in 37 patients who had a recurrence of PCa followed by primary treatment failure in a phase-II trial. Out of 37 patients tested, one patient had a complete response, and 10 patients

responded partially to the treatment. At the end of the study, 30% of study participants had displayed a positive response. A randomized phase-III trial was arranged for this approach in mCRPC patients but has not been completed owing to funding restrictions (Rastogi, Muralidhar and McNeel, 2023). Another example of a DC-based vaccine is DCVAC/PCa for the treatment of mCRPC which consists of autologous DCs pulsed with LNCap cells. The safety and efficacy of this vaccine have been evaluated in a phase III double-blinded placebo-controlled trial. DCVAC/PCa was administered with docetaxel and prednisone was well tolerated in patients with mCRPC but the treatment did not extend the overall survival of patients (Vogelzang *et al*. 2022).

Provenge (Sipuleucel-T) is the first and only FDA-approved autologous immune cell-based vaccine; it consists of autologous PBMCs incubated with prostatic acid phosphatase (PAP) fused with GM-CSF, which has shown improved survival of 4.1 months compared with placebo in phase III clinical trial in men with castration-resistant prostate cancer (Elsheikh, Makram and Nguyen Tien Huy, 2023). Sipuleucel-T vaccine is prepared by obtaining PBMCs from PCa patients by leukapheresis. The PBMCs obtained include $CD54^{bright}$, $CD3^{+}$, $CD14^{+}$, and $CD19^{+}$ cells are centrifuged over a buoyant density solution -which contains colloidal silica and is used to separate the peripheral blood progenitor cell populations according to their distinctive densities - of 1.077 g/mL followed by washing twice to eliminate platelets. This is further centrifuged over a density solution of 1.065 g/mL and washed twice to eliminate granulocytes. The resulting concentration is resuspended in AIM-V medium and incubated with PA2024 (10 µg/mL) at 37° C for 40 hours. PA2024 is a recombinant protein of PCa-associated antigen PAP fused with GM-CSF. Once the incubation is complete, the activated cell products are washed in Lactated Ringer's and CD54, a marker linked with immune activation is used to determine the potency of the vaccine. Activated cells are reinfused to the patient with each infusion containing a minimum of 50 million $CD54^{+}$ cells. The complete procedure is repeated for each of the 3 infusions of sipuleucel-T (Madan and Gulley, 2011).

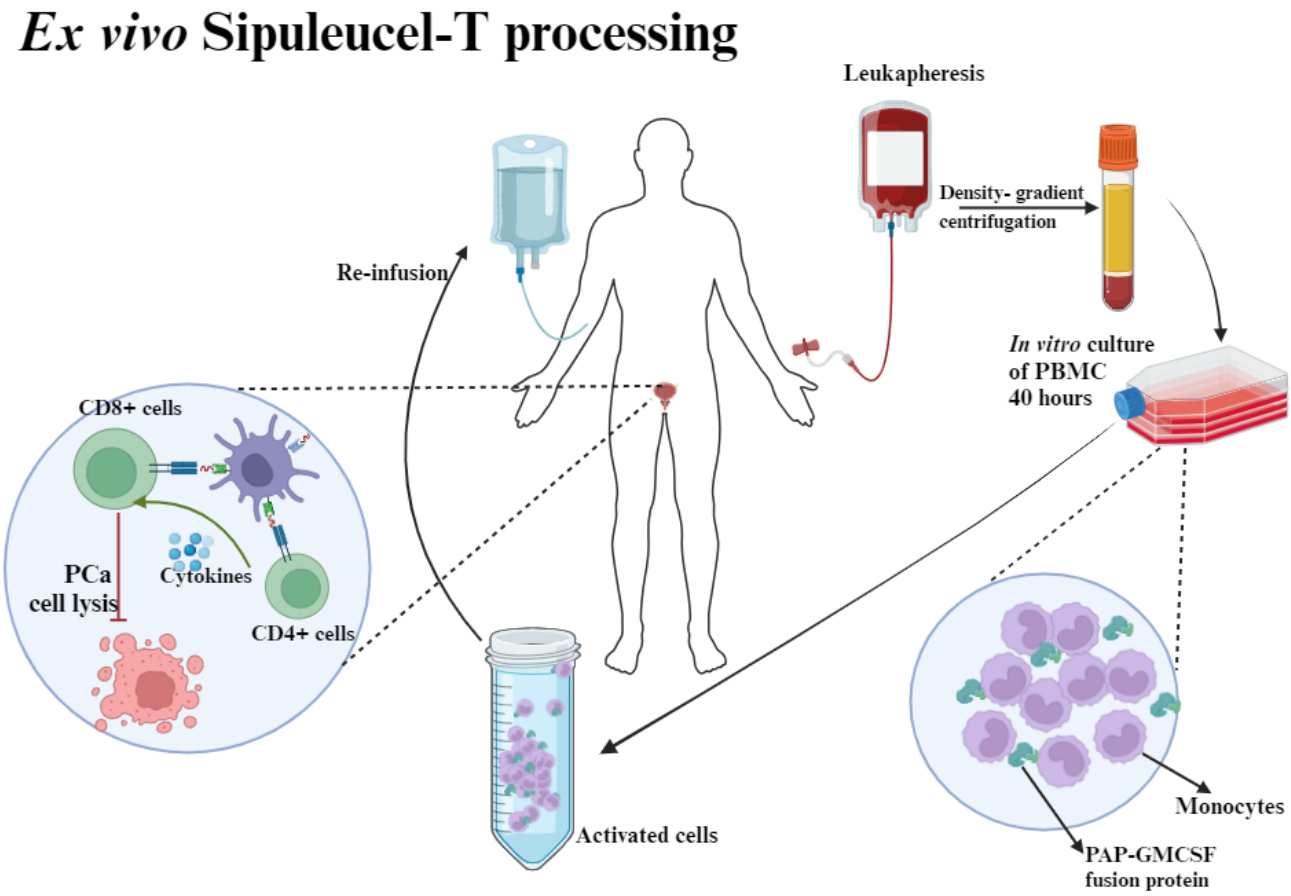

Figure 1.7. Ex-vivo processing of Sipuleucel-T vaccine. *Patient blood is collected via leukapheresis, and immune cells are isolated and stimulated in vitro with a fused PAP-GM-CSF protein for 40 hours and are re-injected back into the patient.*

Preliminary evidence for the clinical efficacy of Sipuleucel-T was collected from phase I/II trials involving patients with hormone-refractory PCa. These trials aimed to determine the safety, effectiveness, and capabilities to break immune tolerance to PAP antigen. Results obtained demonstrated that all patients could develop immune responses to PA2024 and 38% developed PAP-specific immune responses. PSA levels decreased in three patients by more than 50%. Fever was the most associated adverse effect. The study concluded that this treatment was able to break the tolerance to PAP antigen and was safe to use (Small et al. 2000). Another phase II study was conducted on 21 patients with androgen independent PCa. The

treatment was well tolerated, and increased T-cell proliferation was reported in 15 participants. Fatigue and fever were the most associated adverse effects (Burch *et al*. 2004).

Based on the safety and efficacy of Sipuleucel-T observed in phase-I/II studies, 2 simultaneous randomized, placebo-controlled phase III clinical trials were conducted including 225 advanced PCa patients. The placebo used for the study consisted of APCs prepared identically to the vaccine but without the culture with PA2024. Participants received 3 intravenous infusions 2 weeks apart. Following randomisation, patients were monitored for survival until a pre-determined 36-month or until their death. Patients randomized to Sipuleucel-T demonstrated a 33% reduction in the risk of death with an overall survival of 25.9 months for the vaccine vs 21.4 months for the placebo (Higano *et al*. 2009). Following this trial, a double-blinded, placebo-controlled another phase-II trial (NCT00065442) was conducted assigning 512 patients with mCRPC. There was a comparative reduction of 22% in the risk of death representing a 4.1-month improvement in median survival in the treatment group as compared with the placebo group. Adverse events also were more reported in the treatment group than in the control group which included chills, fever, and headache (Kantoff *et al*. 2010). Sipuleucel-T was the first FDA-approved therapeutic cancer vaccine for patients with metastatic CRPC (Madan and Gulley, 2011).

Outcomes of completed Phase II/III PCa immunotherapy trials							
Vaccine	Antigen	Combination agent	patients	Phase	Trail ID	Outcome	Reference
GVAX	PSA, PAP, PSMA	GVAX	Asymptomatic chemo-naïve mCRPC (n=626)	III	NCT00089856	Terminated (the chance of meeting the primary endpoint was <30%) No OS improvement	(Ward and McNeel, 2007)
GVAX		Docetaxel	symptomatic chemo-naïve mCRPC (n=408)	III	NCT00133224	Terminated due to greater death rate in patients	
DCVAC/Pca		Docetaxel and prednisone	mCRPC (n=1170)	III	NCT02111577	No improvement in the overall survival of patients	(Vogelzang et al. 2022)
PROSTVAC-VF/TRICOM	PSA	GM-CSF	mCRPC (n=1200)	III	NCT01322490		(Gulley et al. 2019)
pTVG-HP	PAP	GM-CSF	Casration sensitive-PCa (n=99)	II	NCT01341652	No overall Survival	(McNeel et al. 2019)
Lpilimumab	Anti-CTLA4 Ab		Docetaxel treated mCRPC (n=988	III	NCT00861614	No improved OS (P=0.53) Improved OS on patients with less advanced disease (P=0.0038)	(Kwon et al. 2014)
			Chemotherapy naive mCRPC (n=837	II	NCT01057810	No improved OS (P=0.53). Increased, PFS Improved OS on patients with less advanced disease (P=0.0038	Beer, et al. 2017

Table 1.3. List and outcome of PCa immunotherapies that have completed phase II or phase III clinical trials. *Abbreviations: OS -overall survival; PFS- progression-free survival; PSA- prostate-specific antigen; PSMA- prostate-specific membrane antigen.*

PCa immunotherapy in clinical trial					
Active ingredient/s	Antibody/Antigen	Phase	Clinical trial identifier	Patients	Stage
Nivolumab (in combination with Rucaparib, Docetaxel, or Enzalutamide)	Anti-PD-1 Ab	II	NCT03338790	mCRPC	Active, not recruiting
Nivolumab (Docetaxel)	Anti-PD-1 Ab	III	NCT04100018	CRPC	Recruiting
Nivolumab	Anti-PD-1 Ab	II	NCT03637543	High-risk biochemically recurrent PCa	Active, not recruiting
Nivolumab	Anti-PD-1 Ab	II	NCT02985957	mCRPC	Active, not recruiting
Ipilimumab	Ant-CTLA-4 Ab				
Atezolizumab	Anti-PD-L1 Ab	I-b	NCT03170960	CRPC	Active, not recruiting
Cabozantinib					
Nivolumab	Anti-PD-1 Ab	III	NCT03879122	Metastatic Hormone-sensitive PCa	Active, not recruiting
Ipilimumab	Ant-CTLA-4 Ab	II			
Pembrolizumab	Anti-PD-1 Ab	I	NCT03805594	CRPC	Active, not recruiting
PRO-MERIT (mRNA vaccine)	KLK2, KLK3, PAP, HOXB13 and NKX3-1	I	NCT04382898	mCRPC	Active, recruiting
CCW702	anti-PSMA/CD3 bispecific Ab	1	NCT04077021	mCRPC	Not recruiting
Enoblituzumab	Anti- B7-H3 Ab	II	NCT06014255	high-risk localised PCa	Recruiting
ORCA-010 (oncolytic adenovirus)		I and II	NCT04097002	Localised PCa	Active, not recruiting

Table 1.4. List of PCa immunotherapies currently in phase 1 and 2 clinical trials. *Abbreviations: KLK -kallikrein; PAP- prostatic acid phosphatase; HOXB13- homeobox B13; NKX3- NK3 homeobox 1. The details of the trials are obtained from https://classic.clinicaltrials.gov*

1.5. PCa specific/associated antigen

Many PCa markers that are expressed on prostate cells and their malignant counterparts have been identified so far, Prostate-specific antigen (PSA), and prostate-specific membrane antigen (PSMA). Though these antigens are expressed at a higher rate in PCa, a strong anti-tumour effect is not produced due to the presence of immunosuppressive factors such as prostate tumour microenvironment, Tregs, TGF-β, and MDSCs.

1.5.1. PAP as a suitable antigen for PCa immunotherapy

Human PAP is a 100 kDa glycoprotein secreted primarily by the prostate gland following adolescence and at very low levels by other organs such as the kidney brain, liver, placenta, lung spleen, thyroid, and salivary gland. PAP is also detected in normal breast tissues but not in breast carcinoma (Muniyan *et al*. 2013; Kong and Byun, 2013). In humans, PAP is also known as Prostatic specific acid phosphatase (Accp) and in mouse is known as acid phosphatase (AP3) (Muniyan *et al*. 2013). PAP is expressed in two isoforms both in humans and mice: the secretory form (sPAP) and the cellular form (cPAP). They both are transcribed from the same gene followed by distinct post-transcriptional variations and differ in their biochemical properties, such as glycosylation, antigenicity, and hydrophobicity. sPAP expression is restricted to prostate tissues and is secreted into seminal fluid. In healthy individuals, sPAP is secreted into the plasma at a physiological concentration of 1–3 ng/mL and approximately 1 mg/mL in seminal fluid. Before puberty, cPAP expression is negligible; however, in healthy adults, cPAP expression is found to be at a higher concentration, roughly 0.5 mg/gm wet prostate tissue. cPAP level is high in normal differentiated prostate epithelia, but its level decreases in prostate malignant cells. cPAP level is inversely correlated with PCa progression. In contrast, sPAP levels in the blood are elevated in PCa patients (Muniyan *et al*. 2013; Kong and Byun, 2013) therefore circulating levels of sPAP have long been used as a PCa diagnosis biomarker until the identification of PSA.

Almost 95% of prostate tumours express PAP, and its activity is extremely high in high Gleason score PCa and bone metastasis which makes PAP a suitable target for immunotherapeutic approaches (Le Vu *et al*. 2022; Westdorp *et al*. 2014; Kong and Byun, 2013). Circulating PAP-specific CTLs have also been found in patients with chronic prostatitis. PAP has already been demonstrated to be both safe as a target and immunogenic given the outcome of the Sipuleucel-T vaccine. However, this vaccine is cost-prohibitive and thus is not widely available. Moreover, this vaccine had shown only a moderate improvement in overall survival (4.1 months) (Westdorp *et al*. 2014) and there is a lack of clear-cut proof of $CD8^+$ CTLs generating epitope within the whole PAP protein thus is not cost-effective (Caram *et al*. 2019).

Chapter 1: INTRODUCTION

1.6. Previous work

Previous research conducted in our lab demonstrated that a 15 AA long PAP sequence, PAP 114-128 -MSAMTNLAALFPPEG which is identical to both mouse and human- was effective in eliciting peptide-specific T-cell responses in HHDII/DR1 humanised mice when administrated as a DNA coated onto gold particles. Greater avidity T-cell responses were seen in C57BL/6J and HHDII/DR1 mice following immunisation with the PAP 114-128 in a DNA vector format, called ImmunoBody®. This also generated an anti-tumour response in pre-established TRAMP C1 murine prostate cancer cell-derived tumours (Saif *et al*. 2014). However, this PAP sequence only contains an HLA-A2 class-I restricted epitope within an HLA-DR1 class-II-restricted epitope limiting its obtainability to HLA- $A2^+$ haplotype patients. This 15 AA long peptide was then elongated to 42 AA long [PAP 103- 144] and one amino acid was changed to increase the immunogenicity of the sequence. This new sequence includes additional peptides predicted to bind to more HLA haplotypes (illustrated in Chapter 4, Table 4.2) thereby increasing the number of patients who could potentially benefit from such a vaccine and was also able to induce more efficient and robust immune responses when tested in HHDII/DR1 mice compared to its wild-type counterpart.

The change in the amino acid at position 116 - from an Alanine to a Leucine - was introduced to break the tolerance against PAP while limiting the generation of immunosuppressive PAP-specific regulatory T-cells. The introduction of mutation also increased the predicted MHC binding score of numerous epitopes. MutPAP42mer peptide was found to elicit stronger PAP-specific T-cell responses towards MHC class I and class II epitopes than its WT counterparts and immunogenicity was further improved when combined with the CAF®09b adjuvant. The vaccine has increased secretory IFN-γ and TNFα and PAP-specific splenic T-cells in the context of HLA-A*02:01 and of HLA-DRB1*01:01, however no $CD4^+$ T-lymphocyte mediated responses were demonstrated (Le Vu *et al*. 2022).

Chapter 1: INTRODUCTION

1.7. Hypotheses

This study hypothesis that the MutPAP42mer PCa vaccine, when combined with the CAF®09b adjuvant, will induce a more robust and effective immune response compared to the CpG adjuvant in humanized mice models. Additionally, the combination of MutPAP42mer with novel 15mer PAP-derived sequences will enhance the induction of potent $CD4^+$ T-cell responses, resulting in a more effective anti-tumour response. Furthermore, when administered in prophylactic and therapeutic settings, the MutPAP42mer vaccine will demonstrate significant anti-tumour efficacy in PCa murine models, correlating with enhanced immune responses (both $CD4^+$ and $CD8^+$ T cells). Finally, the study also investigates the immune cell subsets and immunosuppressive regulators in the peripheral blood of PCa patients, comparing them with those of patients with benign disease, to understand the systemic immune environment and its impact on vaccine efficacy.

1.7. Aims of this study

This project aims to improve the already patented MutPAP42mer ("PAP peptide analogues" has been granted in the USA (10/137,185) and Europe (EP3129046)) prostate cancer vaccine owned by NTU and Dr. McArdle given gathering the necessary evidence to proceed to a "First in Man" clinical trial.

More specifically:

1. The study will aim first to confirm the superior efficacy of the MutPAP42mer vaccine when combined with CAF®09b over CpG as an adjuvant in humanised mice HHDII DR1 while in parallel assessing the ability of two novel 15mer PAP-derived sequences to induce potent $CD4^+$ T-cells response. The immunogenicity of MutPAP42mer + PAP 15mer/s will be assessed in HHDII DR1 mice while the wild-type (WT) PAP42mer will be evaluated using C57BL/6J murine models.

2. Following immunisation, vaccine-induced $CD4^+/CD8^+$ immune responses will be assessed, and the capability of vaccine-specific lymphocytes to recognise and lyse PAP-expressing target cells in an MHC-restricted manner will be assessed in vitro.
3. The anti-tumour efficacy of the vaccine will be assessed in vivo using suitable PCa-bearing murine models in both prophylactic and therapeutic settings.
4. In parallel, the characterisation of immune cell subsets, immunosuppressive regulators (MDSCs), and inflammatory molecules that circulate in the peripheral blood of PCa patients will be compared with patients with benign disease

2. Materials and Methods

2.1. Materials

2.1.1. Cell culture reagents		
Product	**Company/Supplier**	**Catalogue number**
2.1.1.1. Cell culture media		
DMEM with 4.5g/L Glucose & L-Glutamine	Lonza/BioWhittaker	12-604F
F-12K with L-glutamine	Corning	10-025-CV
MEM with Earle's salts & L-glutamine	Corning	10-010-CV
Opti-MEM I Reduced Serum Medium	ThermoFisher Scientific	31985062
RPMI-1640 without L-Glutamine	Lonza/BioWhittaker	BE12-167F
SOC Medium	ThermoFisher Scientific	15544034
TexMACS	Miltenyi Biotech	130-097-196
2.1.1.2. Culture media supplements		
Fetal Bovine Serum (FBS) 500mL	Gibco	10270-106
Insulin solution human 5mL	Sigma- Aldrich	I9278
L-Glutamine 100mL	BioWhittaker	17-605E
MEM Non-essential Amino Acid Solution (100x) 100mL	ThermoFisher Scientific	M7145
Sodium Pyruvate 100mM Solution 100mL	BioWhittaker	BE13-115E
1 M Hepes 100mL	BioWhittaker	BE17-737E
Dulbecco's Phosphate-Buffered Saline (DPBS) 500mL	BioWhittaker	17-512F
Dimethyl Sulfoxide (DMSO), cell culture reagent 100mL	ChemCruz	sc-358801
2.1.1.3. Antibiotics		
Ampicillin sodium salt 25g	Sigma- Aldrich	69-52-3
Kanamycin 5g	ThermoFisher Scientific	11815024
Geneticin (G418) sulphate 25g	Santa Cruz Biotechnology	sc-29065B
Penicillin-Streptomycin Mixture 100mL	BioWhittaker	DE17-603E
Puromycin 10mg/mL	Gibco	A1113803
Amphotericin B (Fungizone)	Sigma- Aldrich	A2942
2.1.1.4. Cytokines		
Recombinant Murine IFN-γ	PeproTech	315-05

Recombinant Murine IL-2	PeproTech	212-12
Recombinant human IL-2	PeproTech	200-02

2.1.2. Chemical reagents

Product	**Company/Supplier**	**Catalogue Number**
0.1% formic acid in Acetonitrile	Fisher Scientific	10468704
0.1% formic acid in water	Fisher Scientific	10429474
2-Mercaptoethanol 25mL	Sigma- Aldrich	M3148
2-Propanol 500mL	Sigma- Aldrich	I9516
25x AP Colour Development Buffer 40mL	Bio-Rad	9702818
4x Laemmli Sample Buffer 10mL	Bio-Rad	1610747
Acetic acid, Glacial	Fisher	A/10360/PB17
Agarose, molecular grade 500g	Meridian Bioscience	BIO41025
Ambion Nuclease-Free Water	Invitrogen	AM9932
Ammonium Carbonate ACS reagent 25g	Fisher Scientific	10710292
Ammonium per sulphate (APS) 25g	ThermoFisher	17874
Antifade Mounting Medium with DAPI (VECTASHIELD)	Vector laboratories	H-1200-10
Aquaguard-2, 50mL	Biological Industries	01-916-1E
Benzonase	Merck	E8263-25U
Bovine Serum Albumin	Fisher Scientific	11493823
Calcium Chloride anhydrous, powder 100g	Sigma-Aldrich	C4901
Clarity Western ECL Substrate	Bio-Rad	1705060
Concanavalin A from Canavalia ensiformis (Jack bean) 5mg	Sigma- Aldrich	C5275
Degarelix acetate 5mg	Sigma- Aldrich	SML2856
dNTP mix 200µL	Promega	U151A
Dried skimmed milk 340g	Marvel	n/a
Ethanol, absolute 2.5L	Fisher Chemical	E/0650DF/17
Ethyl Acetate 1L	Fisher Scientific	10724181
Ethylenediaminetetraacetic acid 100g	Sigma- Aldrich	E6758

0.5 M EDTA pH 8	ThermoFisher	15575020
FastGene IC Green 2x qPCR Universal Mix 1mL	NIPPON Genetics EUROPE	LS4001
Glycerol 100mL	Sigma- Aldrich	G5516
Gold Microcarriers 1.0µm	Bio-Rad	1652263
Hexane 2.5L	Fisher Scientific	H/0350/17
Hydrochloric acid 2.5L	Fisher Chemical	H/1150/PB17
LB Agar -Miller	Fisher Scientific	BP1425-500
LB Broth- Miller	Fisher Scientific	10638013
Lipofectamine 3000 Transfection Reagent 0.1mL	ThermoFisher	L3000001
Liquid nitrogen	BOC	
MACS® Tissue Storage Solution	Miltenyi Biotec	130-100-008
Matrigel 5mL	Corning	356277
Methanol 2.5L	Fisher Chemical	M/4000/17
Methylated spirit 99%, 2.5L	Fisher Chemical	M/4450/17
M-MLV reverse transcriptase 10,000u	Promega	M170A
M-MLV RT 5X buffer 1mL	Promega	M531A
Nitrogen gas cylinder	BOC	UN1066
Oligo(dT)15 primer 20µg	Promega	C110A
OneTaq Quick-Load 2X Master Mix with Standard Buffer 1.25mL	New England Biolabs	M0486S
Paraffin wax -soft white	VWR International	29841
Phosphate buffer saline (PBS) tablets	Oxoid- Thermo scientific	BR0014G
Polybrene	Santa Cruz biotechnologies	sc-134220
Polyvinylpyrrolidone (PVP) 100g	Sigma-Aldrich	P5288
Precision Plus Protein StrepTactin-HRP Conjugate 300µL	Bio-Rad	161-0380
Precision Plus Protein WesternC Standards 250µL	Bio-Rad	161-0376
Presept disinfectant tablets 2.5g	ASP	SPR25
Protease inhibitor cocktail 1mL	Sigma- Aldrich	P8340

Protogel (30% Acrylamide mix)	Geneflow	A2-0072
Quick-Load Purple 1 kb Plus DNA Ladder (100ug/mL) 0.1mL	New England Biolabs	N0550G
RNase ZAP 250mL	SIGMA Life Science	R2020
RNasin ribonuclease inhibitor 2,500u	Promega	N251A
Sodium acetate anhydrous	Fisher Scientific	S/2080
Sodium Citrate trisodium dihydrate	Sigma- Aldrich	6132-04-3
Sodium dodecyl sulphate (SDS) 100g	Sigma- Aldrich	133771
Sodium chloride 5kg	OmniPur	7760
Sodium deoxycholate 100g	Sigma- Aldrich	L3771
Solution 18 - AO·DAPI 1mL	Chemometec	910-3018
Spermidine 1g	Sigma-Aldrich	S0266
SYBR Safe DNA Gel Stain 400µL	Invitrogen	S33102
Sucrose 250g	Sigma- Aldrich	84100
T E buffer	Invitrogen	10742317
Testosterone 1g	Sigma- Aldrich	86500
TEMED electrophoresis grade 25mL	Geneflow	EC-503
Tris-Glycine electroblotting transfer buffer 10X, 4L	Geneflow	B9-0056
Tris-Glycine-SDS PAGE running buffer 10X, 4L	Geneflow	B9-0032
Triton X-100, 50mL	Sigma-Aldrich	T8787
Trizma base 1kg (Tris)	Sigma-Aldrich	T1503
Trypan Blue solution (0.4%) 100mL	Sigma-Aldrich	T8154
Trypsin with Versene 100mL	BioWhittaker	BE02-007E
TWEEN 20, 500mL	Sigma-Aldrich	P2287
Xylene	Fisher Scientific	X/0200/17

2.1.3. Antibodies and flow cytometry/western blotting reagents		
Product	**Company/Supplier**	**Catalogue number**
APC anti-human HLA-A2 Antibody (flowcytometry)	Biolegand	343307
Anti-mouse CD4 purified *In Vivo* mAb Clone GK1.5 (ELISpot)	BioCell	BE0003-1
Anti-mouse CD8a *In Vivo* mAb Clone 2.43 (ELISpot)	BioCell	BE0061
Anti-rabbit IgG, HRP-linked Antibody1 mL	Cell Signalling Technology	7074s
FITC anti-mouse H-2K /H-2D Antibody 0.5 mg/ml	Biolegand	114606
Human FcR blocking reagent 1mL	Miltenyi Biotec Ltd	130-059-901
ISOTON sheath fluid 1x 10L	Beckman Coulter	B51503
OneComp eBeads™ Compensation Beads	Invitrogen Europe Limited	01-1111-41
Pharm Lyse lysing buffer 100mL	BD Biosciences	555899
Prostate Specific Acid Phosphatase Recombinant Rabbit Monoclonal Antibody (ARC2124) 100 µL	Thermofisher Scientific	MA5-38108
Precision Protein™ StrepTactin-HRP Conjugate, 300 µl (WB)	Bio-Rad	1610380
Rabbit Anti-VINCULIN monoclonal Ab (WB)	Thermofisher Scientific	700062
Antibodies used for pentamer staining, immunostimulatory/ immune-inhibitory markers, whole blood staining, and MDSC staining are mentioned within the methodology sections.		

2.1.4. Reagent kits		
Product	**Company**	**Catalogue Number**
AP Conjugate Substrate Kit	Bio-Rad	170-6432
Cell Counting Kit (CCK-8)	Sigma- Aldrich	96992
Clarity Western ECL Substrate kit	Bio-Rad	170-5061
EZ-PCR Mycoplasma Detection Kit	Biological Industries	20-700-20
Foxp3 / Transcription Factor Staining Buffer Set	Thermofisher scientific	00-5523-00
KAPA Mouse Genotyping Kit	Merck Life Science UK Limited	KK7301

Mouse IFN-γ ELISpot BASIC kit (ALP)	Mabtech	3321-2A
PerFix-nc Kit (no centrifuge assay kit)	Beckman Coulter	B31168
QIAGEN Plasmid Mini Kit (25)	QIAGEN	12123
RNeasy Mini Kit (250)	QIAGEN	74106
Tumour Dissociation kit, Mouse	Miltenyi	130-096-730
QIAquick PCR Purification Kit	QIAGEN	28104
QIAquick Gel extraction kit	QIAGEN	28704

2.1.5. ELISA kits for PCa patients stress study		
Product	**Company**	**Catalogue number**
Human Interleukin 1 Beta	R&D System	DY201-05
Human intestinal fatty acid binding protein, iFABP	R&D System	DY3078
Human IL-6 (Interleukin 6)	R&D System	DY206-05
Tumor necrosis factor-alpha (TNF-alpha)	R&D System	DY210-05
C-Reactive Protein (CRP)-Human	R&D System	DY1707
Human Haptoglobin	R&D System	DY8465-05
Lipopolysaccharides (LPS) ELISA Kit	Abbexa	abx517692
Human TPH1 (Tryptophan Hydroxylase 1)	NOVUS Biological	NBP2-68157
DuoSet ELISA Ancillary Reagent Kit 2 1 Kit (for 5 Plates)	R&D System	DY008B

2.1.6. Peptides Adjuvants and Plasmids		
Murine and Human PAP Peptides	Genscript	
Adjuvants CAF®09b	Statens Serum Institut, Denmark	
CpG ODN 1826 VacciGrade 1mg	InvivoGen	vac-1826-1
CpG ODN 2395 VacciGrade 1mg	InvivoGen	vac-2395-1
Freund's adjuvant Incomplete (IFA)	Sigma-Aldrich	0151M8727
HHD-pCDNA3.1(-)	Scancell Ltd	
pLV-CMV-MCs-PGK-puro 10uG (vector)	Cellomics Technology LLC	LVR-1001
PAP_pcDNA3.1(1+)	Genscript	U928UGI200

pTVG4-hPAP Plasmid 0.8mL 0.2mg/mL	Douglas McNeel	UV17-PAP-FP--001
pLKO.1-puro with shRNA insert	Sigma-Aldrich	
pMD2.G -Envelope plasmid	Addgene	12259
psPAX2 – Packaginig plasmid	Addgene	12260

2.1.7. Enzymes/cells for transfection		
XL10-Gold Ultracompetent Cells, 10 x 100µL	Agilent	200315
Nhe I restriction enzyme	Promega	R6501
Xba I restriction enzyme	Promega	R6181
T4 DNA ligase and buffer	New England Biolabs	B0202/M0202

2.1.8. Buffers and gels	
Agarose gel	**For 1% gel**
Agarose Powder	1g
1x TAE buffer	Up to 100mL
Heat in the microwave to get a clear solution	
10% Resolving Gel	**For 1 gel**
dH2O	4mL
30% acrylamide mix	3.3mL
1.5MTris pH8.8	2.5mL
10% SDS	100 µL
10% APS	100 µL
TEMED	4 µL
5% Stacking Gel	**For 1 gel**
dH2O	4mL
30% acrylamide mix	3.3mL
1.5M Tris pH8.8	2.5mL
10%SDS	100 µL
10% APS	100 µL
TMED	4 µL
Complete T-cell media	**Concentrations**
RPMI 1640	500mL
FBS	10%
L-glutamine	1%
Penicillin/Streptomycin	2%
HEPES	1%
Fungizone	0.01%
2-mercaptoethanol (to be freshly added)	50mM
LB Agar for bacterial cultures	**For 1L**
LB Agar powder	32g
ddH2O	Up to 1L
Autoclave for 15 minutes	

Chapter 2: MATERIALS AND METHODS

LB BROTH Miller	**For 1L**
LB Miller powder	1g
ddH2O	upto 1L
Autoclave for 15 minutes	
Sodium Citrate antigen retrieval buffer pH6.0	For 1L
Sodium Citrate trisodium dihydrate	2.94g
dH2O	up to 1L
TWEEN 20	0.5 mL
Adjust to pH 6.0 with HCl	
TRIS-Acetate EDTA (TAE) BUFFER	**FOR 50x**
1 M Tris base	242g
Disodium EDTA	18.61g
Acetic acid, Glacial	57.1mL
ddH2O	Up to 1L
TRIS-EDTA (TE) BUFFER	**FOR 500 ML**
1 M Tris pH 8	5 mL
0.5 M EDTA pH 8	1 mL
ddH2O	Up to 500mL
TRIS-BUFFERED SALINE (10 X TBS)	**FOR 1 L**
Trizma base	24.2 g
NaCl	80 g
ddH2O	Up to 1 L
Tris-Buffered Saline with Tween (TBST)	
10 X TBS	100 mL
TWEEN 20	0.5 mL
ddH2O	900 mL

2.1.9. Laboratory Plastics, Sharps and Glass Ware	
Products	**Company**
0.22 µm syringe filter	Sartorius
0.45 µm syringe filter	Sartorius
25mm Gauge needle	BDmicrolance
40 µm nylon strainer	Greiner
70 µm nylon strainer	Greiner
Cell culture flasks (T25, T75, T175)	Sarstedt, UK
Conical flasks (50 mL,100 mL)	Pyrex
Cryovials	TPP
ELISpot plates	Millipore
Eppendorf tubes (0.5 mL, 1.5 mL, 2 mL)	Sarstedt, UK
FACS tubes	Tyco healthcare group
Falcon tubes (50 mL, 15 mL)	Sarstedt, UK
Falcon® Round-Bottom Polystyrene 5 mL tubes	STEMCELL
Filter tips (0.5-10µL, 2-20µL, 20-200µL, 200-1000µL)	Greiner bio-one/ Sarstedt
Flat-bottom culture plates (6, 24, 96-well)	Sarstedt, UK
Glass coverslips	SLS
Glass slides	SLS
Leucosep tube 50 mL	Greiner
Micro tips (0.5-2µL, 10µL,20µL,100µL,200µL and 1000µL)	Sarstedt, UK
Microtome blade MX35 Ultra	Thermo Scientific
Microvette 100 Serum 100 µL tubes 20.1280	Sarstedt
Multichannel pipette	Sartorius
Magnetic cell separators MACS	Miltenyi Biotech
Nitrocellulose blotting membrane 0.22µm	GILSON scientific
Pasteur pipettes	Sarstedt, UK
Petri dishes	Sarstedt, UK
Pipettes (5mL, 10mL, 25mL)	Sarstedt, UK
RNAse Free Syringe with 20G needle	Sarstedt, UK
Round Bottom cell culture plates 96 well	Sarstedt, UK
Scalpels	SLS (Swann Morton)

Syringes (10mL,20mL,50mL)	Becton Dickenson
Tefzal tube (Versilon)	Saint Gobain
Universal tubes (20mL)	Greiner
Bedding and food for preclinical models	**Company**
Chew sticks	Datesand Ltd, UK
Envigo Global Certified Diet	Envigo Laboratories UK Ltd
Sizzle-nest	Datesand Ltd, UK
Techniplast Sealsafe Plus cages and furnished with corncob bedding	International Product Supplies Ltd,UK
Equipment	**Company**
96-well plate reader	Tecan
Analytical balance	Fisher Scientific
Autoclave	Rodwell
Bacterial cell culture plate incubator 37°C	Genlab
Bacterial Cell Orbital Incubator 37°C	Stuart
Centrifuges	Sanyo
Digital tissue section bath	CellPath
Haemocytometers	SLS
Class II safety cabinets	Walker
ELISpot plate reader	Cellular Technology Limited
Flow cytometer	Cytek Aurora
Freezer -20°C	Lec
Freezer -80°C	Revco/ Sanyo
Heat blocks	Lab-Line
Ice Machine Scotsman - AF200	Scotsman
Leica wax microtome	Leica Microsystems
Leica SP5 Confocal	Leica Microsystems
Light microscope	Nikon/Olympus
Microcentrifuge	MSE
Mo FloTM cell sorter	Beckman Coulter

Mixer/agitator	Intelli-mixer (ELMI)
Nanodrop 8000 Spectrophotometer	Thermo Scientific
NanoDrop ND UV-VIS Spectrophotometer version 3.2.1	Thermo Scientific
NucleoCounter® NC-250™	Chemometec
Pipettes and multichannel pipettes	Gilson, Star Labs, Eppendorf
Plate rocker	VWR, Stuart
pH meters	Metler Toledo
Refrigerators 4°C	Lec
Slide-drying hot plate	CellPath
Sonicator	VWR
Speedvac - vacuum drier	Effendroff
Thermo Excelsior AS tissue processor	Thermo Scientific
Thermo Mixer	Effendroff
Tissue culture incubator 37°C, 5% CO2	Sanyo, Binder
Ultracentrifuge Optima TLX	Beckman
Ultrapure water dispenser	Barnstead
Viral cell culture incubator 37°C, 5% CO2	IncuSafe
Vortex	Scientific Industries
Water baths	Clifton
Softwares	
ELISpot CTL ImmunoSpot 7.0.34.0 software	Cellular Technology Limited
GraphPad Prism 10.2	Graph Pad software
Kaluza 1.3 version	Beckman Coulter
ImageJ 1.53t w/Adiposoft 1.16	
SnapGene Viewer 5.2.2	GSL Biotech LLC
FCS Express Data Analysis Version 7.14.0020	Cytek Aurora spectral flow cytometer

Chapter 2: MATERIALS AND METHODS

2.2. Methods

2.2.1. Cell culture

2.2.1.1. Thawing, sub-culturing, and freezing of cell lines.

The cell lines (Table 2.1) used in this project were handled inside the cell culture hood using aseptic techniques. Cryovials of cells were taken from -80°C freezers and thawed quickly in the cell culture hood. The content of the vial was then transferred into a centrifuge tube containing 9mL complete culture medium and spun at 300g for 5 minutes. The supernatant was discarded, and cell pellets were resuspended with the complete medium and dispensed into a 25 cm^2 or a 75 cm^2 culture flask. Cells were incubated at 37°C, 5% CO_2 in air. All cell lines used for this study had adherent growth properties.

When 70%-90% confluency was reached, cells were sub-cultured. Cell culture medium was removed, and cells were washed with sterile PBS, to remove all traces of serum that contains trypsin inhibitors. Trypsin-EDTA solution was added to the cells and incubated at 37°C until the cells detached from the surface. 5-10mL of complete growth media was added onto the cells to neutralise the Trypsin-EDTA and the mixture was transferred into a 15 or 50mL falcon tube and centrifuged at 300xg for 5 minutes at toom temperature. Following centrifugation, the supernatant was discarded, and cell pellets were resuspended in fresh media. Cells were either re-seeded or counted for subsequent use. Cells to be frozen were resuspended in freezing media composed of 90% FCS and 10% DMSO. Usually, $1x10^6$ cells are resuspended in 1mL of freezing media, transferred into a cryogenic vial, labelled, and stored frozen at -80°C.

To harvest the cells for mRNA and protein expression analyses, 2 - $5x10^6$ cells were transferred into a 1.5mL microtube and centrifuged as previously described; the supernatant was discarded, and the cell pellets were resuspended in DPBS to wash off any residual medium. The cell suspension was then centrifuged again, the supernatant carefully removed, and the cell pellets were then stored at -80°C until further downstream processing.

Cell lines	Characteristics				Obtained from	Complete growth medium
	Organism	Disease	Tissue of origin	Growth Properties		
TRAMP C1	Mouse, transgenic (Strain: C57BL/6)	Adenocarcinoma	Prostate	Adherent	ATCC	Dulbecco's modified Eagle's medium (high glucose) + 10% FCS+ 2mM L-glutamine
TRAMP C2				Adherent	ATCC	
DU-145	Human	Carcinoma	Prostrate, derived from metastatic site, brain	Adherent	ATCC	Minimum Essential Medium (MEM)+ 10% FCS+ 2mM L-glutamine +MEM non essential amino acid solution 5%
LNCap			Prostate, derived from metastatic site -left supraclavicular lymph node	Adherent	ATCC	RPMI-1640 Medium+10% FCS+ 2mM L-glutamine
HEK293t			Kidney of a human embryo	Adherent	ATCC	Dulbecco's modified Eagle's medium (high glucose) + 10% FCS+ 2mM L-glutamine

Table 2.1: List of cell lines used in this research and their properties. *This table summarizes the murine and human cell lines utilized in the research. The HEK293t cell line is the only non-cancerous line, while all other cell lines are prostate cancer cell lines.*

2.2.1.3. Cell counting

Cells were counted using a haemocytometer for subculturing purposes. After wiping the haemocytometer with ethanol, a coverslip was positioned in the middle. To obtain a 1:10 dilution, 10µL of cell suspensions were mixed with 90µL of trypan blue. The counting chambers were filled with 10µL of the dilution and viewed under the light microscope using 10x magnification. Live cells exclude trypan blue and appear clear when viewed under the microscope while dead cells take up the dye and appear blue. Viable cells were counted in the four large squares which were equally divided into 16 small squares. The number of cells per mL was calculated according to the following formula.

Concentration = (Total number of cells counted/number of large squares counted) x 10 (dilution factor) x 10^4

Cells obtained from human PBMCs and animal tissues such as spleens, lymph nodes, and tumours were counted using the NucleoCounter to obtain more precise cell concentrations and percentages of viability. The cell suspensions were made by resuspending the cell pellets in 5 mL media (if less pellet, less volume of media was used). To obtain 1:10 dilution, 10µL of cell suspensions was mixed with 90µL of fresh media in a 500µL Eppendorf tube. 50µL of diluted cell suspension was mixed with 2.5µL of 'Solution-18'. 10µL of this mixture was poured into the counting slide, and cell viability and count were measured by the NucleoCounter. Solution-18 contains two dyes; acridine orange, which stains all nucleated cells, and DAPI, which stains non-viable cells. The NucleoView software automatically calculated the cell concentration and viability percentage. The cell count (of viable cells) obtained was multiplied by the dilution factor to compensate for the dilution and calculate the number of cells per mL.

2.2.1.3. Mycoplasma testing

Mycoplasma testing was carried out using the EZ-PCR Mycoplasma Detection Kit following the manufacturer's protocol. 1mL of cell culture medium from each cell line to be tested was transferred under sterile conditions to 1.5mL microtubes and centrifuged at 300 x g for 2 minutes at room temperature to remove cellular debris. To sediment the mycoplasma, the supernatant was poured into a fresh microtube and centrifuged at 16,900 x g for ten minutes at 20ºC. The supernatant was decanted, and the pellet was resuspended in 50µL of buffer solution and heated for 3 minutes at 95ºC using a heating block. The reaction mixture was prepared by mixing 10µL of the reaction mix, 1µL of internal control DNA, 1µL of internal control primers, and 29µL of PCR-grade water added with 5µL of the test sample. The positive control sample in the kit was prepared by mixing it with the reaction mix. A negative control for the experiment was prepared by mixing 1µL of PCR-grade water with the reaction

mix. Samples and controls were placed in a thermal cycler with the following conditions: 94ºC for 30 seconds; 35 cycles of 94ºC for 30 seconds, 60ºC for 120 seconds, and 72ºC for 60 seconds; 94ºC for 30 seconds, 60ºC for 120 seconds and 72ºC for 5 minutes. Once the PCR amplification was completed, amplified products were analysed by 2% agarose gel -stained with SYBR Safe DNA Gel Stain- electrophoresis with a 100bp DNA ladder. The gel was run at 90v until the optimal parting of the bands was achieved. The bands were visualised using a chemiluminescent gel imaging system. Mycoplasma negative samples showed a single 357bp band, whereas mycoplasma positive samples showed a 357bp and a 270bp band like positive control.

2.2.2. Genetic modification of target cell lines

2.2.2.1. HHDII transfection using lipofectamine 3000 reagent.

HHDII plasmids were kindly provided by Scancell Ltd, UK as bacterial glycerol stock and were bulked in LB broth containing 100µg/µL of ampicillin. Plasmid was isolated using QIAGEN Plasmid Midi Kit as described in section 2.2.2.2.5.

For the transfection of DU145 and HEK293t cells with HHDII plasmid Lipofectamine 3000 Transfection Kit was used. Cells were sub-cultured in a 6-well plate, transfection was carried out when the cells were approximately 70% confluent. 500µL of Opti-MEM Medium and 20µL of Lipofectamine 3000 Reagent were added to a 1.5mL microcentrifuge tube and mixed well. 500µL of Opti-MEM, 20µL of P3000 reagent, and 10µg of HHDII plasmid were added to a separate 1.5mL microcentrifuge tube and vortexed for 3 seconds. The contents from both tubes were mixed in a 1:1 ratio and incubated for 15 minutes at room temperature. 250µL of this mixture was added dropwise to cells to be transfected, while the control wells were left untouched. Cells were incubated for 16 hours at 37°C 5% CO_2 in air; then, followed by replacing the media with selection media containing 1mg/mL G418. Transfection was confirmed by flow cytometry analysis.

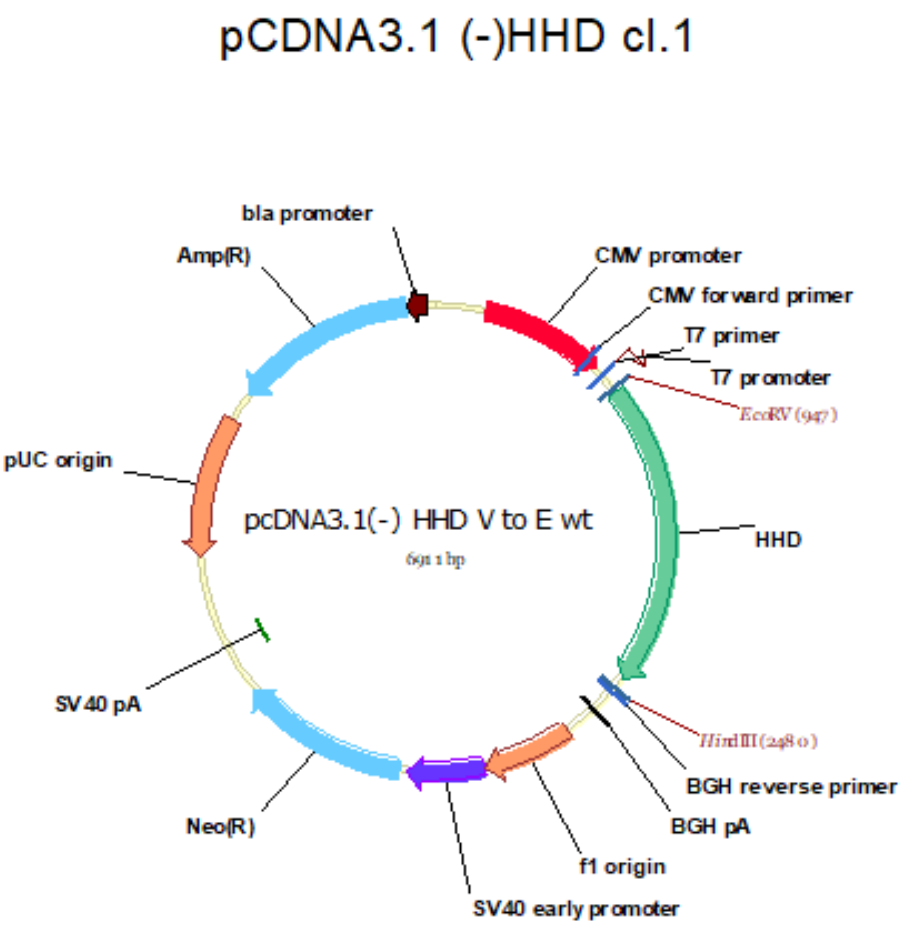

Figure 2.1. pCDNA3.1(-) HHD map. *Map illustrating cDNA encoding HHD (1458bp) inserted into the EcoRV and HindIII restriction sites of the mammalian expression vector pCDNA3.1(-).*

2.2.2.2. Human PAP knock-in

Codon optimised Human PAP Plasmid was obtained from Genscript in a PAP pcDNA3.1(1+) vector between the cloning site BamHI and EcoRI. The human PAP gene was subcloned into Lenti Viral vector (pLV-CMV-MCs-PGK-puro) using NheI and XbaI restriction enzyme and T4DNA ligase. The ligation mixture was transformed into XL-10 gold ultracompetent bacterial cells and grown in selection media (100µg /mL of ampicillin). Transformed bacterial cells were cloned, and suitable colonies with plasmid were bulked in LB growth media containing antibiotic selection to isolate an adequate amount of plasmid using the Qiagen Plasmid isolation kit. The isolated plasmid size was confirmed by agarose gel

electrophoresis, and the orientation and the sequence integrity of the insert were confirmed by sanger sequencing. Isolated plasmids were stored at -20°C for further use.

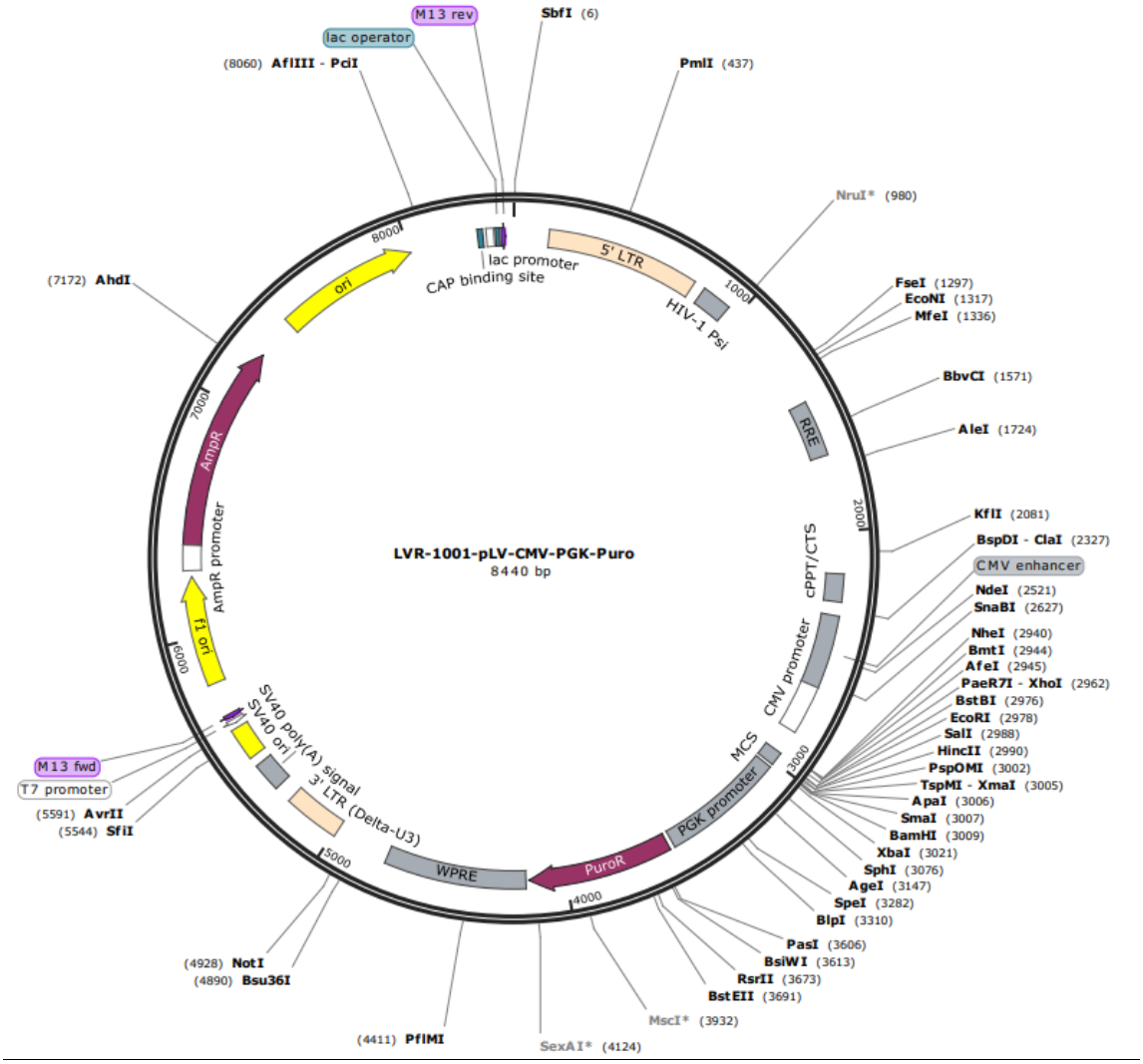

Figure 2.2: pLV-CMV-MCs-PGK-puro vector map. *The vector contains a lentiviral backbone with the human cytomegalovirus promoter driving the expression of a multiple cloning site, followed by a puromycin resistance gene cassette, which is driven by the PGK promoter. The PAP gene was inserted between the NheI and XbaI restriction sites.*

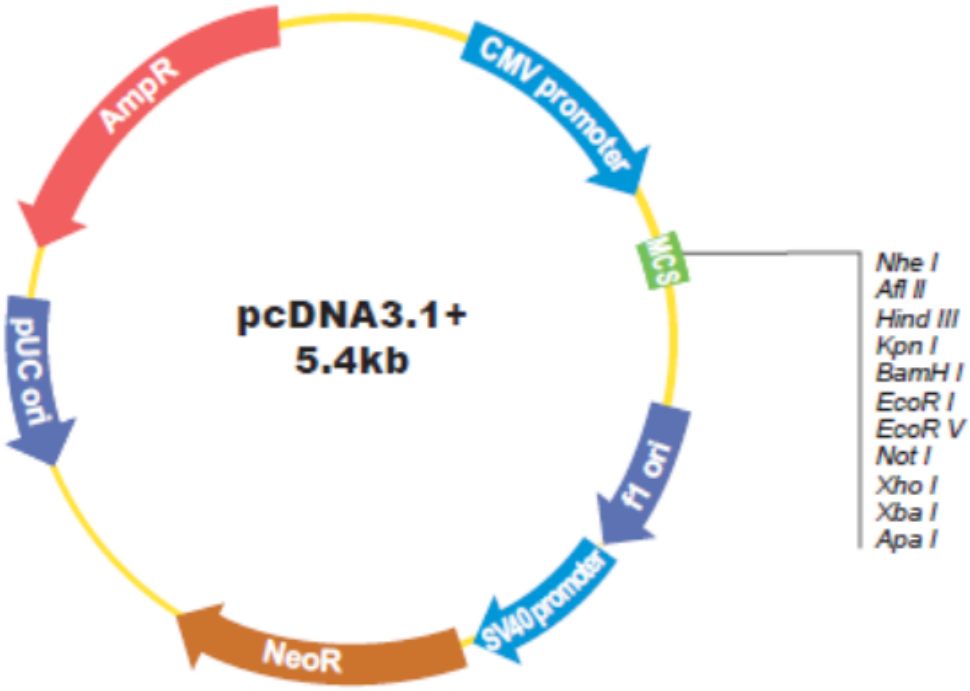

***Figure 2.3: PAP_pcDNA3.1(1+) map**. This vector is a mammalian expression plasmid featuring a CMV promoter, a multiple cloning site in the forward (+) orientation, and a Neomycin resistance gene for the selection of stable cell lines. The human PAP plasmid was inserted between the BamHI and EcoRI restriction sites within the multiple cloning sites.*

2.2.2.2.1. Restriction digestion

PAP_ pcDNA3.1(1+) and PLenti vector were diluted with nuclease-free water to obtain a concentration of 100ng/µL. Restriction digestion mix was prepared by mixing 16.3µL of nuclease-free water, multicore restriction enzyme 10x buffer, and 0.5µL each of restriction enzymes Xba-I and Nhe-I. 1µL of diluted plasmid and empty vector were mixed with the restriction digestion mix in a separate centrifuge tube, and incubated in a water bath at 37^0C for one hour. The digested samples were run on a 1% agarose gel to confirm the digestion of the PAP gene from pcDNA3.1(1+) and linearization of pLenti puro empty vector at cloning sites Nhe-I and Xba-I with a 1kb DNA ladder running parallel to the sample. This was identified according to the desired size of the band obtained on the agarose gel.

2.2.2.2.2. Plasmid extraction from the gel using QIAquick gel extraction kit.

pLenti puro empty vector and PAP DNA fragments were excised from the gel using a clean scalpel and collected in a 1.5 mL centrifuge tube. The gel slices were weighed and dissolved in 3 volumes of Buffer QG by heating at 50^0C for 10 minutes. One gel volume of 100% isopropanol was added to the dissolved gel, passed through the QIAquick spin column, (centrifugation speed here), and discarded the flow through. The column was washed by adding buffer PE and centrifuging at 17,900 x g for 30 seconds. Any residual buffer was removed by centrifuging the column at high speed for one more minute at room temperature. PAP DNA and empty vectors were eluted by adding 20µL of buffer EB, centrifuging at 17,900 x g for one minute. The DNA and empty vectors were quantified using Nanodrop. PAP DNA nucleotide sequence was confirmed by Sanger sequencing.

2.2.2.2.3. Ligation

The digestion of PAP DNA and pLenti puro empty vector using restriction digestion enzymes as described above results in a single-stranded overhang also known as 'sticky ends' on the digested end (Nhe-I and Xba-I) of DNA fragments. Using DNA ligase enzyme PAP DNA overhangs were ligated into the compatible sticky ends of the pLenti puro vector. The quantity of insert DNA needed for the ligation was calculated using the following formula.

(Concentration of Vector x Kb size of Insert)/ Kb size of the vector x molar ratio.

The molar ratio is the ratio of insert: vector to be used. Two different inserts: vector molar ratio (2:1 and 3:1) ligation mixture was prepared by mixing the calculated volume of vector and insert with 1µL of 10x ligation buffer and 0.5µL of DNA ligase, making up the volume to 10µL using nuclease-free water. This mixture was incubated overnight at 4^0C.

2.2.2.2.4. Bacterial transformation

The ligated mixture was transformed into XL-10 Gold Ultracompetent bacterial cells. Bacterial cells were obtained from 'Agilent' and were thawed on ice. 4µL of the β-Mercaptoethanol was added to 100µL of bacteria by swirling gently, and the mixture was incubated on ice for 10 minutes. 2µL of ligation mixture was added to the bacteria, mixed by swirling the tube gently, and incubated on ice for 30 minutes, followed by heat-pulsing the tubes in a 42°C water bath for 30 seconds. 900µL of preheated (37^0C) SOC medium was added to the tubes and incubated at 37°C for 1 hour with shaking at 225-250 rpm. 100µL of the transformed mixture was then plated on LB agar plates containing ampicillin 100µg/mL, incubated at 37^0C overnight. Colonies were picked up and grown in 100 mL LB miller media containing ampicillin 100µg/mL at 37°C with shaking at 225 rpm overnight. The bacterial population of each clone was collected, and plasmids were isolated. Glycerol stocks of each bacterial colony were prepared by mixing an equal volume of bacterial culture and 50% glycerol and stored at -80°C.

2.2.2.2.5. Plasmid isolation

The bacterial glycerol stock was bulked up in 100mL of Luria Broth with 100µg/mL ampicillin by incubating overnight at 37°C in a rotary incubator at 225rpm. The plasmid was isolated using the QIAGEN Plasmid Midi Kit, according to the manufacturer's protocol. All buffers used for plasmid isolation were provided with the kit. Bacterial culture was harvested by centrifuging at 3000 x g for 30 mins at 4°C. Cell pellets were resuspended in the PE buffer and mixed with lysis buffer to lyse the cell pellet. The clear supernatant of cell lysate was allowed to flow through an equilibrated QIAGEN tip, washed twice with washing buffer. DNA was eluted with eluting buffer, precipitated by adding the required volume of isopropanol, washed with 70% ethanol once, and air dried. DNA was then redissolved in 30-50µL of TE buffer, pH 8.0. The DNA concentration was estimated by measuring the absorbance of 1µL of the sample at 260/280 nm using the NanoDrop 8000 spectrophotometer. The digestion mix of isolated plasmids was run on 1% agarose gel to identify the size of the plasmid, and

Sanger sequencing was also carried out. For long-term storage plasmid glycerol stocks were prepared by mixing 500µl of expanded bacterial culture with 500µL of sterile 30% glycerol in a cryogenic vial and stored at -80ºC.

2.2.2.2.6. Antibiotic titration for the positive selection of transfected or transduced cells

The antibiotic titration was carried out in the target cells being modified either to induce PAP/HHDII antigen expression or knock down PAP antigen expression -as detailed in chapter 3, table 3.1-, prior to the transfection/transduction protocol. This was done to determine the lowest lethal antibiotic concentrations that can kill 100% non-transfected cells, an antibiotic titration was performed in a 24-well plate. Each concentration was tested in duplicate, with a negative control consisting of cells grown without antibiotics. When the cells were about 70% confluent the media was replaced with selection media and cell death was monitored daily until complete cell death observed for a week. The effective lethal dose determined at this step used for further antibiotic selection processes.

2.2.2.2.7. Lenti-viral transduction

Transfection of packaging cells:

HEK293t cells were used as packaging cells to produce viral particles. HEK293t cells were seeded in a T-25 culture flask. Cells were transfected at 80% confluency using the lipofectamine 3000 kits following the manufacturer's protocol. 20µL of Lipofectamine 3000 reagent was mixed with 500µL Opti-MEM I medium in a 1.5mL microtube. In a separate microtube tube, 8µg target plasmid, 6µg packaging plasmid (psPAX2), and 2µg envelope plasmid (pMD2.G) were mixed with 500µL Opti-MEM containing 12µL P3000 reagent. The content of each tube was mixed in a 1:1 ratio and incubated for up to 20 minutes at room temperature. After the incubation 1mL of the mix was added to the HEK293t culture flask, and incubated overnight at 37°C, 5% CO_2 in the air. The day of transfection was counted as Day 1. The following day, the media was replaced with 5mL of fresh culture media.

Chapter 2: MATERIALS AND METHODS

Virus Collection:

On day 3 fraction-1 media was collected from the cell culture flask, sterile filtered through a 0.45µm syringe filter aliquoted to 1mL cryovials and stored at -80^{0}C. The culture flask was replaced with 5mL of fresh media, and on day 4, fraction-2 viral particles were collected in the same manner.

Target cell transduction:

Target cells (DU145 HHDII and HEK293t HHDII) were seeded in 6 well plates. At 70% confluency, the media was replaced with 1mL of complete medium containing hexadimethrine bromide at a final concentration of 8µg/mL and 1mL of viral particles per well; one of the wells in the 6-well plates received the lentiviral particles from fraction-1, whereas the other well was received the viral particles from fraction-2. Negative control wells received 1mL of complete medium without lentiviral particles. After 15 hours incubating at 37°C and 5% CO_2, the media were replaced with 2mL of selection medium containing 1µg/mL puromycin. The transduced cells were then expanded, and transduction was confirmed by qPCR and western blot analysis.

2.2.2.3. Murine and human PAP knockdown

MISSION shRNA plasmids to knock down murine and human PAP were obtained from SIGMA as bacterial glycerol stock. Human prostate cancer cell line LNCap, murine prostate cancer cell line TRAMP C1, and TRAMP C2 cells which naturally express PAP were selected as target cell lines for the gene silencing. The glycerol stocks were grown in 100mL of Laurie Broth media with 100µg/mL ampicillin, incubating overnight at 37°C with shaking at 225 rpm. The plasmid was isolated using the QIAGEN Plasmid Midi Kit as described in section 2.2.2.1.5. Knockdown of the gene expression by short hairpin (sh) RNA was carried out by the lentiviral transduction method (section 2.2.2.1.7). Viral particles of target plasmids were generated, which were used to infect the above-mentioned human and murine cell lines. The transduced cells were further selected using their respective media containing puromycin (1µg/mL).

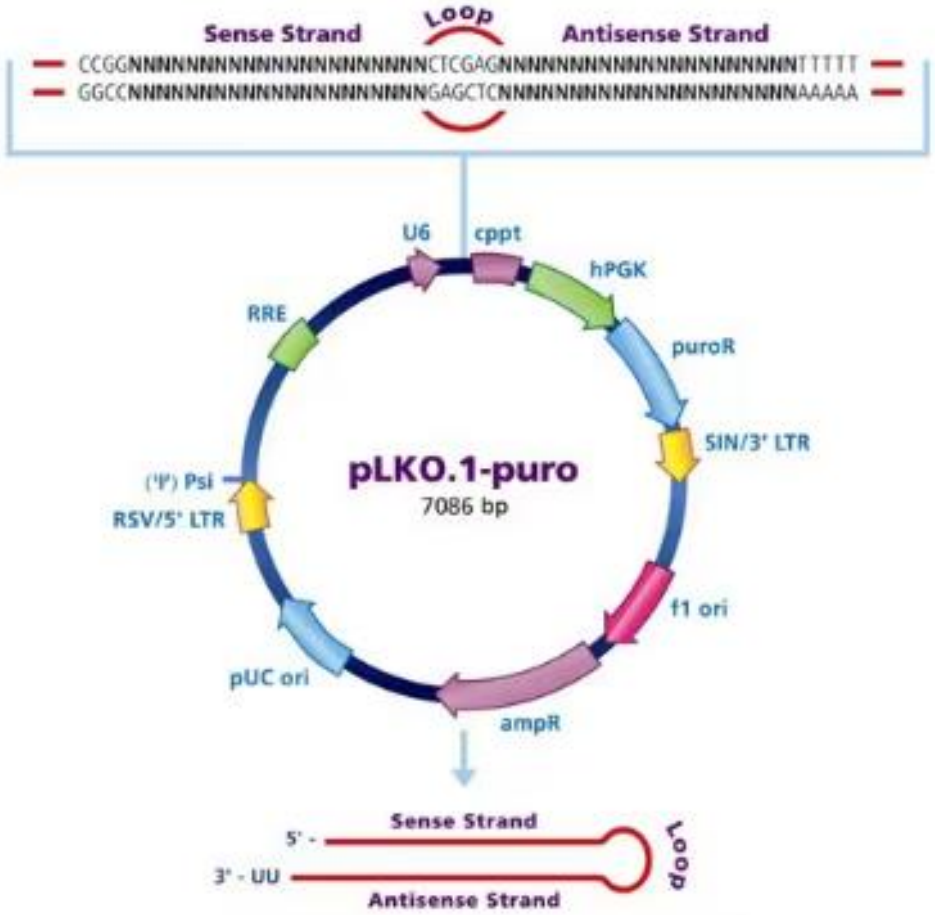

Figure 2.4: Vector map pLKO.1-puro. *The shRNA plasmids for murine and human PAP knockdown were obtained from SIGMA and are based on the pLKO.1-puro lentiviral vector, which includes a puromycin resistance gene for selection of successfully transduced cells and a bacterial ampicillin resistance gene for bacterial selection*.

2.2.2.3.1. Manual clone isolation

Transduced cells were cloned to obtain cell populations with homogeneous protein expression levels. After counting, cell suspension was diluted to a density of 33 cells/mL of complete growth medium. Using a multichannel pipettor, 100µL of the cell suspension was transferred into each well of 96-well tissue culture plate, incubated in a 37°C, 5% CO_2 incubator for 2-3 weeks until the single cell colonies were able to visualise under a

microscope, clonal populations were further expanded to assess the PAP expression by qPCR.

2.2.2.4. CRISPR-Cas9 technique to knockout β2M gene in TRAMPC1 cells

2.2.2.4.1. Transfection

Three different TRUE Guide Synthetic Guide RNAs (sgRNA 1,2 and 3) (Table 2.2) were, reconstituted in 1x TAE buffer to obtain 100 µM solution and the sgRNA forward and reverse primers were reconstituted and diluted in nuclease-free water to a final concentration of 100 pmol/µL. gRNA mouse Rosa 26 was used as positive control reconstituted in TAE buffer to obtain a 3nM solution.

CRISPR/Cas9 reagents		
Target gene: B2M	**Company:** Invitrogen/ ThermoFisher Scientific	
Product	**Sequence**	**Catalogue number**
TrueGuide Synthetic sgRNA (1)	U*U*C*GGCUUCCAUUCUCCGG	CRISPR42443_SGM
TrueGuide Synthetic sgRNA (2)	G*G*A*UUUCAAUGUGAGGCGGG	CRISPR42460_SGM
TrueGuide Synthetic sgRNA (3)	G*G*C*GUAUGUAUCAGUCUCAG	CRISPR42448_SGM
TrueCut Cas9 Protein v2	NA	A36496
Lipofectamine CRISPRMAX Cas9 Transfection Reagent	NA	Cmax00001
GeneArt Genomic Cleavage Detection Kit	NA	A24372
TrueGuid sgRNA Positive Control, Rosa26	NA	A35525

sgRNA forward and reverse Primers for CRISPR/Cas9			
Primer Name	**Company**	**Forward sequence**	**Reverse sequence**
B2M sgRNA (1)	Eurofins	GAGGGGCACAGTTCTTGAGAG	TCAGTCTCAGTGGGGGTGAA
B2M sgRNA (2)	Eurofins	TTTCATCTGTCTTCCCCTGTGG	ACCACAGATCAGTCTTTTGGGG
B2M sgRNA (3)	Eurofins	GTGGGTAGACTTTGGGGGAA	TGGAGCGTCCAGAAAGTAAGG

Table 2.2. *List of CRISPRMAX Reagents and primers used in transfection protocol for synthetic gRNA.*

TRAMP C1 cells were cultured in 24 well plates DMEM high glucose media with 10%FCS, once the cells reached 50% confluency (recommended confluency was 30-70%), cells were transfected with CRISPR constructs according to CRISPMAX transfection protocol- transfection mix prepared by incubating diluted CRISPRMAX reagent in Opti-MEM medium with a solution containing Cas9 nuclease, gRNA solution with Cas9 plus reagent followed by incubation at room temperature for 10 minutes. This complex was then added to TRAMP C1 cells and incubated for 2 days 37^0C under 5% CO_2 growth condition. After two days, cells were trypsinized and divided into two portions; one portion of the total cell population was put back in the culture, while the other was used to perform genomic cleavage detection assay to detect locus-specific cleavage of genomic DNA using the GeneArt Genomic Detection Kit.

2.2.2.4.2. Cleavage assay

For performing the cleavage assay, cells were washed with PBS, lysed using lysis buffer, and DNA extracted using PCR thermal cycle under the following parameters: 68°C for 15 minutes, 95°C for 10 minutes, and 4°C hold. Extracted DNA was amplified using Amplitaq Gold 360 MasterMix, and suitable reverse and forward primers (Table 2.2) under the following PCR setting.

Stage	Temp	Time	Cycles
Enzyme activation	95°C	10	1x
Denature	95°C	30	40x
Anneal	55°C	30	
Extend	72°C	30	
Final extension	72°C	7	1x
Hold	4°C	Hold	1x

The PCR products were then verified using 2% Agarose gel by loading 3µL of PCR product with 10µL water at 75v. A 100 bp DNA ladder was run in parallel to assess the DNA

concentration by visual inspection. A single band with an intensity like 400 bp was crucial to obtain accurate cleavage detection. The PCR products of cells that showed a single band at 400 bp were further proceeded to the denaturing and re-annealing step.

For denaturing and re-annealing, 3µL of PCR products were mixed with 1µL of detection reaction buffer, in a PCR tube making up the volume to 9µL. PCR tubes were briefly centrifuged to remove any bubbles and bring all samples down, then placed onto a thermal cycler with the heated lid to run the program using the following parameters.

Stage	Temperature	Time	Temperature/time
1	95^0C	5 min	
2	95^0C -85^0C		-2^0C/sec
3	85^0C -25^0C		-0.1^0C/sec
4	4^0C		Hold

Following the completion of the annealing reaction, samples immediately proceeded to enzyme digestion where the heteroduplex DNA containing the insertion, deletion, or mismatched DNA (indel) is cleaved by the detection enzyme, allowing for quantification of the percentage of gene modification. For that, 1µL of the detection enzyme was added to the test samples and incubated for one hour at 37^0C. After the incubation, tubes were vortexed briefly and verified by 2% agarose gel electrophoresis at 75v. Bands were visualised using a gel imaging system and the relative proportion of DNA contained in each band was determined by ImageJ software. Cleaved samples produced two cleavage products of 225 and 291 bp in size. Cleavage efficiency was calculated using the following equation:

Cleavage Efficiency = 1- [(1-fraction cleaved)1/2]

Fraction cleaved = Sum of cleaved band intensities / (Sum of the cleaved and parental band intensities)

The cleaved transfected cells were cloned (section 2.2.2.3.1.) to identify the homozygous mutation of the gene B2M. DNA was extracted from the clones and amplified using Amplitaq

Gold 360 MasterMix as described above. PCR products were purified using the QIA quick PCR purification kit following the manufacturer's protocol.

2.2.2.4.3. PCR purification

One volume of the PCR reaction was mixed with five volumes of the buffer provided in the QIAquick PCR purification kit, loaded to the QIAquick column, and centrifuged at 17,900 x g for 30 seconds. The column was washed with wash buffer and centrifuged to discard the flowthrough. Additional centrifugation of the column is carried out to remove any residual wash buffer. Then the column was transferred to a clean 1.5mL microcentrifuge tube and DNA was eluted using 30-50uL of eluting buffer. DNA was quantified by nanodrop and sent for sequencing to identify the mutation.

2.2.2.4.4. Sequencing

PCR products were diluted with nuclease-free water to get a concentration of 10ng/µL. Forward and reverse primers to the appropriate sgRNA were diluted to obtain a concentration of 3.2pmol/µL. 5µL of each PCR product and their primers were sent to Source Biosciences for sanger sequencing. Sequence alignment was matched through the clustal omega website, and samples that showed homozygous mutation were expanded further. In addition to the sequencing, B2M mutation was confirmed by flow cytometry staining (section 2.2.3.1) using FITC anti-mouse H-2K /H-2D Antibody.

2.2.2.5. Assessing the expression of PAP and MHCs (MHC-I/ HLA-A2)

A million HHDII transfected and non-transfected human cells were transferred to flow cytometry sample tubes and washed with 2mL PBS per tube. The supernatant was discarded, and nonspecific binding was blocked by incubating the cells with 1µL of Fc blocking reagent in 50µL FBS for 15 minutes at 4^0C. The cells were incubated with 5µL/test APC conjugated anti-human HLA-A2 Antibody for 30 minutes at 4^0C. After the incubation, cells were washed with 2mL PBS, centrifuged at 400 x g for 5 minutes, and the supernatant

was discarded. Cells were then resuspended in isoton sheath fluid, analysed by flow cytometer. For murine cells, - TRAMP C1 and TRAMP C2 - MHC class-I expression was analysed similarly replacing the HLA-A2 antibody with FITC conjugated anti-mouse H-2K^{b}/H-2Db antibody at a concentration of 1.0µg/million cells.

2.2.2.6. Assessing the expression of the PAP gene at mRNA level

2.2.2.6.1. RNA extraction

Up to 5x10^{6} cells were pelleted by centrifugation at 300 x g for 5 minutes at room temperature. Pellets were washed with DPBS to remove any residual media. Total RNA was extracted using QIAGEN's RNeasy Mini Kit following the manufacturer's protocol. All buffers used were provided in the kit. Pellets were disrupted with 350µL of Buffer RLT (with 1µg/mL β mercaptoethanol). The cell lysate was homogenized by passing through a 29-gauge needle 4-5 times; they were then mixed with 1 volume of 70% ethanol and transferred to RNeasy spin columns placed inside 2mL collection tubes. The columns were centrifuged at 8,000 x g for 15 seconds at toom temperature and the flow-through was discarded. 350µL of Buffer RW1 followed by 500µL of Buffer RPE twice were added to each column and centrifuged at the same parameters. The flow-through was discarded, and the columns were placed in 1.5mL collection tubes, RNA was eluted using 30µL of nuclease-free water. Elutes were stored at -80ºC after RNA, purity check, and quantification were done using NanoDrop 8000 spectrophotometer. The RNA was considered pure if the 260/280 ratio was between 1.8 and 2.2 which was automatically determined by the spectrophotometer.

2.2.2.6.2. cDNA synthesis

cDNA was synthesised from the RNA eluates by reverse transcription. 2µg of RNA in nuclease-free water (final volume 9µL) and 1µL of oligo dT were heated at 70°C for 5 minutes and placed on ice immediately after incubation. To this, a reaction mix containing 5µL of RT buffer, 1µL of reverse transcriptase enzyme, 1µL of dNTPs 0.7µL of RNasin, and 7.3µL of

nuclease-free water was added and incubated at 40°C for an hour. The reaction was heated at 95°C for 5 minutes to inactivate the reaction and frozen immediately at -20°C.

2.2.2.6.3. RT-PCR

Primer efficiency

Primers for RT-PCR			
Primer Name	**Company**	**Forward sequence**	**Reverse sequence**
hGUSB	Sigma Aldridge	ACTGAACAGTCACCGAC	AAACATTGTGACTTGGCTAC
hPAP		GAGAAGGGGGAGTACTTTG	CTGTTTGTGGTCATACACTC
mPAP (M_Acpp_1)		AAAAGCTGGTCATGTATTCC	GAGGCAGAACTCCATTATA
mGAPDH		ACACATTGGGGGTAGGAACA	AACTTTGGCATTGTGGAAGG
HHDII	Eurofins	ATGAGTATGCCTGCCGTGTG	CCGGGACACGGATGTGAAG

Table 2.3*. List of primers used for the qPCR analysis of the expression of the PAP gene in murine and human cell lines.*

The quantitative RT-PCR method was used to assess the expression of the PAP gene at the mRNA level. For the normalisation of qPCR quantification, reference genes GAPDH -for murine PAP expression- and GUSB – for human PAP expression- which are stably expressed in PCa cell lines and were selected. Primers for reference genes and murine/human PAP protein were obtained from 'Sigma-Aldrich' as lyophilized powders and reconstituted in TE buffer to obtain 100mM concentrations. The primers were further diluted with nuclease-free water to obtain a working concentration10mM. The efficiency of each primer obtained was assessed which is essential for accurately calculating fold change using quantitative RT-PCR. The primer efficiency between 90% and 110% with a standard deviation below 0.2 within the technical replicates was considered acceptable.

To assess the efficiency of murine GAPDH and mPAP primers, cDNA synthesised from TRAMPC2 cells was used. Similarly, for assessing the efficacy of human GUSB and hPAP primers, cDNA was synthesised from HEK293t cells transfected with human PAP protein. A fivefold dilution series of the cDNA was prepared (80, 16, 3.2, 0.64, 0.128, and 0.0256 ng/µL) using nuclease-free water. 1 µL of cDNA dilution was mixed with qPCR reaction mix which consisted of 6.75µL of FastGene IC Green qPCR Universal Mix, 0.5µL each of forward and reverse primers (10mM), and 3.75µL of nuclease-free water. Non-template control (NTC) which contained qPCR reaction mix without any cDNA also prepared. cDNA dilution and NTC reaction were performed in triplicate. PCR was performed at the parameters described in Table 2.5 using a RotorGene-Q real-time PCR cycler on a software version Rotor-Gene Q Software 2.3.1.49 which generated a standard curve and calculated reaction efficiency automatically (Appendix, Figure AF.1). The established threshold (Table 2.3) was applied for all further qPCR experiments. All primers used had a comparable amplification efficiency (Table 2.3) within the generally accepted values ranging between 90- 110%.

	GAPDH	**mPAP**	**GUSB**	**hPAP**	**HHDII**
Annealing temperature	58^0C	58^0C	58^0C	58^0C	66^0 C
Threshold	0.0307	0.0352	0.03432	0.0298	0.0264
Efficiency (%)	90.6	104.2	92.8	101.7	97.7

Table 2.4*. The amplification efficiency and threshold to obtain C_T value for each primer used in the qPCR analysis of murine and human PAP expression.*

qPCR analysis

qPCR was performed to assess the mRNA expression of murine and human PAP antigen in the PAP transfected cells and naturally PAP-expressing cells such as LNCaP, TRAMP C1, and TRAMP C2. The reaction for each cDNA sample and NTC was performed in triplicate in a final volume of 12.5µL, consisting of 1µL of cDNA and 11.5µL of qPCR master mix. The RT-PCR parameters were set as described below (Table 2.5).

Cycle	Cycle point
Hold	@95^{0}C,5 minutes (initial denaturation)
Cycling (40 repeats)	Step 1: Hold @95^{0}C, 10s
	Step 2: Hold @ 58°C, 15s (annealing)
	Step 3: Hold @ 72°C, 20s (extension)
Melt	Ramp from 58°C to 95°C
	Hold for 90s on the 1st step
	Hold for 5s on next steps, Melt A

Table 2.5. *RT PCR parameters for analysing the gene expression*.

Once the run was completed, the quantitation report was generated by applying the established threshold, cycling time (C_T) value was obtained. The relative PAP expression was measured using the 2^{-DDCT} method with suitable reference genes.

2.2.2.7. Assessing PAP gene expression at protein level

2.2.2.7.1. Western blotting for PAP

2.2.2.7.1.1. Sample preparation

$5x10^6$ cells were pelleted in 1.5mL tubes by centrifugation at 300 x g for 5 minutes at room temperature. Any residual media is removed by washing the pellet with DPBS, centrifuging down, and discarding the supernatant. Cell pellets were resuspended in 500µL of cold RIPA lysis buffer, vortexed for 30 sec, and left on ice for 10 minutes. This was repeated twice. Lysate was centrifuged at 14,000 x g for 15 minutes at 4ºC. The clear supernatants were transferred to a microtube and kept on ice throughout the protein assay, or it was stored at -80ºC.

2.2.2.7.1.2. Bicinchoninic acid (BCA) assay

The BSA standards were prepared at concentrations ranging from 2000 and 25µg/mL using RIPA buffer. The lysates were diluted by a factor of 4 using RIPA buffer. 200µL of working reagent (bicinchoninic acid and copper (II) sulfate mixed at a 50:1 ratio) was combined with

25µL of the BSA standards and the lysates, which were transferred in triplicate to a 96-well microplate. After covering and incubating the microplate for 30 minutes at 37ºC in the dark, the microplate absorbance was read at 570 nm. A standard curve was drawn from the absorbance reading obtained for BSA standards, and the concentration of protein present in each lysate was calculated from the standard curve.

2.2.2.7.1.3. SDS-PAGE and protein transfer

Samples are prepared by mixing the cell lysates containing protein (calculated for 30 µg) with 3 parts of 4x Laemmli buffer vortexed and then boiled at 95^{0}C for 5 minutes. The sample was loaded into polyacrylamide gels composed of a 5% stacking gel and a 10% resolving gel. 5µL of Precision Plus Protein WesternC Standards were used for protein size evaluation. The polyacrylamide gels were run at 70 volts for 5 minutes, and then at 100 volts, constant for around 1.5 hours or until the dye front reached the bottom of the gel. When the dye reached the bottom of the gel, gels were removed and equilibrated by socking in the transfer buffer for 10 minutes. The polyacrylamide gels and nitrocellulose membranes were sandwiched in between filter paper and sponge and placed into the transfer tank filled with cold transfer buffer. The protein transfer was carried out in a cold room, 100V, for 90 minutes.

2.2.2.7.1.4. Blocking and probing membranes with antibodies

After the protein transfer, the membrane was blocked with 5% skimmed milk powder in TBST for 1 hour at room temperature under constant agitation, washed 5 times for 5 minutes in TBST then incubated overnight at 4°C with 1:1000 rabbit anti-human PAP primary antibody in 5% skimmed milk powder in TBST. Rabbit Anti-Vincullin at 1:10000 dilution with 5% skimmed milk in TBST is used as WB loading control, and bands were detected at 125KDa. After overnight incubation, membranes were washed 5 times for 5 minutes in TBST at RT and incubated with 1:5000 secondary HRP Goat anti-rabbit antibody in 5% skimmed milk powder in TBST for 1 hour at room temperature. BioRad Precision protein Strep-Tactin -HRP conjugate 1:5000 dilution was added to the secondary antibody which will aid in the

detection of BioRad Precision Plus Protein Western C Standards. After 5 washes for 5 minutes in TBST at room temperature, the membranes were developed using Clarity Western ECL Substrate and the bands were visualised using the Chemi gel documentation system.

2.2.3. Mouse models: HHDII/DR1 and C57BL/6J mice

HHDII/DR1 transgenic mice were given by Dr. Lone (CNRS, Orleans, France), and HHDII/DP4 mice were given by Scancell Ltd; and were bred at the Animal unit of Nottingham Trent University animal facility by the Home Office Codes of Practice for the Housing and Care of Animals. C57BL/6J mice were purchased from Charles River. Both were used between 8 to 14 weeks old at the start of treatment.

Tumour studies were conducted according to the Home Office regulations and reviewed by Nottingham Trent University's Animal Welfare Ethical Review Body (Licence number: ID1B4D884). Animals were housed in groups of up to 5 per cage in Techniplast Sealsafe Plus cage furnished with corncob bedding, chewsticks, sizzle-nest and play tunnels. The environmental conditions were maintained at a target temperature of 20- 24°C, and target humidity of 45-65% with twelve hours of continuous artificial light in each 24 hours with at least fifteen air changes per hour. The animals were provided with Rodent 2018C Envigo Global Certified Diet and autoclaved tap water.

2.2.3.1. Genotyping of mice

All HHDII DR1 mice used in this study were assessed for transgenes HLA-A2*0201, HLA-DRA1*0101, and HLA-DRB1*0101 by conventional PCR method. Ear notches of the animals were collected, and DNA was extracted using the KAPA Mouse Genotyping Kit. Ear notches were submerged in a mixture comprised of 90µL of PCR grade water, 10µL of 10x KAPA express extract buffer, and 2µL of 1 U/mL KAPA express extract enzyme and heated at 75ºC

for 10 minutes using a heating block followed by inactivating digestive enzyme by heating at 95ºC for 5 minutes.

For the PCR amplification, 2µL of each sample was combined with a reaction mixture containing 7µL of PCR grade water, 10µL of 2x KAPA 2G Fast Genotyping Mix, 0.5 µL each of forward and reverse primers, of each transgene separately (sequences described in table 2.7). All primers were reconstituted in TE buffer and diluted to 30uM with nuclease-free water. All tubes were placed in a thermal cycler with the following conditions: 95ºC for 3 minutes; 35 cycles of 94ºC for 15 seconds, 60ºC for 15 seconds and 72ºC for 30 seconds; 72ºC for 5 minutes. For analysing the transgenes by gel electrophoresis, PCR products were loaded into a 1.5% agarose gel stained with SYBR Safe DNA Gel stain, with a 100bp DNA ladder running parallel to the sample. The gel was run at 80V until the optimal separation of the bands was achieved. Bands were visualised using the Chemi gel documentation system. HLA-A2 positive samples showed a 400bp band; HLA-DRA1 positive samples showed a 153bp band; HLA-DRB1 positive samples showed a 228bp band (Appendix Figure AF.2).

Genotyping primer sequences			
Primer	**Company**	**Forward sequence**	**Reverse sequence**
HLA- A2	Eurofins	CATTGAGACAGAGCGCTTGGCACAGAAGCAG	GGATGACGTGAGTAAACCTGAATCTT TGGAGTACGC
HLA- DR-A1	Eurofins	CTCCAAGCCCTCTCCCAGAG	ATGTGCCTTACAGAGGCCCC
HLA -DR-B1	Eurofins	TTCTTCAACGGGACGGAGCGGGTG	CTGCACTGTGAAGCTCTCACCAAC

Table 2.6*. Forward and reverse primer sequences used to analyse the expression of HLA-A2, HLA-DR-A1 and HLA-DR-B1 in HHDIIDR1 mice.*

2.2.3.2. Immunisation of mice

2.2.3.2.1. Peptides

All peptides (both long and short) were purchased from GenScript as lyophilized powder (purity > 90%), reconstituted at 10mg/mL in 100% DMSO under sterile conditions, aliquoted, and stored at -80°C until used.

Human	Peptide sequences	Murine
	YIRSTDVDRTLMSAMTNLAALFPPEGISIWNPRLLWQPIPVH	mPAP42merWT
hPAP42merWT	YIRSTDVDRTLMSAMTNLAALFPPEGVSIWNPILLWQPIPVH	2 mutations
hPAP42merMut (1mutation)	YIRSTDVDRTLMSLMTNLAALFPPEGVSIWNPILLWQPIPVH	3 mutations
hPAP15merCPR (WT)	CPRFQELESETLKSE	3 mutations
	CPRFEELKSETLESE	mPAP15mer CPR(WT)

Table 2.7. List of humans, murine and mutated PAP peptides included in the vaccine. *The AA highlighted in red displays the mutation of mPAP peptides to its human or mutated counterparts.*

2.2.3.2.2. Adjuvants

CpG ODN 1826 and 2395 were purchased from Eurofins. CAF®09b adjuvant was a generous gift from Gabriel Kristensen, Statens Institut, Copenhagen. Freund's adjuvant Incomplete (IFA) is purchased from Sigma-Aldrich.

2.2.3.2.3. Immunisation procedures

The peptide vaccine for this study is formulated by mixing an appropriate quantity of PAP peptides with adjuvants in a 1.5 mL sterile centrifuge tube. The mice were immunised with the vaccine composed of 30µg of PAP peptides adjuvanted with either 50µg CpG ODN 1826/ 25µg CpG ODN 2395+ 25µL IFA or 100µL CAF®09band 100µL PBS-9% sucrose. The vaccine composed of CpG/IFA adjuvants was administered subcutaneously at the base of the tail while the vaccine prepared with CAF®09b adjuvant is administered by intraperitoneal injection. Immunisations were given on days 0, 14, and 28. On day 42 animals were culled, spleens, lymph nodes, and terminal blood were collected for downstream processing and analysis (Figure 2.5).

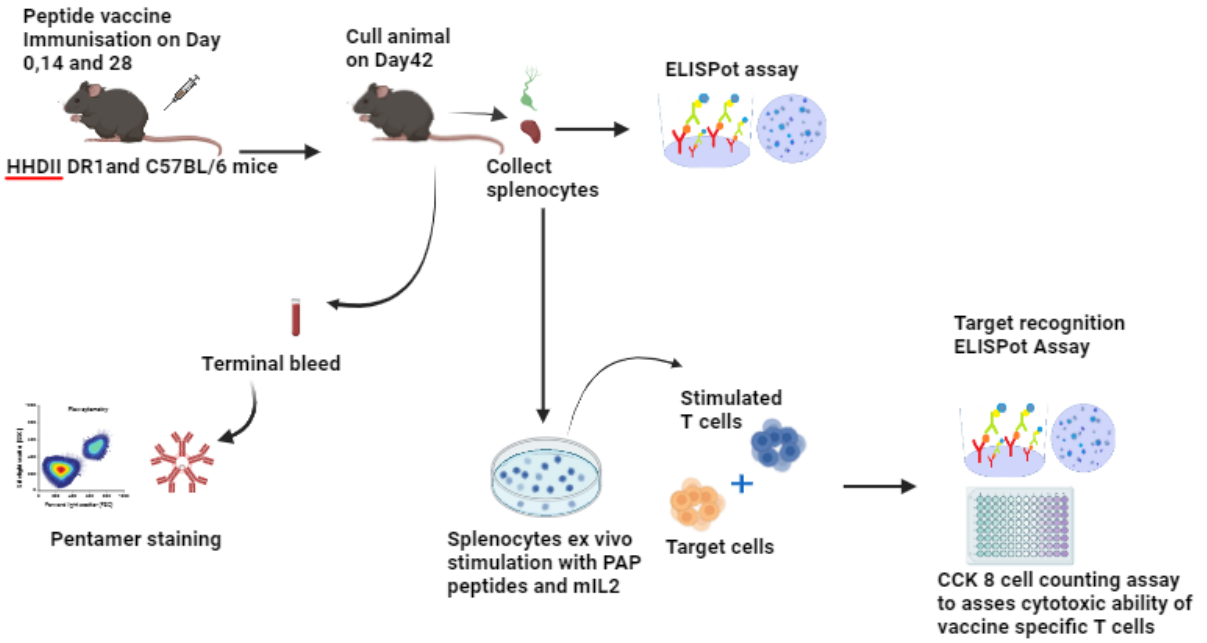

Figure 2.5. Schematic representation of immunisation protocol. *Illustrates the immunisation protocol and invitro assessment of immunogenicity and efficacy of the peptide vaccine. Figure generated using Biorender.com.*

2.2.3.3. Blood sampling for pentamer analysis

Terminal blood samples were collected into labelled Microcuvette 100 Serum tubes via cardiac puncture under terminal anaesthesia when the animal was culled. Blood samples were gently agitated once collected and were used to perform pentamer staining.

2.2.3.4. Processing of tissue samples

2.2.3.4.1. Isolation of splenocytes and lymphocytes

Spleens and Lymph nodes (iliac, inguinal, and axillary) from immunized mice were harvested at the end of the study and conveyed in sterile bijoux containing T-cell media (section 2.1.8). Under laminar air flow, spleens were placed into a sterile petri dish containing 10mL of T-cell media. To extract as many splenocytes as possible, 10mL of T cell medium was carefully flushed through each spleen using a 21G needle attached to a 10mL luer slip syringe. This was accomplished by holding each spleen submerged in the T-cell medium with tweezers while inserting the needle into the spleen before flushing the medium.

The spleen was firmly squeezed using tweezers to extract as many splenocytes as possible, and the cell suspension was transferred to separate 50 mL centrifuge tubes with 40µm cell strainers. After the cell suspensions had been fully filtered, they were centrifuged at 300 x g for 10 minutes at room temperature. The supernatants were discarded, and the splenocytes were resuspended in 5mL of T-cell medium and counted using the NucleoCounter.

To isolate the cells from lymph nodes, each set of lymph nodes was put inside a 40µm cell strainer in a petri dish containing 5mL of T-cell medium. Lymph nodes were cut using sterile scissors and squeezed gently with the thump-rest of the 10mL luer slip syringe plungers, for around 30 seconds. The cell suspension was strained through the filter and collected in a 50mL tube, centrifuged at 300 x g for 10 minutes at room temperature; the supernatants were discarded, and the cells were resuspended in 1mL of T-cell medium and checked for viability and cell count using NucleoCounter.

2.2.3.4.2. IFNγ ELISpot assays

The number of IFNγ releasing PAP-specific T-cells was determined using a murine IFNγ ELISpot assay. The ELISpot plates were activated with 50µL of 35% ethanol and washed 5 times with 200µL of sterile ddH_2O per well. After that, membranes were coated with 50µL of a 1:1000 diluted capture antibody in sterile PBS and left to incubate overnight at 4°C. The following day, plates were washed 4 times with sterile PBS and the membranes were blocked with 100µL/well of T-cell media for 30 minutes at room temperature. After blocking, T-cell media was removed, and $0.5x10^6$ splenocytes/well in a final volume of 100µL/well were plated. Splenocytes were stimulated with MHC class-I and class-II peptides at 2µg/mL and 20µg/mL respectively in 100µL/well so that the final volume in each well was 200µL/well. Since the negative control wells contained only splenocytes, the T-cell medium was added to bring the final volume to 200µL. A 1:200 dilution of Concanavalin A in T-cell media with splenocytes was used as a positive control. All treatments are done in triplicates. For the target recognition ELISpot assay, splenocytes or isolated $CD3^+$ T-cells were co-cultured with

suitable target cells in a 50:1 (Effector: Target) ratio. The plates were then incubated for 40 hours at 37ºC, 5% CO_2. After 40 hours of incubation, the plates were washed 5 times with 200µL/well of PBS using the HydroFlex microplate washer, followed by the addition of 50µL/well of the biotinylated-detection- antibody diluted 1:100 in PBS for 2-4 hours at room temperature. Then, 50µL/well of streptavidin-AP diluted 1:100 in PBS was added after 5 washes with PBS for 1 hour and 30 minutes at room temperature. Finally, plates were washed 5 times with PBS and coated with 50µL per well of colour development solution and incubated for 10 to 30 minutes in the dark. Once the spots were visible, the reaction was stopped by washing the plates under running tap water. Plates were dried; number of spots was quantified using the ImmunoSpot ELISpot plate reader.

2.2.3.4.3. *In vitro* stimulation and Isolation of $CD3^+$ T cells

Splenocytes along with lymph node cells ($4x10^6$ cells/mL) were stimulated *ex-vivo* with hPAP42mer at 0.1µg /mL and 50U/mL mIL2 for 5 days. Cells were harvested, washed, and resuspended in fresh T-cell media containing 50U/mL mIL2 for one day. After that, cells were collected and assessed for viability and count. Using the Mouse T-cell isolation kit from Stem Cell Technologies, $CD3^+$ T-cells were extracted from ex-vivo stimulated splenocytes following the manufacturer's instructions.

EasySep Mouse T-cell isolation kit allows the isolation of T-cells from a single-cell suspension of splenocytes by negative selection. Biotinylated antibodies and streptavidin-coated magnetic particles are used to label and eliminate unwanted (non-T-cells) cells. A magnet is used to separate the labelled cells leaving intended T-cells in the cell suspension which is collected in a fresh tube. *Ex vivo* stimulated splenocytes were resuspended in a suitable volume of T-cell isolation buffer (PBS containing 2% FBS and 1 mM EDTA) as instructed in the manufacturer protocol and transferred to sterile round-bottom polystyrene tubes. 20µL/mL FcR blocker was added followed by the addition of the isolation cocktail 50µL/mL and incubated for 10 minutes at room temperature. After the incubation 75µL/mL rapid spheres were added to the sample, mixed well by pipetting up and down, and

incubated for 2.5 minutes at room temperature. The volume of the cell suspension was made up to 2.5mL using the isolation buffer. The tube was then placed into the magnet without the lid, and incubated for 2.5 minutes, which allowed the separation of T-cells from other cells which was labelled with magnetic particles. The cell suspension enriched with T-cells was collected in a fresh tube and centrifuged at 300x g for 5 minutes. The cell pellets were resuspended in fresh T-cell media. The total cell counts and viability of the $CD3^+$ T cells were identified using NucleoCounter.

2.2.3.4.4. Cytotoxicity assay

Cytotoxicity was performed by Cell Counting Kit (CCK-8). $CD3^+$T-cells were co-cultured with target cells at 50:1(Effector: Target) ratio in flat bottom 96-well microplates in a final volume of 100µL /well and incubated for 24 hours at 37ºC, 5%CO_2. T-cells alone and target cells alone were plated in separate wells to determine the total number of cells. Target cell treated with 0.1%SDS is used as a positive control to identify the maximum cell death. After 24 hours of incubation, 10µL of CCK-8 solution (provided in the kit) was added per well and incubated for 4 hours at 37ºC, 5%CO_2. The absorbance was measured with a microplate reader at 450nm.

2.2.3.4.5. Cell surface pentamer staining of murine cells.

Cells derived from the spleens and blood of naïve and vaccinated mice were stained for downstream analysis using spectral flow cytometry. $1x10^6$ splenocytes and 100µL blood were used. The cell suspensions or blood volumes were transferred to round bottom polystyrene test tubes and incubated for 15 minutes at 4ºC with 1 µL of Fc Blocker in 50µL of FBS per tube added to block non-specific binding to Fc receptors. After that, the cells were incubated with a Pro5 MHC Pentamer which is specific for the desired peptide and incubated for 10 minutes at room temperature in the dark. Each sample was then stained with a cocktail of antibodies listed in Table 2.8 followed by 30 minutes of incubation at 4ºC in the dark. The blood samples were mixed with 2mL of 1x PharmLyse to lyse red blood cells,

incubated for 25 minutes at room temperature in the dark, centrifuged at 300 x g for 5 minutes, the supernatant was discarded. The pellets from samples derived from spleens and blood were resuspended in 2mL of PBS and centrifuged at 400 x g for 5 minutes. The supernatant was then discarded, and the pellets were resuspended in 350µL of Isoton sheath fluid, ready for analysis using the spectral flow cytometer.

Antibody	Clone	Fluorochrome	Company	Catalogue number
CD45	S18009F	FITC	Biolegend	157213
CD3	17A2	BV421	Biolegend	1000228
CD8a	53-6.7	APC-Cy7	Biolegend	100714
Live/dead Yellow			ThermoFisher Scientific	L23105
Pentamer	N/A	PE	Pro Immune	

***Table 2.8**. List of antibodies used in the pentamer staining flowcytometry analysis.*

2.2.3.5. Assessing the efficacy of the vaccine *in vivo*

2.2.3.5.1. Tumour implantation

The cells used for tumour implantation were tested for mycoplasma contamination a day before tumour implantation. The cells are harvested and counted using the NucleoCounter for accurate cell count. 1- $5x10^6$ cells/100µL sterile PBS or Matrigel were used for tumour implantation. The cell suspension was injected subcutaneously, at the right flank. Animals were observed closely for tumour development. The tumour size and body weight of each tumour-bearing mouse were measured every 3-4 days until the animal was culled to collect the tumour.

2.2.3.5.2. Tumour harvesting

Animals were culled when the tumours reached 15mm size or if there was any ulceration at the tumour site or any clinical signs - for example, weight loss, drowsiness, toe-tipping- presented by the animals. Tumours are harvested and collected in bijoux containing RPMI-

1640 or MACS® Tissue Storage Solution. Tumours were weighed and measured. Tumour cells were collected by dissociating the tumours using the Miltenyi tumour dissociation kit.

2.2.3.5.3. Isolation of tumour cells

Tumours are dissociated using the Miltenyi murine tumour dissociation kit. Tumours were cut into small fragments with a scalpel and mixed with dissociation enzymes in 2.35 mL of serum-free RPMI-1640 media. The tumour fragments were then incubated for one hour in Incu-shake at 225rpm rotation. After the incubation, tumour dissociates were filtered through a 40µm strainer into the 50mL Falcon tube and centrifuged at 300 x g for 10 minutes. The cell pellets were resuspended in 1mL T-cell media and counted using NucleoCounter.

2.2.3.5.4. Immunophenotyping of tumour cells using 22 colour flow cytometry panel

2.2.3.5.4.1. Optimisation of antibodies for 22 colour panel

All surface and intracellular antibodies used in the 22-colour flow cytometry panel were titrated under the same experimental condition (as described in section 2.2.3.5.4.2) using naïve splenocytes. A series of dilutions of antibodies were prepared; neat (recommended concentration by the manufacturer), and further four dilutions, 1 in two, 1 in four, 1 in 8, and 1 in 16. Each antibody was stained separately. Cells that were not treated with any antibody were used to identify the negative population in the stain index. The acquisition was set for 10,000 live cells, live single cells were gated to define the positive and negative populations.

2.2.3.5.4.2. Flowcytometry staining protocol.

Tumour cells were stained with different surface and intracellular antibodies (Table 2.9) to identify immune stimulatory and immune suppressive cells by flow cytometry analysis. 1 x 10^6 splenocytes/tumour cells and 100µL of blood were blocked with 50µL of FCS and 1µL FcR blocking reagent, incubated for 15 minutes at 4^0C. A cocktail of surface antibodies was prepared, added to the cells, and incubated for 30 minutes at 4^0C in the dark. After surface markers staining, cells were washed, fixed, and permeabilized for intracellular staining. For

that, 1mL FoxP3 Fixation/permeabilization working solution was added to the cells and incubated overnight at 4^0C. After the overnight incubation, 2 mL 1x permeabilization buffer was added to the tubes and centrifuged at 400x g for 5 minutes, discarded the supernatant. Cells were resuspended in the residual volume of 1x permeabilization buffer, incubated with the cocktail of intracellular markers for 30 minutes at room temperature, followed by washing with 2mL PBS, cells were resuspended in 350µL of isoton for flowcytometry analysis.

Antibody		Company	Catalogue number	Fluorochrome	Clone
Surface staining	CD45	Thermofisher	58-0451-82	Alexafluor532	30-F11
	Ly6G	Thermofisher	48-9668-82	Efluor 450	1A8-Ly6g
	CD8	Thermofisher	46-0081-82	PerCP-efluor 710	53-6.7
	GITR	BD Biosciences	747402	BV750	DTA-1
	PD-1	BioLegend	114118	PE	RMP1-14
	CD3	Biolegend	100218	PerCP-Cy5.5	17A2
	CD11b	Biolegend	101263	BV510	M1/70
	Ly6C	Biolegend	128049	BV650	HK1.4
	CD4	Biolegend	100430	Alexafluor700	GK1.5
	CD25	Biolegend	102017	Alexafluor488	PC61
	CD62L	Biolegend	104438	BV605	MEL-14
	OX40	Biolegend	119421	BV711	OX-86
	CD44	Biolegend	103062	APC/Fire750	IM7
	CD69	Biolegend	104510	PE-Cy5	H1.2F3
	LAG3	Biolegend	125226	PE-Cy7	C9B7W
	TIM3	Biolegend	119725	BV785	RMT3-23
	IFNγ	Biolegend	505830	BV421	XMG1.2
Intracellular staining	TNFα	Biolegend	506314	Alexafluor647	MP6-XT22
	CTLA4	eBioscience	61152282	PE-eFlupor610	UC10-4B9
	FoxP3	Thermofisher	17-5773-82	APC	FJK-16s
	Ki67	BD Biosciences	566109	BV480	B56
	Live/dead yellow stain	ThermoFisher Scientific	L34959		

***Table 2.9**: List of surface and intracellular antibodies used for 22 colour flow cytometry analyses.*

2.2.3.5.5. Analysing the effect of castration in mice

2.2.3.5.5.1. Castration of mouse

Castration was performed in two different ways, chemical castration, and surgical castration. Animals that underwent surgical castration were anaesthetised before the surgery; a small incision was then made to expose the testis (Valkenburg, Amend and Pienta, 2016). Animals that underwent chemical castration were injected with 0.625mg of Degarelix Acetate (GnRH receptor antagonist) in 100µL PBS subcutaneously into the right-hand side flank (Jayusman, Mohamed and Shuid, 2018; Shen *et al*. 2017).

2.2.3.5.5.2. Blood sampling and serum isolation

50µL of blood samples were collected from each animal before castration and after castration into labelled Microvette blood collection tubes. The tubes containing blood were kept at room temperature undisturbed for one hour for clotting. The clot was removed by centrifuging at 14,000x g for 30 minutes at 4^{o}C, which separated the serum layer at the top was collected with P200 pipette carefully without disturbing the blood clot and was transferred to cryovials and stored at -80^{o}C until analysis.

2.2.3.5.5.3. Testosterone isolation

Serum samples were mixed with 100µL of anhydrous ethanol. 100µL of 0.5M sodium acetate solution pH5.5 was added to this mixture and vigorously mixed for 2 hours at room temperature on an electric shaking thermomixer. After two hours of mixing, liquid-liquid extraction was performed twice by adding 400µL of ethyl acetate: hexane (60:40 v/v) mixture. Solvents of combined organic layers were collected into a 1.5mL Eppendroff tube and evaporated using the Eppendroff Speedvac drier connected to a vacuum and the application set for vacuum-alcohol at room temperature for 15-20 minutes. The sample extract was dissolved in 150µL of 0.2M ammonium carbonate solution pH 9.8. The sample solution was extracted twice by mixing with 300µL of Hexane. Organic layers were collected, combined,

and evaporated using the Speedvac as described above. The sample extract was stored at -20^{0}C until analysed by Mass spectrophotometer.

2.2.3.5.5.4. Mass Spectrometry analysis

Samples were reconstituted in 20µL of 0.1% formic acid in water:0.1% formic acid in acetonitrile, 80:20v/v and vortexed mixed for 1 min before injection by autosampler onto a Waters M-Class UPLC system hyphenated to a Sciex ZenoTOF 7600 mass spectrometer. The chromatography method was as follows, samples were directly injected onto a Phenomenex Kinetex XB C-18, 2.6µm column at a flow rate of 10µL/min. mobile phase A: 0.1% formic acid; mobile phase B: acetonitrile with 0.1% formic acid with gradient elution (10% B initial conditions, rising to 70% at 12 min), a wash 95% at 13 min until 15 min and re-equilibration to 10 again for a total run time 16.5 min. The mass spectrometry method was as follows – Time -of- flight mass spectrometry scan from 100 -1000 m/z (mass/charge number), collision energy 10V, de-clustering potential voltage 80V and accumulation time of 250ms. Data was analysed via Sciex OS 3.3.1.43, analytics module automatically integrating the peak area using the transition 289.22 to 109.06 as quantifier and 289.22>97.06 as qualifier.

2.2.4. Characterisation of immune cells and biomarkers in the periphery of PCa patients

2.2.4.1. Ethical approval for using Human clinical material.

Ethical approval for collecting blood from PCa patients has been obtained (Reference number: 18/WM/0377) and the patients who donated their blood were consented by the consultant. The inclusion criteria included patients with BPH as well as those with low, intermediate, and high-risk PCa, irrespective of tumor size. Blood samples were obtained from 32 participants aged 47 to 78 years between September 2021 and May 2023 which included 12 benign prostate conditions, 3 low-grade, 9 intermediate-grade, and 8 high-grade prostate cancer (PCa). Clinical characteristics of patients included age, PSA levels, volume, pathology stage, Gleason score, and D'Amico classification (described in chapter 6, table6.1). All samples were processed within 3 hours of collection.

2.2.4.2. Sample collection

Whole blood samples from patients with higher PSA levels than age-related normal levels were provided by Dr Massod Khan, Leicester General Hospital, Leicester, UK. Blood samples were collected in tubes containing Heparin 1000 U/ml. Approximately 70mL of blood was received from each patient, of which 2 mL of whole blood was taken out, and centrifuged at 14000 rpm, for 30 minutes at 4°C, to separate the plasma which was stored at -80^{0}C for further analysis by ELISA. 100µL of whole blood from each patient was taken by reverse pipetting for the whole blood flow cytometry analysis. The remaining blood was used for PBMC isolation.

2.2.4.3. Peripheral blood mononuclear cells (PBMC) isolation

PBMCs were isolated from whole blood by using the density gradient method. Leucosep tubes were prepared by adding 15mL of Ficoll-Paque Plus solution and centrifuge at 1000x g for 30seconds at room temperature. Blood samples were mixed with sterile PBS to 1:1 dilution. 30mL of diluted blood was poured slowly through the edge of the tube without disturbing the filter and centrifuged at 800x g in a swing bucket rotor at room temperature, with break-off for 20 minutes. As seen in Figure 2.6, a sequence of layers was formed during centrifugation with plasma at the top, cell-enriched fraction (PBMCs), separation medium, porous barrier, separation medium, and erythrocyte/granulocyte pellet at the bottom. Cell enriched fractions were collected carefully and transferred to a 50mL sterile falcon tube, washed with 45mL of PBS by centrifuging at 600x g for 10 minutes with breaks on at room temperature. The supernatant was discarded, repeated the washing step with PBS centrifuging at 400x g for 5 minutes. After washing the PBMCs were resuspended in 5mL FCS, viability and total count were assessed using NucleoCounter. Appropriate volume for 1x10^6 cells was taken for flow cytometry. The remaining PBMCs, 10x10^6 per vial were frozen in freezing media made up of 10% DMSO and 90% FCS, immediately stored at -70^{0}C. The following day the cryogenic vials containing PBMCs were transferred to a liquid nitrogen tank for long-term storage.

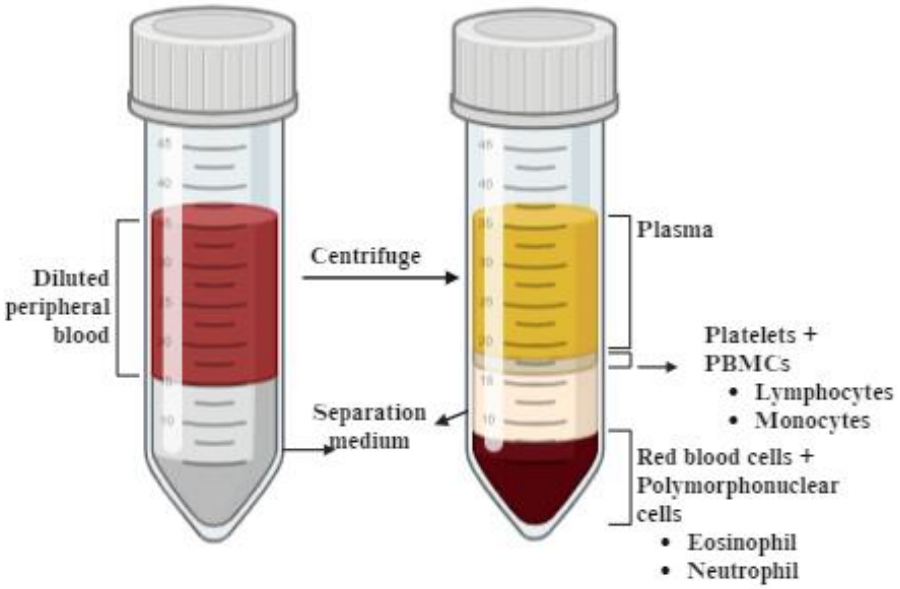

Figure 2.6. PBMC isolation by density gradient centrifugation. *Various layers obtained after the centrifugation include the plasma layer, enriched cell fraction (interphase consisting of PBMC), separation medium, separation medium, and erythrocytes/granulocytes. Diagram generated using biorender.com.*

2.2.4.4. Assessing MDSCs subpopulation present in PBMC.

Antibodies used for MDSC staining were titrated to obtain optimal Ab concentration resulting in the highest signal of positive population and the lowest signal of negative population.

2.2.4.4.1. Optimisation of antibodies-MDSC staining

One drop of OneComp eBeads™ Compensation Beads was used for the titration. 20µL Fc blocking reagent was added and incubated for 15 minutes at 4°C in the dark to block non-specific binding and background fluorescence. 100µL PBS with an appropriate volume of antibodies was added and incubated for 20 minutes at 4°C in the dark. All the antibodies (Table 2.10) were titrated at the concentration suggested by the manufacturer (neat) and 4 further dilutions, 1 in 2, 1 in 4, 1 in 8, and 1 in 16. Since Arginase-1 required intracellular staining, the PerFix-NC kit was used to maintain similar conditions as in the experiment. The

kit includes fixative reagent R1, permeabilizing reagent R2, and Buffer R3. 25µL Fixative reagent R1 was added and incubated for 15 minutes at 4°C in the dark, which was followed by the addition of 300µL permeabilizing reagent R2 and vortexed immediately, incubated for 15 minutes at 4°C in the dark. For staining with Arg-1, the antibody was added after the addition of the permeabilizing reagent and was then incubated for 20 minutes at 4°C in the dark. 3mL of 1x R3 was added, and centrifuged. The supernatant was discarded, and the cells were resuspended in 350 µL 1x R3 and analysed by a flow cytometer.

Antibody	Fluorochrome	Clone	Supplier	Catalogue number
CD33	eFluor 450	P67.6	eBioscience	48-0337-42
CD11b	BV570	ICRF44	Biolegend	301325
CD14	BV480	M5E2	BD Bioscience	746304
CD16	BV711	3G8	Biolegend	302044
CD66	APC	G10F5	Biolegend	305118
CD15	PE-Dazzle594	W6D3	Biolegend	323038
CD84	AlexaFluor 700	CD84.1.21	Novus Biologicals	NB100-65929AF700
PD1-L1	APC eFluor 780	MIH1	Thermo Fisher	47-5983-42
HLA-DR	BV605	G46-6	BD Bioscience	562845
CD3/CD19 dump channel	BV421	(CD3) OKT3	Biolegend	317343
		(CD19) HIB19		302233

***Table 2.10**. List of antibodies used for the flow cytometry analysis of subpopulation of MDSCs present in isolated PBMCs of PCa patients.*

2.2.4.4.2. Flow cytometry for immunophenotypic analysis of MDSCs

To investigate the distinct subpopulations of MDSCs and the expression of various molecular markers on the MDSCs of benign vs PCa patients $1x10^6$ PBMCs were used. An appropriate volume of cell suspension was transferred to the flow cytometry tube and

washed with 2mL of PBS by centrifuging at 400x g for 5 minutes. The supernatant was disposed of, and 20µL FC blocking was added, and incubated for 15 minutes at 4°C. Cells were stained with the cocktail of all surface antibodies at optimised volumes for 20 minutes at 4°C in the dark. Cells were fixed and permeabilized for the intracellular staining of Arginase-1 for 20 minutes at 4°C in the dark. After incubation, cells were washed with 3mL 1x R3 buffer, resuspended the pellet in 350µL 1x final reagent, and kept in the dark at 4^0C until analysed by flow cytometer.

2.2.4.5. Immunophenotyping of cell population from whole blood

2.2.4.5.1. Optimisation of antibodies- whole blood staining

The list of antibodies and details are shown in Table 2.9. One drop of OneComp eBeads was used for the titration. 20µL FcR blocking reagent was added and incubated for 15 minutes at 4°C followed by the incubation of antibodies for 30 minutes at 4°C in the dark. To lyse the red blood cells, 1 mL of BD Pharm Lyse lysing buffer was added, vortexed, and incubated for 15 minutes at 4°C. This was then analysed by FCS express using a 5-point template for antibody optimisation. Patient samples were stained using the determined antibody volume.

Antibody	Fluorochrome	Clone	Supplier	Catalogue number
CD8	FITC	SK1	BioLegend	344704
CD19	PE	HIB19	BioLegend	302208
CD28	PE-Texas Red (ECD)	CD28.2	Beckman Coulter	6607111
CD56	PE-Cy5	NCAM	BioLegend	362516
CD3	PE-Cy7	HIT3a	BioLegend	300316
CD45RA	APC	HI100	BioLegend	304112
CD27	APC eFluor 780	O323	eBioscience	47-0279-42
CD45	Pacific Blue	J33	Beckman Coulter	A74763
CD4	Pacific Orange	13B8.2	Beckman Coulter	A96417

Table 2.11. *List of antibodies used for whole blood immunophenotyping.*

2.2.4.5.2. Flow cytometry analysis of whole blood

100 µL of whole blood was transferred to polystyrene tubes by reverse pipetting method, and 20 µL Fc blocking reagent was added and incubated for 15 minutes at 4°C. Cells were then stained using surface antibodies shown in Table 2.11 and incubated for 20 minutes at 4°C in the dark. The erythrocytes were lysed using 2 mL of 1x BD Pharm Lyse lysing Buffer and analysed by flow cytometer.

2.2.4.6. ELISA

The ELISA employed is a sandwich ELISA which uses the specificity of antibodies to recognize a particular antigen. The analytes investigated by ELISA include Human IL 1 β, intestinal fatty acid binding protein (iFABP), IL-6, C-Reactive Protein (CRP), Haptoglobin, Lipopolysaccharides (LPS), and Tryptophan Hydroxylase 1 (TPH1). The details of the company and catalogue numbers are provided in section 2.1.5. The ELISA plates were prepared by adding 100µL per well of working concentration of capture Ab in PBS, incubated overnight at room temperature. following incubation, plates were washed 3 times with 400µL/well of wash buffer (0.05% Tween® 20 in PBS). The membranes were then blocked by adding 300µL of 1% BSA in PBS, incubated at room temperature for an hour followed by 3 times washing with wash buffer. Samples and standards were prepared in reagent diluent (1% BSA in PBS), and 100µL were loaded into the respective wells. The plate was covered with an adhesive strip and incubated for 2 hours at room temperature followed by 3 times washing with 400µL wash buffer. 100µL of the detection Ab, diluted in Reagent Diluent, was added, and incubated for 2 hours at room temperature. The wells were washed, and 100µL of the working dilution of Streptavidin-HRP in Reagent Diluent was added to each well and incubated for 20 min at room temperature protecting from direct light. 100µL of substrate solution (mixture of H_2O_2 and Tetramethylbenzidine) was then added after washing the plates and incubated for 20 minutes at room temperature in the dark. Finally, 50µL of Stop Solution (2N sulfuric acid) was added, and optical density was determined using a microplate reader set to 450nm with a wavelength correction set to 570nm.

2.2.4.7. Data analysis

For antibody titration, the data acquired using Cytek Aurora spectral flow cytometer was analysed using FCS Express data analysis software version 7.14.0020. the Stain Index (SI) which is the ratio of the separation between the positive and negative populations divided by the standard deviation of the negative population twice, is automatically calculated by the software. The patient's sample staining and all other flow cytometry staining of surface and intracellular antibodies were analysed using Kaluza software (Beckman Coulter). To aid the interpretation of quantitative results, statistical tests were carried out using GraphPad Prism version 10.2.

For comparisons of marker expression between the benign and PCa groups in the MDSC study, two-way analysis of variance (ANOVA) was used, followed by Sidak's multiple comparisons test to adjust for multiple group comparisons. Data are presented as the mean ± standard error of the mean (SEM). An unpaired t-test was used to assess the correlation between PSA and cancer and evaluate the pattern of one specific phenotype in the two study groups -benign vs cancer. Mass spectrometry data were processed using Sciex OS (version 3.3.1.43), with peak area integration automatically performed using the transition 289.22 → 109.06 as the quantifier and 289.22 → 97.06 as the qualifier.

ELISpot data were analyzed using GraphPad Prism (version 10.2). For normally distributed data, parametric tests were applied, including unpaired t-tests for two-group comparisons and one-way ANOVAs for comparisons involving more than two groups. In cases where the data did not follow a normal distribution, nonparametric tests such as the Mann-Whitney U test were used for two-group comparisons, and the Kruskal-Wallis test was used for comparisons involving more than two groups. Post-hoc pairwise comparisons, following significant one-way ANOVAs, were conducted using the Dunn's multiple comparisons test.

Chapter 2: MATERIALS AND METHODS

Spearman's rho correlation was employed to assess the significant association between biomarkers measured in ELISA analysis. Statistical significance was determined by P-values, with the following thresholds: *P < 0.05, **P < 0.01, ***P < 0.001, and ****P < 0.0001.

For qPCR data analysis, the threshold cycle (CT) method was used to determine relative gene expression. CT values were obtained at a fixed threshold level as indicated in Table 2.3, derived from amplification efficiency experiments. Relative gene expression levels were calculated using the $2-\Delta\Delta Ct$ method, as described by Li et al. (2022).

Chapter 3: TARGET CELLS PREPARATION

3. Target Cell Preparation

3.1 Introduction

3.1.1. MHC molecule

Professional APCs including DCs, B cells, macrophages, and thymic epithelial cells process the antigen and present it to the lymphocytes via their major histocompatibility complex (MHC) surface protein. All vertebrates possess unique MHC, with many conserved genes some of which encodes for its functionality. There are two major types of MHC- class I and class II; for human beings, it is also called human leukocyte antigen (HLA) located on chromosome 6, and in the mouse, they are known as the H-2 genes, located on chromosome 17 (de Winde, Munday and Acton, 2020) (Blum, Wearsch and Cresswell, 2013). MHC class I molecules are ubiquitously expressed on all nucleated cells, while MHC class II molecules are selectively expressed on APCs (Nanda et al. 2006). In humans within the HLA complex, there are three classical MHC-I genes, HLA-A, -B, and -C, and three MHC-II molecules, HLA-DR, -DQ, and -DP. Depending on the strain, mice have two or three genes within the H-2 complex that encode classical MHC-I molecules -H2-D, H2-K, and H2-L- and two MHC-II molecules known as I-A and I-E. MHC-I and -II molecules each have a structurally homologous groove capable of binding peptides with high affinity towards T-cell receptors. MHC class I groove typically bind peptides of 8-11 AA long which are recognised by $CD8^+$ T-cells, whereas MHC class II molecules bind peptides of 12-25 AA long that are recognised by $CD4^+$ T helper cells (Blum, Wearsch, and Cresswell, 2013; Wu *et al*. 2021).

3.1.2. Antigen processing and presentation

Endogenous or intracellular antigens such as proteins of phagocytosed microbes or viruses that reside in the cytoplasm of infected cells are processed in the cytoplasm by protease or proteasomes and then transported into the endoplasmic reticulum by TAP transporter, where they bind with newly generated MHC class I molecules and travel to the cell surface ready for presentation. MHC class II molecules bind to exogenous or extracellular antigens that are internalised by phagocytosis or endocytosis. APC internalised exogenous or extracellular antigens are degraded and directed by the CLIP-DM pathway to be presented

on the cell surface via a newly synthesised MHC class II molecule. Exogenous proteins may also undergo a phenomenon known as "cross-priming," in which they are either processed by the proteasome and enter the class I pathway, or they may first undergo class II pathway cleavage before being transferred to the endoplasmic reticulum, where they are further trimmed to fit into the MHC class I groove (Nanda *et al*. 2006).

3.1.3. T-cell activation and target lysis

T-cells recognise the antigens only when they are processed into small peptides and presented *via* MHC molecules on the surface of the cells. Each T-cell expresses multiple copies of the same TCRs. Each T-cell will have a different TCR, with a unique specificity that is achieved through the VDJ recombination process, which allows the antigen receptor gene segments to be cleaved through cleavage proteins called RAG1 and RAG2 and re-joined by non-homologous DNA end. Along with TCRs, co-receptors CD4 and CD8 dictate the specificity of the MHC molecule-peptide complex to bind to the CD8 coreceptor present on cytotoxic T-cells. CD8 coreceptor binds to the peptide-MHC I complex to generate cytotoxic effect whereas CD4 is present on T helper cells and binds to the peptide-MHC class II complex to activate B cells or to induce or activate macrophages to kill their intracellular pathogens (Nishana and Raghavan, 2012). Peptide/MHC complexes binding to the TCRs trigger T-cell activation. Activated CTLs follow the death ligand pathway, cytotoxic granule pathway, or cytokine IFNγ-mediated pathway for target cell lysis. CTLs mainly eliminate target tumour cells using cytotoxic granules such as perforin and granzymes. The granzyme cytotoxic pathway is dynamic and situation-specific due to the differential expression of granzymes within T-cells based on their activation state and environment. In the death ligand pathway, target cell death is induced by T-cell Fas ligand or TNF-related apoptosis-inducing ligand (TRAIL), interaction with its receptor on the target cell. IFNγ activates the STAT1 transcription factor to reduce tumour cell proliferation or increase the expression of Fas and TRAIL (Hay and Slansky, 2022).

Chapter 3: TARGET CELLS PREPARATION

3.1.4. Tumour cells recognition

Presentation of tumour antigens *via* MHC is fundamental for building a vigorous immune response against cancer cells. Especially, MHC class I antigen presentation is vital for granzyme- and perforin-producing cytotoxic $CD8^+$ T-cell activation. To promote an effective antitumor response, tumour antigens must be cross presented by professional antigen APCs, primarily DCs, for the priming of naive $CD8^+$ T cells. After that, the tumour antigens must be directly presented by tumour cells for recognition and killing by primed CTLs (Heimberger, Brat, and Lesniak, 2023).

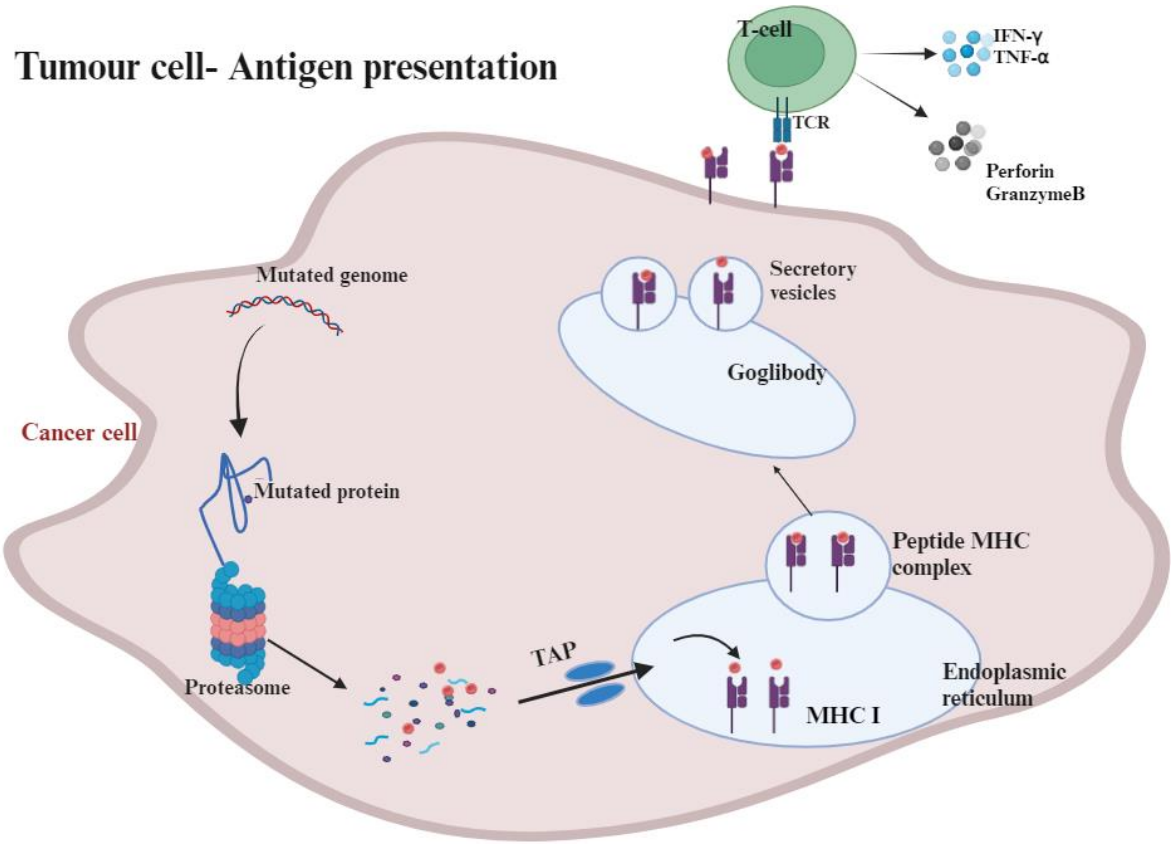

Figure 3.1. Tumour antigen presentation. *Mutated proteins undergo proteasomal degradation into smaller peptides, which are transported to the endoplasmic reticulum where they are complexed with MHC molecules. The peptide–MHC complexes are transported to the cell surface by Golgi vesicles. Figure generated using Biorender.com.*

Chapter 3: TARGET CELLS PREPARATION

3.1.4.1. Cancer cell lines to study cytotoxic T-cells' antigen recognition *in vitro*

The cytotoxic potential of vaccine-primed CTLs to recognise and lyse tumour cells in an antigen-specific manner can be studied *in vitro* by coculturing the vaccine-specific T-cells with murine or human cell lines that present antigen on its surface via MHC molecule. Cell lines are *in vitro* model systems that are extensively employed in many medical research domains, particularly drug discovery and basic cancer research. Under the right growth conditions - temperature, hygrometry, and CO_2-controlled environment- authenticated cancer cell lines retain most of the genetic properties of the cancer of origin thus used as an indefinite source of biological material for experimental purposes (Dowling, Berthon Eliche, and Bagasra, 2022).

3.1.4.1.1. Modifying cell lines to aid its use as an *in vitro* tumour model.

Cells that do not have similar genomic functions to host cancer cells can be modified using knockout, knockdown, or knock-in gene methods to facilitate the elucidation of gene functions to generate a suitable *in vitro* model (Ishibashi *et al*. 2020) (Han, 2018). The gene knockdown/ gene silencing method reduces the gene expression in contrast to gene knockout where the target gene is completely erased (Zhan *et al*. 2023). Gene knockdown traditionally involves interfering with RNA molecules (either mRNAs or non-coding RNAs) and is achieved by introducing small double-stranded interfering RNA (siRNA) or short hairpin RNA (shRNA) into the cytoplasm or using CRISPR-based catalytically dead Cas9 or Cas13 proteins. Gene knockdown is a temporary stop to the expression of the targeted gene, often reversible if the model organisms survive the knockdown event, they eventually begin to express the gene as before (Han, 2018) (Zhan *et al*. 2023). Gene knockout methods mutate the target gene to irreversibly stop its expression. CRISPR-Cas9 system which is based on the prokaryotes' adaptive immune system genome editing mechanism is the widely genome editing approach to generate knock-out cancer cell lines. This technique involves a single guide RNA (sgRNA) that leads Cas9 protein to induce an indel - insertion/deletion- mutation to a precise location in the host genome where it introduces a double-stranded break in the genomic DNA (Ishibashi *et al*. 2020; Komori *et al*. 2023).

Chapter 3: TARGET CELLS PREPARATION

Cells can be genetically modified to enhance the expression of specific genes by transfection (knock-in) techniques, by which foreign nucleic acids are artificially introduced into the cells. Transfection can be either; transient transfection- where the introduced transgene expression stays for a short period, eventually lost as the host replicates-, or stable transfection- which allows the foreign DNA to be integrated into the host genome causing sustained transgene expression introduced through their multiple progenies. Foreign DNA can be introduced into eukaryotic cells by various methods such as direct microinjections, through nanoparticle carriers, using chemical reagents such as lipofectamine, or using biological particles such as viruses as carriers. Virus-mediated transfection also known as transduction involves recombinant-deficient viral vectors to transduce dividing cells and is the most efficient way to introduce sustainable transgene expression *in vivo* or *in vitro* (Chong, Yeap, and Ho, 2021).

Cancer cell lines or genetically modified cell lines provide excellent *in vitro* model systems to study cancer cell biology and to understand the mechanism of cancer therapy, yet these models cannot completely depict the biological reality of tumours and their TME, thus *in vivo* models are crucial for understanding the working mechanisms and evaluating the efficacy of immunotherapies in the context of the TME (Kapałczyńska *et al*. 2016).

Murine and human MHC molecules differ in their peptide binding groove and from the same protein different peptides will be displayed on their surface which makes them poor models to translate results obtained to humans. However, the use of transgenic mouse models expressing human alpha 1 and alpha 2 from HLAs have allowed researchers to test the immunogenicity of vaccines with increase chances of the results to translate to human.

3.1.5. Chimeric HLA -A2 and humanised *in vivo* models to study CTL response.

Chimeric HLA -A2 (HHD II) is a fusion molecule consisting of a human HLA-A2 leader, the human β2 macroglobulin molecule covalently linked via a glycine serine linker to the α1 and α2 domains of the human HLA *0201 molecule, and the α3, transmembrane and cytoplasmic domains of the murine MHC class I (H-2Db) molecule. The HHD construct was amplified with designed primers from cDNA synthesised from total RNA isolated from EL4-

HHD cells. HHD (1458bp) was inserted into the EcoRV/HindIII sites of the mammalian expression vector pCDNA3.1(-) obtained from Invitrogen (Xue *et al*. 2016).

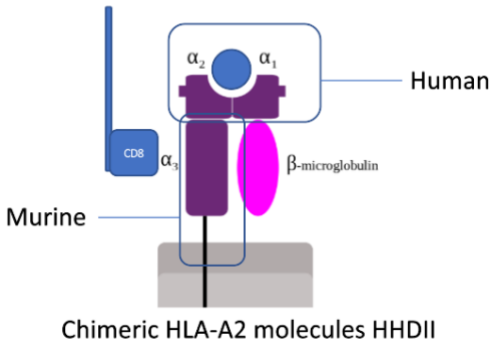

Figure 3.2*. Schematic representation of chimeric HLA -A2 molecule. This molecule consists of the human HLA-A*0201 α1 and α2 chains, which are fused with the α3 chain of the murine H-2Dd allele, covalently bound to human β2-microglobulin. Figure generated using Biorender.com.*

HHDII/DR1 and HHDII DP4 are double transgenic mice knockout for murine H-2 genes (MHC class I H-2b and MHC class II I-Ab), instead, they express an MHC class I molecule consisting of human HLA A*0201 α1 and α2 chains chimeric with α3 chain of murine H-2Dd allele called (HHDII) which is covalently bound to human β2-microglobulin and an MHC class II molecule consisting of human HLA-DRB*0101 for HHDII/DR1 (Pajot *et al*. 2004) or human HLA DP*0401 and human CD4 for HHDII/DP4 mice (Victoria Anne Brentville et al. 2022). This provides a good model for the study to assess immunogenic responses of different vaccines encoding multiple epitopes for HLA class-I and class-II peptides, or whole protein sequences within the context of the murine host system (Le Vu *et al*. 2022; Saif *et al*. 2014; McArdle, 2009).

Aim of this chapter

This chapter aims to generate *in vitro* target cell lines and *in vivo* models to assess the efficacy of Mut/WT hPAP42mer/ CPR/CAF®09b vaccine *in vitro* and *in vivo*.

Chapter 3: TARGET CELLS PREPARATION

3.2. Results

3.2.1. Generation of relevant target cells for the *in vitro* assessment of vaccine capabilities.

Given that the vaccine is made of hPAP peptides (section 2.2.3.2.1), tumour cell lysis by vaccine-induced CTLs is mediated by the PAP-derived antigen presentation via MHC molecule followed by its CTL recognition. Target cells that naturally express or cells modified to express PAP antigen can be used to study the cytotoxic capabilities of hPAP-derived vaccine-specific CTLs to lyse tumour cells *in vitro*. To assess the cytotoxic capabilities of the vaccine-specific CTLs two murine cell lines -TRAMP C1 and TRAMP C2 -, and three human cell lines -LNCap, DU145, and HEK93t were selected. Their MHC expression, PAP expression, and whether any adaptations are required are summarized in Table 3.1.

	Cell line	**Origin**	**MHC expression**	**PAP expression**	**Adaptation needed**
Murine cell lines	TRAMP C1	Mouse prostate adenocarcinoma	H2-K^b-D^b	Murine PAP^+	Murine PAP knockdown
	TRAMP C2		H2-K^b-D^b		
Human cell lines	LNCap	PCa bone metastasis	HLA $A2^+$	Human PAP^+	HHDII transfection / human PAP knockdown
	DU145	PCa brain metastasis	HLA $A2^-$	-	HHDII and human PAP transfection
	HEK293t	Human embryonic kidney cells	HLA $A2^+$	-	

Table 3.1. *The list of murine and human cell lines used for this research as target cells to assess vaccine efficacy.*

3.2.1.1. Human cell lines

As mentioned in (Table 3.1) two human PCa cell lines (LNCap and DU145) derived from metastatic deposits and non-cancerous human HEK293t cells were selected to assess the vaccine capabilities *in vitro*. LNCap cell line was established from a supraclavicular lymph node lesion in a 50-year-old Caucasian male, diagnosed with stage-D prostate cancer sequentially failed hormone therapies and chemotherapies and developed bone metastases. LNCap is commonly used as an androgen sensitive PCa model (Saranyutanon

et al. 2020). DU145 cells were established from the brain metastasis of a 69-year-old Caucasian diagnosed with advanced prostate carcinoma with widespread metastasis. This cell line is commonly used as *in vitro* PCa models and is shown to be tumorigenic when orthotopically injected into mice (Dowling, Berthon Eliche, and Bagasra, 2022) (Saranyutanon *et al*. 2020). HEK293t is one of the derivatives of HEK293- a transforming human embryonic kidney cell with sheared adenovirus type 5 DNA- modified to express a temperature-sensitive mutant SV40 T-antigen which facilitates them to generate recombinant proteins within plasmid vectors containing the SV40 promoter. The ease of transferability and high protein productivity make them a suitable *in vitro* model for immunotherapy developmental studies (Iuchi *et al*. 2019).

3.2.1.1.1. Assessment of MHC class I expression on human cell lines

The human cell lines (LNCap, Du145, and HEK293t) are HLA class I genotyped, with LNCap and HEK293t, being described as positive for HLA *A0201 (Carlsson *et al*. 2007; Vogel *et al*. 2013). The HLA -A2 expression on LNCap has been reported to be low without any increase in response to IFN-g stimulation (Carlsson *et al*. 2007). However, when assessing the expression of HLA -A2 in the LNCap cell line by flow cytometry, cells were found to be positive (Figure 3.3). Nonetheless, LNCap and HEK293t cells were transfected with HHDII to match the alpha3 loop and transmembrane domain of the HHDII/DR1 mice. This is because, the CD8+ T-cells require not only contact with MHC/peptide and T-cell receptors, but also the CD8 chain and the alpha 3 domain of the MHC class I molecule (Pennock *et al*. 2013) (Koh *et al*. 2023) from the same species to increase the contact between the TCR/peptide/MHC molecules thereby increasing the chance for a signal to be generated. Therefore, human target cell lines, naturally expressing HLA A2, transfected with HHDII enhance their recognition and lysis by CD8+ T-cells generated in HHDII mice. DU145 does not express HLA -A2 (Carlsson *et al*. 2007). Therefore, all human cell lines used in this study were transfected with chimeric HLA-A2 molecules.

Chapter 3: TARGET CELLS PREPARATION

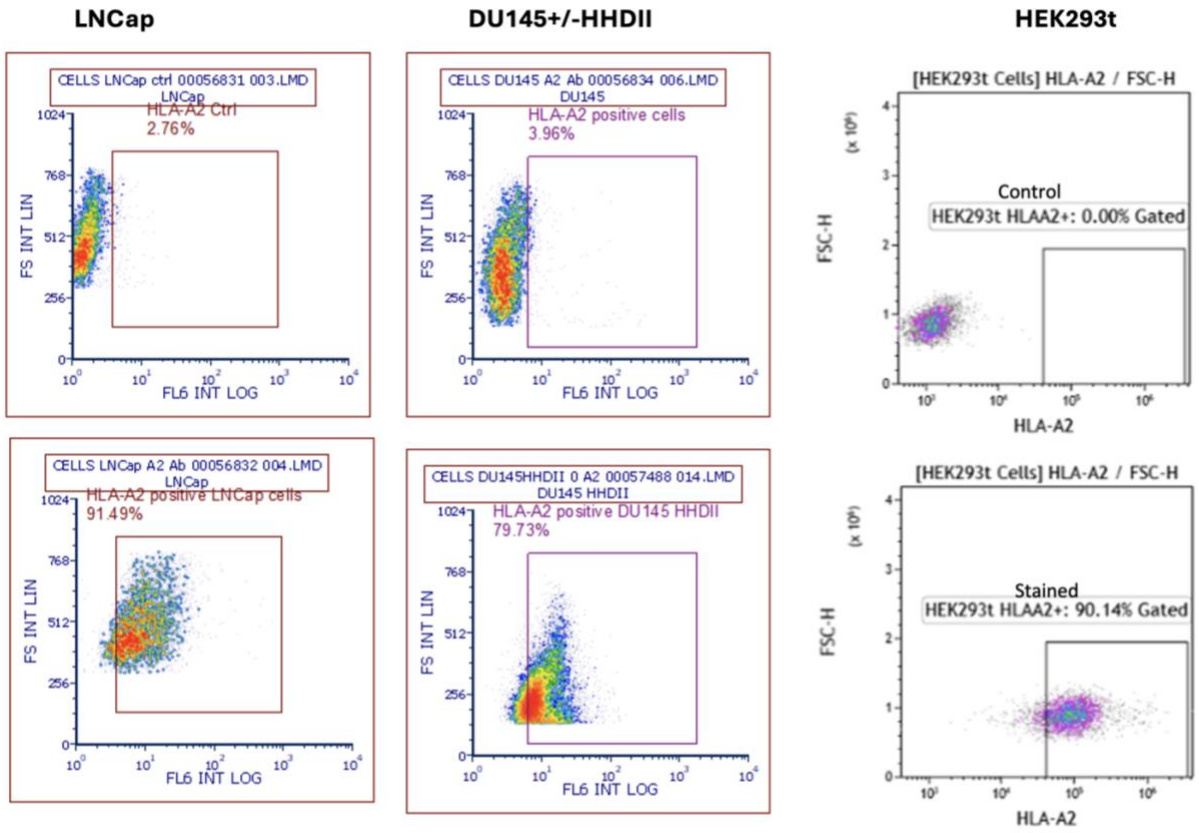

Figure 3.3. Flow cytometry analysis of HLA-A2 expression on human cell lines *LNCap, DU145-/+HHDII and HEK293t. LNCap and HEK293t cells naturally express HLA -A2 whereas DU145 and PC3 cells that do not express HLA-A2 were transfected with chimeric HLA-A2 plasmid. The expression of the HLA-A2 molecules was confirmed by flow cytometry staining with APC conjugated anti-human HLA-A2 antibody and compared with non-transfected cells.*

Before the cells were transfected, the lowest lethal geneticin (G418) concentration (1mg/mL) was determined by subjecting them to various geneticin concentrations for 14 days. Transfection of chimeric HLA-A2 molecule was then carried out using lipofectamine 3000 reagents (section 2.2.2.2); successfully transfected cells were retained by 1mg/mL geneticin. Following transfection, the expression of the chimeric HLA-A2 molecules on the cell surface was first verified by flow cytometry using APC conjugated anti-human HLA-A2 antibody (Figure 3.2). The selection of successfully HHDII transfected cells for LNCap and HEK293t was solely based on antibiotic selection (1mg/mL of G418) as the expression of the chimeric HLA-A2 cannot be differentiated from that of the wild-type HLA-A2 molecules.

3.2.1.1.2. Assessment of endogenous hPAP expression on human target cells

In human cell lines, LNCap cells have been described as PAP protein expressing naturally (Carlsson et al. 2007), hPAP expression on LNCap was confirmed by RT-PCR in comparison with PC3 cells which are known to be PAP negative (Figure 3.4(A)). To evaluate the role of hPAP expression in their sensitivity to killing by vaccine induced CTLs, suitable controls were generated by hPAP gene knocked down in LNCap HHDII cell lines. The lentiviral transduction method was used (described in section 2.2.2.3) and mRNA from successfully transduced cells (selected in 1µg/mL of puromycin) was extracted to assess the expression of the hPAP gene. The expression of hPAP was lower in LNCaP HHDII shRNA (hPAP knockdown) cells (Figure 3.4 (B)) compared to the empty vector control transduced cells: 100 to 5.5%. Western blotting analysis was also carried out to analyse the hPAP expression at the protein level. Cell lysate volume (µL) equivalent to 30µg of protein was run onto the SDS- PAGE gel, transferred to a nitrocellulose membrane, and probed with anti-PAP and anti-vinculin (internal control) primary antibody separately by cutting the membrane into two parts between 100kD and 70kD. Membranes were washed and incubated with HRP conjugated secondary antibody, put together, and developed using Clarity Western ECL Substrate. The bands were visualised using the Chemi gel documentation system. Internal control Vincullin bands were visualised at 125 kD and PAP at 55kD (Figure 3.4. (D))

Chapter 3: TARGET CELLS PREPARATION

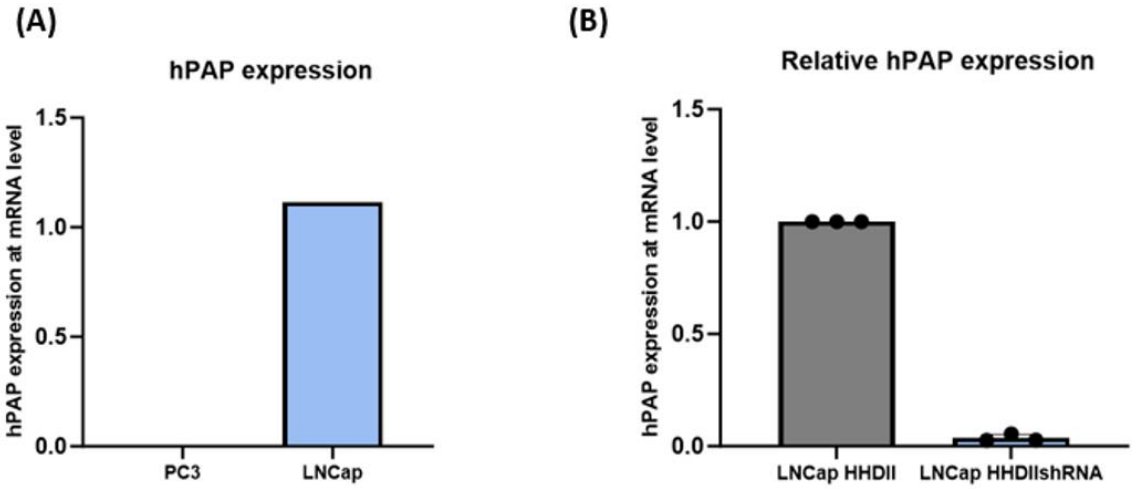

(C)

Cell line	$\Delta\Delta C_T$	% expression	% knockdown
LNCap HHDII	1	100	
LNCap HHDII shRNA	0.055510013	5.551001	94.449

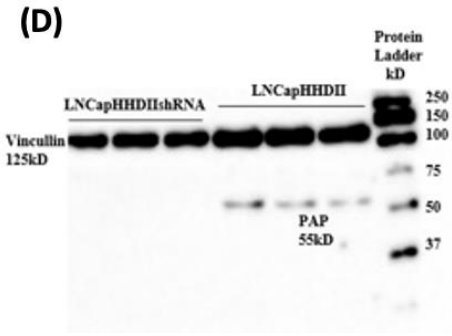

Figure 3.4. Endogenous hPAP expression and knockdown of hPAP in LNCap human cancer cell line*. (A) LNCap cells naturally expressing PAP were assessed by qPCR (B) Relative expression of the hPAP gene following knockdown with shRNA, results obtained are from three passages (n=3). PAP expression was reduced from 100% (LNCap HHDII) to 5.5% in LNCap HHDII shRNA cells. (C) % PAP expression calculated using $\Delta\Delta C_T$ method (% PAP Knockdown = (1-$\Delta\Delta C_T$) *100). (D) Western blot analysis of PAP protein expression in LNCap HHDII and LNCap HHDII shRNA cells (n=3). GUSB was used as reference gene for qPCR analysis and anti-Vincullin antibody used as western blot loading control for PAP analysis.*

DU145 and HEK293t cells do not (Carlsson *et al*. 2007) express PAP protein naturally, hence, were transfected to express human PAP protein using the lentiviral transduction method. Successfully transduced cells were selected with 1µg/mL of puromycin and hPAP knock-in was confirmed by RT-PCR and Western blot analysis (Figure 3.5). Since the PAP expression in HEK293t HHDII PAP was higher and consistent across successive passages, these cell lines were not cloned, however, DU145 HHDII PAP was cloned to obtain the highest PAP-expressing clone. Compared to non-transfected cells, the qPCR analysis of hPAP transfected HEK293t HHDII PAP cells revealed an approximately 8000-fold increase in hPAP

expression; fold change expression was determined using the $2^{-\Delta\Delta CT}$ method. ‘Clone-C4’ of DU145 HHDII PAP transfected cells showed the highest PAP expression, nearly 500-fold higher than DU145HHDII cells. Flow cytometry analysis also confirmed the HHDII expression on DU145HHDII PAP ‘clone -C4’.

Chapter 3: TARGET CELLS PREPARATION

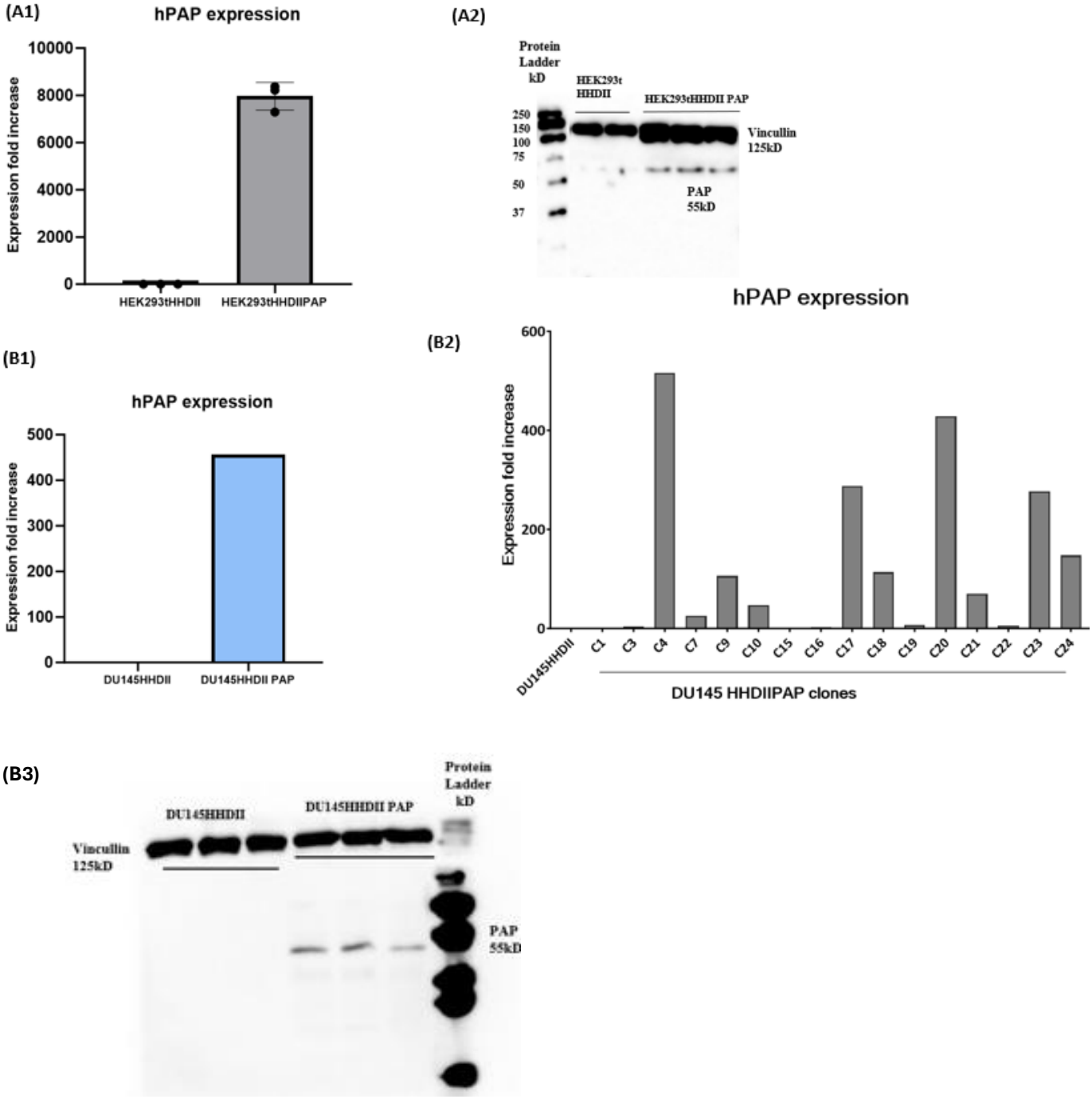

Figure 3.5. Endogenous hPAP expression in PAP transfected human cell lines. *(A1) Relative expression of human PAP gene before and after transfection using GUSB as reference gene in HEK293t HHDII cells (N=3). (A2) Protein expression of human PAP in HEK293t HHDII cells before and after transfection (n=3). (B1) qPCR analysis of PAP expression at RNA level on DU145 HHDII PAP cells. (B1) Relative human PAP gene expression in specific clones of DU145 HHDII PAP, (B2) clone C4 showed the highest expression which was 500-fold higher than non-PAP transfected cells. (B3) Western blot analysis of protein expression of hPAP in DU145 HHDII PAP clone C4 using anti-Vinculin antibody as western blot loading control.*

Chapter 3: TARGET CELLS PREPARATION

3.2.1.2. Murine cell lines

The mouse PCa cell lines TRAMP C1 and TRAMP C2 were derived from the transgenic adenocarcinoma of the mouse prostate (TRAMP), developing in C57BL/6 male mice transgenic for the tumour antigen coding region SV40 under the transcriptional control of the prostate-specific rat probasin promoter. These cell lines have been proven to be tumorigenic in syngeneic C57BL/6 mice and they no longer express SV40 (Martini *et al*. 2010). They grow in an androgen-independent manner (Philippou *et al*. 2020), can express MHC class I (K^b and D^b) and are liable to specific lysis by cytotoxic T lymphocytes (Yu *et al*. 2012). Besides, their tumorigenic properties, both TRAMP C1 and TRAMP C2 have demonstrated a diversity of prostate-specific genes including PAP, PSA, PSMA, and STEAP (Martini *et al*. 2010; Jachetti *et al*. 2013) which is highly expressed in human PCa, making these cell lines ideal to use as preclinical targets for PCa disease intervention.

3.2.1.2.1. Assessing MHC class-I expression on murine cell lines

TRAMP C1 and TRAMP C2 cells have been described as having MHC class I molecule (K^b and D^b) expression on their surface. The MHC expression on TRAMP cells was demonstrated to decline with *in vitro* passages, which can be reversed with *in vitro* IFNγ treatment (Yu *et al*. 2012). Though IFNγ treatment upregulates the MHC class I expression in TRAMP cells, it has also demonstrated that IFNγ induces immunosuppressive PD-L1 expression which can bind to the PD-1 receptor expressed on T-cells and obstruct the anti-tumour immunity (Yu *et al*. 2012; Martini *et al*. 2010). For this research, an *in vivo* passage of TRAMP C1 and TRAMP C2 cells were obtained by implanting TRAMP C1 and TRAMP C2 tumours in NOD SCID mice. To detect MHC class I (H2-Kb -Db) expression on TRAMP-C1 and TRAMP C2 cells, flow cytometry surface staining was performed using FITC conjugated anti-mouse H-2K /H-2D Antibody. Results obtained demonstrate the expression of MHC Class I in both TRAM P C1 and TRAMP C2 cells (Figure 3.6).

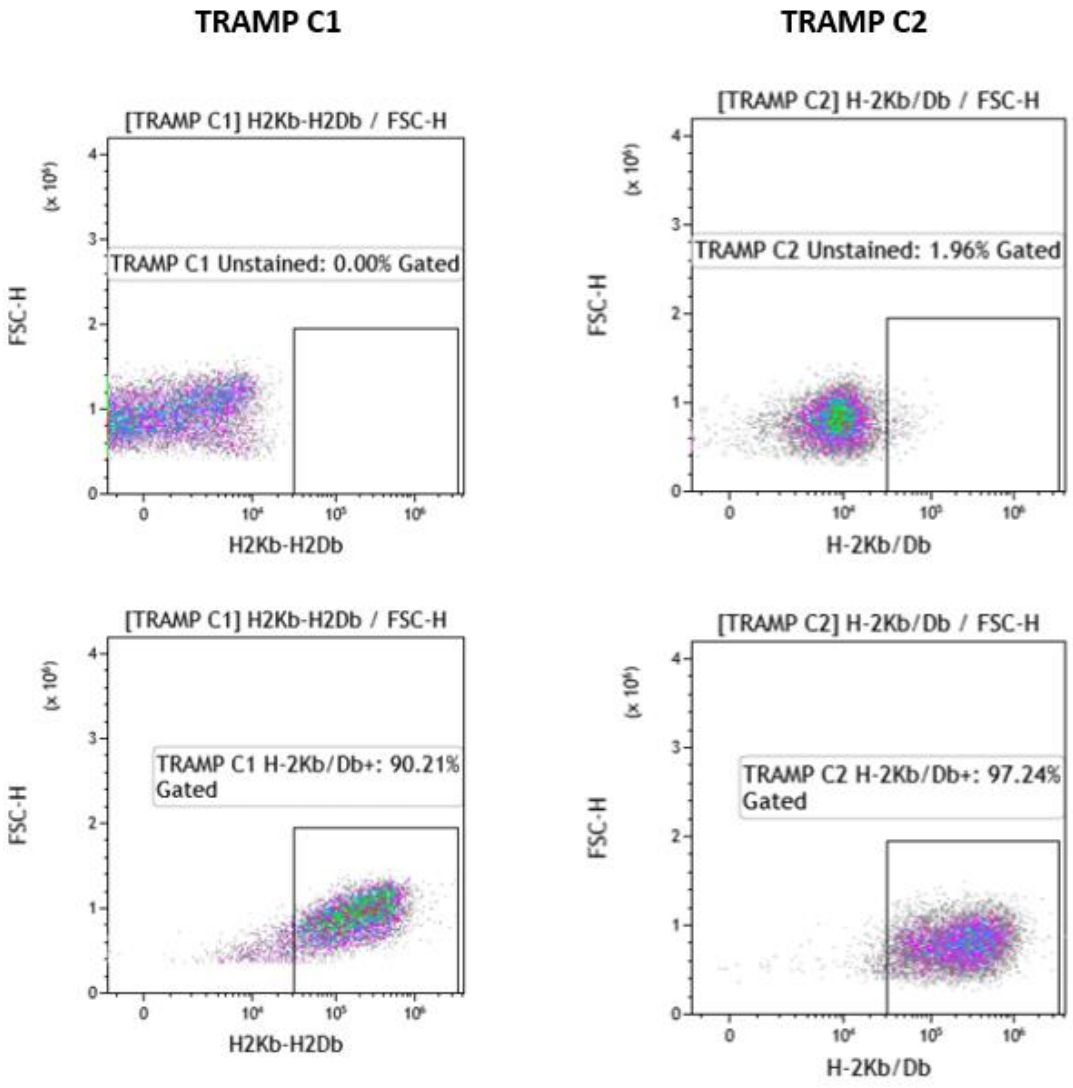

Figure 3.6. Flow cytometry analysis of MHC class I expression on murine cell lines. *TRAMP C1 and TRAMP C2 cells were stained with FITC conjugated anti-mouse H-2K /H-2D Antibody, analysed by a flow cytometer. Results confirm the MHC class I expression on TRAMP C1 and TRAMP C2 cells.*

3.2.1.2.2. Assessing endogenous mPAP expression and knockdown of mPAP

TRAMP C1 and TRAMP C2 express murine PAP protein naturally (Yu *et al*. 2012; Jachetti *et al*. 2013); which was confirmed by RT-PCR (Figure 3.7 (A)). To create appropriate controls for the study, the mPAP expression in the TRAMP-C1 and TRAMP-C2 cell lines was knocked down by the lentiviral transduction method following the selection of successfully transduced cells in 1µg/mL of puromycin. mPAP gene expression with both TRAMP cell lines

before and after the knockdown was analysed by qPCR (Figure 3.7 (B) and (C)) and Western blot analysis (Figure 3.7 (D)). The mPAP knockdown decreased the expression of PAP by around 90% in TRAMP C1 shRNA and about 98% in TRAMPC2 shRNA cells.

Chapter 3: TARGET CELLS PREPARATION

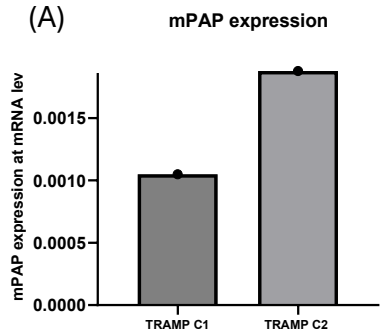

Cell line	$\Delta\Delta C_T$	% expression	% knockdown
TRAMPC1	1	100	
TRAMPC1 shRNA	0.09942786	9.942786	90.05721
TRAMPC2	1	100	
TRAMPC2 shRNA	0.01034354	1.034354	98.96565

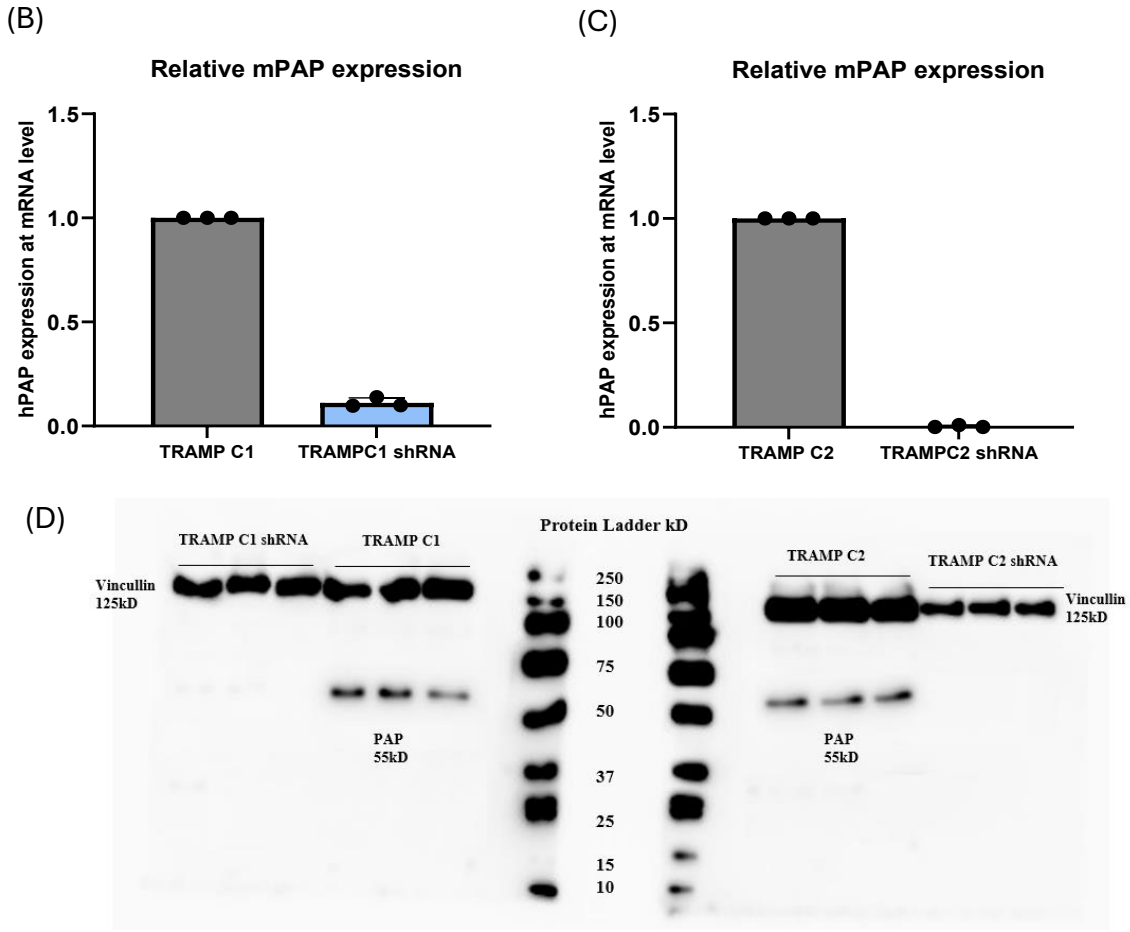

Figure 3.7. Endogenous hPAP expression and knockdown of hPAP in murine PCa cell lines. *TRAMP C1 and TRAMP C2 naturally expressing murine PAP were knocked down for the PAP gene, and the murine PAP expression was confirmed by qPCR and western blot analysis. (A) qPCR analysis of mPAP expression on TRAMP C1 and TRAMP C2 cells. Relative mPAP expression in (B) TRAMP C1 and (C) TRAMP C2 before and after PAP knockdown. (D) Western blot analysis of TRAMP C1+/- shRNA and TRAMP C2 +/-shRNA (n=3). No protein bands were detected for both TRAMPC1 shRNA and TRAMP C2 shRNA. GAPDH used as the reference gene for qPCR analysis, while anti-Vinculin antibody was employed as the loading control in the Western blot for PAP analysis.*

Chapter 3: TARGET CELLS PREPARATION

3.2.2. Generation of relevant tumour models to assess the vaccine efficacy *in vivo*.

3.2.2 .1. HHDII DR1 humanised mouse model.

HHDII DR1 double transgenic mice express a human HLA A*0201 α1 and α2 chain chimeric with the α3 chain of the murine H-2Dd allele, corresponding to a knockout of murine H-2 genes (Le Vu *et al*. 2022; Saif *et al*. 2014). The results obtained using these models will be transferrable to clinical settings because these animals are genetically modified with human genes. Because the human HLA heavy chains are chimeric with the murine H-2Dd α3 chain, the tumorigenicity of human cancer cells is not feasible with these models. Genetically altered murine cancer cells that are knockout for murine genes and then transfected with HHDII (Chimeric HLA A2) molecule can be used to generate tumour in HHDII mice. Therefore, TRAMP C1 murine prostate adenocarcinoma cells which are known to be carcinogenic in syngeneic C57BL/6 mice (Martini *et al*. 2010) were selected to apply the genetic modification to be implanted in HHDII mice. For this, the cell line was subjected to murine gene β2M knockout using the CRISPR-Cas9 technique followed by transfection with chimeric HLA- A2, murine PAP knockdown, and human PAP transfection.

3.2.2.2. β2M knockout in TRAMP C1 cells

TRAMP C1 cells were transfected with commercially obtained β2M sgRNA (described in Chapter 2, Table 2.2) following CRISPRMAX™ Reagent Cas9 nuclease transfection protocol (section 2.2.2.4). Transfected cells were cleaved, and PCR products of the cleavage detection assay were verified in a 2% agarose gel power system under low voltage. The percentage of cleavage was calculated using the following equation, which was calculated as 30%.

Cleavage Efficiency = 1- [(1-fraction cleaved)1/2]

Fraction Cleaved = Sum of cleaved band intensities / Sum of cleaved and parental band intensities

To identify the mutated single clone, sgRNA-cleaved cells were cloned, and the DNA of different clones was isolated, amplified by PCR, and analysed by 2% agarose gel

electrophoresis. At the same time, these clones were sent for Sanger DNA sequencing to identify the homozygous mutation. All clones were shown mutation in their nucleotide sequence but only clone 2 showed homozygous mutation in the sequencing report. The nucleotide sequences for 'clone 2' obtained by Sanger sequencing are shown below (Figure 3.8). Further to confirm the β2M knockout, mutated cells were stained with FITC conjugated anti-mouse H-2K /H-2D Antibody which was compared against the TRAMP C1 cells. Flow cytometry analysis confirms the β2M knockout in TRAMPC 1 cells (Figure 3.9).

(A) **Forward nucleotide sequencing of B2M knockout gene.**

```
B2M   ACTCGTAGGATTTTGAGGAAAAGATACTACGTTTTCAAAATGTGGGTAGACTTTGGGGGA  60
2F    ------------------------------------------------------------    0

B2M   AGCAGATCACTTATCCAGAGTAGAAATGGAACAGGGAGAAATAGAGGAACAAATGTAAGA  120
2F    ----------------------------------------GAGGAACAAATGTAAGA     17
                                               ******************

B2M   TGGTGCACGGTGCAGACTGAGCTCTGTTTTCATCTGTCTTCCCCTGTGGCCCTCAGAAAC  180
2F    TGGTGCACGGTGCAGACTGAGCTCTGTTTTCATCTGTCTTCCCCTGTGGCCCTCAGAAAC   77
      ************************************************************

B2M   CCCTCAAATTCAAGTATACTCACGCCACCCACCGGAGAATGGGAAGCCGAACATACTGAA  240
2F    CCCTCAAATTCAAGTATACTCACGCCACCCACCGGAGAATGGGAAGCCGAACATACTGAA  137
      ************************************************************

B2M   CTGCTACGTAACACAGTTCCACCCGCCTCACATTGAAATCCAAATGCTGAAGAACGGGAA  300
2F    CTGCTACGTAACACAGTTCCACCCGCCTCACATTGAAATCCAAATGCTGAAGAACGGGAA  197
      ************************************************************

B2M   AAAAATTCCTAAAGTAGAGATGTCAGATATGTCCTTCAGCAAGGACTGGTCTTTCTATAT  360
2F    AAAAATTCCTAAAGTAGAGATGTCAGATATGTCCTTCAGCAAGGACTGGTCTTTCTATAT  257
      ************************************************************

B2M   CCTGGCTCACACTGAATTCACCCCACTGAGACTGATACATACGCCTGCAGAGTTAAGCA  420
2F    CCTGGCTCACACTGATACCT--------------------ACCCCTGCGAAGTTAACCC  296
      ***************   *                     ** *****  ****** *

B2M   TGCCAGTATGGCCGAGCCCAAGACCGTCTACTGGGGTAAGCCTCAAGTTCTTCCTTACTT  480
2F    TGGCAGAATGGCCCATGCCAATACCGTCTACTGCGGTAAGCCTCACGGTCTTCCTTACTT  356
      ** *** ****** *  **** *********** *********** * ************

B2M   TCTGGACGCT----------------------                              490
2F    TCTGGACCCTCCAATTCTGGACGCTCCAAAA                              387
      ******* **
```

(B) **Reverse nucleotide sequences of B2M knockout gene**

```
B2M    ACTCGTAGGATTTTGAGGAAAAGATACTACGTTTTCAAAATGTGGGTAGACTTTGGGGGA 60
2R     ------------------------------------------------GNATCAGGGGGA 12
                                                        *  *  ******

B2M   AGCAGATCACTTATCCAGAGTAGAAATGGAACAGGGAGAAATAGAGGAACAAATGTAAGA 120
2R    AGCAGTTCAATTATCCCGAGTAGAAATGGAACAGGGAGAAATAGAGGAACAAAGGTACGG  72
       ***** *** ****** ************************************ *** *

B2M  TGGTGCACGGTGCAGACTGAGCTCTGTTTTCATCTGTCTTCCCCTGTGGCCCTCAGAAAC 180
2R   TGGTGCATGGGGCAGAATGAGTTTTGTCTTCATGCCTTTTGACACGCGTCCATCTGAAAC 132
     ******* ** ***** **** * *** *****   * **  *  * * ** ** *****

B2M  CCCTCAAATTCAAGTATACTCACGCCACCCACCGGAGAATGGGAAGCCGAACATACTGAA 240
2R   CCATTCAATTCAAGCATACTCGAGCCAGACACCGGAGAATGGGAAGCGGAACGTAACGCA 192
     ** *  ******** ******  ****  ****************** **** **  * *

B2M  CTGCTACGTAACACAGTTCCACCCGCCTCACATTGAAATCCAAATGCTGAAGAACGGGAA 300
2R   GTTCCACGTAACACAGTTCCAAATGCAAAACATGAAAATCCAAAAAAAAAAAGAACGGGAA 252
      * * ****************   **   ****  *********     ***********

B2M  AAAAATTCCTAAAGTAGAGATGTCAGATATGTCCTTCAGCAAGGACTGGTCTTTCTATAT 360
2R   AAAAATTCCTAAAGTAGAGATGTGCANGGAGTCGTTCAGCAAGGNNNN------------ 300
     ************************       *** **********

B2M  CCTGGCTCACACTGAATTCACCCCCACTGAGACTGATACATACGCCTGCAGAGTTAAGCA 420
2R   ----------NCTCACANTAACTTCACTCACACTGATACATACGCCTGCAGAGTTAAGCA 350
                ** *    * *  **** * ******************************

B2M TGCCAGTATGGCCGAGCCCAAGACCGTCTACTGGGGTAAGCCTCAAGTTCTTCCTTACTT  480
2R  TGCCAGTANGGCCGAGCCCAAGACCGTCTAC----------------------------  381
    ******** **********************

B2M TCTGGACGCT                                                    490
2R  ----------                                                   381
```

Figure 3.8. Sanger sequencing reports showing the mutation in the β2M gene of TRAMP C1 cells. *(A) Forward and (B) reverse nucleotide sequences of mutated clone were obtained by Sanger sequencing. The targeted site mutation is highlighted in yellow.*

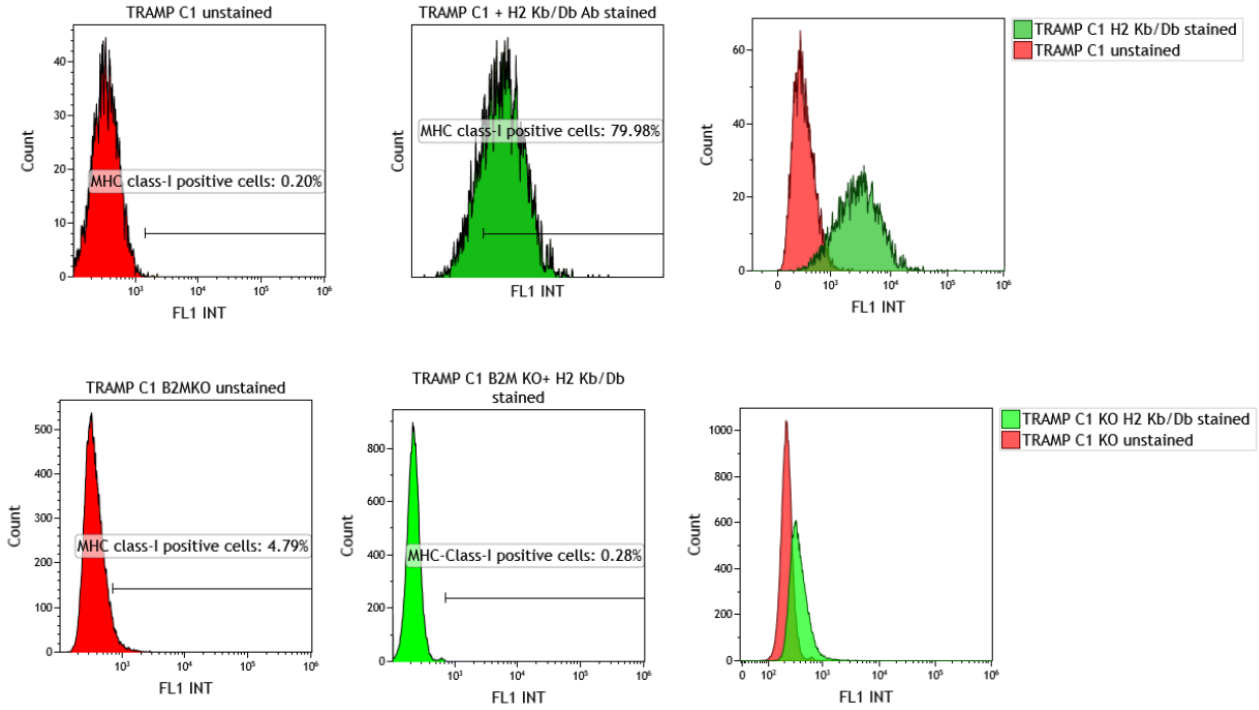

Figure 3.9. Flow cytometry analysis showing the mutation in the β2M gene of TRAMP C1 cell. *Flow cytometry surface staining of TRAMP C1 cells before and after knockout with FITC anti-mouse H-2K /H-2D Antibody. Red and Green histograms represent unstained (control) and Antibody-stained cells. A shift in the green histogram (antibody-stained cells) in TRAMP C1 cells indicates the MHC class I expression whereas there is no shift is seen in the stained TRAMP C1 β2M knockout cells indicating mutation in the B2M gene which is a component of MHC class I molecule.*

3.2.2.3. Murine PAP knockdown and human PAP knock-in.

The β2M knock-out TRAMP C1 cells were further modified to silence the murine PAP protein using MISSION shRNA plasmids and the knock-down of murine PAP was confirmed by qPCR analysis. There was about 99% of murine PAP knockdown was noticed (Figure 3.10). These cells were then transfected with human PAP by lentiviral transfection methods and successfully transduced cells were selected in puromycin 1µg/mL selection medium. The human PAP expression was confirmed by qPCR analysis using human PAP primers. The transfected cells were cloned to generate a population of cells with homologous PAP expression. The results obtained are shown below.

Chapter 3: TARGET CELLS PREPARATION

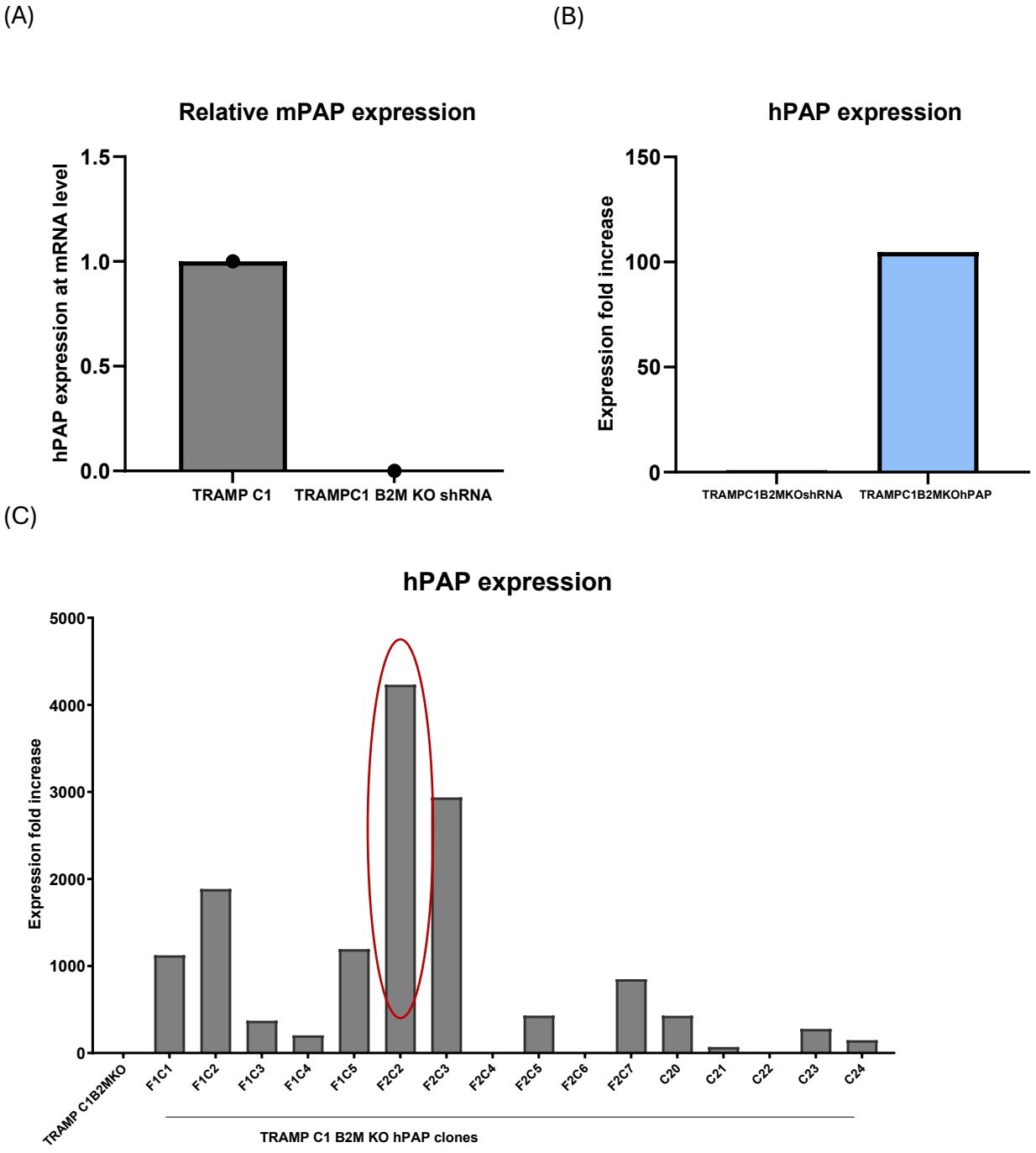

Figure 3.10. Murine PAP knockdown and human PAP transfection in TRAMP C1 β2M knock-out cells*. (A) q PCR analysis confirms a 99% reduction in the expression of the murine PAP gene. (B) qPCR analysis shows a 110-fold increase in the expression of the human PAP gene. (C) TRAMP C1 β2M knockout hPAP transfected clones, clone F2C2 showed a 4000-fold increased expression of the human PAP gene.*

3.2.2.4. Chimeric HLA-A2 transfection

The TRAMP C1 cells that were knockout for murine gene β2M and were transfected with the chimeric HLA-A2 gene. This step is necessary for the cell line to achieve characteristics to develop tumour in humanised (HHDII/DR1) mice. Cells were assessed by flow cytometry for the expression of the chimeric HLA-A2 using an anti-HLA-A2-APC conjugated antibody. Initial staining performed using the recommended amount of antibody did not show a significant level of staining which led to the initial wrong conclusion that the cells kept the plasmid (as they were able to grow in the presence of antibiotic while the non-transfected died), they did not express the HHDII gene at protein level. The transfection was repeated several times and led to the same conclusions. However, the antibody was then re-titrated, and the cells was found to be positive Figure 3.11(B). The expression of HHDII was also confirmed by qPCR analysis as shown in Figure 3.11(A), the result reveals a 4000-fold increase in the expression of HHDII at the mRNA level.

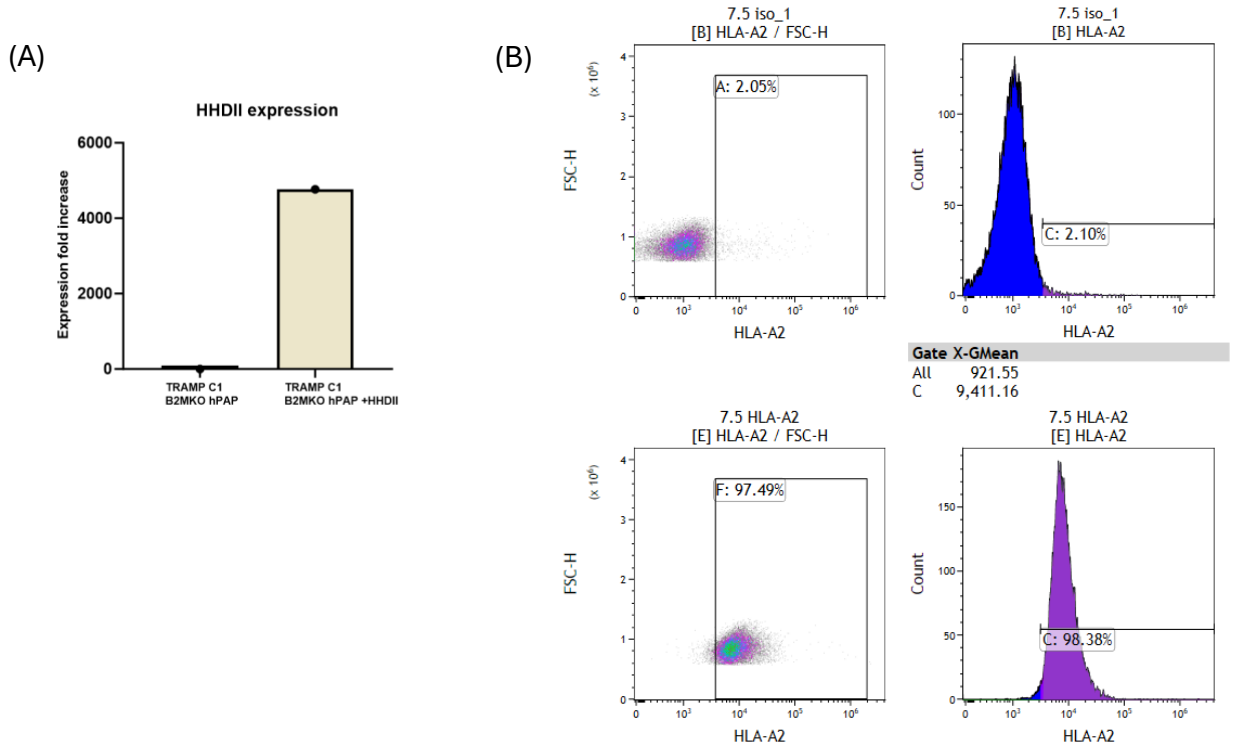

Figure 3.11. Chimeric HLA -A2 expression in TRAMP C1 B2M knock out cells. *TRAMP C1 B2MKO hPAP cells were transfected with HHDII molecule. (A) HHDII expression by qPCR analysis. (B) Surface protein expression of the chimeric HLA-A2 as assessed by Flow cytometry using isotype control and anti-human HLA A2 antibody (7.5 μL).*

Chapter 3: TARGET CELLS PREPARATION

3.3. Discussion

Under the right *in vitro* growth conditions (in temperature, hygrometry, and CO_2-controlled environment) authenticated cancer cell lines retain most of the genetic properties of the cancer of origin thus used as *in vitro* model systems, particularly in drug discovery and basic cancer research (Mirabelli, Coppola, and Salvatore, 2019). Two human PCa cell lines with different metastatic origins (DU145- Brain metastasis and LNCap- Lymph node metastasis) were selected as target cell lines to assess the *in vitro* efficacy of the vaccine. Since the vaccine was formulated with PAP peptides (section 4.2.1 and table 4.1), it was necessary to confirm the expression of PAP antigen on the target cells. Thus, the cell lines that do not naturally express PAP were transfected to express PAP antigen. The lentiviral transduction method was used which is a widely recognised and highly effective stable transfection method. The lentiviral PAP transfection was successful, and the efficiency of transfection was assessed by qPCR and western blot analysis respectively. qPCR allowed a relative measurement of PAP expression between transfected and wild-type cells, while the western blot confirmed the protein expression of the PAP gene. Moreover, the target cells (LNCap, TRAMP C1, and TRAMP C2) that naturally express PAP were knocked down for PAP to obtain suitable controls for the study. 98% of PAP knockdown was achieved for TRAMP C2 shRNA cells, whereas TRAMP C1 shRNA knockdown cells showed a 10% expression of PAP at the RNA level. Similarly, LNCap shRNA cells were shown a 94.4% reduction in endogenous PAP expression. The PAP knock-in and knockdown were assessed in three biological replicates to confirm the stable gene expression or its reduced PAP expression.

In addition to the antigen expression, MHC class I expression is also necessary for the tumour cells to present their tumour antigen to be recognised by the CTLs. Though MHC class I is expressed on all nucleated cells, cancer cells tend to downregulate its expression as a mechanism to evade recognition by T-cells (Blum, Wearsch, and Cresswell, 2013). Therefore, all target cell lines selected to assess the cytotoxic capabilities of the vaccine were confirmed for their MHC class I expression. The human cell lines chosen for this research were HLA class I genotyped, however, T-cells generated in the HHDII mouse

models have better responses towards antigen epitopes presented on chimeric HLA-A2 (HHDII) molecule. Therefore, all human cell lines were transfected with HHDII molecule by chemical (lipofectamine-3000) transfection method and its expression was confirmed by flowcytometry analysis.

HHDII DR1, HHDII DP4 and C57BL/6J mice were the murine models selected for this research to evaluate the vaccine efficacy in preclinical settings. The C57BL/6J mouse strain encoding the $H2^b$ MHC Haplotype is widely used in biomedical research. C57BL/6 mice are notable for their well-known cell-mediated immunity and NK cell activity, which have an important role in antitumor activity (Simon *et al*. 2013) (Bryant, 2011). Moreover, the pilot tumour implantation study as part of this research showed that TRAMP C2 cells naturally expressing MHC class I molecule and murine PAP gene were able to generate tumour in C57BL/6J mice. Therefore, these tumour models are efficient in evaluating the immune responses and tolerance of PAP peptides.

HHDII DR1/DP4 models are double knockout mice which represent a potent tool in translational cancer research when evaluating the potential validity of targeted therapy. Assessing the immunogenicity and *in vitro* efficacy of the HLA -A2, HLA- DR1 and HLA-DP4 epitopes of the hPAP42mer peptide is achievable using these models. HHDII DR1 mice have been shown to have HLA-A2-restricted CTL responses against HAGE peptides (Rukaia Almshayakhchi *et al*. 2021) and PAP peptides (Saif *et al*. 2014) when studied in our lab. Identification of $CD4^+$ T-cell responses that are restricted through HLA -DP*401 and HLA-DR*0101 alleles has also been studied using HHDII DP4 and HHDII DR1 transgenic mice in the presence of $CD4^+$ and $CD8^+$ blocking antibodies, with a significant reduction shown in HHDII DP4 transgenic strain responses suggesting a $CD4^+$ mediated (DP*0401 restricted) response (Victoria Anne Brentville *et al*. 2022).

In vivo assessment of vaccine efficacy in humanised tumour models is necessary to translate the therapeutic outcome to the clinic. A murine PCa cell line, that is modified to mimic human PCa characteristics in terms of its MHC and PAP antigen expression was necessary to generate HHDII DR1 models. For this reason, TRAMP C1 cells were knocked

out for the murine β2M gene encodes MHC class I and transfected with HHDII and human PAP gene to implant the tumour in these models. CRISPR-Cas9 gene editing technology was used to knockout the β2M gene. This technique causes a constant mutation in the gene guided by synthetic guide RNA leading to the elimination of gene expression. Nonetheless, a major challenge with CRISPR gene editing is off-target DNA cleavage leading to nonspecific alteration to the genome. For the β2M knockout in TRAMP C1 cells, three sgRNAs were obtained and there were up to 30% DNA cleavage obtained with two sgRNAs. All the clones showed mutation however, the homozygous mutation was confirmed in the nucleotide sequence of one of the clones. This clone was further modified to incorporate HDDII and human PAP. Though CRISPR-Cas9 technique was effective, the process was extensive, had taken no less than three months to obtain a clone with a homozygous mutation. Moreover, transfection with the HHDII plasmid was initially thought the be unsuccessful and several more attempts were made before the antibody concentration was adjusted and the cells were found to be positive by which time it was not possible to use them for tumour studies.

Chapter 4: VACCINE OPTIMISATION USING HHDII DR1 MICE

4. **Vaccine optimisation using HHDII DR1 mice.**

4.1. Introduction

Peptide-based vaccines are promising immunotherapeutic options for treating metastatic cancers. They elicit a cell-mediated antitumor response through antigen presentation of selected tumour epitopes to T-cells. Several factors, such as the choice of the competent target antigen, adjuvants, and immunisation regimes, must be taken into consideration to develop a peptide vaccine that is both clinically safe and more effective (Feola *et al.* 2020).

4.1.1. Choice of antigen for the development of the peptide-based cancer vaccine.

The antigen for vaccine development should be exclusively expressed by tumour cells, or expressed at a much higher level, and must be capable of being recognised by the patient's T-lymphocytes. Tumour-associated antigens (TAAs) and Tumour-specific antigens (TSAs) are used in developing peptide cancer vaccines. TAAs are antigens constitutively overexpressed by malignant cells but are also expressed in some healthy tissues at lower levels; for example, PAP and PSA (PCa antigens). Cancer testis antigens (CTAs) are TAAs expressed only by the human tumour cells with varying histological origins but not in somatic normal tissue, except in testis and placental tissues (Nelde, Rammensee and Walz, 2021). Unlike TAAs, TSA expression is specific to malignant cells, for example, antigens derived from HPV or EBV in cervical cancers and Hodgkin lymphomas respectively. Neoantigens are also TSA, they are mostly unique to each patient and are produced directly from non-synonymous single-point mutations, frameshifts, or insertions/deletions. T-cells do not develop immune tolerance to neoantigens and thus can induce a potent immune response to the neoantigens (Takahashi *et al.* 2021; Feola *et al*. 2020).

4.1.2. Choice of adjuvant in developing a peptide-based vaccine

In addition to the antigen selection, antigen presentation to the APCs followed by T-cell receptor stimulation and expansion by appropriate co-stimulatory molecules, and specific cytokines are crucial to achieve optimal antitumour effect. Therefore, antigens must be delivered correctly to be processed and presented by the APCs. Incorporating an adjuvant/

delivery vehicle to the peptide in the vaccine formulation enhances the peptide uptake by APCs (Nelde, Rammensee and Walz, 2021). Adjuvants enhance the immune response by regulating antigen localisation, preventing possible serum protease-associated antigen degradation, and extending antigen presentation time (Khong and Overwijk, 2016).

Adjuvants used in vaccine formulations can be categorised as; delivery systems (particulate), immune potentiators (immunostimulatory), and Mucosal adjuvants - which act as both immunostimulatory and delivery systems- (Apostólico *et al*. 2016). Delivery systems function as antigen carriers, with some specially made to promote the localisation of antigens to peripheral draining lymph nodes (LN), resulting in increased antigen presentation to the T-cells (Khong and Overwijk, 2016). They also activate innate immunity by initiating pro-inflammatory responses that recruit innate immune cells to the site of injection (Apostólico *et al*. 2016). Delivery systems cover a wide range of materials such as mineral salts (aluminium salts or alum), lipid particles, and microparticles (Apostólico *et al*. 2016; Khong and Overwijk, 2016). Immune stimulators activate innate immune responses directly by expressing costimulatory molecules such as CD80/CD86 and cytokines such as IL-12 by activated APCs (Khong and Overwijk, 2016) or through pattern-recognition receptors (PRRs) - that are widely expressed on immune cells- such as Toll-like receptors (TLRs), nucleotide-binding oligomerization domain- (NOD-) like receptors (NLRs), and the retinoic acid-inducible gene-I- (RIG-I-) like receptors (RLRs) (Apostólico *et al*. 2016; Pulendran, S. Arunachalam and O'Hagan, 2021). Apart from toll-like receptor agonists, cytokines such as IL-2, GM-CSF and IFNs are also used as immunostimulatory in vaccine preparation.

Incomplete Freund's adjuvant (IFA): IFA is water in oil emulsion without heat-killed mycobacteria. Its adjuvant activity is the result of a continuous release of the antigen from the oily depot, an increased antigen lifetime, and the stimulation of local innate immunity, as it enhances phagocytosis, leukocyte infiltration, and cytokine production. IFA has been used in human trials such as melanoma, renal carcinoma, and HIV infection, besides its high potency it has shown severe adverse reactions (Apostólico *et al*. 2016). In animal studies, IFA has been shown to increase immunogenicity, however, minimal epitope-sized

short peptides adjuvanted with IFA vaccines have led to T-cell retention and exhaustion at the vaccination site due to the long-term and chronic release of antigen by IFA. This was explained as prolonged antigen presentation and subsequent T-cell recognition and cytokine release at the vaccination site triggered chronic tissue inflammation and chemokine production led to the retention of effector T-cells at the injection site, preventing them from reaching the tumour site which ultimately, resulted in T-cell exhaustion and Fas/FasL-mediated T-cell apoptosis. When long peptides -which contain both MHC class I and class II epitopes - were emulsified with IFA T-cell trafficking to vaccine sites was eased thereby improving T-cell infiltration to the TME. When the peptide vaccine was formulated with IFA and TLR agonists, expression of co-stimulatory molecules was increased due to the induction of additional maturation signal via TLRs, hence improved $CD8^+$ T-cell priming was noticed in the lymph node. Apart from its use in animal studies development of clinical-grade IFA with reduced toxicity (Montanide incomplete seppic adjuvant (ISA)-51 and Montanide ISA-720) have been widely used clinically in experimental peptide and protein-based cancer vaccines (Melssen *et al*. 2022; Khong and Overwijk, 2016).

CpG-ODN as a TLR9 Ligand agonist: Synthetic oligodeoxynucleotide (ODN) sequences which contain unmethylated deoxycytidine-deoxyguanosine (CpG) dinucleotides (CpG-ODN), mimic bacterial CpG motifs and stimulate TLR9. TLR9 activation initiated by CpG ODN has been shown to activate plasmacytoid DCs (pDCs) and B-cells, leading to $CD8^+$ T-cell cytotoxicity, NK cell cytotoxicity and antigen-specific antibody responses (Guillem Montamat *et al*. 2021). Different classes of CpG (A, B, C and P) with different structural immunogenic properties have been classified. CpG adjuvant induces both humoral and cellular responses and has been used in clinical trials of cancer vaccines against breast/lung/ovarian cancers, sarcoma, melanoma, and glioblastoma (Guillem Montamat *et al*. 2021). Class A CpG-ODNs induce high IFN-α production through the activation of pDCs however are weak inducers of TLR9-dependent NF-κB signalling and pro-inflammatory cytokines such as IL-6 production. Class-B CpG, is a potent Th1 adjuvant and a strong activator of B cell and NK cells. Unlike class-A CpG, they are weak stimulators for IFN-α secretion from pDCs. Class C CpG displays combined features of class A and class B CPGs.

They stimulate B cells, induce pDCs' type I IFN secretion and are strong Th1-inducing adjuvants (Tosi *et al*. 2018).

CAF®09b- TLR 3 agonist: Liposome-based cationic adjuvant formulations are a family of adjuvants comprised of core component dimethyl-dioctadecyl ammonium (DDA) liposomes (Pedersen, Christensen, and Andersen, 2018). CAF®09b is a novel vaccine adjuvant formulated electrostatically combining cationic surfactant DDA with two immune-stimulatory components: The TLR3 agonist poly (I: C) and C-type lectin receptor MINCLE agonist monomycoloyl glycerol (MMG) (Zimmermann *et al*. 2022; Sofie Kirial Mørk *et al*. 2023). The liposomal vaccine adjuvant CAF®09b contains the TLR3 agonist polyinosinic: polycytidylic acid, which induces a type-I interferon (IFN-I) response and an antiviral state in the affected tissues. CAF®09b combined with viral/ cancer antigens has been studied for its immunostimulatory properties preclinically and clinically. In preclinical settings, CAF®09 liposomes have induced an influx of innate immune cells into the nose and lungs and upregulated IFN type-I gene expression when administered intranasally (Zimmermann *et al*. 2022). CAF®09b was shown to induce cellular ($CD8^+$ driven) mediated immune responses when combined with PAP-derived peptides (Le Vu *et al*. 2022). CAF®09b increases antigen intake by APCs and activates the APCs to induce cross-presentation and proinflammatory signalling for the activation of vaccine-specific $CD4^+$ and $CD8^+$ T-cells (Sofie Kirial Mørk *et al*. 2023). A first-in-man phase I clinical trial in locally advanced PCa patients was undertaken to investigate the safety and immunogenicity of a peptide vaccine comprising Bcl-XL_42 peptide-42 AA sequence of an anti-apoptotic protein Bcl-XL- and CAF®09b administered by different administration routes. The study demonstrated that the Bcl-XL_42-CAF®09b is safe and efficient in inducing $CD4^+$ and $CD8^+$ T-cell responses both by intramuscular and intraperitoneal injections in clinical settings where patients received concurrent anti-androgenic therapy (Sofie Kirial Mork *et al*. 2023).

Chapter 4: VACCINE OPTIMISATION USING HHDII DR1 MICE

4.1.3. Aim of this chapter

This chapter aims to validate the immunogenicity of the 'mutated human PAP 42mer' (MutPAP42mer) combined with CAF®09b over CpG as an adjuvant in HHDII transgenic models. The immunogenicity of two novel PAP 15mer peptides will be assessed in parallel. The vaccine formulations containing MutPAP42mer, and PAP15mer/s will be assessed for their ability to induce strong $CD8^+$ and $CD4^+$ specific immune responses against PAP antigen. The vaccine-induced CTLs will then be tested for their ability to recognise and kill human PCa cell lines *in vitro* in an HLA-restricted manner.

Chapter 4: VACCINE OPTIMISATION USING HHDII DR1 MICE

4.2. Results

4.2.1. Mutated human PAP42mer and epitope selections.

Given the immunogenic potential, safety, and specificity of PAP antigen to be used as a target for developing immunotherapies for PCa, a PAP 114-128, 15mer PAP sequence which is identical in both mouse and human was identified and tested in our laboratory (Chapter 1, section 1.4). This sequence was further elongated to 42mer (PAP 103- 144) long and one mutation was introduced at PAP 116th position -replacing leucine with Alanine- (Table 4.1).

Human PAP (GenBanl accession no. NM_001099)

MRAAPLLLARAASLSLGFLFLLFFWLDRSVLAKELKFVTLVFRHGDRSPIDTFPTDPIKESSWPQGFGQLTQLGMEQHYELGEYIRKRYR
KFLNESYKHEQVYIRSTDVDRTLMSAMTNLAALFPPEGVSIWNPILLWQPIPVHTVPLSEDQLLYLPFRNCPRFQELESETLKSEEFQKRL
HPYKDFIATLGKLSGLHGQDLFGIWSKVYDPLYCESVHNFTLPSWATEDTMTKLRELSELSLLSLYGIHKQKEKSRLQGGVLVNEILNHM
KRATQIPSYKKLIMYSAHDTTVSGLQMALDVYNGLLPPYASCHLTELYFEKGEYFVEMYYRNETQHEPYPLMLPGCSPSCPLERFAELVG
PVIPQDWSTECMTTNSHQGTEDSTD

Peptides	Sequence
Human PAP42mer WT	YIRSTDVDRTLMSLMTNAAALFPPEGVSIWNPILLWQPIPVH
Human PAP42mer Mutated	YIRSTDVDRTLMSLMTNLAALFPPEGVSIWNPILLWQPIPVH
Novel PQG 15mer	PQGFGQLTQLGMEQH
Novel CPR 15mer	CPRFQELESETLKSE

Table 4.1: Human PAP protein and PAP peptide selection for the development of vaccine. *The long sequence highlighted in yellow is PAP 42mer, PAP 114-128 sequence underlined is identical in both humans and mice. The AA highlighted in red displays the mutation of hPAP peptides to its human WT counterparts. The sequences highlighted in green at position PAP 64-78 and PAP 161-175 are the novel peptides that were identified to optimise the immunogenicity of MutPAP42mer (section 4.2.2).*

PAP42mer includes epitopes that are predicted to bind to HLA-A, HLA-B and HLA-DR haplotypes, which were identified using SYFPEITHI and IEDB databases and are illustrated in Table 4.2. Tools like SYFPEITHI and the Immune Epitope Database (IEDB) are commonly used to predict the binding affinity of peptides to individual HLA molecules. These databases containing a large collection of experimentally verified MHC binding peptides, also use algorithms to predict which peptides from a protein are likely to bind to specific MHC molecules (Sarkizova *et al*. 2019; Fleri *et al*. 2017). T-cell mediated immune response is initiated when peptides presented on MHC molecules are recognised by T-lymphocytes,

thus identifying the vaccine-derived MHC epitopes is crucial to understanding the pathways that vaccine effectively generates target-specific immune responses. Moreover, identifying epitopes that bind to common MHC alleles ensures the efficiency of the vaccine in a wide range of demographics (Sarkizova *et al*. 2019; Fleri *et al*. 2017).

Haplotype	Epitope	SYFPEITHI Score/IEDB rank	HLA subtype	Length
HLA-A	STDVDRTLMS	22/1.2	HLA-A*01	10mer
	ALFPPEGVSI	25/0.18	HLA-A*02:01	
	ILLWQPIPVH	22/0.1		
	EGVSIWNPIL	23	HLA-A*26	
	SAMTNLAAL	24/2.7	HLA-A*02:01	9mer
	DVDRTLMSA	23/5.1	HLA-A*02 *06	
HLA-B	FPPEGVSI	23	HLA-B*51:01	8mer
	LFPPEGVSI	25	HLA-B*15:16	9mer
	PEGVSIWNP	24	HLA-B*45:01	
	AALFPPEGV	21	HLA-B*51:01	
	FPPEGVSIW	25	HLA-B*53:01	
	RSTDVDRTL	31	HLA-B*58:02	
	IRSTDVDRTL	23	HLA-B*27:05	10mer
	RSTDVDRTLM	25	HLA-B*58:02	
	RTLMSAMTNL	23		
	VSIWNPILLW	23		
HLA-DRB1	DRTLMSAMTNLAALF	26/3.60	HLA-DRB1*0401 (DR4Dw4)	15mer
	DRTLMSAMTNLAALF	26/26	HLA-DRB1*0701	15mer
	VSIWNPILLWQPIPV	22	HLA-DRB1*1101	15mer
	PEGVSIWNPILLWQP	34/1.20	HLA-DRB1*1501	15mer
	RTLMSAMTNLAALFP	24/8.80		
	MSAMTNLAALFPPEG	24/57		
	LAALFPPEGVSIWNP	24/80		

Table 4.2: In silico analysis using the SYFPEITHI database and IEDB analysis revealed the predicted MHC binding scores of the peptides derived from the hPAP42mer WT. *The higher the SYFPEITHI score or lower the IEDB score, the stronger the binding of the peptide to the HLA allele indicated. SYFPEITHI maximum score for HLA-A2*0201 peptides are 36. Peptides used for the in vitro stimulation of splenocytes from vaccinated HHDII/DR1 humanized mice were chosen using this method. IEDB analysis resource NetMHCIIpan (ver. 4.1) tool. (http://tools.iedb.org/mhcii/) and SYFPEITHY algorithms* (http://www.syfpeithi.de/bin/MHCServer.dll/EpitopePrediction.htm).

4.2.1.1. Confirmation of better immunogenicity of hPAP 42mer mutated when combined with CAF®09b adjuvant.

The immunogenicity of the MutPAP42mer using either CpG1826 or CAF®09 adjuvant was assessed by the previous PhD student -Pauline Le Vu- and is demonstrated in Figure 4.1. The HHDII DR1 mice were injected with MutPAP42mer along with either CAF®09 or CpG 1826 adjuvant, and the ex vivo responses were subsequently re-challenged using smaller PAP peptides. The MutPAP42mer + CAF®09 vaccine induced a higher number of IFN-γ specific spots when splenocytes were co-cultured with smaller vaccine-derived peptides (Le Vu *et al*. 2022).

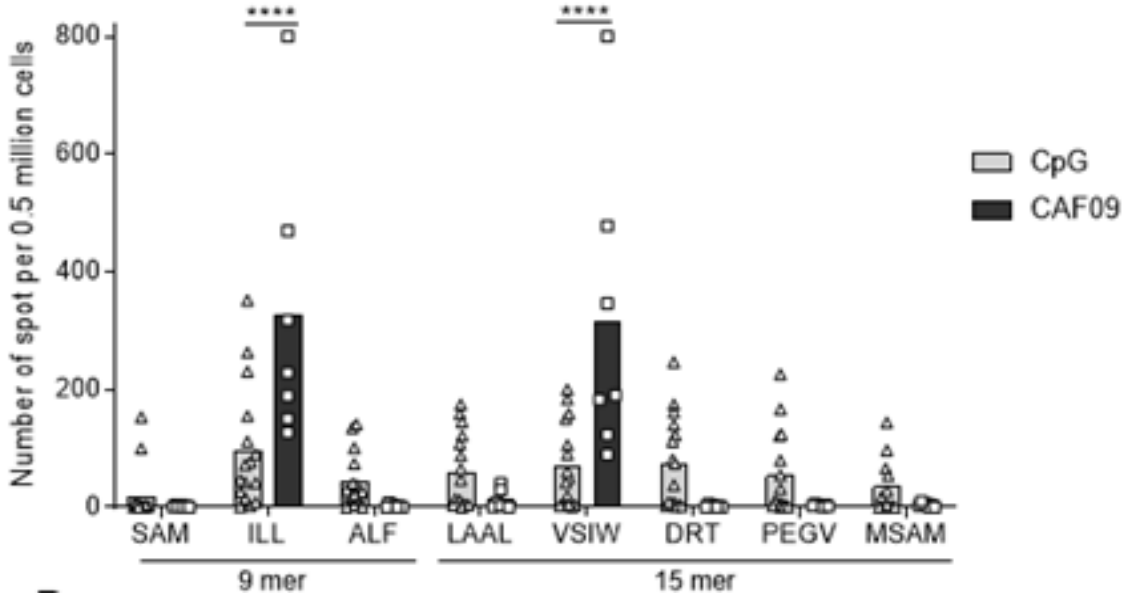

Figure 4.1. IFN-γ specific response of MutPAP42mer vaccine with CpG1826 or CAF®09b adjuvant. *hPAP42mer mutated peptide induces a higher number of IFN-γ specific spots released by splenocytes derived from the spleen of HHDII DR1 mice when CAF®09b is used as an adjuvant compared with CpG 1826. This experiment was done by Dr Pauline Le Vu whilst her PhD research, the graph is adapted from (Le Vu et al. 2022).*

To optimise the immunogenic capabilities of the hPAP42mer vaccine, the previously obtained results were first validated by conducting an immunisation study under the same experimental conditions using 3 HHDII DR1 mice per group. The group of mice immunised with the CAF®09b adjuvant received the vaccine (30µg MutPAP42mer + 100µL CAF®09b) 3 times (day -7, day 0, and day 15) while CpG 1826 was only administrated (30µg

hPAP42merMut+ 50μg CpG 1826) twice on day 0 and day 15 with the hPAP42mer mutated peptide. Animals were culled after a week of the last immunisation, splenocytes were isolated, and IFN-γ ELISpot assay was performed coculturing the vaccine-specific splenocytes with hPAP42merWT and MHC class-I and Class-II epitopes of hPAP42merWT (Table 4.2) to assess the immunogenicity.

As can be seen in Figure 4.2, similar results were obtained, confirming CAF®09 as a better adjuvant compared to CpG 1826. The results also confirmed that peptides ILL(9mer) and VSIW (15mer) were the only two peptides with a significant increase in the number of IFN-γ spots produced. LAAL (15mer) and MSAM (15mer) also produced IFN-γ spots however these were not significantly different between the two adjuvants nor were they when compared with cells alone. Additionally, in this experiment, the hPAP42merWT was used for the *in vitro* co-culture with vaccine-induced splenocytes and was found to induce a significantly greater number of spots with CAF®09b as an adjuvant. The number of spots was also higher than those with either ILL or VSIW peptide albeit not significantly different indicating more mice per group might be required to achieve significance. In addition, it was decided that all groups in subsequent experiments would use the same number of immunisations to confirm the better adjuvanticity of the CAF®09b based vaccine over the CpG adjuvanted vaccine.

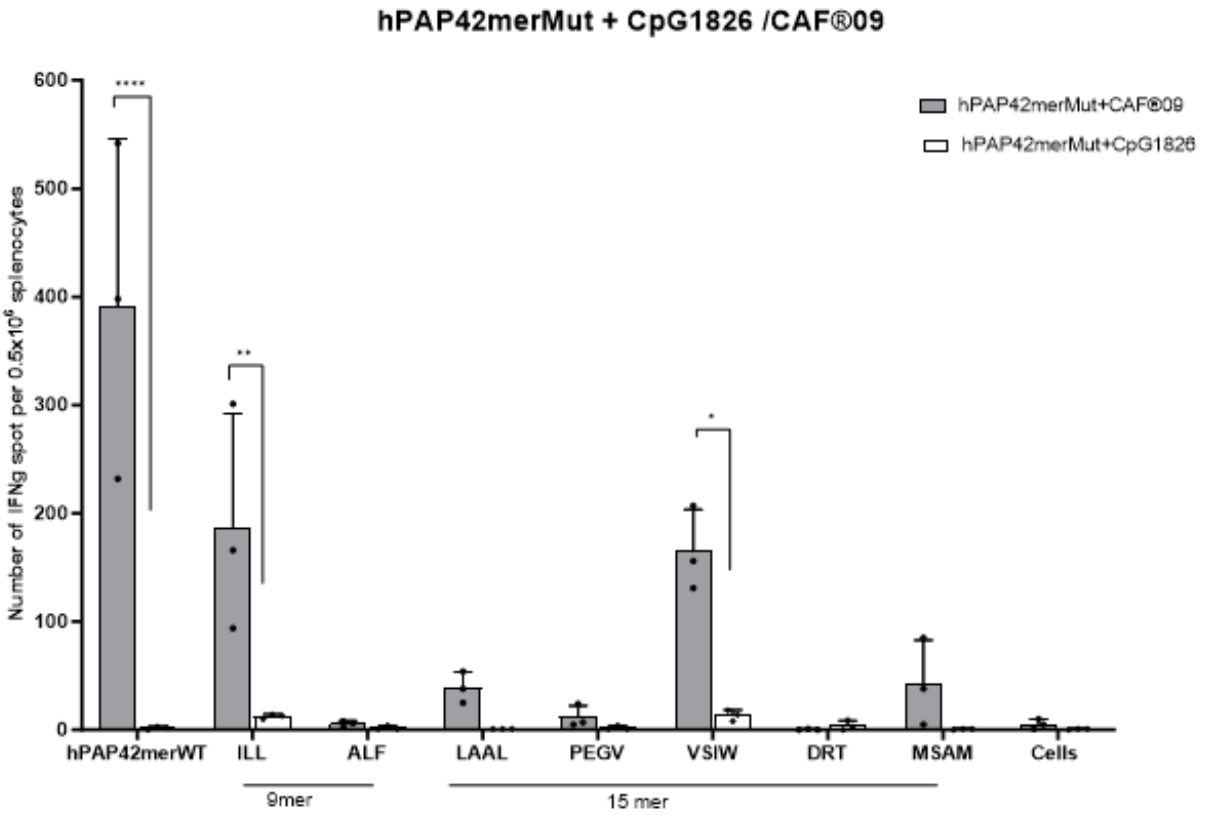

Figure 4.2. Confirm the superior immunogenicity of the hPAP42merMut CAF®09b based vaccine over the hPAP42merMut CpG1826 vaccine*. n=3/group. Bars represent the mean number of spots. A significant difference in the induction of peptide-specific IFN-γ releasing T-cells between immunisation groups was determined using a two-way ANOVA comparison test. **** P<0.0001; **P=0.0051; * P=0.0140*

The Mut hPAP42mer- CAF®09b vaccine was shown to induce high avidity and ILL-specific cytotoxic T lymphocytes capable of killing ILL-presenting cells *in vitro*, however, no $CD4^+$ T-cells response was previously demonstrated (Le Vu *et al*. 2022). Effective tumour elimination needs the activation of both $CD4^+$ and $CD8^+$ T-cells. $CD8^+$ T-cells directly lyse the tumour cells by identifying MHC class-I bound tumour antigens; however, activated $CD4^+$ T-cells are necessary for the induction of tumour-specific CTL responses that are dependent on activated $CD4^+$ T-cells. Moreover, $CD4^+$ cells enhance the cross-priming of $CD8^+$ cells through their interaction with APCs and are essential for the generation of memory T-cells including $CD8^+$ memory T-cells. Additionally, $CD4^+$ T cells demonstrate cytolytic effector

functions towards tumour cells expressing MHC class II- antigen complex (Riazi Rad *et al*. 2015).

4.2.2. Selection of hPAP 15mers to improve the anti-tumour efficacy of MutPAP42mer.

Consequently, two novel 15mer sequences (Table 4.1) - outside of the PAP42mer- were identified from whole PAP protein, these were predicted to bind strongly to HLA-DR molecules (Table 4.3) and were tested in combination with/without MutPAP42mer peptide.

Haplotype	Peptide	SYFPEITHI Score/IEDB rank	HLA subtype	Length
HLA-DRB1	PQGFGQLTQLGMEQH	28/24	HLA-DRB1*0401 (DR4Dw4)	15mer
		28/7.20	HLA-DRB1*0101	
		28/13	HLA-DRB1*0301 (DR17)	
HLA-DRB1	CPRFQELESETLKSE	33/0.29	HLA-DRB1*0101	15mer
		28/14	HLA-DRB1*0401 (DR4Dw4)	
		26/3.20	HLA-DRB1*0701	

Table 4.3. *hPAP 15mer peptides and their predicted MHC-II binding were analysed using the IEDB analysis resource NetMHCIIpan (ver. 4.1) tool and SYFPEITHY algorithms.*

4.2.2.1. Immunogenicity of novel human PAP 15mers compared using strong adjuvants CpG +/- IFA by IFN-γ ELISpot assay.

The immunogenicity of the two novel hPAP 15mers (PAP 64-78 (**PQG**FGQLTQLGMEQH) and PAP161-175 (**CPR**FQELESETLKSE)) was tested using CpG ODN (either 1826 or 2395) +/- IFA in HHDII DR1 mice using 3 mice per group. CpG 1826 and CpG 2395 are class B and class C CpG ODNs respectively; they strongly activate B-cells and generate TLR-9-mediated immune responses. CpG 2935 is a strong inducer of type I IFNs compared to CpG 1826 (Tosi *et al*. 2018). CpG 1826 when used as an adjuvant with the Mucin 1 oncogene vaccine, has been shown to induce Th1 immune responses, generation of CTLs, and Mucin 1 -specific antibodies in vivo in B16 tumour-bearing mice (Jie *et al*. 2018). CpG 2395 had demonstrated substantial DC activation and anti-tumour activity in melanoma mouse models (Zhang *et al*. 2021). IFA ensures the sustained release of antigens from the oily depot at the injection site, enhancing APCs to capture and process antigens effectively (Apostólico *et al*. 2016). CpG

ODN when used in combination with IFA as an adjuvant had further improved the Th1 immune response, and high IFN-γ production in C57BL/6J mice immunised with hepatitis B surface antigen (LUO *et al*. 2012).

Initial experiments were carried out using 50μg of CpG 2395 however this proved toxic to the animals for CpG 2395 and 10μg of CpG 2395 produced a smaller number of IFN-γ (Data not shown). Therefore, 25μg of CpG 2395 and 50μg of CpG 1826 were used in further experiments. HHDII DR1 mice were immunised (day 0 and day15) with hPAP15mer PQG or CPR + CpG2395 25μg /CpG1826 50μg +/- (1:1) IFA. Vaccine-induced immunogenicity was identified by co-culturing the splenocytes -which were isolated from the immunised mice 7 days after the last immunisation - with the same peptide *in vitro*. Figure 4.3 shows the findings of these experiments. Overall, immunisation with hPAP CPR peptide induced the highest numbers of peptide-specific IFN-γ secreting T-cells. In addition, IFA was found to improve the response obtained with CpG. Out of two classes of CpG adjuvants used to generate a robust immune response, CpG2395 with IFA produced more spots however this was not statistically significant. Since hPAP CPR was found to be more immunogenic than hPAP PQG; hPAP CPR was decided to incorporate along with MutPAP42mer in the future vaccine formulations.

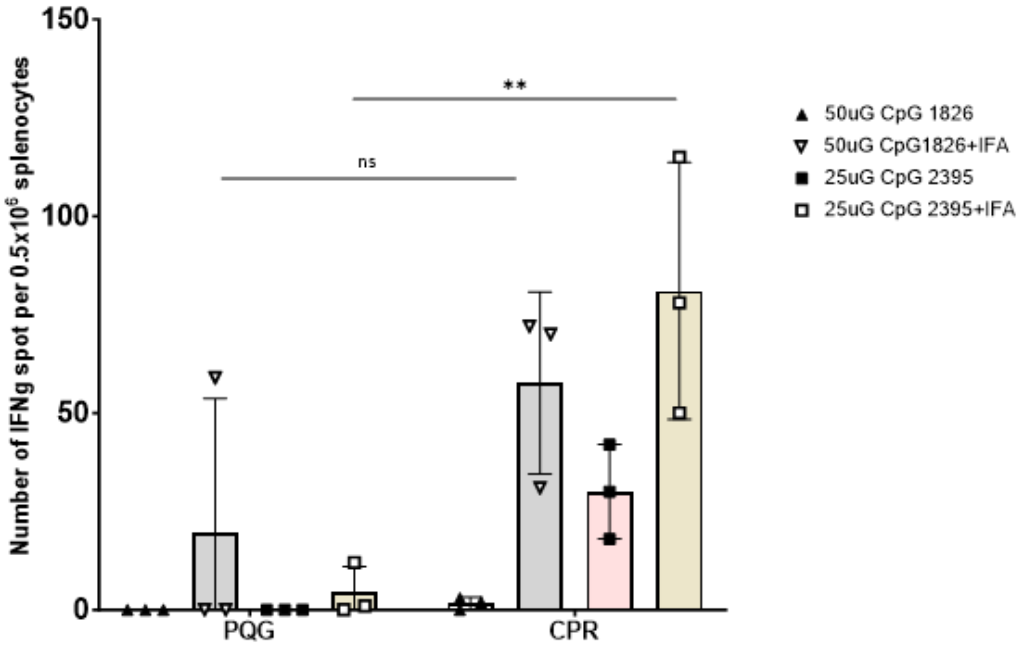

Figure 4.3. Immunogenicity of novel hPAP derived 15mers in HHDII DR1 with CpG (1826 or 2395) adjuvants +/-IFA. *n=3 per group. hPAP15mer CPR induced the highest number of IFN-γ spots when it is combined with CpG1826/CpG2395+/-IFA compared to hPAP15mer PQG. Bars represent the mean number of spots. A significant difference in the induction of peptide-specific IFN-γ releasing T-cells between immunisation groups was determined using a two-way ANOVA comparison test. **P=0.0019.*

4.2.3. Assessing the immunogenicity of MutPAP42mer +PAP 15mer CPR using adjuvants CAF®09b, CPG1826+IFA or CPG 2395+IFA.

The combined immunogenicity of the Mut hPAP42mer + 15mer CPR peptides was tested with either CAF®09b or CpG (1826 or 2395) +/- IFA, in HHDII DR1 mice; n = 9-11 mice per group over 4 different experiments. All animals received 3 doses of vaccine containing 30µg MutPAP42mer+30µg hPAP15mer CPR with adjuvant (100µL CAF®09b or 50µg CpG 1826 + 50µL IFA or 25µg 2395 +50µL IFA) on day 0, day 14 and day 28.

In the previous experiment performed to confirm the superior efficacy of MutPAP42mer with the CAF®09b adjuvant compared to the CpG adjuvant, the vaccine with CAF®09b was administered in three doses, while the CpG-adjuvanted vaccine was given in only two doses. This experiment was designed to replicate the results of the previous research student; thus, their experimental protocol was followed. The results obtained confirmed that the CAF®09b -adjuvanted vaccine was more immunogenic compared to the CpG-adjuvanted

vaccine. However, this conclusion is questionable because the higher immunogenicity observed with the CAF®09b -adjuvanted vaccine could be attributed to the additional dose administered. Therefore, the immunisation protocol was modified in the subsequent experiments, where all groups would receive the same number of immunisations.

Moreover, at this point, the splenocytes collected 7 days after the last immunization were found to generate IFN-γ spots non-specifically, even the internal control (splenocytes alone) produced a higher number of IFN-γ spots in the ELISPot experiment (data not shown). This phenomenon could be attributed to the sharp peak in the immune response kinetics, characterized by the activation, expansion, and proliferation of T-cells, which is typically followed by a contraction phase and memory phase (Kumar, Connors, and Farber, 2018). Consequently, splenocytes from immunized mice were collected 14 days after the last immunisation, and the ELISpot experiment was conducted by co-culturing the splenocytes ($0.5x10^6$) with long PAP42mer, hPAP-derived peptides 9mer (ILL), and 15mers (LAAL, VSIW) and CPR. Figure 4.4 shows the findings of these experiments. Immunisation with CAF®09b based vaccine was found to induce a greater number of peptide-specific IFN-γ secreting T-cells compared to immunisation with CpG 1826/2395+IFA following stimulation with all hPAP-derived peptides 9mer (ILL), and 15mers (LAAL, VSIW, and CPR) but was significant only with CPR peptide.

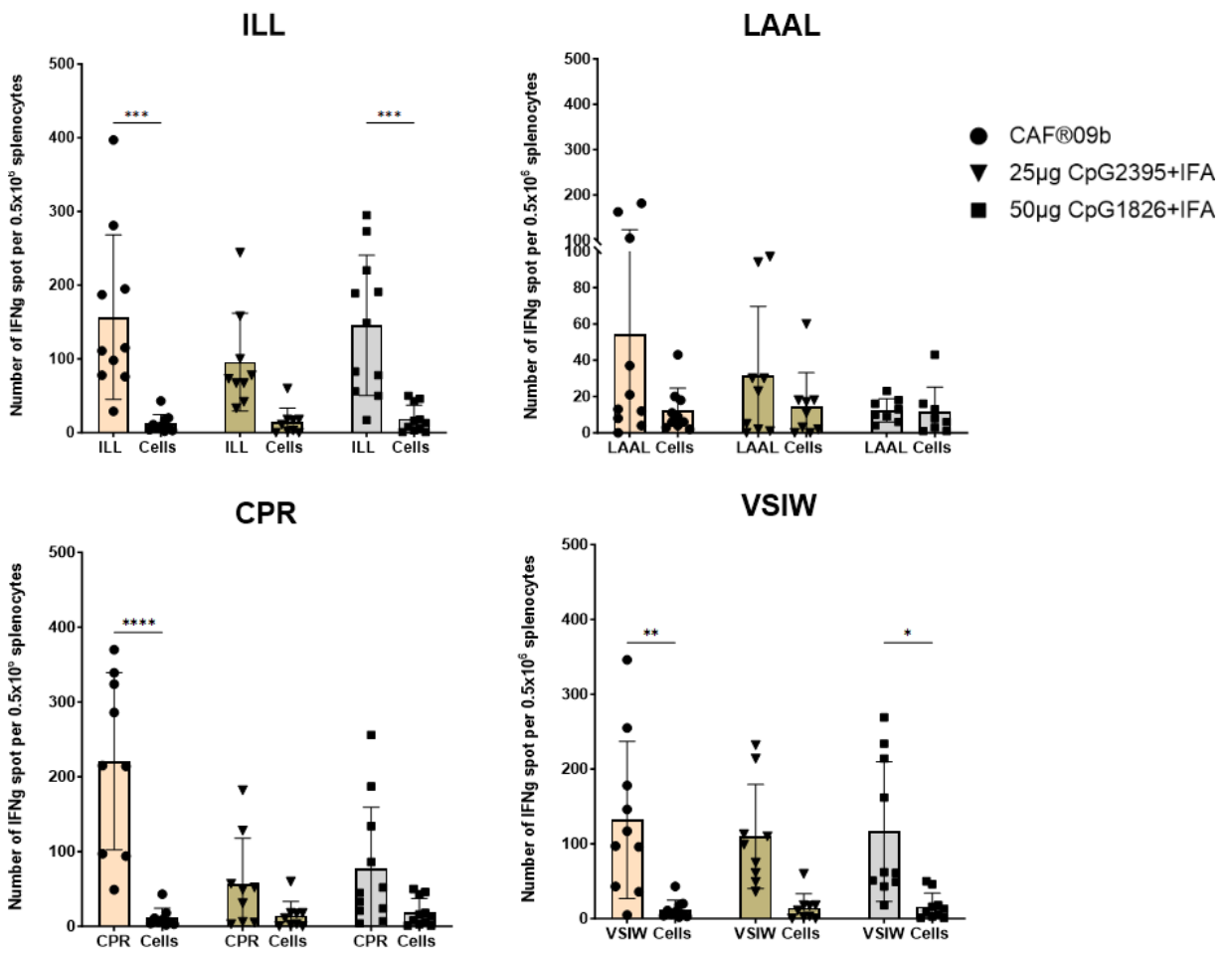

Figure 4.4. ELISpot results of immunisation of HHDII DR1 mice with MutPAP42mer + hPAP15mer CPR vaccine containing either CAF®09b / CpG 1826 +IFA/ CpG 2395 + IFA. *n= 9-11 per group between four different experiments. Mice immunised with MutPAP42mer+ hPAP CPR with adjuvant CAF®09b induced highest number of IFN-γ secreting T-cells compared to immunisation with CpG 1826/2395+ IFA following co-culture with hPAP-derived short peptides 9mer (ILL), and 15mers (LAAL, VSIW, and CPR) and there was a significant response noticed when splenocytes were co-cultured with CPR peptide. Bars represent the mean number of IFN-γ spots. A significant difference in the induction of peptide-specific IFN-γ releasing T-cells between immunisation groups was determined using a two-way ANOVA comparison test. * P= 0.0357; **P= 0.0031; ***P< 0.0002; ****P <0.0001.*

4.2.3.1. MutPAP42mer +hPAP15mer CPR + CAF®09b vaccine induced $CD8^+/CD4^+$ specific responses in HHDII DR1 mice.

The combined immunogenicity of the Mut hPAP42mer + hPAP15mer CPR peptides and the $CD8^+/CD4^+$ responses were tested in HHDII DR1 mice using CAF®09b. Vaccine-induced $CD8^+/CD4^+$ responses were identified by co-culturing the splenocytes of immunised mice with the hPAP-derived MHC class I peptides +/- Anti-mouse CD8a mAb Clone 2.43 and Class II peptides +/- Anti-mouse CD4 purified mAb Clone GK1.5 andin vitro. In addition to using IFN-γ ELISpot assay, MHC pentamer flow cytometry was performed to quantify epitope-specific $CD8^+$ T-cells.

4.2.3.1.1. Vaccine-specific $CD4^+/CD8^+$ responses assessed by IFN-γ ELISpot assay.

HHDII DR1 mice were immunised with the MutPAP42mer +CPR +CAF®09b vaccine on day 0, 14, and 28. Two weeks following the last immunisation, animals were culled, and spleen and terminal bleeds were collected. Vaccine-induced $CD8^+/CD4^+$ responses were identified by co-culturing the splenocytes ($0.5x10^6$) of immunised mice with the hPAP-derived peptides 9mer (ILL and ALF) +/- anti $CD8^+$, and 15mers (LAAL, VSIW, CPR and MSAM) +/- anti $CD4^+$ antibodies *in vitro*. The addition of antibodies was used to determine whether the response detected was due to $CD8^+$ T-cells or $CD4^+$ T-cells. The results obtained are shown below (Figure 4.5).

The co-culture of splenocytes with hPAP42mer WT long peptide and peptide-derived MHC class I and class II epitopes (Table 4.2) showed a significant reduction in the number of IFN-γ spots upon adding antibodies against CD8 and CD4. When vaccine-specific splenocytes were co-cultured with long peptide hPAP42mer WT + anti-CD8 / anti-CD4 antibody, 18 of the 22 animals that were tested showed a reduction in IFN-γ spots compared to the response obtained by hPAP42merWT alone (Figure 4.5). This indicates the presence of both $CD8^+$ and $CD4^+$ T cell epitopes within hPAP42mer to initiate MHC class I cross-presentation and MHC class II endosomal processing of antigen presentation. Further to analyse the $CD8^+$ specific T-cell activation, splenocytes were co-cultured with vaccine-derived MHC class I epitopes -

ILL, ALF, and SAM +/- anti-CD8 antibody. Results obtained demonstrate CD8 TCR blocking for all three epitopes with a significant blocking observed with ILL upon the addition of the anti-CD8 antibody (Figure 4.5). Similarly, to analyse the vaccine-induced CD4 T-cell activation, splenocytes were co-cultured with MHC class II epitopes of hPAP42mer WT (LAAL, VSIW, and MSAM) and CPR+/- anti-CD4 antibody. All class II epitopes tested showed a higher number of IFN-γ production which was inhibited by the addition of anti-CD4 except for VSIW (Figure 4.5). Inhibition of CD4 co-receptor with anti-CD4 antibody not shown any reduction in the immune responses generated by VSIW may be due to the presence of class I epitope (ILL) within 15mer VSIW sequence (VSIWNPILLWQPIPV), therefore immune responses generated were $CD8^+$ driven. Table 4.4 illustrates the number of mice tested vs the number of mice that were responsive to antibody blocking.

Peptide	**Antibody blocking**	**Number of mice tested**	**Number of mice responded**	**Comments**
42mer WT	Anti- CD4 and anti- CD8 Ab	22	18	
CPR 15mer	Anti- CD4 Ab	18	18	
LAAL 15mer		14	13	
VSIW 15mer		20		No CD4+ blocking observed
MSAM 15mer		6	6	
ILL 9mer	Anti- CD8 Ab	16	15	
ALF 9mer		14	13	No significant difference
SAM 10mer		6	6	

Table 4.4. *The list of the number of mice used to test the MutPAP42mer+ CPR+ CAF®09b vaccine for $CD8^+$/$CD4^+$ driven responses, along with the total number of mice that responded with Anti-mouse CD4 purified mAb Clone GK1.5 and Anti-mouse CD8a mAb Clone 2.43 blocking.*

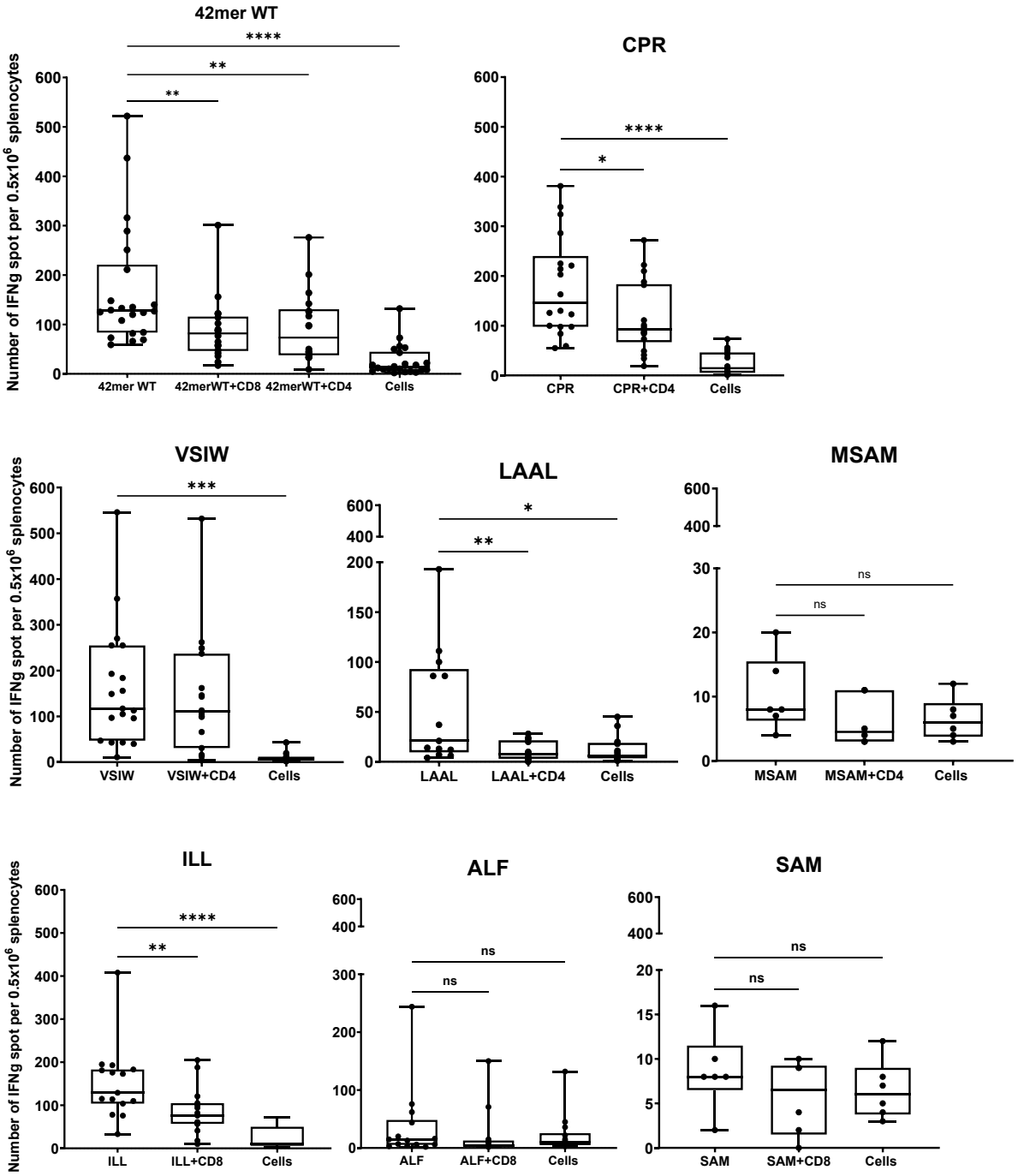

Figure 4.5. ELISpot results of CD4+/CD8+ driven immunogenic response generated by the immunisation of MutPAP42mer + hPAP15mer CPR CAF®09b in HHDII DR1 mice. *HHDII DR1 mice were immunised on day 0, day 15, and day 28 with MutPAP42mer +CPR +CAF®09b vaccine. Animals were euthanized two weeks following their last immunisation, splenocytes were isolated and co-cultured with hPAP42mer WT, class I (ILL, ALF, and SAM), and class II (CPR, VSIW, LAAL, and MSAM) vaccine-derived peptides along with anti-CD8 or*

*anti-CD4 antibodies. A significant difference in the induction of peptide-specific IFN-γ releasing T-cells and antibody blocking was determined using a one-way ANOVA comparison test. Co-culture of vaccine-induced splenocytes with hPAP42mer WT generated IFN-γ that was significantly blocked by both Anti-mouse CD4 purified mAb Clone GK1.5 and Anti-mouse CD8a mAb Clone 2.43. *P= 0.0360; ****P <0.0001. MHC class I epitopes (ILL, ALF, and SAM) responses were blocked by an anti-CD8 antibody with ILL showing a significant difference **P= 0.0088. MHC class-II epitopes (CPR, LALL, and MSAM) responses were blocked by the anti-CD4 antibody with a significant reduction in the immune response of CPR * P= 0.0160 and LAAL **P= 0.0069. The presence of anti-CD4⁺ antibodies did not show any reduction in the immune responses generated by VSIW.*

4.2.3.1.2. Vaccine-induced CD8⁺ T cells assessed by pentamer staining.

MHC pentamer is composed of five MHC peptide complexes arranged in a planar configuration that has improved staining sensitivity for T-cells with low-affinity TCR (Chang, 2021). Pentamers of vaccine-specific MHC class-I peptides (ILL and ALF) were obtained from Pro5® Proimmune. The presence of vaccine-induced splenic and circulating CD8⁺ cells was detected and compared with non-vaccinated mice. Splenocytes ($1x10^6$) and 100µL of blood samples of immunised mice and non-immunised mice collected at the end of the immunisation study were stained with phycoerythrin (PE)-conjugated pentamer along with CD45⁺, CD3⁺, and CD8⁺ antibodies as described in table 4.5. The gating strategy used to analyse the percentage of pentamer positive cells are shown in figure 4.6.

Antibody	Fluorochrome	Volume per test
CD45	FITC	2µL
CD3	BV421	1µL
CD8a	APC-Cy7	2.5µL
Live/dead yellow		0.5µL
Pentamer (ILL/ALF)	PE	10µL

Table 4.5. *List of antibodies used for pentamer immunophenotyping of MutPAP42mer+ CPR+ CAF®09b vaccine-induced splenocytes and blood cells.*

Before the splenocytes and blood samples were incubated with these surface antibodies and pentamers, both splenic and blood cells were incubated with FcR blocker in FCS to prevent the Fc receptor non-specific binding. Fc receptors on cells have a strong affinity for the Fc region of antibodies, therefore adding an FcR blocker to samples prevents the non-specific binding of antibodies to cells and significantly reduces potential nonspecific

antibody staining caused by IgG receptors (Andersen *et al*. 2016). Following staining, red blood cell lysis was performed according to the manufacturer's protocol for the determination of pentamer-specific $CD8^+$ blood lymphocytes. RBC lysis is an essential immunophenotypic analysis of leukocytes as this results in good light scatter separation of lymphocytes and red blood cell debris when analysed by flow cytometry without losing the viability of leukocytes (Einwallner *et al*. 2013). ILL and ALF pentamer staining demonstrated an increase in the percentage of antigen specific $CD8^+$ cells in the blood and spleen of vaccinated mice compared to non-vaccinated mice, with ILL pentamer showing a significantly higher increase (Figure 4.7). These findings corroborated the findings of the IFN-γ ELISpot experiment (Figure 4.5).

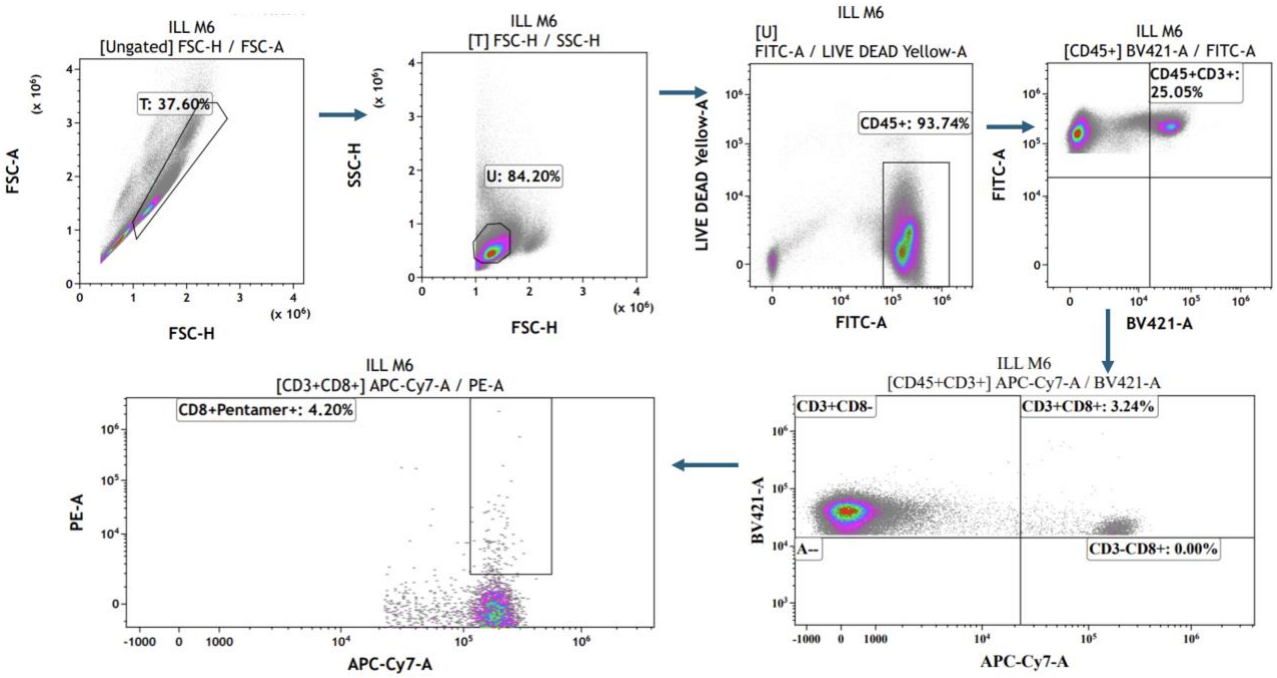

Figure 4.6. The gating strategy used to analyse the pentamer staining with example plots from ILL pentamer. *CD45+ cells were first gated from forward scatter/side scatter singlets. CD3+ cells were then selected from the CD45+ population, and further gating identified the CD3+CD8+ cell subset. Finally, the pentamer-positive cell population was identified within this gated population.*

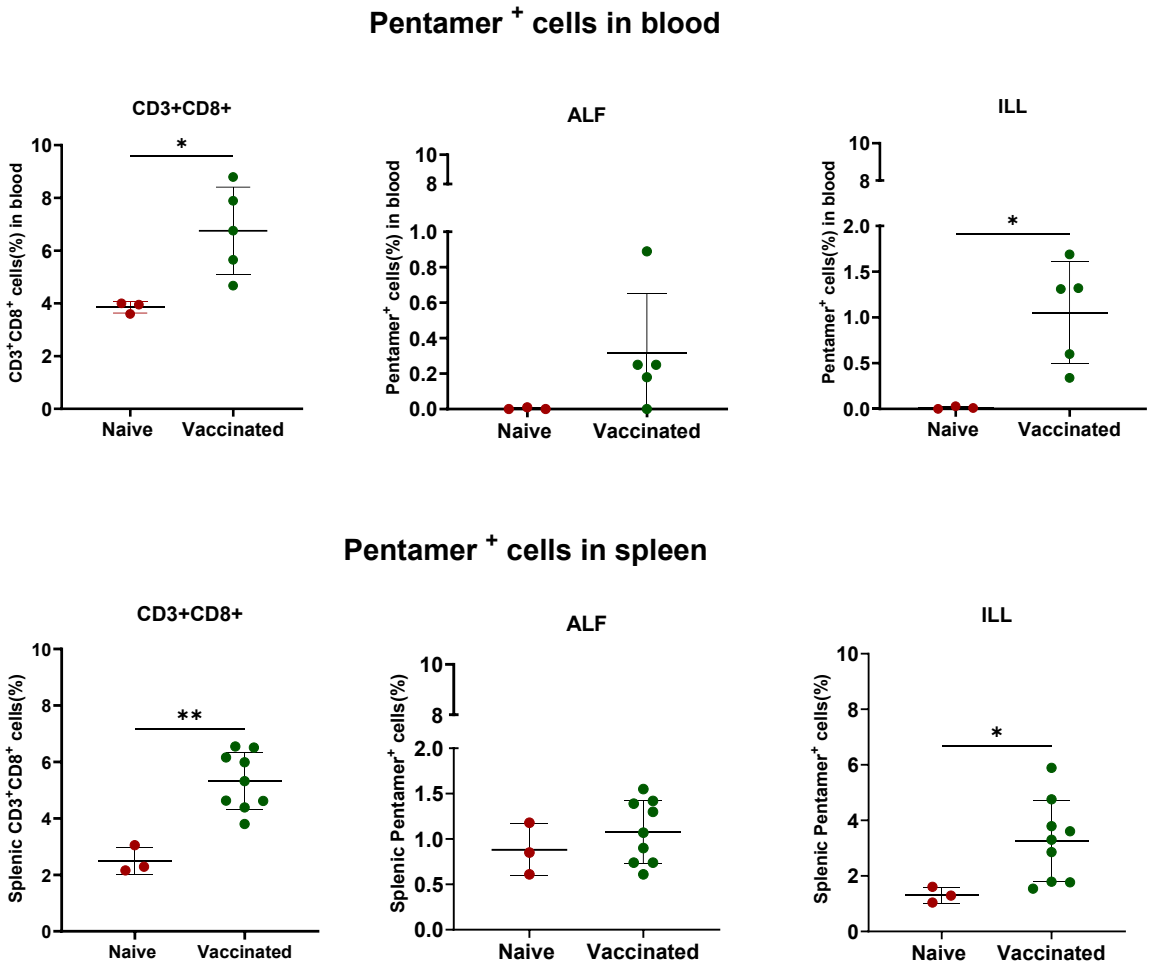

Figure 4.7: MutPAP42mer +CPR + CAF®09b vaccination increased circulating and splenic CD8⁺ CTLs in HHDII DR1 mice. *Illustrates the total number of CD8⁺ and ILL and ALF pentamer positive CD8⁺ cells present in the spleen and blood. HHDII DR1 mice were immunised with 3 doses of MutPAP42mer+ CPR+ CAF®09b vaccine two weeks apart, splenocytes (1x10⁶) and 100 µL of terminal blood collected from naïve mice and vaccinated mice at the end of the study, and phenotype with CD45⁺, CD3⁺ and CD8⁺ surface antibodies and PE-conjugated ILL or ALF pentamer after blocking potential nonspecific antibody staining with FcR Blocker in FCS. Samples were analysed by flow cytometry analysis. Results obtained show that vaccination has increased the number of total CD8⁺ cells. With regards to the ILL and ALF pentamer, there were ILL and ALF pentamer-specific CD8⁺ cells identified. *P ≤ 0.0357 has been determined by the Mann-Whitney test (n= 5-9).*

4.2.4. Cytotoxic capabilities of the hPAP vaccine assessed *in vitro* using relevant target cells.

Given that, the MutPAP42mer/CPR/ CAF®09b vaccine can generate $CD4^+/CD8^+$ specific CTLs in HHDII DR1 humanised mice, the next step was to evaluate, the ability of vaccine induced CTLs to recognise and eradicate prostate cancer cells *in vitro*. To assess the cytotoxic capabilities of vaccine-specific T-cells *in vitro*, target cell lines (LNCap, DU145 and HEK293t) were prepared. Vaccine-induced T-cells derived from HHDII DR1 immunised mice required the expression of the chimeric HLA-A2 molecule (HHDII) and PAP protein. In human prostate cancer cell lines, DU145 is known to be HLA-A2 and PAP negative, while LNCap is positive for both, and HEK293t is known to be positive for HLA-A2 but not PAP. All human target cell lines were transfected to express HHDII. Additionally, DU145 and HEK293t were transfected with hPAP and the LNCap naturally expressed PAP gene was knocked down for its PAP expression to be used as a specific control for the experiment as described in Chapter 3 section 3.2.1.

4.2.4.1. Vaccine-specific target recognition on vaccine-induced splenocytes.

T-cell co-culture assay was initially performed to analyse whether the T-cells can recognise the target cells. This was done in two different ways: either using vaccine-induced splenocytes directly isolated from immunised mice or using $CD3^+$ T-cells isolated from vaccine-specific splenocytes stimulated *ex vivo* with murine IL2 (mIL2) PAP peptides. When co-cultured with hPAP-expressing target cells under IFN-γ ELISpot experimental conditions, T-cells should recognise the PAP-derived MHC/peptide complexes presented by the target cells and release IFN-γ against the antigen. The PAP-dependent immune response is then measured and compared against its target control- which does not express the hPAP and T-cells alone response generated.

To measure the target recognition by vaccine-induced splenocytes, an IFN-γ ELISpot assay is performed, where $5.0x10^5$ splenocytes of immunised mice were co-cultured with hPAP expressing target cells and their controls (LNCap HHDII +/- shRNA, DU145 HHDII +/- PAP

and HEK293t HHDII +/- PAP). At the lowest effector: target (10:1) ratio target recognition was identified; however, no difference was seen between cells expressing PAP and those not expressing PAP or with anti-CD8^{+} antibodies blocking (data not included). Additional experiments were carried out with different effectors (T-cells) to target cells, there was evident recognition noticed at 50:1 (Effector: Target) ratio. The results are shown below (Figure 4.8). Vaccine-induced T-cells were able to identify the PAP fragments presented by the target cells (LNCap HHDII, DU145 HHDII PAP and HEK293t HHDII PAP) in an HLA-restricted manner and were able to generate antigen-specific IFN-γ comparatively higher than that of its control (LNCap shRNA, DU145 HHDII and HEK293t HHDII) and T-cells alone response.

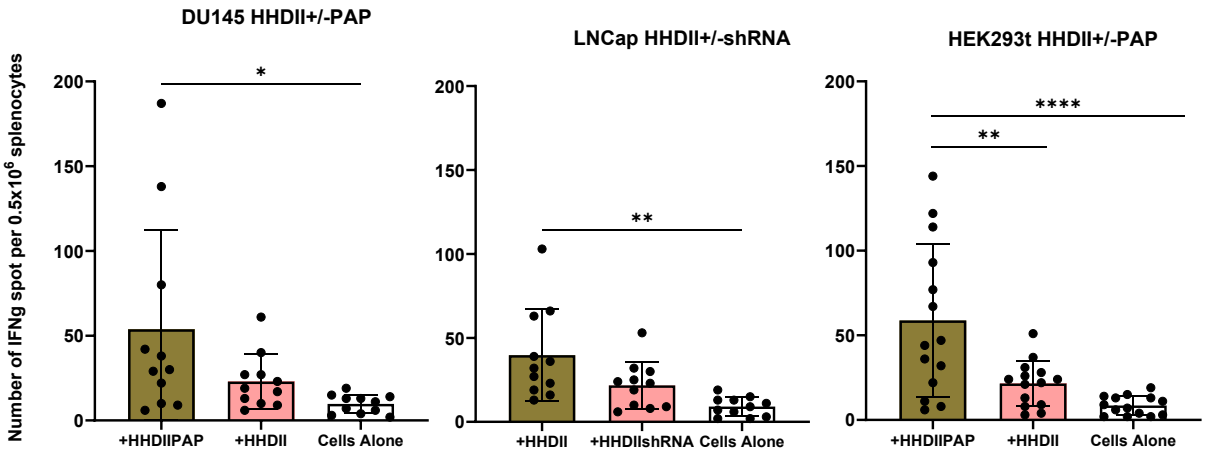

Figure 4.8. IFN-γ ELISpot results of target cell recognition by vaccine-induced splenocytes. *HHDII DR1mice received 3 doses of the MutPAP42mer +CPR +CAF®09b vaccination spaced two weeks apart. Animals were culled 14 days after the last immunisation, splenocytes were isolated and co-cultured with DU145 HHDII +/-PAP, LNCap HHDII +/- shRNA or HEK293t HHDII +/- PAP at a 50:1 (effector: target) ratio. * p ≤ 0.02, ** p ≤ 0.002 and **** p ≤ 0.0001 as determined by an ordinary one-way ANOVA test (n= 11-14 over 2-3 independent experiments).*

4.2.4.2. Vaccine-specific target recognition assessed on isolated $CD3^+$ T-cells.

Vaccine-induced splenocytes were stimulated *ex vivo* with hPAP42mer WT and 50U/mL mIL2 for 5 days, followed by one day of rest during which the splenocytes were treated only with 50U/mL mIL2. When splenocytes are cultured with IL-2 *in vitro*, it promotes the proliferation and differentiation of T-cells, especially $CD8^+$ CTLs and $CD4^+$ helper T-cells. The presence of vaccine-derived peptides in the culture enhances the expansion of T-cells that are specific to the antigen thereby promoting a higher frequency of antigen-specific T-cells within the culture (Bachmann and Oxenius, 2007; Look *et al*. 2023). However, the presence of a higher concentration of peptide in the culture can lead to high-affinity T-cell death. This can be explained as a phenomenon known as 'activation-induced cell death' which occurs because of intense and prolonged TCR signals triggering pro-apoptotic pathways, including the Fas-Fas Ligand interaction and mitochondrial apoptosis mechanisms (Zhan *et al*. 2017). In this study, a concentration (1µg /mL) of hPAP42merWT used for *ex vivo* stimulation of splenocytes, was found lethal to the cells. As a result, splenocytes were treated with a ten times lower concentration (0.1µg /mL) of peptide and 50U/mL mIL2, which restored the viability of cells to 80-90%. $CD3^+$ T-cells were isolated from *ex vivo* stimulated splenocytes using 'Mouse T-cell isolation kit- Stem cell Technologies', following the manufacturer's protocol. The total cell counts and viability of the $CD3^+$ T cells were identified using NucleoCounter NC250.

IFN-γ ELISpot assay was performed using $0.2x10^6$ $CD3^+$ T-cells co-cultured with hPAP expressing target cells and their controls (LNCaP HHDII +/- shRNA, DU145 HHDII+/- PAP and HEK293t HHDII +/- PAP) at 50:1 (E: T) ratio. The results obtained are shown in Figure 4.9A. $CD3^+$ T-cells were able to identify the antigen presented by the targets (LNCap HHDII +/- shRNA, DU145 HHDII +/- PAP, and HEK293t HHDII +/- PAP), released IFN-γ in HLA and PAP restricted manner. Nonetheless, the results obtained with LNCap HHDII and DU145 HHDII PAP were not significantly higher than its control LNCap HHDII shRNA and DU145 HHDII.

To further analyse whether recognition was $CD8^+$ driven, $CD3^+$ T-cells were co-cultured with prostate cancer target cells LNCaP HHDII and DU145 expressing HHDII and PAP, with and without the presence of anti-CD8 antibodies. T-cells blocked with Anti-mouse CD8a mAb

Clone 2.43 before coculturing with target cells showed a significant reduction the target recognition, indicating a strong CD8⁺-driven immune response (Figure 4.9B).

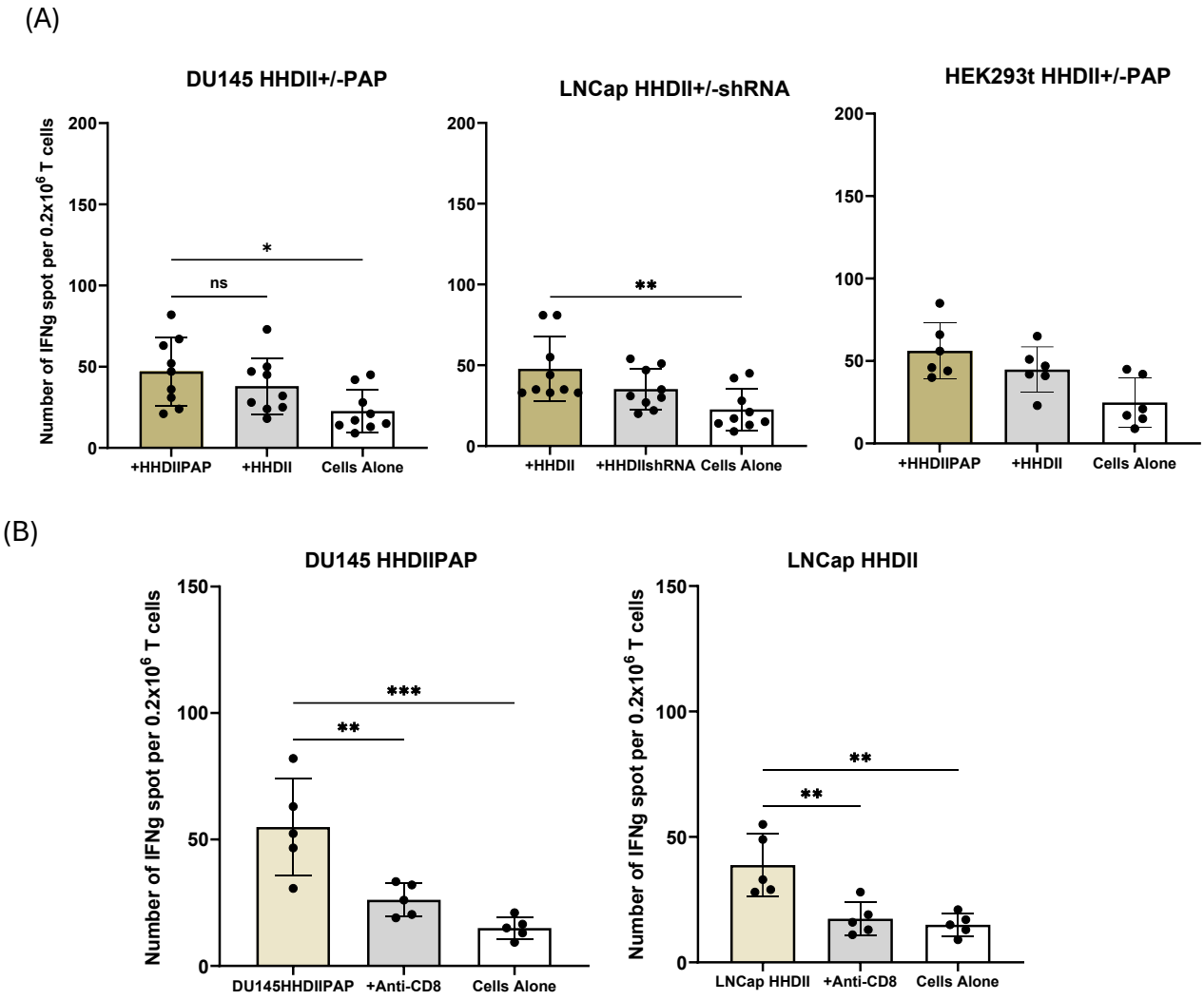

Figure 4.9. Vaccine-induced CD3⁺ T-cells recognise PCa target cells in HLA and PAP-restricted manner. *Splenocytes of immunised mice were restimulated for 5 days in vitro in the presence of low levels of hPAP42mer WT and mIL2. After one day of rest, CD3⁺ T-cells were isolated by negative selection using STEMCELL* EasySep™ *Mouse* T-Cell Isolation *Kit, following manufacturer instructions. Isolated CD3⁺ T cells were co-cultured with target cells (LNCap HHDII +/- shRNA, DU145 HHDII +/- PAP and HEK293t HHDII +/- PAP) at a 50:1 (E: T) ratio in an IFN-γ ELISpot plate to assess (A), target recognition, (B) in the presence of anti- CD8 antibody for identifying CD8⁺ driven response. For the IFN-γ ELISpot, * P ≤ 0.002, ** P ≤ 0.007, and *** P ≤ 0.001 as determined by an ordinary one-way ANOVA test (n = 5-9).*

4.2.4.3. Vaccine-specific target killing

The cytotoxicity of vaccine-specific $CD3^+$ T-cells to PAP-expressing target cells was tested by WST-8 cell viability assay using a commercially available CCK-8 kit following the manufacturer's protocol. CCK-8 solution contains a water-soluble tetrazolium (WST-8) salt, which is reduced by the dehydrogenase activities in cells to give a yellowish formazan dye. The amount of formazan dye generated is directly proportional to the number of live cells present in the well (Xia *et al*. 2020). Target cells or their controls along with $CD3^+$ T-cells were seeded into 96-well cell culture plates at a 50:1 (E: T) ratio and incubated at 37 °C and 5% CO_2 for 24 hours. A comparable quantity of target cells was treated with 0.1% SDS, either to determine the maximum amount of cell death or as a positive control. The total number of live cells can be calculated by adding the absorbance of each well where the same number of T-cells or target cells were cultured separately. WST-8 solution 10µL per 100µL of culture media was added, followed by further incubation for 4 hours under the same conditions. The absorbance was measured at 450nm, percentage of live cells was calculated using the following formula.

% Live cells = [Absorbance of T-cells with targets and controls ÷ (Absorbance of T cells alone + Absorbance of Target alone) *100

% Dead cells = 100 - live cells

The results showed (Figure 4.10) that the T-cells from vaccinated mice recognize and kill LNCap HHDII and HEK293t cells expressing HHDII and PAP at higher levels than their controls LNCap HHDII shRNA and HEK293t HHDII, which showed less or no PAP expression. The killing observed with DU145 HHDII PAP cells was at a higher rate compared with DU145 HHDII. The highest cell lysis rates that were noticed by LNCap HHDII, DU145 HHDII PAP, and HEK293t HHDII PAP were 67%, 67%, and 53%, respectively.

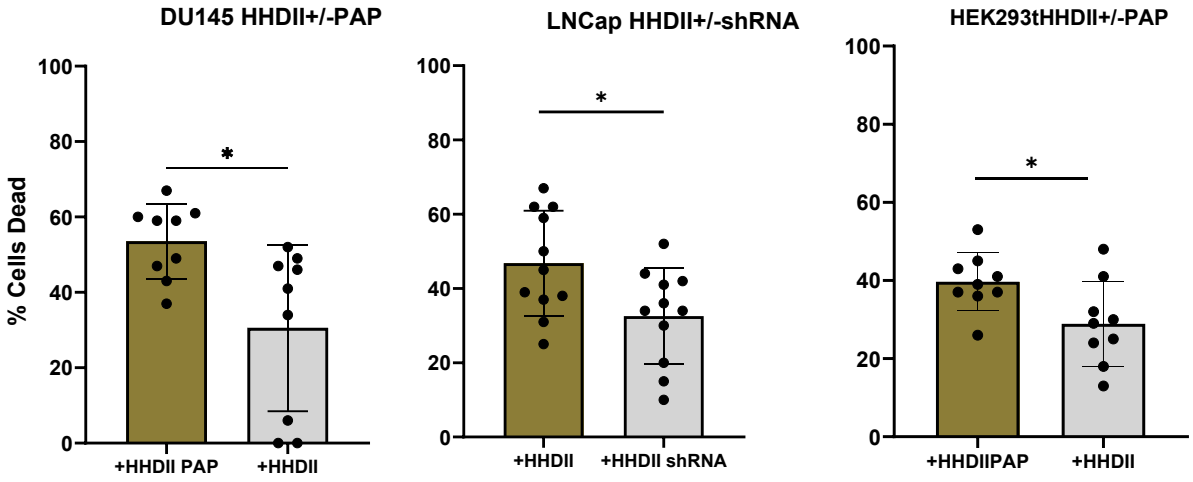

Figure 4.10. MutPAP42mer+ CPR+ CAF®09b vaccine induced CD3⁺ T cells recognise and kill target cells in vitro. *Results of the WST-8 cytotoxicity assay demonstrate that when coculturing the target cells and their controls LNCap +/- shRNA, DU145 HHDII +/- PAP and HEK293t HHDII +/- PAP with CD3⁺ T-cells isolated from in vitro hPAP42mer WT and mIL2 stimulated splenocytes from immunised mice. A maximum of 67% for LNCap HHDII and 67% for DU145 HHDII PAP and 53% for HEK293t HHDII PAP cell lysis were observed. *** P= 0.0007, ****P= <0.0001as determined by an unpaired t-test (n = 8 over two independent experiment).*

4.2.5. MutPAP42mer+ CPR+ CAF®09b vaccine capabilities assessed using HHDII DP4 mice. HHDII DP4 mice are genetically modified to express chimeric HLA-A2 and HLA-DP4 molecules. HLA-DP4 specifically involves at least two molecules; DP*401 (HLA-DPA1*0103/DPB1*0401) and DP*402 (HLA-DPA1*0103/DPB1*0402) and together they have an allelic frequency of 20–60% worldwide and are the most prevalent human *HLA class II* alleles. These mouse models allow vaccine-specific HLA *A2, HLA *DRA1, and HLA DP*401 mediated immune responses to be evaluated (Castelli *et al*. 2002). HLA-DP4 epitopes of hPAP42mer and hPAP 15mer CPR predicted HLA DP*401 binding were identified using the IDEB algorithm (Table 4.6), however, due to the lack of time synthesizing these peptides, DP4 epitopes were not obtained.

Peptide	Epitope (15mer)	IEDB rank	HLA-DP4 subtype
hPAP 42mer	LMSLMTNAAALFPPE	21	HLA-DPA1*01:03/DPB1*04:01
	PEGVSIWNPILLWQP	28	
	TLMSLMTNAAALFPP	29	
	MSLMTNAAALFPPEG	33	
	SIWNPILLWQPIPVH	34	
	PPEGVSIWNPILLWQ	44	
	VSIWNPILLWQPIPV	54	
	SLMTNAAALFPPEGV	58	
	DVDRTLMSLMTNAAA	59	
	FPPEGVSIWNPILLW	60	
	DRTLMSLMTNAAALF	61	
hPAP 15mer CPR	CPRFQELESETLKSE	13	HLA-DPA1*01:03/DPB1*04:01

Table 4.6. HLA-DP4 epitope derived from hPAP 42merWT and hPAP15mer CPR. *Prediction binding of the DP*401 epitopes was revealed using IEDB analysis resource NetMHCIIpan (ver. 4.1) tool (http://tools.iedb.org/mhcii/). Lower the IEDB rank, stronger the binding. All epitopes identified were predicted to have strong binding to HLA-DP4 alleles.*

HHDII DP4 mice were immunised with the vaccine composed of 30µg MutPAP42mer + 30µg CPR + 100µL CAF®09b on day 0, 14, and 28. Splenocytes of immunised mice were collected two weeks after the last immunisation. Immunogenicity of the vaccine was identified by IFN-γ ELISpot assay; co-culturing the splenocytes ($0.5x10^6$) of immunised mice with the hPAP-derived peptides 9mer (ILL and ALF) and 15mer CPR and hPAP42mer WT. The results (Figure 4.11) obtained show that, *in vitro* stimulation with long peptide hPAP42mer WT generated the highest number of IFN-γ responses. The splenocyte co-culture with MHC class I (ILL and ALF) and class II (CPR) peptides tested did produce IFN-γ significantly different from that of splenocytes alone response. The presence of vaccine-specific $CD4^+/CD8^+$ responses in HHDII DP4 mice was not assessed by blocking $CD4^+$ and $CD8^+$ co-receptors, yet the highest IFN-γ response obtained by hPAP42mer WT long peptide *in vitro* stimulation confirming the presence of $CD4^+/CD8^+$ epitopes within the sequence.

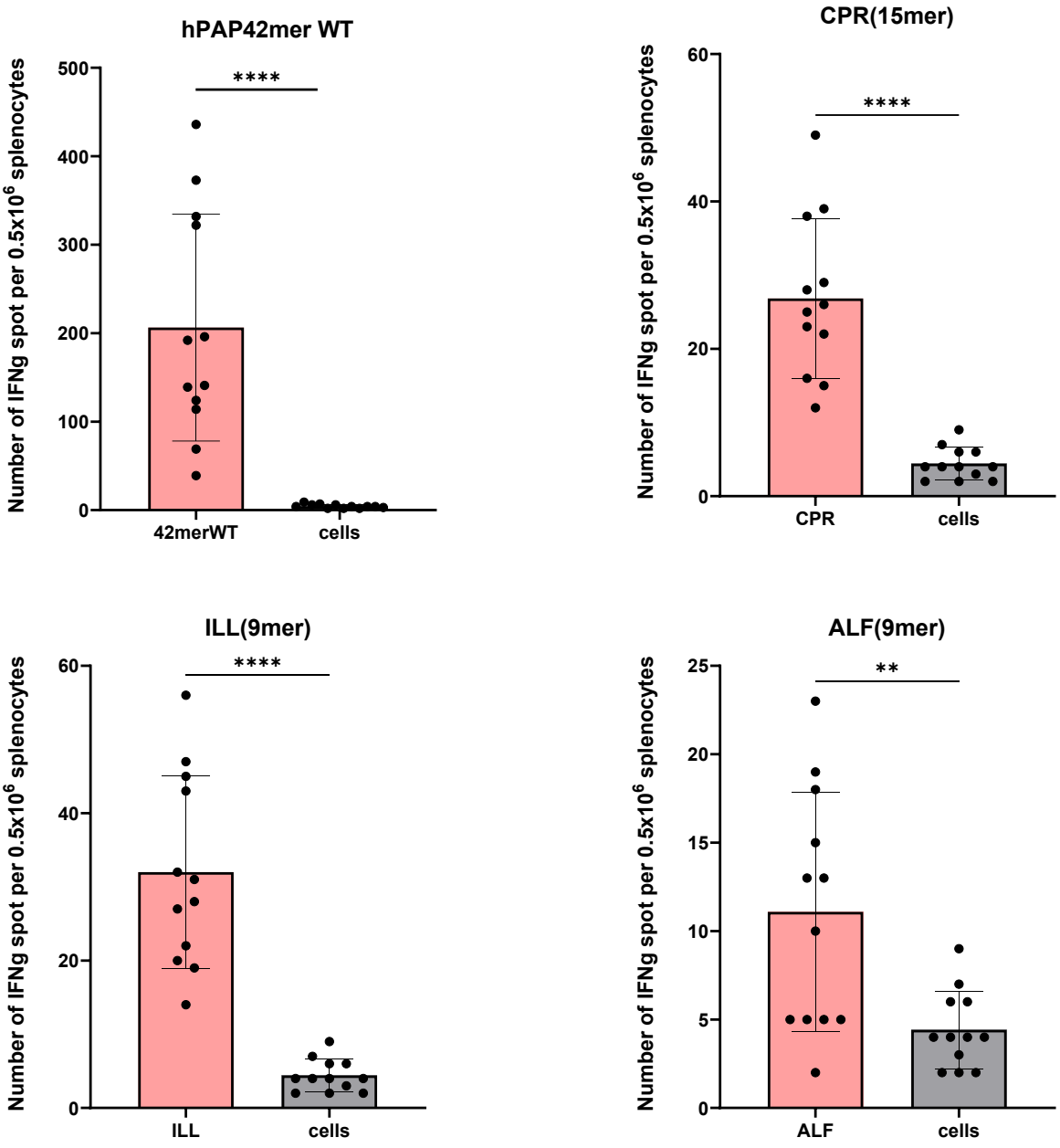

Figure 4.11. ELISpot results of co-culture of Mut hPAP42mer + CPR + CAF®09b vaccine-induced splenocytes with vaccine-derived long and short peptides using HHDII DP4 mice. *The co-culture results of vaccine-induced splenocytes with hPAP42merWT, Class I (ILL and ALF), and Class II (CPR) induced a higher number of IFN-γ responses. ****P <0.0001, **P= 0.0038. The significant difference in the immune responses among the groups was calculated using an unpaired t-test. n=12, over two independent experiments.*

4.2.5.1. Vaccine-specific target recognition.

MutPAP42mer+ CPR+ CAF®09b vaccine-induced splenocytes were re-stimulated *ex vivo* with a lower concentration (0.1μg/mL) of hPAP42mer WT and 50U/mL mIL2 for 5 days. After

one day of rest cells were harvested, and CD3⁺ T-cells were isolated using a Mouse T-cell isolation kit- Stem Cell Technologies, according to the manufacturer's protocol. The total cell count, and viability of the cells were identified using NucleoCounter NC250 before and after the T-cell isolation. An ELISpot assay is performed, co-culturing the CD3⁺ T-cells with HHDII and hPAP expressing target cells and their controls (LNCaP HHDII+/-anti-CD8 antibody, DU145 HHDII PAP +/- anti-CD8 antibody and HEK293t HHDII +/-PAP). The results (Figure 4.12) obtained indicate an evident CD3⁺ T-cell target recognition in an HLA and PAP-restricted manner. CD8 co-receptor blocking with anti-CD8 antibody to T-cells showed a specific reduction in the IFN-γ production demonstrating the vaccine's capabilities to generate CD8⁺ CTLs. The results obtained were promising, nonetheless, as a next step, an *in vitro* target-killing assay could not be performed because not enough HHDII DP4 was available due to breeding difficulties encountered with this breed.

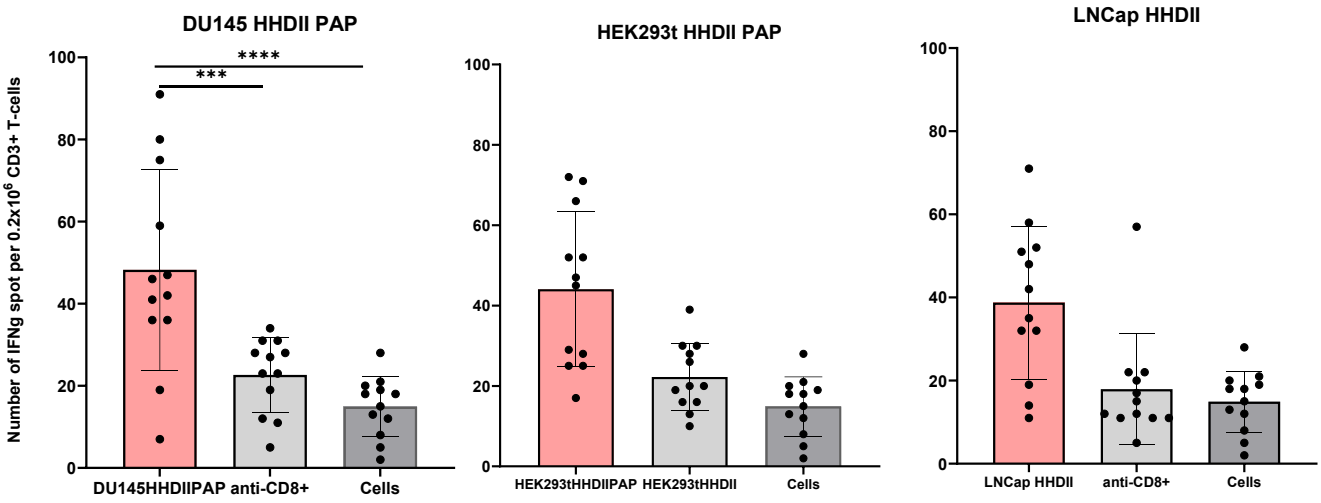

Figure 4.12. Vaccine-induced CD3⁺ T-cells recognise HHDII and PAP-expressing target cells. *CD3⁺ T-cells were isolated from in vitro stimulated vaccine-induced splenocytes, and co-cultured with target cells that express HHDII and human PAP protein. Target cells LNCap HHDII, HEK293t HHDII PAP, and DU145 HHDII PAP were recognized by the CD3⁺ T-cells Assessed by an IFN-γ ELISpot assay. For the IFN-γ ELISpot assay, **P= 0.002, *** P ≤ 0.0006, and **** P ≤ 0.0001 as determined by an ordinary one-way ANOVA test. n=12 between 2 independent experiments.*

Chapter 4: VACCINE OPTIMISATION USING HHDII DR1 MICE

4.3. Discussion

The immunogenicity of the vaccine was evaluated *in vitro* using HHDII DR1 and HHDII DP4 humanized models, which are applicable and transferable to the clinical setting. Initially, it was discovered that the hPAP42mer mutated sequence and 15mer CPR peptide were more immunogenic when injected with the CAF®09b adjuvant than when injected with the CpG and IFA adjuvants. The long hPAP42mer sequence contained both MHC class I and class II epitopes, and the hPAP15mer CPR is predicted to bind to HLA-DR1, suggesting the vaccine can generate MHC class I and class II-mediated immunogenicity. This has been supported by the findings presented in this chapter, that the vaccination was able to generate a $CD4^+/CD8^+$-driven immune response which is necessary for effective tumour cell lysis. Poncette, Bluhm and Blankenstein, (2022) support the fact that both $CD4^+/CD8^+$ induced IFN-γ and TNF-α are necessary for effective tumour elimination. $CD8^+$ cells perform direct cell lysis by recognising tumour antigens presented *via* MHC class I molecules. On the other hand, activated $CD4^+$ T cells are necessary for the generation of effector and memory CTLs.

Strong antigen-specific $CD8^+$ T-cell responses are elicited by CAF®09b adjuvant; nevertheless, studies reveal that the mode of administration significantly affects the quality of these responses. Intraperitoneal or nasal immunisation has been shown to induce strong $CD8^+$ T-cell responses whereas subcutaneous or intramuscular administration elicits weak $CD8^+$ T-cell responses suggesting that intraperitoneal immunisation of CAF®09b facilitates the concomitant delivery of the antigen for the professional cross-presentation to $CD8\alpha^+$ DCs in the lymphoid tissues (Tandrup Schmidt *et al*. 2016). In this study, the CAF®09b adjuvanted vaccine was administered *via* the intraperitoneal route to maximise the immunostimulant competence of CAF®09b. Furthermore, total splenocytes were stimulated *in vitro* with hPAP42mer WT and mIL-2 before conducting cytotoxicity assays. IL-2 cytokine has been demonstrated to regulate the proliferation and differentiation of T-cells to promote the expansion of $CD8^+$ CTLs (Ross and Cantrell, 2018).

Chapter 4: VACCINE OPTIMISATION USING HHDII DR1 MICE

Antigen-expressing human cancer cells were modified to express chimeric HLA-A2 (HHDII) for assessing the cytotoxic capabilities of the vaccine *in vitro*. This was because, target cell recognition by $CD8^+$ T-cells generated in HHDII mice involves both the CD8 co-receptor and the α3 domain of the MHC class I molecule from the same species in addition to contact between the MHC-peptide and TCR (Nishana and Raghavan, 2012; McArdle, 2009). The results obtained showed that vaccine-induced $CD3^+$ T-cells were able to recognise and lyse the target cells that express HHDII and human PAP. Up to 67% of the target lysis was observed, this indicates the activation of $CD8^+$ T-cells and their subsequent differentiation into CTLs. T-cells blocked with anti-$CD8^+$ antibodies before coculturing with target cells demonstrated a significant decrease in target recognition, supporting the direct tumour cell lysis mechanism by activated $CD8^+$ CLTs. However, the control cells, which express less or no PAP, showed an average of 25% of the cells lysed demonstrating some non-specific killing.

The lack of significant differences between the killing of two LNCap HHDII PAP and LNCaP HHDII shRNA (PAP low) could be explained by the fact that the LNCap HHDII shRNA cells were ‘knocked down’ rather than ‘knocked out’ for PAP and hence still express PAP. The qPCR data showed there is still 6.65% of PAP mRNA in the LNCaP HHDII PAP knockdown cells. Consequently, the expression at the protein level could be sufficient for a similar number of PAP-derived class-I epitope and HLA-A2 complexes to be presented at their surface. PAP-knockout within LNCaP HHDII cells would address this question. To conclude whether the lysis was HLA-A2 restricted would require the use of an HLA-A2 blocking antibody. While this may account for the lysis of LNCaP HHDII shRNA cells, vaccine-induced $CD3^+$ T-cells also lysed an average of 25% of the other two control cells, HEK293t HHDII and DU145HHDII. Considering the absence of PAP antigen expression in these cells suggests that there were antigen-nonspecific $CD8^+$ memory T-cells with non-MHC-restricted cytotoxic capabilities.

For the assessment of target cell death, a WST-8 cytotoxicity assay was performed using a Cell Counting Kit-8. WST-8 assay measures the absorbance of the amount of formazan product produced by cellular dehydrogenase activity. The reading obtained correlates with

the number of living cells which indirectly measures the percentage of cytotoxicity (Scarcello *et al*. 2020). Chromium release assay- a highly sensitive assay that quantifies the density of lysed target cells by measuring the percentage of intracellular chromium-labelled molecule release should have been a better option, but this was not accessible due to safety concerns.

In addition to HHDII DR1 mice, HHDII DP4 models were used to evaluate the vaccine's capabilities, which verified the vaccine's immunogenicity. HHDII DP4 allows the vaccine capabilities to be tested in HLA -A2, HLA -DRA*0101, and HLA -DP*401 context. PAP42mer long peptides had several HLA -DP4 epitopes identified by IEDB algorithm that have predicted strong binding to HLA DP*401. In addition, the novel PAP 15 mer CPR also showed a strong predicted binding to HLA DP*401 allele. However, due to the limited time frame, DP4 epitopes were not obtained, consequently, were not tested. Since HLA-DP4 is the most prevalent HLA Cass II allele with an allele frequency of 20-60% worldwide (Castelli *et al*. 2002), it would have been ideal if the vaccine-derived DP*401 epitopes were to be tested to identify the immunogenic capabilities of the vaccine. The *in vitro* coculture of hPAP42mer WT with splenocytes of HHDII DP4 immunised mice generated a significant increase in IFNγ release compared to splenocytes alone indicating the MHC class I and Class II epitopes present within the hPAP42mer long peptide. Moreover, the vaccine-induced $CD3^+$ isolated T-cells recognised the target cells in a highly HLA -A2/$CD8^+$ -dependent manner. Nonetheless, additional experiments could not be carried out due to the HHDIIDP4 models' inaccessibility and time constraints.

Although the vaccine can induce robust PAP-specific immune response in non-tumour-bearing animals, its efficacy must be assessed in prostate tumour-bearing animals. The immuno-suppressive mechanisms within the TME would render the tumour infiltrated T-cells non-functional or exhausted, which leaves them inefficient in initiating CTL functions. Thus, the vaccine capabilities must be studied within the physiological context of TME *in vivo*, using tumour-bearing animal models (Jubelin *et al*. 2022). However, the *in vivo* efficacy of MutPAP42mer +CPR +CAF®09b was not tested in HHDII mouse models. HHDII mouse

models do not support the tumorigenicity of human cancer cells since these models have chimeric HLA- A2. Tumours in HHDII mice can be produced using genetically modified murine cancer cells that are knockout for murine genes and then transfected with the HHDII (Chimeric HLA -A2) molecule. As described in (Chapter 3, section 3.2.2.2) TRAMP C1 cells were subjected to murine B2M knockout and transfected with human PAP and HHDII plasmid. However, modification of these cell lines took longer than expected. Therefore, while the tumour-bearing HHDII DR1 models were being generated, C57Bl/6J mouse models were used as proof of concept. The immunogenicity and efficacy of the vaccine were assessed on C57Bl/6J mice, as explained in Chapter 5. Since C57BL/6J models are not double transgenic, wild type (WT) form of hPAP 42mer.
(YIRSTDVDRTLMSAMTNLAALFPPEGVSIWNPILLWQPIPVH) and its epitopes will be used for vaccine formulation and *in vitro* stimulation respectively.

Chapter 5: VACCINE EFFICACY IN C57BL/6J MICE

5. Vaccine Efficacy in C57BL/6J mice

5.1. Introduction

In vitro studies, conducted in cell culture systems, allow researchers to assess vaccine candidates in controlled environments, but the absence of all TME components in these models may limit their translational relevance. Conversely, *in vivo*, studies using animal models offer a broad understanding of tumour initiation, progression, metastasis, and immune evasion mechanisms, TME, immune responses within a physiological context and for the preclinical investigation in the development of anti-tumour therapies (Jubelin *et al*. 2022; Guerin *et al*. 2020).

5.1.1 Mouse models for *in vivo* cytotoxic studies

The mouse as a human cancer research model has proven to be an effective tool because the genomic and physiological features of tumour biology in mice and humans are relatively similar (Lampreht Tratar, Horvat and Cemazar, 2018). Furthermore, 80% of mouse genes have a human ortholog, making them an excellent experimentally tractable model system for studying the fundamental mechanisms underlying the development of cancer and how it responds to therapy (Lampreht Tratar, Horvat and Cemazar, 2018). Tumours are generally investigated in mice using two different approaches: transplantable tumours and spontaneous tumours.

5.1.1.1. Transplantable tumours

Transplantable tumours are established by injecting tumour cell lines or primary tumour cells subcutaneously or orthotopically (Guerin *et al*. 2020) and are classified into two; syngeneic (allograft) models and xenograft models. In syngeneic models the tumour cells are implanted in syngeneic, immunocompetent mouse strains like BALB/c mice, and C57BL/6 mice (Lechner *et al*. 2013) whereas in xenograft models the human tumour cells grafted in immunocompromised or humanized mice (Chulpanova *et al*. 2020).

Syngeneic (allograft) models: Tumours are grafted in syngeneic (genetically identical) mice, allowing the establishment of mouse tumour and its TME, which provides an effective

approach for understanding tumour immunity and immunotherapy responses in the context of the complete functional murine immune system. The fundamental characteristic of an inbred strain is that they are genetically identical since they all carry the same homozygous allele for every DNA sequence in the genome. Spontaneous, oncogenic, or transgenic tumour cell lines can be implanted subcutaneously, orthotopically, or intravenously into such mouse strains as C57BL/6 or BALB/c, which allows tumour development within a few weeks (Chulpanova *et al*. 2020). Though these model systems are immunocompetent, featuring functional murine immunity and comprehensive stroma, they often lack the genetic complexity of human tumours, or may not possess a similar metastatic distribution of human malignancy, such as bone metastasis (Chakrabarti and Kang, 2015). Their peptide repertoire on MHC -I and MHC -II surface will also be specific to that strain and therefore not relevant to humans. Thus, tumour immunity and immunotherapy responses studied in the setting of a fully functional murine immune system are difficult to translate to a clinical trial (Guerin *et al*. 2020; Zeng *et al*. 2021).

Xenograft models are generated by grafting human tumour cell lines into immunodeficient mice, such as NOD-SCID mice (lack T-cell and B-cell function), nude mice (lack T-cell function), or NSG mice (lack T-cells, B-cells, and NK cells) (Chakrabarti and Kang, 2015). These models have demonstrated superiority in reiterating the features of human cancer, such as the spatial structure and the intratumor heterogeneity of cancer. Tumour stromal interaction may be less studied using a xenograft model, due to the species difference between tumour and host. Patient-derived xenograft models that contain tumour tissue fragments derived directly from human tumours without an extensive *in vitro* passage which mimics the original characteristics of the human tumours serve as an effective platform for developing personalized anticancer therapies (Chulpanova *et al*. 2020; Liu *et al*. 2023). However, the use of xenograft models in immunocompromised mice is mainly used for the development of conventional anti-tumoral therapies such as radiotherapy chemotherapy, or immunotherapy, which require endogenous immune cells to study the optimal drug efficacy (Guerin *et al*. 2020). Xenografts generated in humanized mice may circumvent this

problem, however, obtaining a mouse model with a fully functioning humanized immune system is very expensive and complicated (Guerin *et al*. 2020).

5.1.1.2. Spontaneous or induced malignant tumours.

Spontaneous or induced malignant tumours consist of de novo generation of cancer, either using genetically engineered animal models or inducing mutation by exposing animals to chemical carcinogens, viruses, or radiation (Jubelin *et al*. 2022). Genetically engineered mouse models are engineered to express an oncogene or to lose a tumour suppressor gene, which advances tumour growth. These tumours grow slowly, allowing prolonged immunotherapeutic study within the murine tumour microenvironment. One drawback of these models is that, in contrast to human tumours, they exhibit a low mutational burden. (Cogels *et al*. 2021).

5.1.1.2.1. Genetically engineered mouse models of prostate cancer

To study the PCa molecular mechanisms and tumour progression from prostate intraepithelial neoplasia (PIN) to metastasis, various transgenic mouse models have been developed; among them are TRAMP/LADY transgenic models and PTEN/P53 (tumour suppressor genes) knockout mouse models. A key tumour suppressor, PTEN deficiency has been connected to many cancers. In PCa, approximately 35% of primary PCa and 63% of metastatic tissues have PTEN loss of function (Wu *et al*. 2013; Parisotto and Metzger, 2013). The TRAMP (Transgenic Adenocarcinoma of the Mouse Prostate) is the first genetically modified PCa model to display distant organ metastasis. TRAMP mice represent a transgene containing the minimal probasin promoter driving viral SV40 large-T and small-t antigens, which leads to the inactivation of *pRb* and *p53*, in the prostatic epithelium. Prostatic intraepithelial neoplasia is seen in these models by 6 weeks, which develops to high-grade neoplasia by 12th weeks, and to an invasive adenocarcinoma by 24 weeks of its age. They are unable to develop bone metastases is a drawback of these models. Additionally, the inherent probasin promoter, which is regulated by androgen, Therefore, the observed

androgen sensitivity is caused by transgene down expression, would be confound in the interpretation of the consequences of castration (Irshad and Abate-Shen, 2012).

5.2. Aim of this chapter

This chapter aims to assess the efficacy of the PAP42mer + CAF®09b vaccine in C57BL/6J mouse models. Specifically, the immunogenicity of the vaccine will be assessed initially to evaluate the capability of the vaccine to generate $CD4^+$ and $CD8^+$ specific immune responses. The cytotoxic ability of vaccine-induced T-cells will be assessed *in vitro* using murine PCa cell lines. Thereafter, the efficacy of the vaccine will be assessed in PCa tumour-bearing C57BL/6J models.

Chapter 5: VACCINE EFFICACY IN C57BL/6J MICE

5.3. Results

5.3.1. Assessment of immunogenicity of hPAP42mer WT +CAF®09b vaccine

PAP is a self-antigen expressed also in normal prostate tissue, the C57BL/6J model is a good choice for assessing whether the derived vaccine was sufficiently immunogenic to elicit an effective immune response against PAP and, consequently, break tolerance against PAP protein. The PAP42mer peptide sequences in humans and mice differ from one another by two amino acids, as Table 5.1 illustrates.

Human	Peptide sequences	Murine
	YIRSTDVDRTLMSAMTNLAALFPPEGISIWNPRLLWQPIPVH	mPAP42merWT
hPAP42merWT	YIRSTDVDRTLMSAMTNLAALFPPEGVSIWNPILLWQPIPVH	2 amino acid differents
hPAP42merMut (1 mutation)	YIRSTDVDRTLMSLMTNLAALFPPEGVSIWNPILLWQPIPVH	3 amino acid differents
hPAP15merCPR (WT)	CPRFQELESETLKSE	3 amino acid differents
	CPRFEELKSETLESE	mPAP15mer CPR(WT)
Mouse PAP (GenBanl accession no. NP_062781.2)		
MRAVPLPLSRTASLSLGFLLLLSLCLDPGQAKELKFVTLVFRHGDRGPIETFPTDPITESSWPQGFGQLTWGMEQHYELGSYIRKRYG RFLNDTYKHDQIYIRSTDVDRTLMSAMTNLAALFPPEGISIWNPRLLWQPIPVHTVSLSEDRLLYLPFRDCPRFEELKSETLESEEFLKR LHPYKSFLDTLSSLSGFDDQDLFGIWSKVYDPLFCEVHNFTLPSWATEDAMIKLKELSELSLLSLYGIHKQKEKSRLQGGVLVNEILKN MKLATQPQKYKKLVMYSDTTVSGLQMALDVYNGVLPPYASCHMMELYHDKGGHFVEMYYRNETQNEPYPLTLPGCTHSCPLEKFA ELLDPVISQDWATECMATSSHQGRN		

Table 5.1. List of humans, murine and mutated PAP-derived peptides included in the vaccine. *In the murine whole PAP, PAP42mer and 15mer CPR are highlighted in yellow. The AA in 'Red' represents the sequential difference of mPAP peptides to its human or mutated counterparts.*

The immunogenicity of hPAP42mer WT and CPR with CAF®09b adjuvant was evaluated and compared against peptide alone or CAF®09b alone formulations. C57BL/6J mice were immunised with hPAP42mer WT + CPR + CAF®09b or hPAP42mer WT + CPR or CAF®09b as described in Figure 5.1. The spleens from immunised mice were collected 14 days following the last immunisation and splenocytes were isolated, and cocultured with vaccine-derived mPAP peptides (Table 5.2) in an IFN-γ ELISpot assay. The MHC class-I (H2-Db/H2-Kb) and

Chapter 5: VACCINE EFFICACY IN C57BL/6J MICE

MHC class-II (H2IAb) peptides were determined by the SYFPEITHI algorithm and/or IDEB resources for better MHC binding, listed in Table 5.2. Only murine WT peptides were used in the *in vitro* experiments, and the amino acids altered by the mutation are presented in red.

MHC Type	**SEQUENCE** (murine WT)	**SYFPEITHI Score/ IEDB rank** Human WT	**SYFPEITHI Score/ IEDB rank** **Mouse WT**	**LENGTH**	**Haplotype**
Class I	SAMTNLAAL	28	28	9mer	H2-Db
	ISIWNPRLL	25	26	9mer	
	SAMTNLAALF	27	27	10mer	
Class II	ISIWNPRLLWQPIPV	25 /63	18 /63	15mer	H2-Ed/H2-IAb
	PEGVSIWNPRLLWQP	51(IEDB rank)	N/A	15mer	H2-IAb
	VDRTLMSLMTNLAAL	5 (IEDB rank)	5 (IEDB rank)		
	DRTLMSLMTNLAALF	20 /6	26/6	15mer	H2-Ab/H2-IAb
	MSAMTNLAALFPPEG	20 /55	24/55		
	CPRFQELESETLKSE	28 (IEDB rank)	30 (IEDB rank)	15mer	H2-IAb

Table 5.2. List of MHC class-I H2-Kb/H2-Db and Class-II H2-IAb peptides derived from mPAP42mer/CPR sequence. *MHC-II binding predictions were made using the IEDB analysis resource NetMHCIIpan (ver. 4.1) tool (http://tools.iedb.org/mhcii/) and SYFPEITHY algorithms. (http://www.syfpeithi.de/bin/MHCServer.dll/EpitopePrediction.htm)*

The results show that CAF®09b or peptides alone immunisations demonstrated no higher immunogenic response than 'splenocytes alone' (experimental control). The group of animals that received hPAP42mer WT + CPR + CAF®09b immunisation, showed the highest IFN-γ responses which demonstrated the immunostimulant properties of adjuvant to the peptides. Although the human WT 15mer CPR was predicted to bind to H2-IAb with higher affinity than that of its murine counterparts with three AA mutations, there were no CPR-driven production of IFN-γ was observed when the vaccine-induced splenocytes were cocultured *in vitro* with CPR (Figure 5.1).

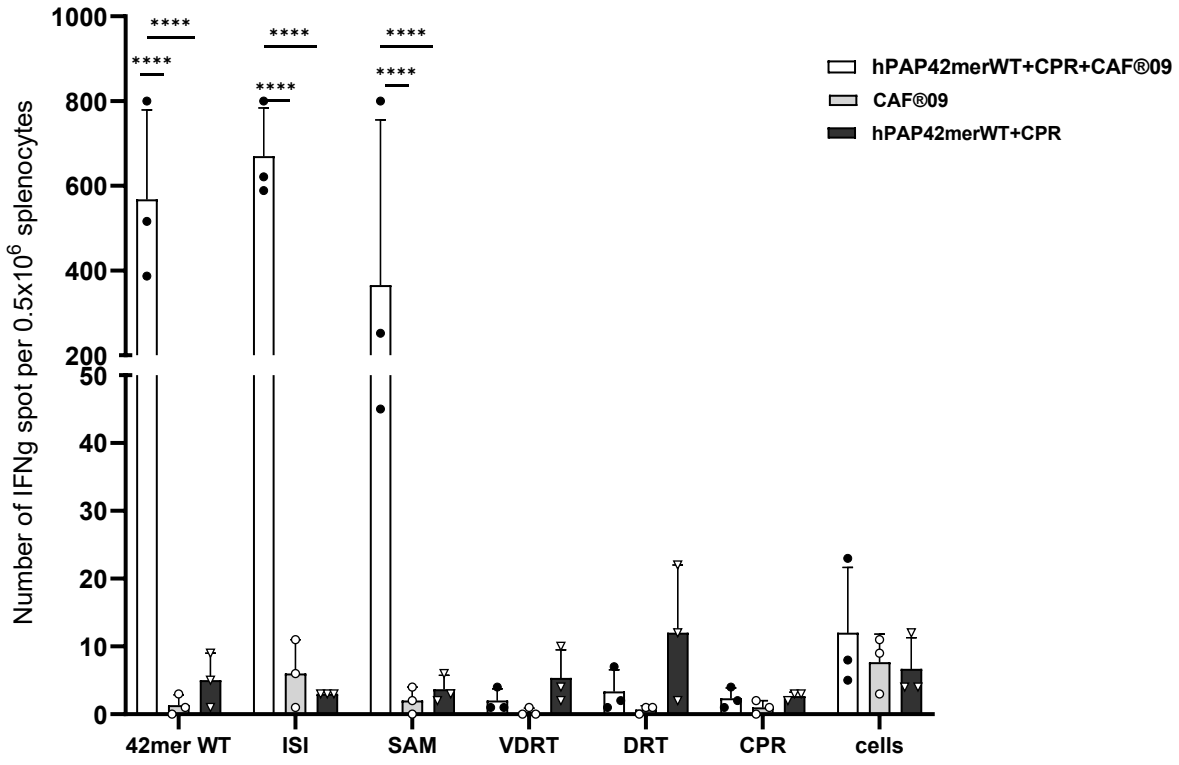

Figure 5.1. Immunogenicity of PAP42mer WT+ CPR+ CAF®09b contrasted with the results of CAF®09b or PAP42mer WT +CPR alone. *C57BL/6J mice were immunised with hPAP42mer WT+ CPR+ CAF®09b or hPAP42mer WT +CPR or CAF®09b on days 1, 15 and 29. n=3 per group. 14 days after the last immunisation, splenocytes were isolated, and an in vitro IFN-γ ELISpot assay was performed. Splenocytes were stimulated with mPAP-derived class I (ISI and SAM- 9mer), class II (15mers – DRT, VDRT, and CPR), and 42merWT for 40 hours at 37ºC. Bars indicate the mean number of IFN-γ spots, and the error bars represent the SD. A significant deviation in the generation of peptide-specific IFN-γ releasing T-cells between immunisation groups was determined using a two-way ANOVA comparison test **** P <0.0001.*

5.3.1.1. hPAP42mer WT +CAF®09b vaccine induced $CD8^+/CD4^+$ specific responses.

To assess the vaccine induced $CD8^+/CD4^+$ responses, C57BL/6J mice were immunised with 3 doses of hPAP42mer WT + CAF®09b vaccine at two weeks intervals. The splenocytes from immunised mice were isolated two weeks after the last immunization and cocultured with mPAP 42mer derived class I and class II peptides with or without anti- $CD8^+/CD4^+$ antibodies (Table5.2) in an *in vitro* IFN-γ ELISpot assay. In addition to the IFN-γ ELISpot assay, MHC pentamer flow cytometry was performed to quantify ISI epitope-specific $CD8^+$ T-cells.

5.3.1.1.1. Vaccine-induced $CD4^+$/$CD8^+$ responses assessed by ELISpot assay.

Splenocytes extracted from the spleen of immunised mice were cocultured with mPAP 42mer +/- anti- CD8 / CD4, mPAP-derived Class I peptides (SAM (10mer), GIS (8mer), and ISI (9mer)) +/- anti- CD8 and Class II peptides (15mers- ISIW, MSAM, and PEG) +/- anti-CD4 antibodies *in vitro*. By blocking CD8, and CD4 co-receptors with antibodies, the ability of T-cells to recognise antigens presented by MHC class I and class II molecules was reduced. This led to a reduction in the IFN-γ production as measured by ELISpot assay, where T-cell activation and cytokine secretion in response to MHC Class I or Class II specific antigens are being evaluated. The results obtained are shown below (Figure 5.2). When antibodies against CD8, and CD4 co-receptors were added to the coculture of splenocytes containing the mPAP42mer WT long peptide, a significant decrease, in the IFN-γ spots, was observed. This suggests that the hPAP42mer WT was processed and presented by MHC class I molecules after cross-presentation and by MHC class II endosomal processing of antigen presentation to both $CD8^+$ and $CD4^+$ T-cell respectively. The total number of animals tested for each epitope and the number of animals that responded are listed in (Table 5.3).

In addition to testing the long peptide mPAP42mer to assess vaccine induced $CD8^+$/$CD4^+$ driven responses, class I (for $CD8^+$) and class II (for $CD4^+$) peptides were also tested individually. For that, splenocytes were cocultured with vaccine-derived MHC class I epitopes- GIS(8mer), ISI(9mer), and SAM (10mer) +/- anti-CD8, antibody. The results show that the addition of an anti-CD8 antibody to the coculture blocked the immune response generated by all three epitopes which was found to be significant for GIS and ISI peptides (Figure 5.2). Similarly, splenocytes were cocultured with MHC class II epitopes of mPAP42mer (ISIW, PEG, and MSAM) +/- anti CD4 antibody to analyse vaccine-induced $CD4^+$ T-cell activation. The addition of anti-CD4+ inhibited the increased production of IFNγ in all tested class II epitopes (Figure 5.2).

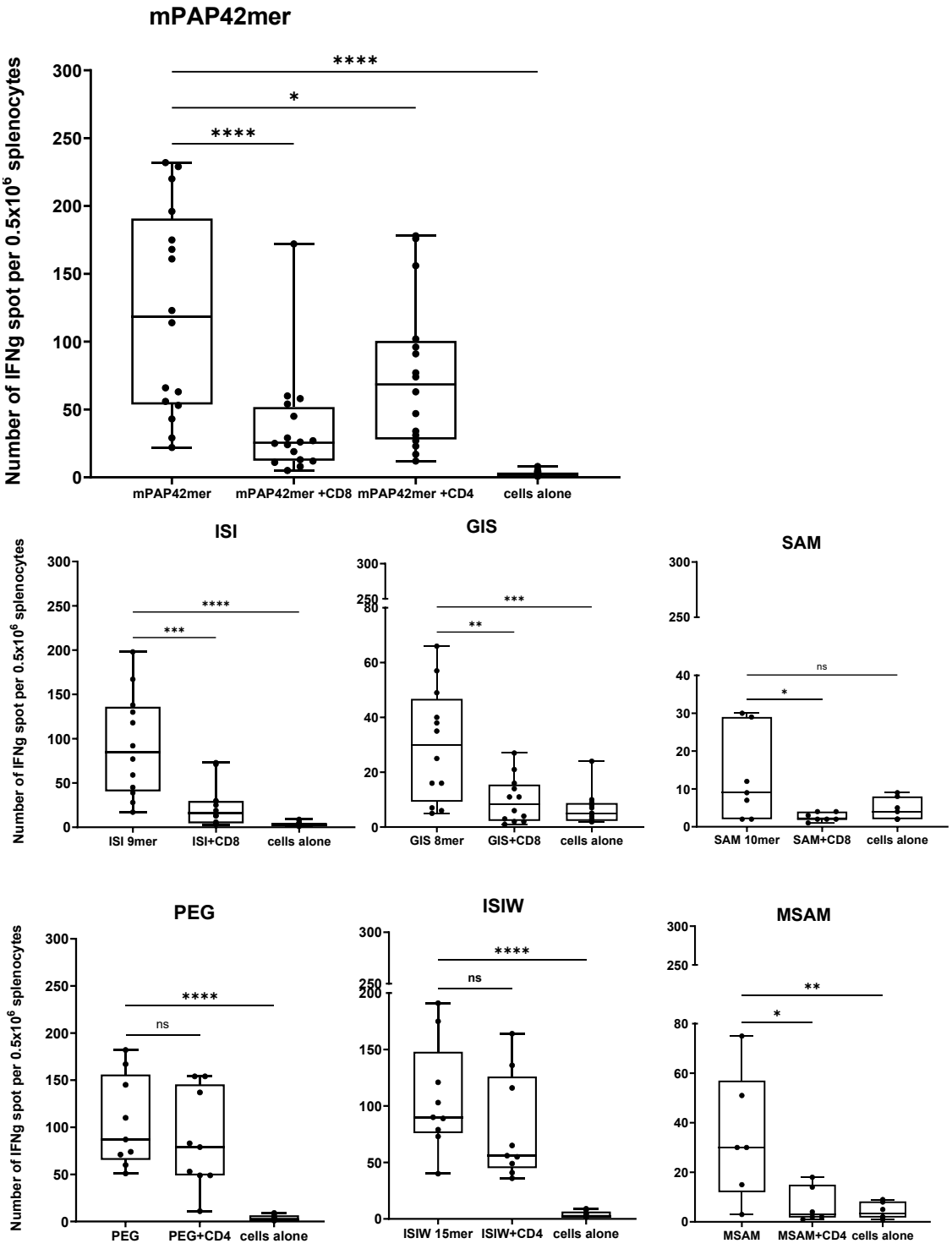

Figure 5.2. *h**PAP42merWT/ CAF®09b vaccine induced CD4⁺/CD8⁺, responses in C57BL/6J mice.** C57BL/6J mice were injected with 3 doses of PA42mer WT +CAF®09b immunisation two weeks apart. Splenocytes were extracted from spleens 14 days following the last immunisation, and an in vitro IFN-γ ELISpot assay was carried out. Splenocytes were stimulated with (mPAP 42mer and mPAP42mer-derived class I epitopes (GIS- 8mer, ISI-9mer) +/- anti CD8 antibody, and class II epitopes (15mers – ISIW and PEG) +/- anti-CD4 antibody for 40 hours at 37°C. The bars show the average number of spots, while the SD is represented by error bars. A one-way*

*ANOVA comparison test was used to determine whether there was a significant difference between the immunization groups in the induction of peptide-specific IFN-γ releasing T-cells. *P≤ 0.02**P≤0.0095, ***P=0.0001 and ****P <0.0001.*

Peptide	**Antibody blocking**	**Number of mice tested**	**Number of mice responded**
mPAP42mer	Anti- CD4 and anti- CD8 Ab	18	16
ISIW 15mer	Anti- CD4 Ab	12	9
PEG 15mer		9	9
MSAM 15mer		6	6
GIS 8mer	Anti- CD8 Ab	12	12
ISI 9mer		12	12
SAM 10mer		7	7

Table 5.3. *The list of the number of mice used to test the hPAP42merWT+ CAF®09b vaccine for $CD8^+/CD4^+$ driven responses, along with the total number of mice that responded with CD8/CD4 antibody blocking.*

5.3.1.1.2. Vaccine-induced $CD8^+$ T-cells assessed by pentamer staining.

MHC class I epitope (ISI) pentamer was purchased from Pro5® pro immune, to detect and compare the presence of peptide-specific vaccine-induced splenic and circulating $CD8^+$ cells with non-vaccinated mice. At the end of the immunisation study, splenocytes and blood samples from immunised and non-immunised mice were obtained. $1x10^6$ splenocytes and 100µL of terminal bleed were stained using anti-CD45, anti-CD3, and anti-CD8, antibodies along with phycoerythrin (PE)-conjugated ISI pentamer following the protocol described (section 2.2.3.4.5), analysed by flow cytometer Cytek Aurora (and Kaluza software). The results (Figure 5.4) obtained supported the findings of the ELISpot splenocyte-peptide coculture experiment (Figure 5.2). The percentage of antigen specific $CD8^+$, cells in the blood and spleen of vaccinated mice was found to be significantly higher than that of non-vaccinated mice, as shown by ISI pentamer staining.

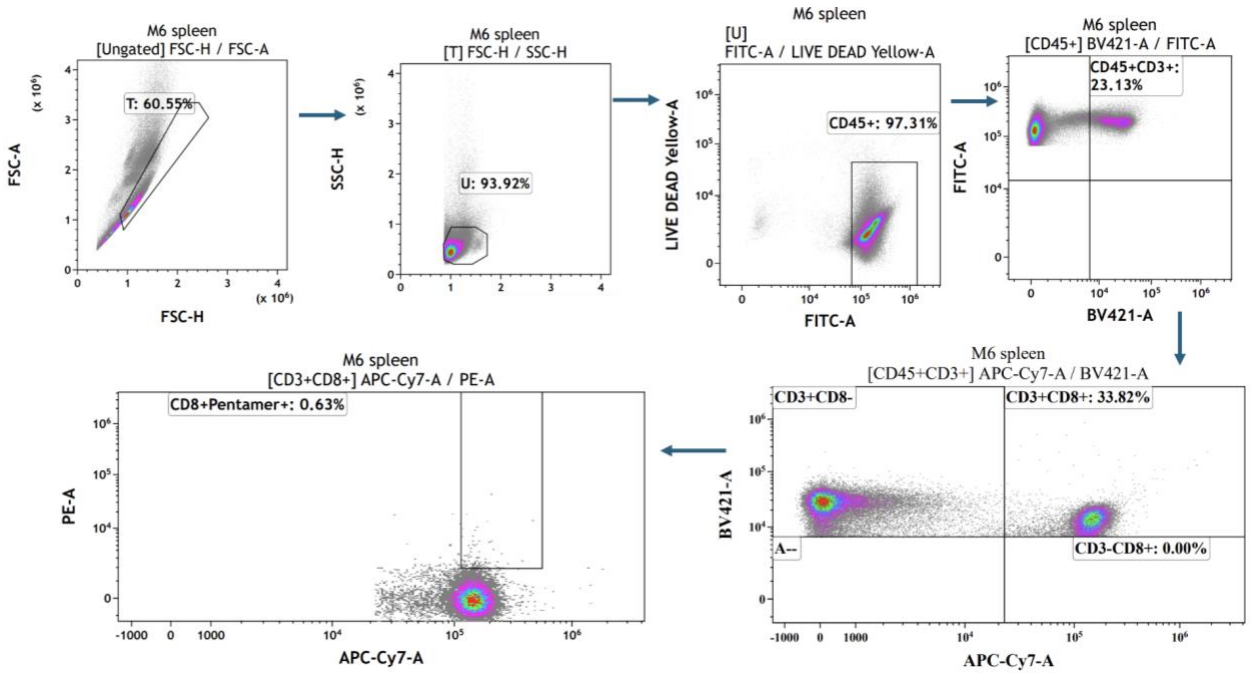

Figure 5.3. Schematic representation of the gating strategy employed to analyse the ISI pentamer staining. *Initially, CD45⁺ cells were gated from the live cell population. Subsequently, CD3⁺ cells were identified within the CD45⁺ subset, followed by gating on CD8⁺ cells within the CD3⁺ population and finally, CD8⁺ pentamer⁺ cells.*

Chapter 5: VACCINE EFFICACY IN C57BL/6J MICE

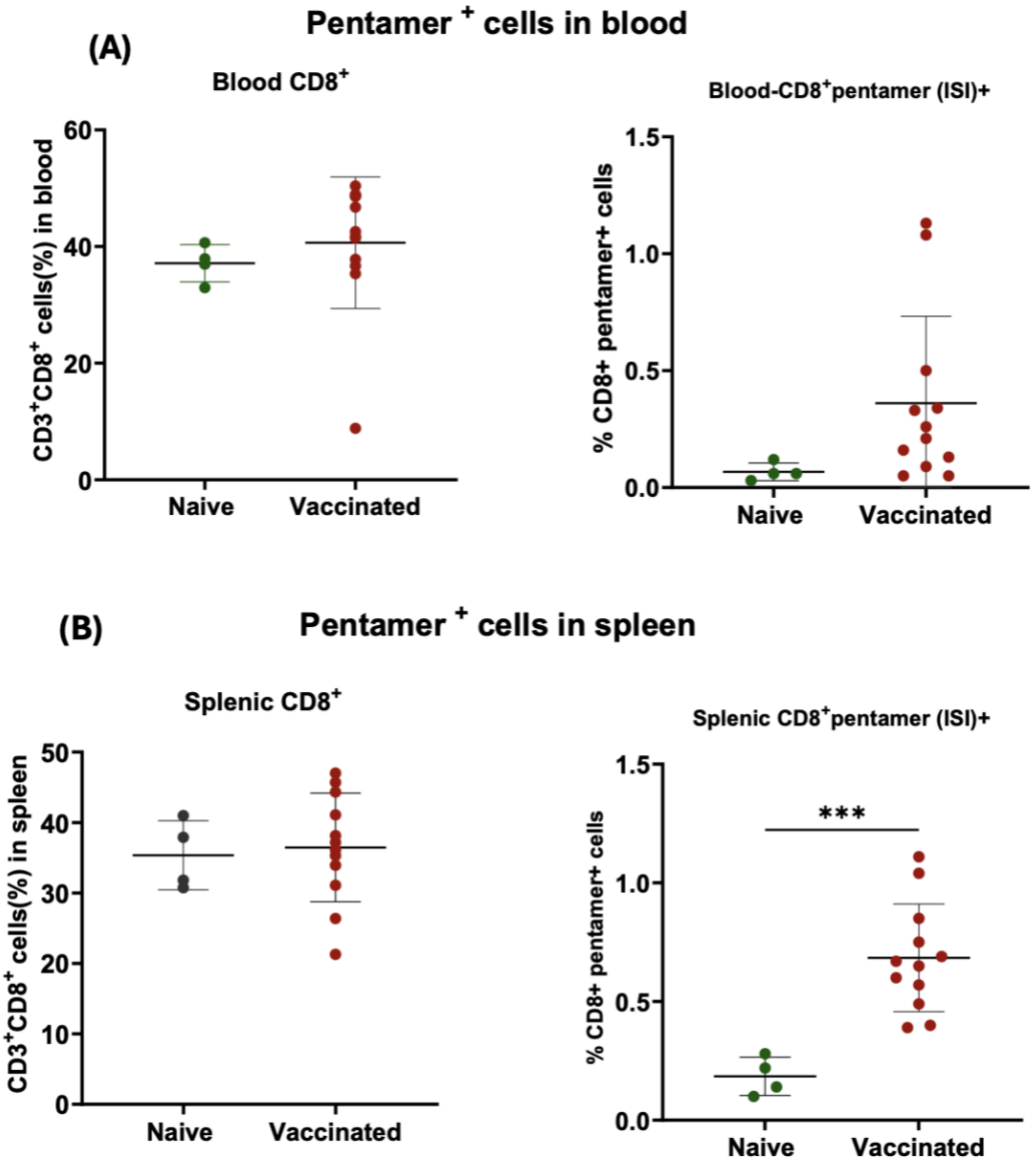

Figure 5.4. hPAP42merWT +CAF®09b immunisation increased circulating and splenic CD8⁺ CTLs in C57BL/6J mice. *(A) Illustrates a percentage of CD8⁺ and ISI pentamer positive CD8⁺ cells present in the blood. (B) Demonstrates a percentage of CD8⁺ and ISI pentamer positive cells present in the spleen. 1x10⁶ splenocytes and 100µL of terminal blood were taken from naïve mice and hPAP42mer WT + CAF®09b vaccinated mice. After blocking any potential nonspecific antibody binding with FcR Blocker in FCS, the cells were stained with anti-CD45, anti-CD3, and anti-CD8 surface antibodies and PE-conjugated ISI pentamer. Flow cytometry analysis shows that vaccination has increased the number of total CD8⁺ cells in spleen *P=0.0091 and in blood *P=0.0357; with regards to pentamer ISI in spleen *P= 0.0182 and in blood P=* 0.0357 has determined by Mann-Whitney test. n= 4 (naïve), n=11(vaccinated).*

Chapter 5: VACCINE EFFICACY IN C57BL/6J MICE

5.3.2. *In vitro* assessment of cytotoxic capabilities of hPAP42mer WT + CAF®09b vaccine induced CTLs to recognise and lyse target cells that express mPAP.

The experiments conducted thus far have confirmed the immunogenicity and ability of the hPAP42mer WT + CAF®09b vaccine to generate vaccine-specific $CD8^+$/$CD4^+$ T-cells in C57BL/6J mice. The next step was determining whether these vaccine-induced CTLs could recognise and kill endogenously processed PAP protein by PAP-expressing cell lines. TRAMP C1 and TRAMP C2 that naturally express MHC class I (chapter 3 Figure3.6) and mPAP expression (chapter 3 Figure 3.7) were used as targets to assess the cytotoxic capabilities of hPAP42mer WT + CAF®09b vaccine-derived T-cells *in vitro*. The mPAP expression of these target cells was knocked down to obtain suitable controls -TRAMP C1shRNA and TRAMP C2shRNA - for the study. The target cells and their controls were cocultured with either the splenocytes isolated from immunised mice or $CD3^+$ T-cells isolated from the vaccine-specific splenocytes that were stimulated *ex vivo* with 0.1µg/mL PAP42mer peptide and 50U/mL IL-2 for 5 days, followed by one day of rest. Target cell recognition and killing were evaluated using the ELISpot assay and the WST-8 assay, respectively.

5.3.2.1. Vaccine-specific target recognition by vaccine-induced splenocytes/ $CD3^+$ T cells.

An IFN-γ ELISpot assay was used to measure the target recognition by vaccine-induced splenocytes. The splenocytes ($0.5x10^6$) of immunised mice were cocultured with target cells that express mPAP and their controls, TRAMP C1+/-shRNA and TRAMP C2 +/-shRNA, at a 50:1 (effector: target) ratio. Results obtained (Figure 5.5A) show that splenocytes of immunised mice were able to recognise the PAP fragments presented by TRAMP C1 and TRAMPC2 cells and generated higher IFN-γ response, than its PAP knockdown control TRAMP C1 shRNA and TRAMP C2 shRNA and splenocytes alone response. To validate these results, target cells and their controls were cocultured with $CD3^+$ T-cells which were isolated from the splenocytes of immunised mice following *ex vivo* stimulation of splenocytes with 0.1µg/mL PAP42mer and 50U/mL mIL2 for 5 days and then one day of rest where the stimulated splenocytes were maintained with 50U/mL mIL2 alone. $CD3^+$ T cells were

isolated using the mouse T-cell isolation kit from Stem Cell Technologies (section 2.2.3.4.3). NucleoCounter NC250 was used to determine the viability and total cell count before and after T-cell isolation.

IFN-γ ELISPOT assay was performed, coculturing $0.2x10^6$ $CD3^+$ T-cells with target cells and their controls (TRAMP C1+/-shRNA and TRAMP C2 +/-shRNA) at a 50:1 (E: T) ratio. Like the splenocyte-target recognition ELISpot findings, $CD3^+$ T-cells were able to recognise the mPAP-derived antigens presented by the target cells (Figure 5.5B). In comparison to their controls and T-cells alone response, target cells TRAMP C1 and TRAMP C2 induced a significantly higher number of IFN-g responses.

Chapter 5: VACCINE EFFICACY IN C57BL/6J MICE

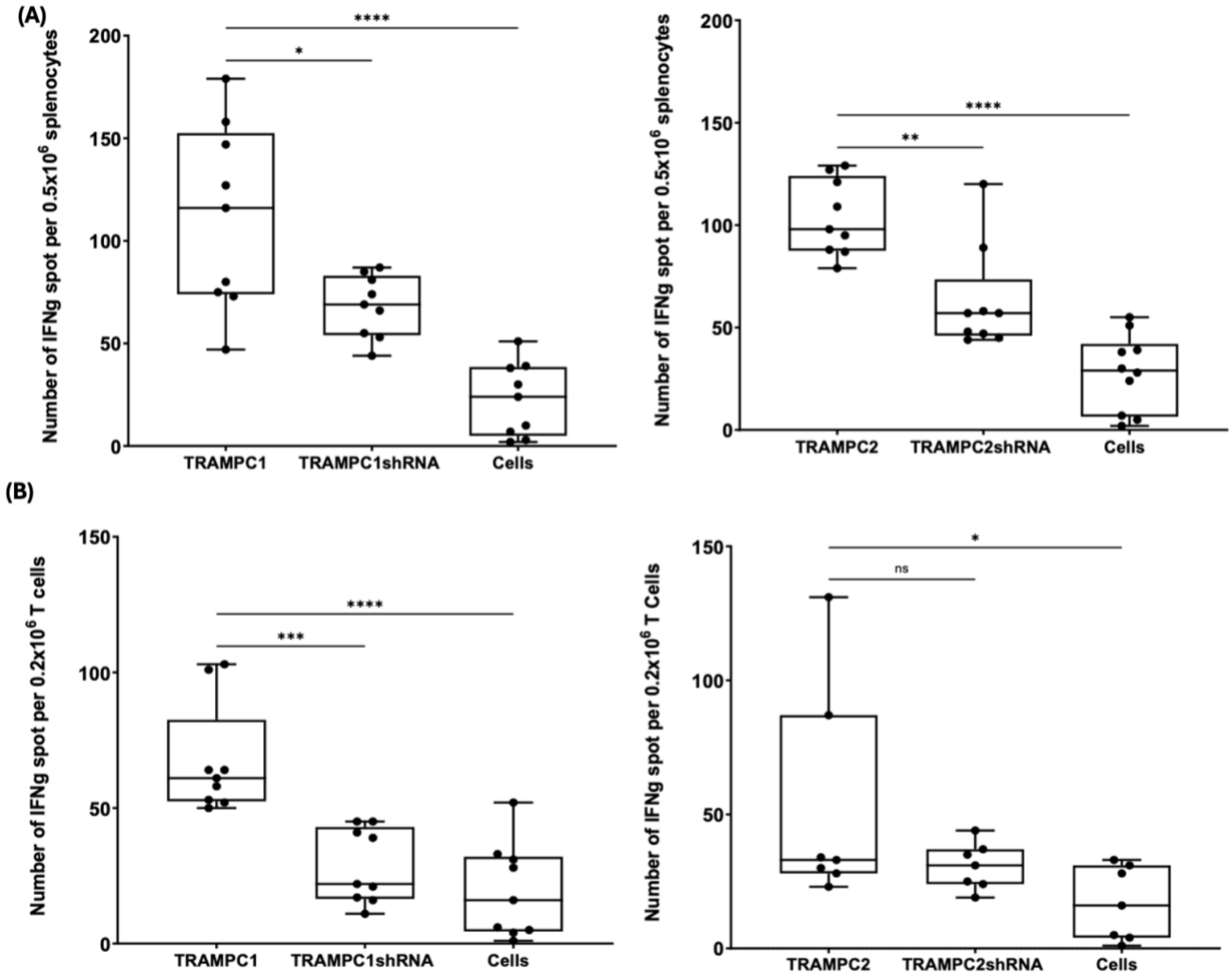

Figure 5.5. IFN-γ ELISpot results of target cell recognition by vaccine-induced splenocytes or CD3⁺ T-cells. *C57Bl/6J mice received 3 doses of the hPAP42merWT +CAF®09b vaccination spaced two weeks apart. Animals were culled 14 days after the last immunisation, splenocytes were isolated and cocultured with TRAMP C1+/- shRNA and TRAMP C2 +/-shRNA (E: T - 50:1), (n = 8)* ***(A)*** *Splenocytes were able to recognise endogenously processed PAP fragments by PAP-expressing TRAMP C1 and TRAMP C2 cell lines. The significant increase in IFN-g was determined by an ordinary one-way ANOVA test.* ***(B)*** *ELISpot results of the coculture of the target cell with isolated CD3⁺ T-cells after ex vivo stimulation with hPAP42mer and mIL2 for 5 days. The STEMCELL EasySep™ Mouse T-Cell Isolation Kit was used to isolate CD3⁺ T-cells by negative selection following the manufacturer's instructions. For the IFN-γ ELISpot, * P≤ 0.04, ** p ≤ 0.008, *** P= 0.0002, and **** P <0.0001 as determined by an ordinary one-way ANOVA test. (n = 6-9 over 2 independent experiments).*

5.3.2.2. hPAP42merWT +CAF®09b vaccine-specific target killing.

The cytotoxic ability of vaccine-specific $CD3^+$ T-cells to lyse PAP-expressing target cells was assessed by WST-8 cell viability assay following the manufacturer's protocol. $0.2x10^6$ $CD3^+$ T-cells together with TRAMP C1, TRAMP C2 cells or their controls TRAMP C1shRNA/ TRAMP C2 shRNA were seeded into 96-well cell culture plates at a 50:1 (E: T) ratio and were incubated at 37 °C and 5% CO_2 for 24 hours. In separate wells, the same number of target cells or T-cells were cultured alone. The total number of live cells was calculated by adding the absorbance values from target cells alone or T-cells alone. An equivalent number of target cells was treated with 0.1% SDS, to determine the maximum amount of cell death. After incubation for 24 hours, WST-8 solution 10µL per 100µL of culture media was added to each well and was incubated for an additional 4 hours at -37 °C and 5% CO_2. The absorbance was measured at 450 nm, and the formula below was used to determine the percentage of live cells.

% Live cells = [Absorbance of T-cells with targets/controls ÷ (Absorbance of T cells alone + Absorbance of Target alone) *100

% Dead cells = 100 - live cells

The results obtained showed that the $CD3^+$ T-cells from vaccinated mice were able to lyse TRAMP C1 and TRAMP C2 cells that expressed MHC class I and mPAP. TRAMP C2 cells exhibited the highest level of cell lysis, percentage of killing shown in the individual mice varied from 40- 76%. TRAMP C1 cells demonstrated an average killing rate of 60% and a maximum rate of 65% cell lysis. TRAMPC2shRNA which was knockdown for its PAP expression also exhibited up to 40% killing when these cells were cocultured with $CD3^+$ T-cells; this may be due to the expression of PAP protein but at a lower level by TRAMP C2shRNA cells, where the PAP gene was not completely knockout but silenced for its expression. A maximum of 25% of cell lysis was observed in TRAMP C1shRNA cells. Overall, there is a significant increase in cell lysis seen with TRAMP C1 and TRAMP C2 compared to its controls TRAMP C1shRNA and TRAMP C2shRNA, upon the interaction with vaccine-induced $CD3^+$ T-cells.

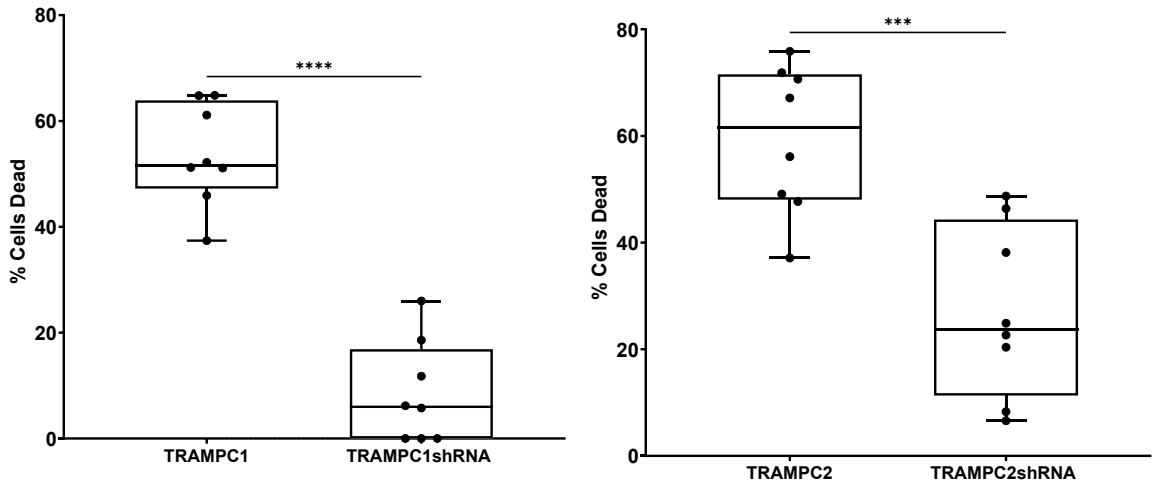

Figure 5.6. hPAP42merWT +CAF®09b vaccine-induced CD3⁺ T-cells target killing in vitro. *Results of the WST-8 cytotoxicity assay demonstrate that when coculturing the target cells TRAMP C1 and TRAMP C2 with CD3⁺ T-cells isolated from in vitro PAP peptides and mIL2 stimulated splenocytes from immunised mice, 65% (TRAMP C1) and 76% (TRAMP C2) cell lysis was observed, which was higher than the lysis observed with CD3⁺ T-cell and target controls -TRAMP C1shRNA and TRAMP C2shRNA- coculture. *** P= 0.0007, ****P= <0.0001as determined by an unpaired t-test (n = 8 over two independent experiment).*

5.3.3. Assessment of the anti-tumour capacity of the PAP42mer vaccine *in vivo*

5.3.3.1. C57BL/6J syngeneic mouse model

TRAMP C1 and TRAMP C2 cells are tumorigenic in C57BL/6J mice (Martini *et al*. 2010). TRAMP C2 cells were injected subcutaneously at the right flank of C57BL/6J male mice to generate suitable PCa tumour models to assess the *in vivo* vaccine efficacy. Tumour studies were conducted according to the Home Office regulations and reviewed by Nottingham Trent University's Animal Welfare Ethical Review Body. C57BL/6J male mice aged 9-10 weeks at the start of the treatment were used for all tumour studies conducted. Animals were closely monitored for any clinical signs, reduced body mass, or behavioural discomfort. The endpoint for the study was based on the tumour size; animals were culled when tumours reached the maximum size of 15mm or when ulceration was observed at the tumour site.

Due to the previously inconsistent growth obtained when TRAMP-C2 cells were injected in C57BL/6J mice, it was decided to grow them first in NOD-SCID mice by injecting TRAMP-C2

cells/ 100µL PBS or Matrigel (Figure 5.7A). TRAMP C2 tumours were developed on day 3, when the tumour reached the size of 250 mm^3 on day 24, they were collected from NOD-SCID mice. Tumour was dissociated using the Miltenyi Tumour dissociation kit, tumour cells were isolated and cultured in DMEM high glucose media with 10% FCS. These cells were used to generate tumours in C56BL/6J models for the study. A pilot study was conducted by injecting two different doses of TRAMP C2; $3x10^6$ cells and $5x10^6$ cells to identify the tumorigenicity of *in vivo* passaged TRAMP C2 cells. Both doses were able to generate tumours in C57BL/6J mice (Figure 5.7B).

The tumours were measured using callipers at every 3-4 days intervals. The mice that received $5x10^6$ cells, developed palpable tumours on day 7 while the mice that received $3x10^6$ cells developed tumours on day 14 of tumour cells injection. However, once the tumour developed, the tumour growth was consistent in both groups, the group of mice that received $3x10^6$ number of TRAMP C2 cells showed tumour growth like that of the group of mice that received $5x10^6$ cells; it was, therefore, decided to use the $5x10^6$ cells for tumour implantation.

Chapter 5: VACCINE EFFICACY IN C57BL/6J MICE

(A)

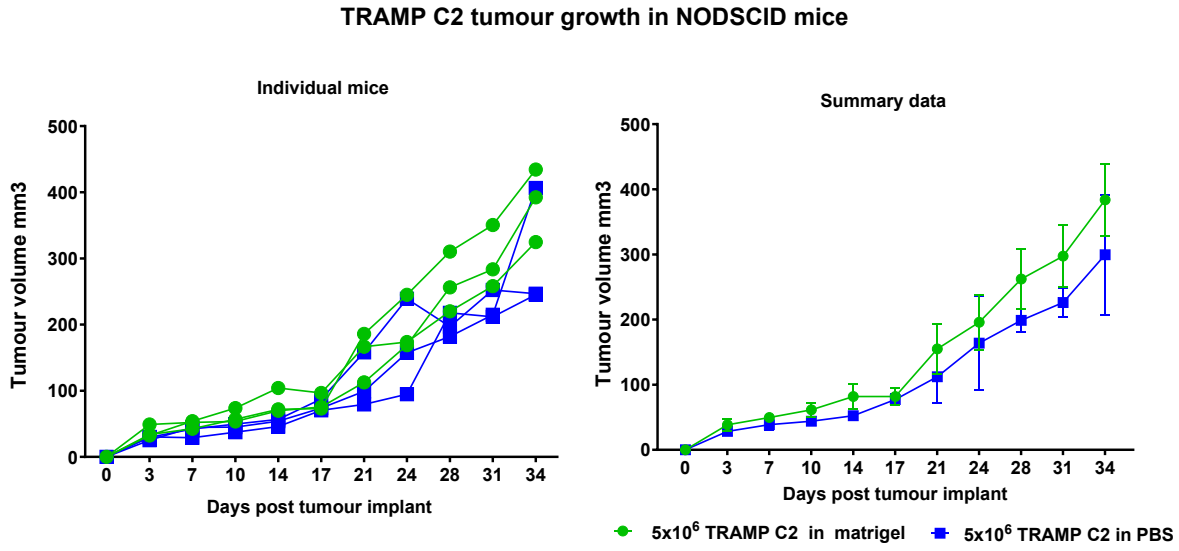

(B)

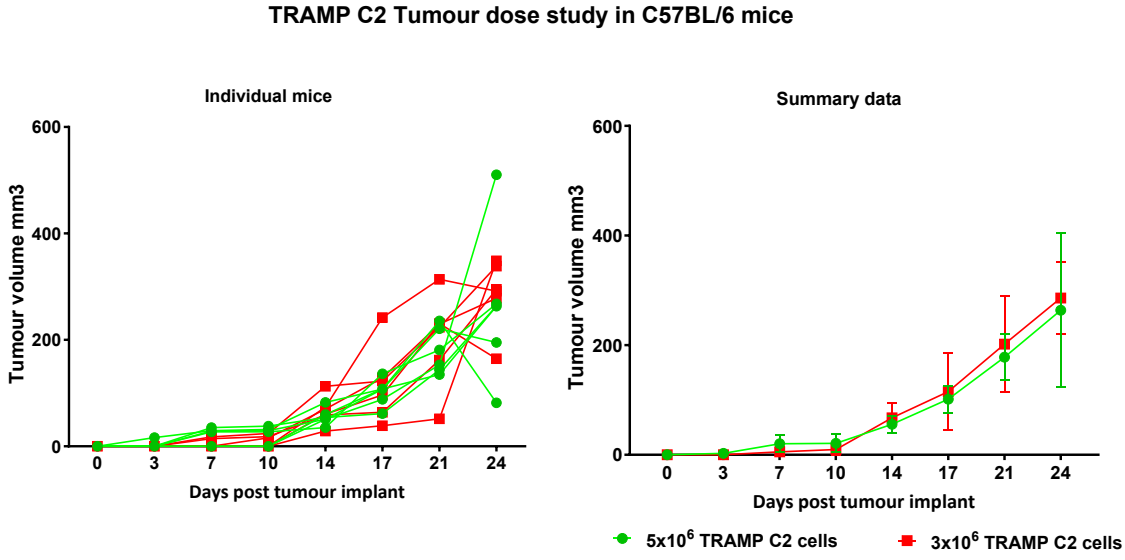

Figure 5.7. TRAMP C2 tumour growth in NODSCID and C57BL/6J mice. *(A) Tumour growth of individual NODSCID mice and summary data of tumour growth in NODSCID mice. 5x10^6 TRAMP C2 cells were injected in 100µL PBS/Matrigel (3 mice per group) subcutaneously at the right flank, and all animals developed palpable tumours on day 3. (B)Tumour growth of individual mice in C57BL/6J mice. Summary data of tumour growth in C57BL/6 mice. Mice received either 3x10^6 or 5x10^6 TRAMP C2 cells (3 mice per group) in 100µL PBS, and measurable tumours were developed on day 7 and day 14 respectively.*

Chapter 5: VACCINE EFFICACY IN C57BL/6J MICE

5.3.3.2. Assessing the vaccine efficacy in TRAMP C2 bearing tumour models in prophylactic settings.

The efficacy of the hPAP42merWT CAF®09b vaccine was assessed *in vivo* in two different settings: (1) The antitumour efficacy of the vaccine was assessed in prophylactic settings, where 3x doses of vaccine were administered before tumour implantation, (2) The antitumour efficacy of the vaccine was assessed in prophylactic settings where the vaccine was administered before or after an androgen deprivation therapy drug 'degarelix'.

5.3.3.2.1. Effect of immunisation in TRAMP C2 tumour bearing C57BL/6J animals.

5.3.3.2.1.1. Tumour growth and survival analysis of tumour models

C57BL/6J mice were challenged with $5x10^6$ TRAMP C2 cells subcutaneously into the right-hand side flank. Tumours developed in all animals, with most of the animals developing solid measurable tumours within 6 days after the implantation. Animals in the prophylactic treatment group received three doses of the hPAP42mer WT CAF®09b vaccine on (Days 0, 14 and 28) before being challenged with $5x10^6$ TRAMP C2 cells per mouse, while the animals in the control group received the same number of TRAMP C2 cells alone.

Tumour growth of individual mice was measured with callipers and is shown in Figure 5.9 (A). Although the individual tumour size increased abruptly in all groups, on day 23 there was a significant delay in the growth noticed in prophylactic groups of animals compared to the control group. There was no statistically significant difference in the survival of mice between groups (Figure 5.9 (B)), the study ended on day 36 post-tumour implantation.

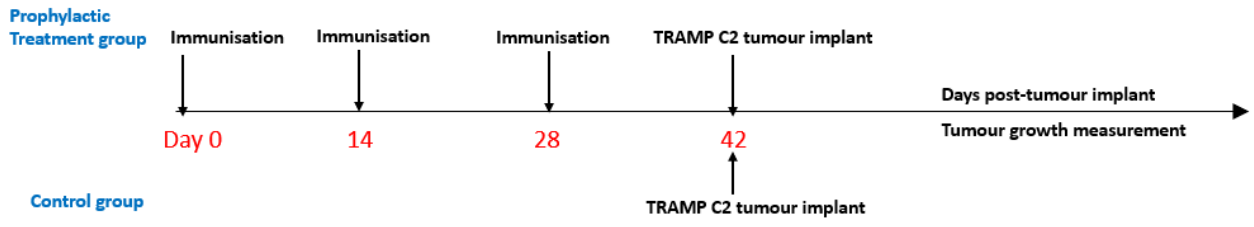

***Figure 5.8**. Schematic representation of immunisation and tumour implantation protocol for the tumour study.*

Chapter 5: VACCINE EFFICACY IN C57BL/6J MICE

(A)

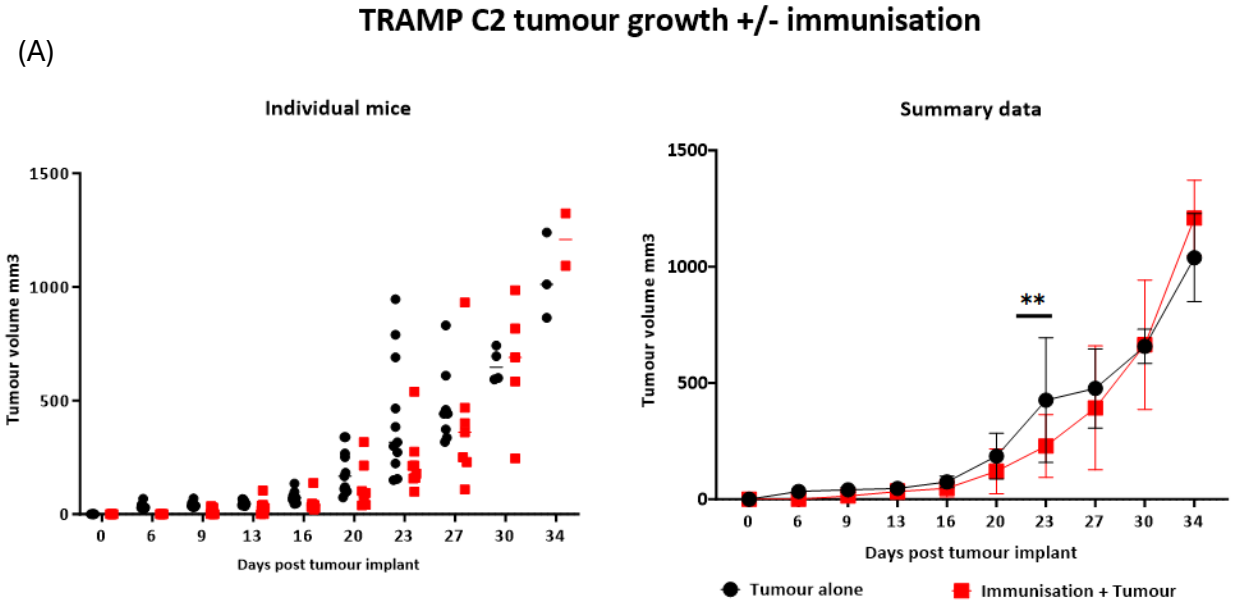

(B)

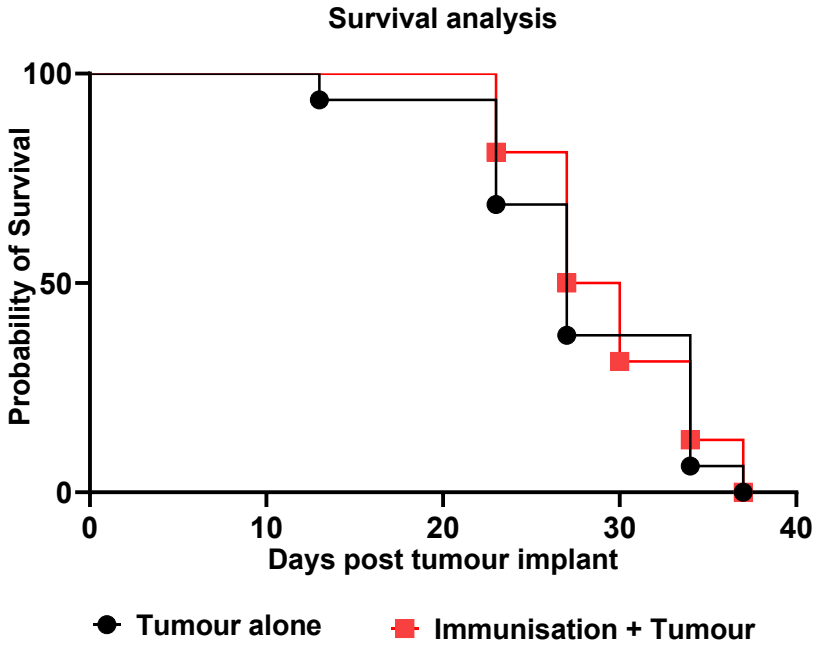

Figure 5.9. Effect of the hPAP42merWT CAF®09b peptide vaccine on tumour growth in C57BL/6J mice bearing TRAMP C2 tumours in prophylactic settings. *(A) Individual tumour growth is measured by callipers measurements. Summary data of tumour growth between three different groups (Control group: n=11; prophylactic group: n=8. A significant difference in tumour growth on day 23 **P≤ 0.0017 was determined by a 2-way ANOVA test. (B) Survival analysis of mice, no difference in survival between the groups were observed.*

Chapter 5: VACCINE EFFICACY IN C57BL/6J MICE

5.3.3.2.1.2. Flowcytometry analysis of gene expression in tumour models

The effect of immunisation on tumour infiltrating immune cells was evaluated by phenotyping of tumour cells (Figure) using the 22-colour flow cytometry staining panel (Table 2.9) At the end of the tumour study, tumours were collected from each mouse and were dissociated using the Miltenyi tumour dissociation kit following manufacturer protocol to obtain single-cell suspension. A total of $1x10^6$ tumour cells were subjected to surface and intracellular antibody staining as described in chapter 2 section 2.2.3.5.4. Table 2.9 displays the list of surface and intracellular antibodies used to detect cell surface markers and intracellular molecules and Table 5.4 illustrates their functions.

Antibody	**Identification marker**	**Properties/Function**	**Reference**
CD45	All nucleated hematopoietic cells except for erythrocytes and platelets.	Lymphocyte survival, and TCR signalling	(Ye et al. 2022)
CD3	T- lymphocytes	T-cell development	(Pennock et al. 2013).
CD8	$CD8^+$ T-cell subtype	Interact with antigen presented on MHC class I molecule	(Koh et al. 2023)
CD4	CD4+ T-cell subtype	Interact with antigen presented on MHC class II molecule	(Koh et al. 2023)
CD44 and CD62L	Naïve/memory T-cell subsets	Adhesion molecules linked to the differentiation of naïve and activated/ memory T-cells	(Pennock et al. 2013)
CD69	Activated lymphocytes	T-cell receptor stimulation expression marker	(Cibrián and Sánchez-Madrid, 2017)
Ki67	Quantitative indicator of T-cell proliferation	Cell proliferative activity	(Sun and Kaufman, 2018)
PD1	Immune checkpoint molecule	Immune suppression by binding to their respective ligands present on APCs	(Mateusz Kciuk et al. 2023).
TIM3			(Tian and Li, 2021) (Tang et al. 2023)

LAG3			(Maruhashi et al. 2020)
CTLA4			Stultz and Fong, 2021).
Ly6G and Ly6C	MDSCs	Suppress T-cell-mediated immune responses	(Veglia, Sanseviero and Gabrilovich, 2021)
CD25 and FoxP3	Regulatory T-cells identification	Suppress the activation, proliferation, and effector function of immune cells	(Xu et al. 2022)
IFN-γ and TNF-α	Cytokines produced by inflammatory cells	Cytotoxic capabilities	(Koh et al. 2023)
GITR and OX40	Co-stimulatory molecule expressed on regulatory T-cells and activated T-cells	T-cell activation	(Gubser et al. 2023) (Fu et al. 2020)

Table 5.4. List of markers used for the immunophenotyping of TILs.

The percentage of tumour infiltrating $CD4^+$/ $CD8^+$ T-cells, immune suppressive Tregs and MDSCs, presence of inflammatory IFN-γ and TNF-α and expression co-stimulatory/exhaustion markers on TILS was determined using Kaluza software. The statistical analysis was performed using GraphPad Prism. An example of the gating strategy used for the stained population of cells is shown in Figure 5.10.

Chapter 5: VACCINE EFFICACY IN C57BL/6J MICE

Gating strategy for 22 colour flowcytometry panel

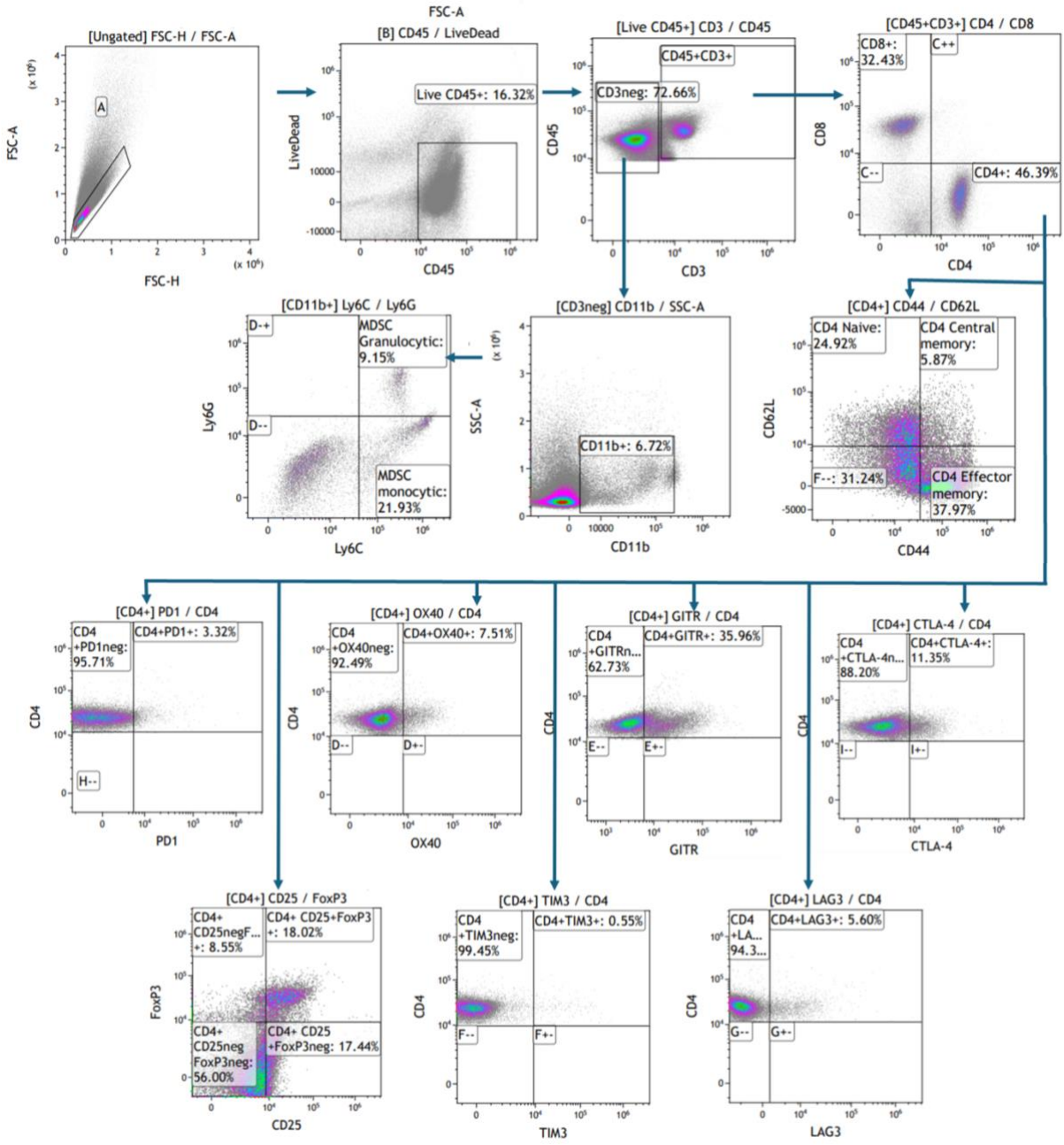

Figure 5.10. The gating strategy used to phenotype the TILs. *CD45 was gated from the forward scatter/side scatter singlets. CD3⁺ and CD3neg cells were gated from CD45⁺ cells. CD4⁺ and CD8⁺ T-cells were identified from CD3⁺ population. CD4⁺ and CD8⁺ T-cells were further gated on individual markers to identify naive/memory subsets (CD44/CD62L), T-regs (CD25⁺FoxP3), costimulatory molecules (GITR/OX40), cytokines (IFN-γ/TNF-α) and immune checkpoints (CTLA4, PD1, TIM3 and LAG3). CD8⁺ subsets also were identified using the similar gating strategy used for the CD4⁺ T-cells population. CD3 negative populations were further gated on CD11b and Ly6C/Ly6G to identify the monocytic and granulocytic MDSCs ($CD3^{neg}CD11b^{+}Ly6C^{+}$ and $CD3^{neg}CD11b^{+}Ly6G^{+}$).*

Chapter 5: VACCINE EFFICACY IN C57BL/6J MICE

In the forward scatter/side scatter (FSC/SSC) singlets, CD45 was gated, and dead cells were excluded by gating on Live/Dead. CD45 is a leucocyte common antigen expressed in almost all immunological and haematological cells except for mature erythrocytes and platelets (Ye *et al*. 2022). $CD45^+$ live cells were further gated to identify $CD3^+$ and $CD3^{neg}$ cells. Among the CD3 negative cell population, $CD11b^+$ cells were gated to identify the MDSC cells. The two subpopulations of MDSCs- granulocytic or monocytic- were identified by further gating the $CD3^{neg}CD11b^+$ cells using Ly6G or Ly6C markers respectively. All T-cells express CD3 (Pennock *et al*. 2013), CD3 positive cells were further gated on CD4/CD8 markers to identify the CD4 or CD8 T-cell subpopulation. Regulatory T-cells that suppress the effector function of immune cells can be identified by CD25 and FoxP3 functional markers (Xu *et al*. 2022), therefore, regulatory CD4 and CD8 T-cell populations were identified by gating as $CD4^+CD25^+FoxP3^+$ and $CD8^+CD25^+FoxP3^+$. Immune checkpoints such as PD-1, TIM-3, LAG-3, and CTLA-4 on T-cells were identified by gating $CD4^+$ and $CD8^+$ T-cells with respective inhibitory checkpoint markers- $CD4^+$PD-1/TIM-3/LAG-3/CTLA-4 and $CD8^+$ PD-1/TIM-3/LAG-3/CTLA-4.

CD44 and CD62L surface markers were used to define naïve, effector memory, and central memory $CD4^+/CD8^+$ T-cells. Naïve T-cells were gated as $CD4^+/CD8^+$ $CD44^{low}CD62L^{high}$, central memory as $CD4^+/CD8^+CD44^{high}CD62L^{high}$, and effector memory as $CD4^+/CD8^+CD44^{high}CD62L^{low}$.

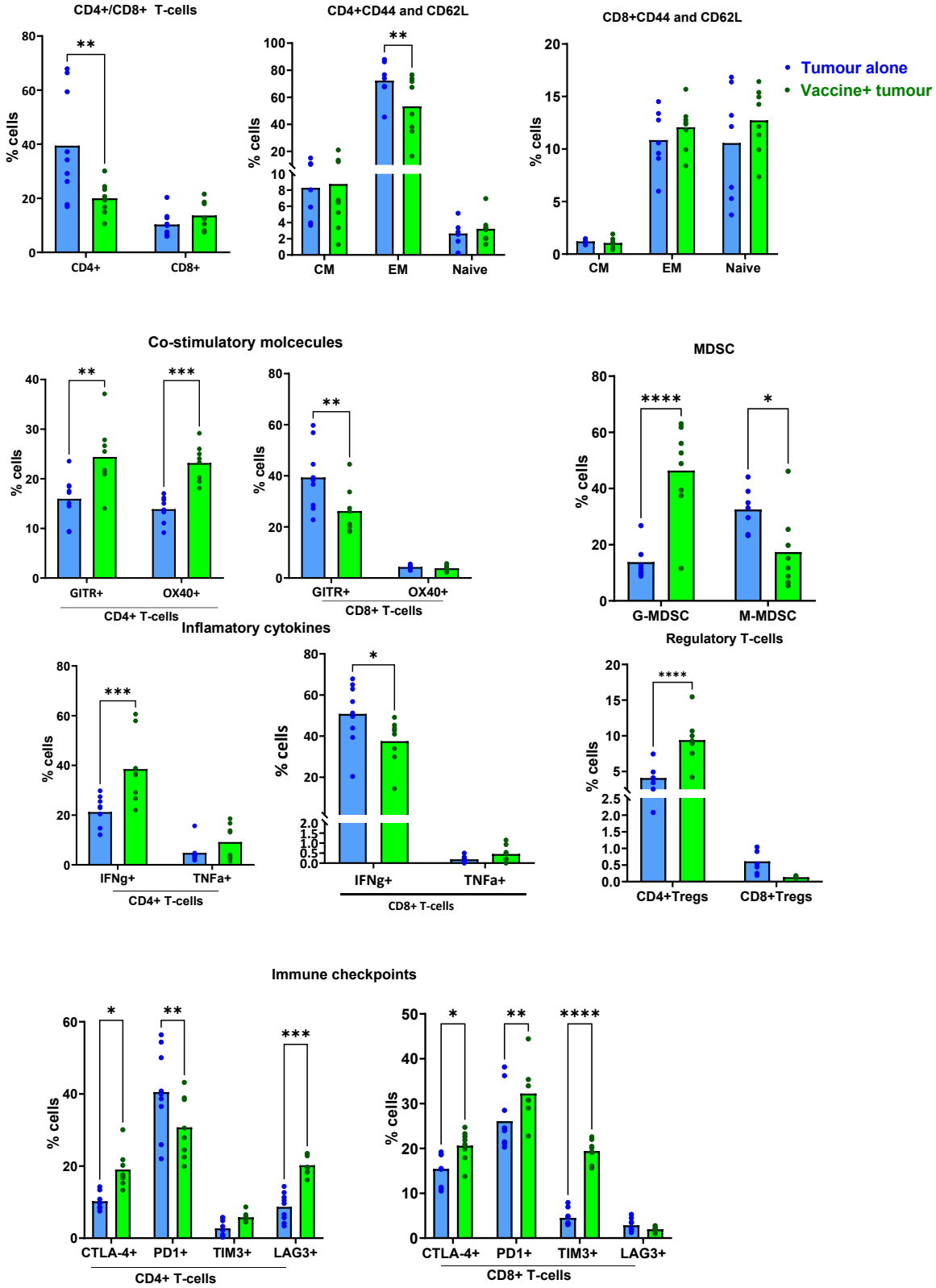

Figure 5.11. Immunophenotyping of the TILs of the immunised (prophylactic) and non-immunised TRAMP C2 tumour models. *Tumour alone represents the control group, where the animals challenged with tumours*

*but not received any immunisation. Vaccine+ tumour represents the group of animals that received 3 doses of immunisation and TRAMP C2 tumours at two weeks intervals. The graphs represent the difference in the expression of costimulatory molecules, inflammatory cytokines, and immunosuppressive elements (FoxP3, PD1, TIM3 and, LAG3 and MDSCs) of $CD4^+$/$CD8^+$ T-cells and MDSCs in in TILs of immunised mice (vaccine +tumour) to that of tumour alone mice. The significant difference between the groups *P≤ 0.0340, ** P≤ 0.0082, *** P≤ 0.006 and **** P<0.0001 were determined by two-way ANOVA test.*

TIL staining (Figure 5.11) revealed no increase in $CD4^+$/$CD8^+$ TILs, in the immunised groups compared to the control group indicating that the immunisation did not positively influence the migration/retention of T-cells into the TME. The percentage of CD8+ Naïve ($CD44^{neg}CD62L^+$) and effector memory ($CD44^+$ $CD62L^{neg}$) T-cell subsets were found to be increased with the immunisation however, no significant increase was observed. The expression of co-stimulatory molecules GITR and OX-40 on $CD4^+$ T-cells was significantly higher in the immunised group, whereas the $CD8^+GITR^+$ cells were significantly less in the immunised group compared to the tumour-alone group. The proportion of $CD4^+$ IFN-γ^+ cells also were found to be more expressed by the immunised group animals however, the IFNg-releasing $CD8^+$ T-cells were significantly reduced comparatively in the treatment group.

Immunisations given in the prophylactic settings significantly reduced the expression of immune checkpoint molecule PD1 in $CD4^+$ helper cells, however, other immune checkpoints such as TIM3, LAG3, and CTLA4 were found to be highly expressed. The proportion of MDSC remained consistent across all groups; in fact, the granulocytic MDSCs and $FoxP3^+$ Tregs were found to be highly expressed in the immunised group. The elevated presence of inhibitory checkpoint receptors such as CTLA4, TIM3, and LAG3 on $CD4^+$ TILs and PD1, CTLA-4, and TIM 3 on $CD8^+$ TILs indicate the level of T-cell exhaustion in the TME. Moreover, the higher expression of immunosuppressive factors such as MDSCs and Tregs contributed to a suppressive TME where T-cells were functionally inactive. There was no upregulation of CD69 (activation marker) and Ki67 (proliferation marker) observed in the TILs of immunised mice indicating a lack of proliferation or activation in naïve and central memory cells (data not shown).

These results reveal that the administration of 3 doses of the vaccine was not sufficient to delay the growth of TRAMP-C2 cells. Some immunostimulatory elements were upregulated however the elevated expression of immune checkpoints, and immunosuppressive Tregs and MDSCs limited the efficacy of the vaccine when it administered alone. Therefore, the efficacy of the vaccine in combination with ADT was tested. ADT (also known as castration) is a primary treatment option for treating advanced PCa (Desai, McManus, and Sharifi, 2021). Androgens function to promote the survival and maintenance of normal and cancerous prostate cells by binding and activating androgen receptors expressed in normal or malignant prostate cells (Murray, 2021). Androgen depletion achieved surgically or chemically inhibits the growth of prostate cancers therefore is a universally accepted treatment option for men with advanced PCa. However, most of the PCa cells become resistant to ADT therapy and continue to grow even when the androgen levels are significantly reduced – also known as castration-resistant PCa (CRPC). Metastatic CRPC is a lethal disease (Sekhoacha *et al*. 2022). The TRAMP C2 cells grow in an androgen-independent manner (Philippou *et al*. 2020), therefore TRAMP C2 grown in castrated mice would mimic the clinical setting of CRPC, thereby the efficacy of PAP42mer peptide vaccine in CRPC can be tested in castrated mouse models bearing PCa tumours. Moreover, all advanced PCa patients are likely to undergo some form of ADT since it is the standard treatment option for advanced PCa. Therefore, it is important to understand how castration will affect the efficacy of the PAP42mer vaccine.

Researchers have discovered that PCa immunotherapies demonstrate an improved immune response when administered in castrated mice. Yi Ting Koh *et al (*2009) found that castration enhanced the immune response of the immunotherapy formulated with prostate stem cell antigen when administered before castration. Tang *et al* (2012) also observed that concomitant castration increased the proportion of antigen-specific $CD8^+$ T-cells of immunisation containing an H-$2K^b$–restricted antigen in castrated C57BL/6J models.

5.3.3.2.2. Efficacy of vaccine in TRAMP C2 tumour bearing castrated C57BL/6J models.

The castration +/- immunisation tumour study aimed to assess the efficacy of the hPAP42mer WT+ CAF®09b vaccine in castrated mice. To ensure that the castration does not impact the growth of the tumour (as is the case for men who develop ADT resistance) TRAMP C2 cells were grown in chemically and surgically castrated mice and compared to mice without castration interventions.

5.3.3.2.2.1. Effect of castration in TRAMP C2 tumour growth

TRAMP C2 cells were shown to grow independently of androgen level in a pilot study (n=4 per group), where the C57BL6/J mice were castrated chemically by injecting an FDA-approved GnRH antagonist degarelix (0.625mg) or by surgically creating an incision on the ventral surface of the scrotum after exposing the testes under anaesthesia. Ten days post-chemical castration and 3 days post-surgical castration, the animals were challenged with $5x10^6$ TRAMP C2 cells. The growth of TRAMP tumours in castrated mice was compared against the growth of TRAMP C2 tumours in non-castrated mice. The results obtained (Figure 5.12(A)) confirmed that TRAMP C2 cells grow in an androgen-independent manner. Measurable tumours were developed by day 4 of post-tumour implantation in all the groups and growth of the tumour was consistent in all the groups. The experiment was concluded on day 17. Additionally, blood samples were collected on day 14 of post-castration and serum was isolated to confirm the reduced serum testosterone levels in castrated mice. Testosterone was extracted from the serum samples by following the protocol mentioned in section (2.2.3.5.5.3.) and was analysed by mass spectrophotometry. The graph (Figure 5.12 (B)) shows the reduction of serum testosterone observed in the surgically and chemically castrated mice.

Chapter 5: VACCINE EFFICACY IN C57BL/6J MICE

(A)

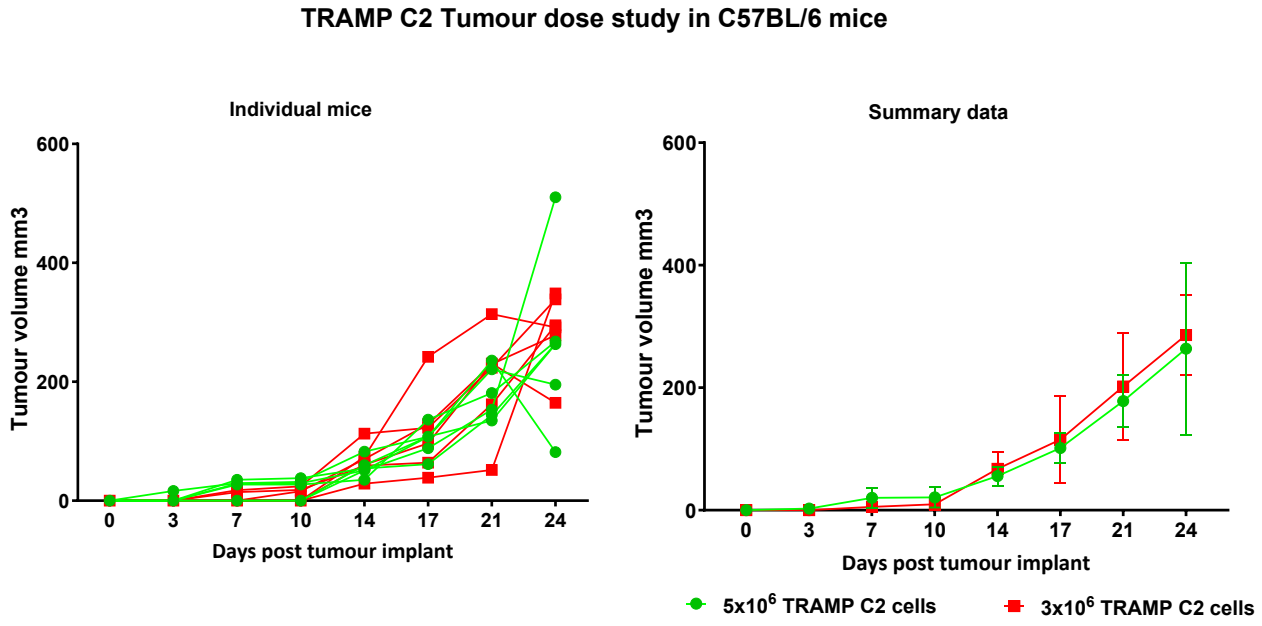

(B)

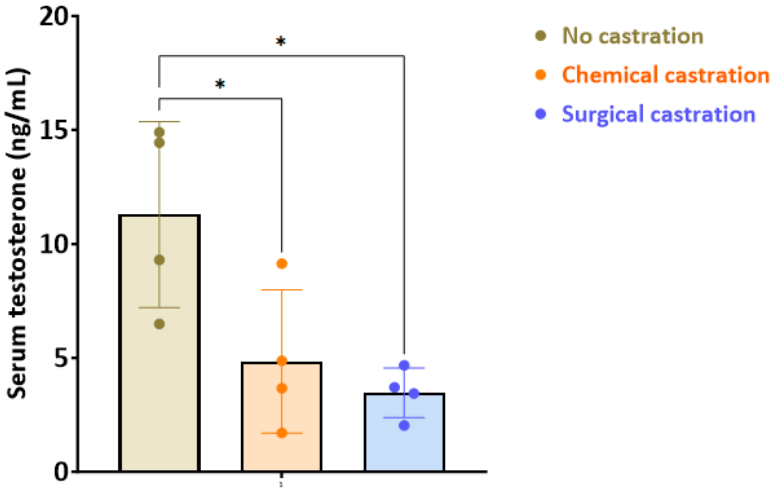

Figure 5.12. Effect of chemical or surgical castration in C57BL/6J TRAMP C2 tumour models. *(A) TRAMP C2 tumour growth in castrated mice. n=4 per group. Chemical or surgical castration was shown to not affect tumour growth. (B) Serum testosterone level of castrated and non-castrated mice. Chemical or surgical castration reduced the serum testosterone level.*

Chapter 5: VACCINE EFFICACY IN C57BL/6J MICE

5.3.3.2.2.2. TRAMP C2 tumour dose optimisation

In the previous tumour study (section 5.3.3.2.1) tumours grew abruptly in the prophylactic treatment group although a delay in tumour growth was noted on day 23. The use of a higher number ($5x10^6$) of TRAMP C2 cells for tumour implantation may have contributed towards the rapid tumour growth. Therefore, a lower dose of TRAMP C2 cells was then considered, and a tumour titration dose was repeated before the next study. Three different doses ($1x10^6$, $2x10^6$ and $3x10^6$) of TRAMP C2 cells were used to optimise the tumour dose with N=5 per group. Tumours were developed in all experimental groups. Mice in the groups that received $2x10^6$ and $3x10^6$ tumour cells developed the tumours by day 14 and the group of animals that received $1x10^6$ tumour cells developed palpable tumours by day 17 which was notably slower compared to the group that received $5x\ 10^6$ cells where all tumours were developed in by day 7. The study was concluded on day 41. The animals that received $2x10^6$ cells were found to be consistent for tumour growth, therefore, it was decided to use the same number of TRAMP C2 cells for tumour implantation in the following tumour study.

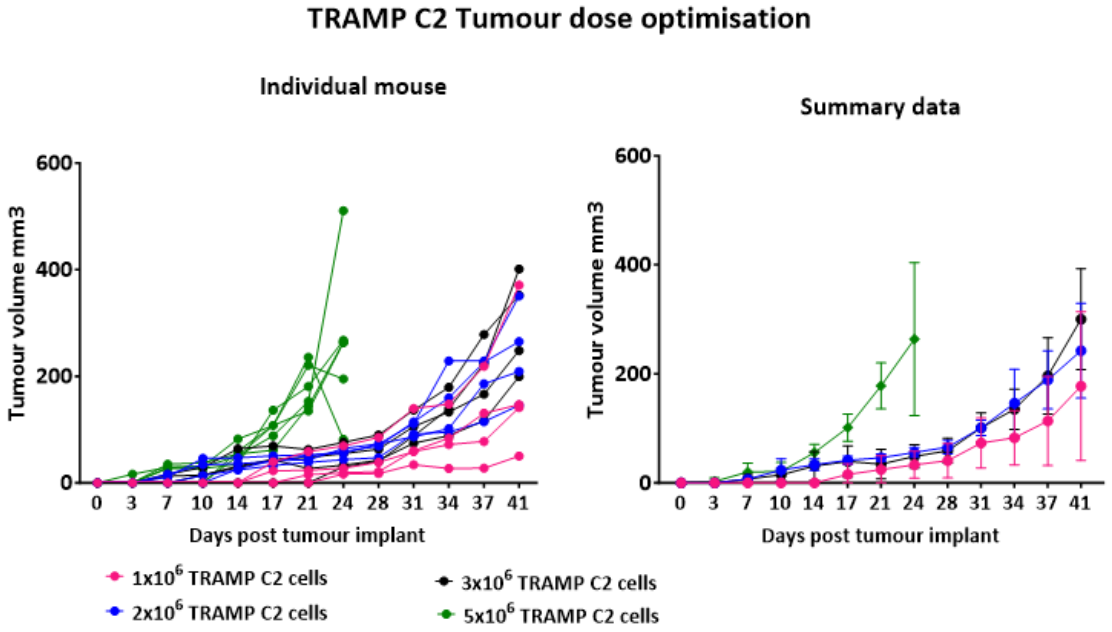

Figure 5.13. TRAMP C2 tumour dose optimisation. *C57BL/6J mice were challenge with $1x10^6$, $2x10^6$ or $3x10^6$ TRAMP C2 cells. The growth of tumours was measured by callipers. The animals that received $2x10^6$ cells were shown to have more consistent tumour growth. The dose optimisation graphs were compared against the tumour growth of $5x10^6$ TRAMP C2 cells (represented as a green-coloured graph) which demonstrated rapid and aggressive tumour growth.*

Chapter 5: VACCINE EFFICACY IN C57BL/6J MICE

5.3.3.2.2.3. Effect of immunisation on tumour growth and survival in castrated mice.

The study was designed as illustrated in (Figure 5.14). The efficacy of the vaccine was tested in C57BL/6J animals bearing TRAMP C2 tumour, where the immunisation was administered before and after degarelix treatment. The experiment included three groups of 13 mice each and all animals were challenged with TRAMP C2 tumour by injecting $2x10^6$ cells into the right flank.

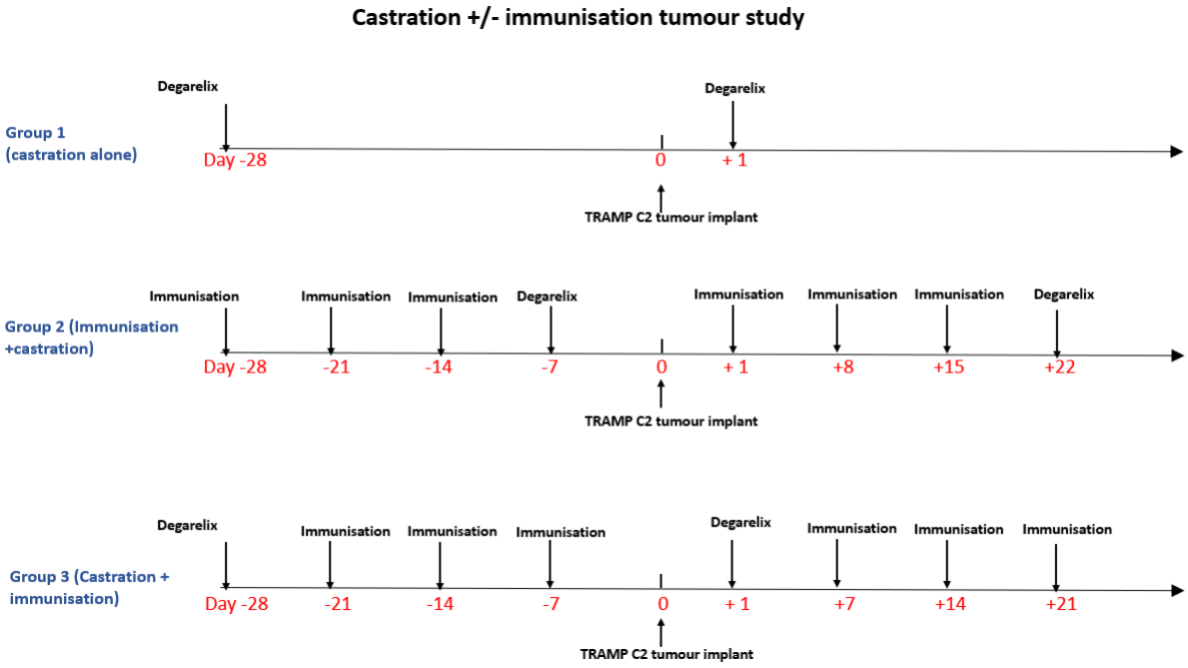

Figure 5.14. Schematic representation of castration, immunisation, and tumour implantation protocol for the tumour study. *While the immunisations were initially planned according to the diagram, not all immunisations were administered post-tumour implantation due to the clinical signs observed in the animals. The control group received two doses of degarelix. Group 2 received immunization three prior to tumour implantation and two post tumour implantations along with one dose of degarelix. Group 3 received four doses of immunisation -three prior to tumour implantation and one post tumour implantation- and two doses of degarelix.*

The control group, Group 1 (Degarelix alone)- animals were subjected to castration alone, received 2 doses of degarelix injection: the first dose of injection was given 28 days before tumour implantation and the other was given the following day after tumour implantation. In the treatment group, Group 2 (Immunisation+ Castration), C57BL/6J mice were immunised with three doses of 30ug hPAP42mer+100µL CAF09 vaccine and a dose (0.625mg) of

degarelix injection a week apart. One-week later animals were subjected to tumour implantation. Whereas in the treatment group, Group 3 (Castration+ Immunisation), C57BL6/J mice were castrated at the start of the study and 7 days later, they received 3 doses of immunisation and then challenged with TRAMP C2 cells at weekly intervals.

The previous prophylactic tumour study failed to show any effect and therefore it was hypothesised that a stronger immune response would be achieved if the mice were to receive the vaccine every week instead of every two weeks. Unfortunately, following the fifth injection of the vaccine, 6 out of 13 animals in group 2 lost significant body weight and showed clinical signs, therefore these animals had to be culled. It appears that a change in the formulation of the CAF®09b caused toxicity to the animals, and from then on, the animals were never again able to be immunised with CAF®09b. The control group animals that received only castration developed measurable tumours later compared to the treatment groups. The tumour development of each grouped animal is summarised in Table 5.5. The growth of the tumours was measured by callipers and the tumour growth between the control and treatment groups is illustrated in Figure 5.15(A). Kaplan-Meier survival analysis (Figure 5.15 (B)) shows no improvement in survival in the treatment groups compared to the control group.

Days post tumour implantation	The number of mice that developed tumours on Day X		
	Group 1 (Castration)	Group 2 (Immunisation+ Castration)	Group 3 (Castration+ Immunisation
Day 11			2
Day 14		4	9
Day 18	5	2	1
Day 21	3	1	
Day 24	4		
Day 27			1

Table 5.5. Incidence of tumour occurrence between the test groups. *In the control group (castration alone) the occurrence of visible tumours was noticed on day 18 whereas in treatment groups tumours started to develop by days 11 and 14. Notably, in the treatment group where immunisation was administered after castration, almost all animals developed tumours by day 18.*

Chapter 5: VACCINE EFFICACY IN C57BL/6J MICE

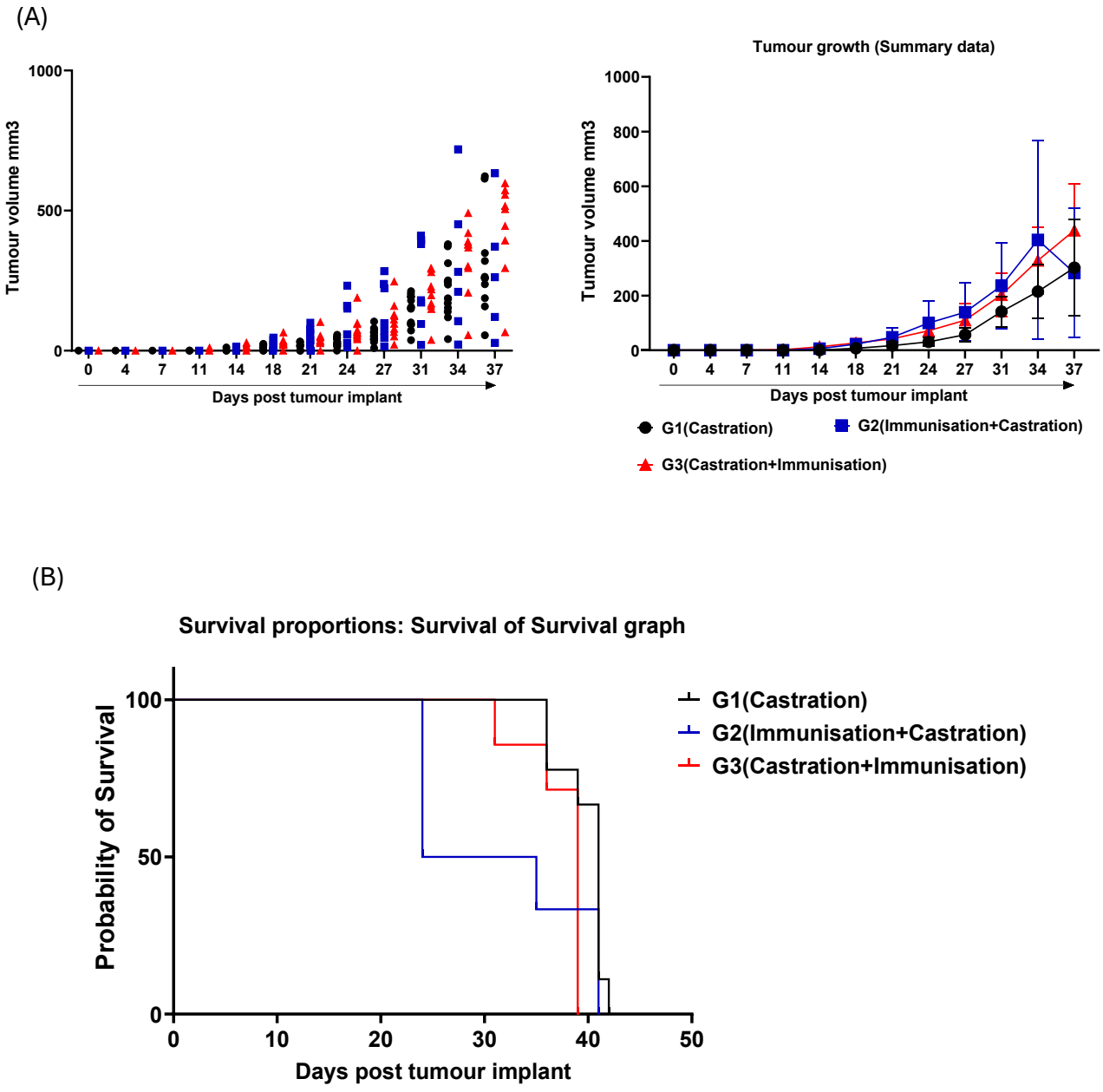

Figure 5.15. Effect of the hPAP42merWT CAF®09b peptide vaccine on tumour growth in castrated C57BL/6J mice bearing TRAMP C2 tumours. ***(A)*** *Callipers measurements of tumour growth in individual and grouped mice (summary data). Immunisation has not shown any reduction in tumour growth, whether it was administered before or after the degarelix treatment.* ***(B)*** *Survival analysis of mice showed no difference in survival between the groups. (Control group: n=12; Immunisation+ castration, n=7; Castration+ immunisation n=13).*

5.3.3.2.2.4. Immunophenotyping of TILs

The effect of immunisation (before and after castration) in modulating the immune system of tumour-bearing castrated mice was evaluated by 22 colour panel flow cytometry. As discussed earlier, one of the treatment groups received immunisation before castration (group 2) and the other group received it after castration (group 3). Group 2 had received 5 doses of immunisation (3x before and 2x after the tumour implant) and one dose of degarelix in total whereas group 3 received 4 doses of immunisation (3x before and 1x after tumour implant) and two doses of degarelix. Before evaluating the effect of immunisation in TRAMP C2 tumour-bearing castrated mice, the impact of castration in modulating the immune system in the presence of TRAMP C2 tumour was evaluated by comparing the TILS flowcytometry analysis of castrated tumour models from this experiment with the flow cytometry analysis of tumour alone (that underwent no castration) from the previous experiment (section 5.3.3.2.1.2); the comparative results of phenotypic analysis are shown below (Figure 5.16). The results show that castrated mice had more (but not significant) tumour infiltrating $CD4^+$ and $CD8^+$ T-cells compared to the non-castrated tumour-bearing models, however, the presence of effector memory T-cells was found to be reduced with castration. The IFN-γ -releasing $CD4^+$ and $CD8^+$ TILs were found to be decreased significantly in castrated tumour models whereas the TNF-α -releasing $CD4^+/CD8^+$ cells were higher in these mice. In addition, castration also showed a reduction in the expression $CD4^+$Tregs, monocytic MDSC in TILs, overexpression of $LAG3^+$ CD8/CD4 T-cells and $CTLA4^+$ CD8 T-cells in the TILs of castrated mice was observed.

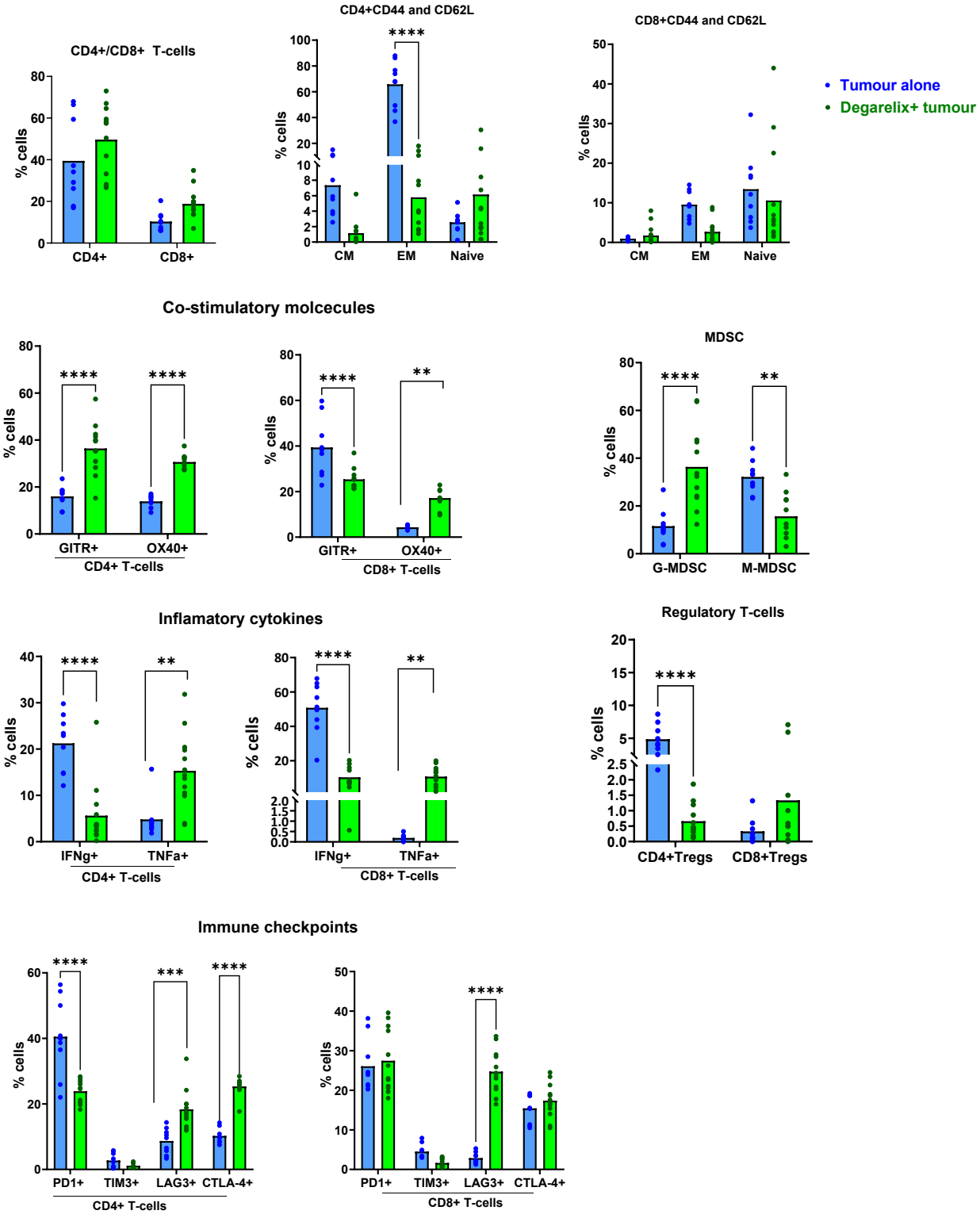

Figure 5.16. The effect of castration in modulating the immune system on TRAMP C2 tumour bearing C57BL/6J models (Tumour alone vs Degralix+ tumour). *The statistical analysis shows a reduction of co-stimulatory molecule GITR, and elevated expression of immune checkpoint PD1, and CTLA -4 in the CD4+ T-cells of castrated mice. Notably, there was a reduction in immunosuppressive G-MDSC and CD4+ Tregs. The*

*significant difference between the groups ** P≤ 0.008, *** P≤ 0.002 and **** P<0.0001 were determined by a two-way ANOVA test.*

The TILs immunophenotyping shows an increased number of CD4 phenotype T-cells in both immunisation+ castration and castration+ immunisation treatment groups compared to the 'castration alone' control group. When compared to the tumour alone non-castrated this was a 20% increase in group 2 (vaccine+ castration) and a 15 % increase in group 3 (degarelix+ vaccine). Castration alone had been shown to decrease the effector memory cells, however, the immunisation was shown to reverse this effect, and the presence of $CD4^+$ and $CD8^+$ effector memory ($CD44^+CD62L^{neg}$) in both treatment groups was higher. Moreover, $CD8^+$ effector memory cells were also found to be activated in both treatment groups indicating the efficacy of the vaccine to generate cytotoxic $CD8^+$ lymphocytes. Interestingly, the presence of $CD69^+$ effector memory T-cells ($CD4^+/CD8^+$ $CD44^+$ $CD62L^{neg}$ $CD69^+$), indicates the increase of activated functional effector cells following immunisation (Figure 5.17). However, vaccination did not improve the generation of central memory subsets when it was administered before or after degarelix.

Immunisation also reduced exhaustion markers such as PD1, CTLA4, TIM3 and LAG3 in castrated TRAMP C2 tumour-bearing mice, specifically the presence of PD1 and $CTLA4^+$ in both $CD8^+$ CTLS and $CD4^+$ T-helper cells when vaccination was administered before castration. When immunisation was administered after castration, the expression of $CTLA4^+$ was significantly reduced in the $CD8^+$ and $CD4^+$ subset of T-cells and the expression of PD1 in $CD8^+$ CTLs. The exhaustion marker PD1 expression on $CD4^+$T-cells was lowered in castrated mice, which was found to be further reduced significantly with immunisation. However, the presence of granulocytic MDSC was higher in castration immunisation-grouped animals. The expression of costimulatory molecules OX40 and GITR in TILs was not altered with vaccination. IFN-γ -generating $CD8^+$ cytotoxic cells also were higher in both treatment groups with significantly higher in the Castration+ Immunisation group compared to the castration alone group. The presence of regulatory T-cells was reduced with castration (Figure 5.16) and was found to be further reduced when immunisation was given before castration.

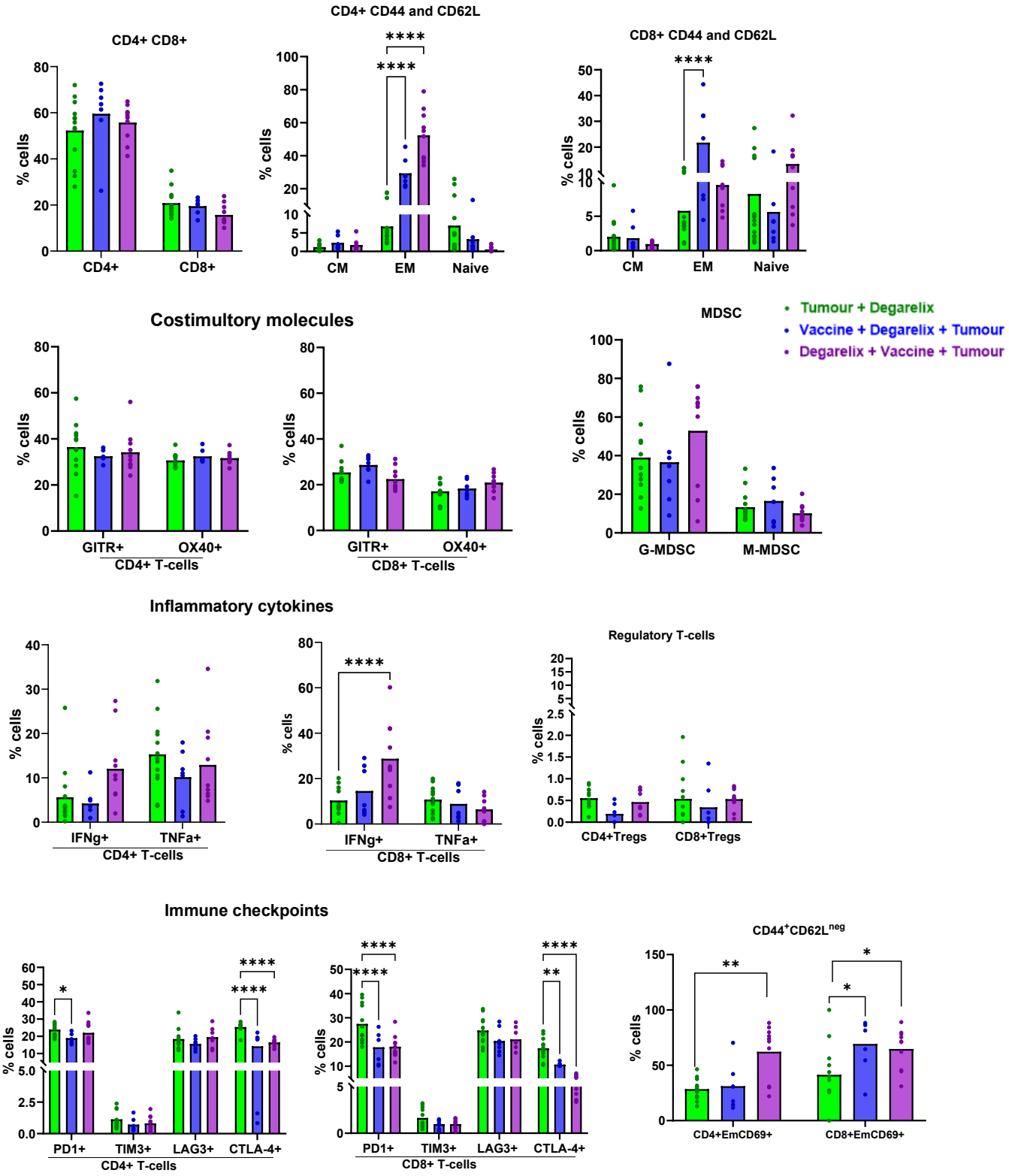

Figure 5.17. Flow cytometric analysis of the effect of hPAP42mer WT + CAF09 vaccine in castrated C57BL/6J TRAMP C2 tumour models. *Immunophenotyping of TILs shows immunisation improved the*

*functioning $CD4^+$ and $CD8^+$ effector T-cells and reduction in T-cells exhaustion markersPD1 and CTLA4. The presence of suppressive Tregs was also reduced, however presence of MDSC was elevated in the immunised group, especially when castration had been applied before immunisation. Both CD4 and CD8 effector memory cells ($CD44^+CD62L^{neg}$) were shown to have high expression of CD69 activation markers in immunised groups. The significant differences between the groups * P≤ 0.037, ** P≤ 0.006 and **** P<0.0001 were determined by a two-way ANOVA test.*

5.3.3.2.2.5. Effect of castration in reducing serum testosterone level confirmed in degarelix-treated mice.

The blood samples of the animals were collected before and 7- and 14-days post castration, serum was isolated (section 2.2.3.5.5.2.), and testosterone was extracted by following the protocol mentioned in section (2.2.3.5.5.3.). The mass spectrophotometric analysis reveals a reduction in the testosterone level one week and two weeks after castration as shown in Figure 5.18.

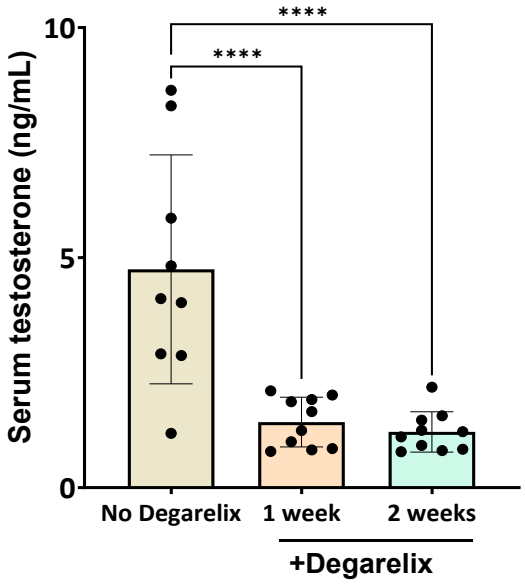

Figure: 5.18. Castration reduces the serum testosterone level in C57BL/6J mice. *Mass spectrophotometry analysis of serum testosterone level in the C57BL/6J tumour-bearing models before castration and at one week and two weeks post castration.*

Chapter 5: VACCINE EFFICACY IN C57BL/6J MICE

5.4. Discussion

The immunogenicity and antitumour efficacy of the hPAP42mer WT+ CAF®09b vaccine were tested in the C57BL/6J syngeneic mouse models. These genetically identical mouse models are ideal models for understanding tumour immunity in the context of a complete functional murine system. Though the results obtained using these models cannot be transferrable to the clinic, the results obtained are proof of concept. Since the immunogenicity was assessed in a complete functional murine immune system, the human wild-type form of the 42mer was used in this study, which differs in two amino acids from the mouse sequence (Table 5.1). The human WT 15mer CPR (CPRFQELESETLKSE) was predicted to bind to H2-IAb with higher affinity than that of its murine counterparts, however no CPR-driven IFN-γ production was observed in vaccine-induced splenocytes and CPR co-culture ELISpot. This could be due to three AA changes in the murine sequence (CPRFEELKSETLESE) to the WT human CPR. Thus, further vaccine formulations only included hPAP42mer WT and CAF09. hPAP42mer WT was identified to be immunogenic to generate vaccine-specific CD8+ and $CD4^+$ T-cell mediated response in mice. Moreover, the vaccine-induced CLTs were able to lyse murine PCa cells TRAMP C1 and TRAMP C2 *in vitro*; 65% cell lysis for TRAMP C1 and 76% lysis for TRAMP C2 cells were observed, which was higher than the cytotoxicity observed with $CD3^+$ T-cell and target controls (TRAMP C1/TRAMP C2 + shRNA) coculture. However, the TRAMP C2 shRNA cells exhibited 40% cytotoxicity, in which PAP expression was knocked down but not completely ablated. To enhance the robustness of the control, it would have been advantageous to include a cell line that lacks PAP expression, such as the MC38 murine colon adenocarcinoma cell line, also derived from C57BL/6 mice.

Though the *in vitro* cytotoxicity assays provide valuable insight as an initial step in tumour efficacy, the ability of the vaccine needs to be assessed *in vivo* using specific tumour models to understand the complexity of immune response within the TME. *In vivo* studies also provide a comprehensive understanding of how effectively and safely vaccine interacts with the immune system and tumour in the physiological context which is essential for developing effective and safe immunotherapies (Jubelin *et al*. 2022).

Chapter 5: VACCINE EFFICACY IN C57BL/6J MICE

Therefore, as the next step of the research, the vaccine efficacy was tested *in vivo* using C57BL/6J -TRAMP C2 tumour-bearing models. TRAMP C2 was shown to express a higher level of PAP (section 3.2.1.2.2.) compared to TRAMP C1 and demonstrated a high percentage of killing by vaccine-induced T-cells *in vitro*. In addition to the PAP expression, TRAMP C2 cells also were confirmed to have the expression of MHC class I molecule, which is necessary for antigen presentation and thereby recognition by CTLs.

Tumour models were generated by injecting TRAMP C2 cells subcutaneously into the right flank of C57BL/6J mice, which makes a transplantable tumour model for the study. The tumours were established quickly allowing the assessment of the efficacy of the vaccine in shorter study timelines, however, the tumours grown across the animals were not consistent, in some animals the tumours were established faster, whereas some animals within the same treatment group showed variability in tumour incidence. Moreover, the tumours were implanted by injecting the tumour cells subcutaneously into the right flank, which does not mimic the TME of PCa. Thereby the interactions between cancer cells and the stromal components of the PCa TME are less accurately represented. An alternative approach is to inject the tumour cells orthotopically into the prostate would have better mimicked the PCa TME. However, to be able to monitor the tumour growth *in vivo* would require either access to an MRI or to modify the tumour cells to express a gene whose expression can be used to monitor the growth using bioluminescence of fluorescence. The MRI is expensive, and the genetic alterations of the cells may change their immunogenicity (Bausart *et al*. 2023). Spontaneous tumour models that develop tumours naturally over time (For example: TRAMP mice) will provide a realistic representation of cancer development and progression and would have been another alternative to consider. For these mice, the use of MRI will therefore be needed. The TRAMP mice are also notoriously known to be difficult to breed and many tend to develop a neuroendocrine type of PCa (Wu *et al*. 2013).

The efficacy of the vaccine was tested in prophylactic settings in non-castrated and castrated mice. In the initial study (non-castrated), no initial tumour growth delay was observed as would have been anticipated if the vaccine had generated T-cells capable of migrating to and recognising the tumour cells. A reduction in tumour growth was observed

in the immunised mice on day 23, but the tumour grew aggressively after that. The TILs immunophenotyping analysis showed that while the proportion of T-cells was not increased, there was an increased expression in co-stimulatory molecules $GITR^+/OX40^+$ on $CD4^+$ T-cells, (indicating $CD4^+$ T-cell activation) as well as an increase in IFN-γ releasing CD4+ cells was noted in the immunised group. Co-stimulatory molecule signals are essential for T-cell activation in addition to antigen stimulation through TCRs. Both GITR and OX40 are expressed on activated $CD4^+$ and $CD8^+$ T-cells. OX40 plays a crucial role in regulating effector and memory T-cell responses, supporting the survival and expansion of $CD4^+$ and $CD8^+$ T-cells (Gubser *et al*. 2023; Fu *et al*. 2020). Nonetheless, the presence of higher expression of G-MDSC and $CD4^+$ $CD25^+$ FoxP3 cells along with the immune suppressive checkpoints CTLA -4, PD -1, and TIM -3 in CD8+ cells, and CTLA -4, LAG -3 in $CD4^+$ cells were also observed in the immunised group. These results explain why immunisation had less effect on tumour growth. MDSCs and Tregs are the major components of immunosuppressive PCa TME, in addition, the increased expression of immune checkpoint leads to T-cell anergy rather than activation (Mateusz Kciuk *et al*. 2023).

The use of a dose that was too high ($5x10^6$) of TRAMP C2 cells was also thought to be the reason for the rapid tumour growth observed. Therefore, in the subsequent study (castrated mice), tumour dose optimisation was carried out again and a lower number ($2x10^6$) of TRAMP C2 cells was used to mitigate the issue. Despite adjusting the number of TRAMP C2 cells, no reduction in the tumour growth was observed in the treatment groups that received immunisation either before or after degarelix treatment, compared to the control group that received degarelix alone. It was also observed that the tumours in the control (degarelix alone) group developed more slowly, occurring 4-7 days later than in the treatment groups; the reason behind this difference was not clear. Before the castration and/or immunisation tumour study, it was confirmed that the degarelix administration in tumour-bearing mice reduced the serum testosterone levels without affecting the growth of TRAMP C2 tumours (section 5.3.3.2.2.1). However, the effect of castration in modulating the immune system in tumour-bearing models was not studied at the time. It would have been beneficial to assess

how castration modulates the immune system in TRAMP C2 models while also evaluating tumour growth.

Tang *et al*. 2012 indicates that the ability of androgen ablation to augment immune responses to prostate cancer antigens may vary depending on the antigen and the strength of the T-cell response generated. To understand the immune response to the prostate gland and investigate PCa immunotherapy, Drake *et al* (2005) adoptively transferred prostate-specific CD4 T-cells in transgenic mice that express model antigen influenza hemagglutinin in the absence and presence of spontaneous PCa. It was found that naive prostate-specific CD4 T-cells were mostly ignorant of the prostate gland, but in the presence of tumour, naive T-cells were able to recognize the prostate gland. Nonetheless, the recognition was tolerogenic -causing an abortive proliferation, lack of effector cytokine production, and impaired responsiveness to vaccination. They have observed that castration mitigated this tolerance—allowing prostate-specific T-cells to expand and develop effector function after vaccination. Based on these results Drake *et al* (2005) suggested that immunotherapy for PCa may be most effective when administered after androgen deprivation. In contrast, Yi Ting Koh *et al* (2009) studied the effects of castration on DC and whether it could enhance the efficacy of PCa immunotherapy and found that androgen deprivation accentuated immune responses to vaccination only when applied after immunisation that contained prostate stem cell antigen (Yi Ting Koh *et al*. 2009).

To model T-cell interactions with prostate antigens, Tang *et al* (2012) immunised male C57BL/6J mice with UV-8101-RE cells that express an H-2K^{b}–restricted immunodominant antigen either castrated or sham-treated. Their findings show that concomitant castration increased the proportion of antigen-specific CD8^{+} T-cells in the spleen and increased their function early after the immunisation, which declined by 5 weeks post-immunisation. An increased proportion of CD4^{+}CD25^{+}Foxp3^{+} Tregs in the castrated and immunized animals were also reported (Tang *et al*. 2012).

In this research, the flow cytometric analysis of castrated tumour-bearing mice was compared against the immunophenotyping of tumour-alone mice and found that effector memory T-cells, IFN-γ releasing CD4^{+}/CD8^{+} T-cells were found to be reduced with castration.

The $CD4^+CD25^+$ FoxP3 Tregs also were found to be reduced with androgen deprivation. Moreover, the elevated presence of monocytic MDSCs, over-expression of immune checkpoint LAG3 on CD4 and CD8 T-cells and increased CTLA-4^+CD8^+ T-cells observed in this study suggests that castration had an immunosuppressive effect in PCa tumour bearing mice. However, the tumour alone group had received $5x10^6$ TRAMP C2 cells while the castrated mice had received only $2x10^6$ TRAMP C2 cells. The difference in the cell numbers for tumour implantation may affect the comparison, making it difficult to draw a definite conclusion.

Interestingly, the results obtained reveal that immunisation was shown to reverse the effect of castration by enhancing the effector function of $CD4^+$ and $CD8^+$ cells in both treatment groups. Exhaustion markers such as PD1, CTLA-4, TIM-3, and LAG-3 were also found to be reduced in $CD4^+$ and $CD8^+$ T-cells with immunisation in castrated mice. Additionally, the percentage of IFN-g-releasing $CD8^+$ T-cells was higher in both treatment groups, with significantly higher when the vaccine was administered after degarelix treatment. The presence of Tregs was reduced with castration and further reduced when immunisation was given before castration which contrasts with what Tang *et al* (2012) observed in their study. However, the presence of MDSCs was higher in the mice that received immunisation after castration. These results indicate that immunisation stimulated the immune system to cancer cells, and the effect was further enhanced when immunisation was administered with androgen ablation. Immunisation administered before and after castration had positive effects, yet the increased presence of MDSC in the immunised animals should be considered to improve the vaccination's efficacy further.

Future work would focus on assessing the immunogenicity of the vaccine in mice which have been castrated either before or after the administration of the vaccine and aim to increase this response by incorporating means to suppress Treg and/or MDSC before repeating any tumour studies.

Chapter 6: IMMUNOPHENOTYPING OF PCa PATIENTS' BLOOD

6. Immunophenotyping of PCa Patients' Blood

6.1. Introduction

Although preclinical models, enable researchers to assess the therapeutic potential, efficacy, and safety of drugs before proceeding to human trials, they do not reflect the full complexity of clinical situations. In clinical settings, the nutritional, physical, and psychological status of patients are indeed critical for improving their "immunological fitness." The factors affecting general, physical, and psychological health also influence immunological functions in humans. Therefore, the development of vaccines and their translation into the clinic must consider these factors.

The PCa risk increases with increasing age and is mostly seen in men aged over 65 years old (Ng, 2021; Rawla, 2019). Ageing weakens both the innate and adaptive immune systems and is manifested, as a general decline in the diversity of the T-cell repertoire, a drop in the number of naïve T-cells and a relative increase in the prevalence of memory T-cells (McArdle *et al*. 2014). Moreover, in general people over 60 exhibit a marked decline in intestinal microflora. Gut bacteria play a crucial role in influencing various immunological functions, including generating anti-inflammatory responses.

Gut dysbiosis is triggered by gut bacterial metabolite leaks due to the disruption of the intestinal barrier leading to a leaky gut syndrome which is characterised by bacterial metabolites and endotoxins such as lipopolysaccharides (LPS) being released into the circulation. Leaked LPS in turn leads to systemic inflammation and increases the risk of cancer. In PCa, LPS activates mast cells via toll-like receptor 4 which favours angiogenesis and proliferation and evasion of PCa cells. Gut microbiota also serves as a source of testosterone which can interfere with ADT treatments and facilitate the development of CRPC (Fujita *et al*. 2023). The effect of LPS on PCa cell metastasis has been investigated by Jain *et al* (2018) in plasma that was isolated from LPS-stimulated human and rodent blood and found that LPS-induced inflammation increases PCa metastasis (Jain *et al*. 2018).

Numerous inflammatory markers in circulation have been investigated for their potential correlations with PCa risk. PCa risk is inversely correlated with IL-10, platelet-derived growth

factor subunit B homodimer, and C-X3-C motif chemokine ligand 1 (CX3CL1) and positively associated with C–C motif chemokine ligand 21 and 11 (CCL21, CCL11) (Henrik Ugge *et al*. 2019). Elevated Serum C-reactive protein CRP levels and haptoglobin were associated with increased probabilities of high-risk and metastatic PCa, with high PSA levels (≥20 ng/mL) (Arthur *et al*. 2018). PCa cells produce several inflammatory cytokines including IL-1 (Xu *et al*. 2022), IL-6, IL-8 and TNF-α (Mao, Ding, and Xu, 2021), which modify the TME to contribute to tumour cell growth, survival, invasion, and progression. Serum levels of IL-6 and TNF-α are elevated in patients with mCRPC and are recognised as a potential biomarker for PCa progression. Michalaki *et al* (2004), compared the serum levels of IL-6 and TNF-α in 80 mCRPC patients against 38 controls with small bulk localised PCa and was found that serum IL-6 and TNF-α levels were significantly elevated in mCRPC patients compared to the controls with localised PCa.

In addition to ageing, gut dysbiosis, and inflammation, chronic stress also leads to the decline of the body's immune surveillance capabilities that are associated with tumorigenesis. Chronic stress enhances tumour angiogenesis in the body and promotes the proliferation of malignant cells mainly by catecholamines mediated β2 adrenergic receptor activation of the cAMP-protein kinase A signalling pathway (Dai *et al*. 2020). The essential amino acid tryptophan (TRP) catabolism plays a part in many biologically active metabolites involved in inflammation, immune response, and neurotransmission. The dysregulation of TRP and its metabolite kynurenine is associated with various health conditions including neurodegenerative disorder and cancer. Kynurenine functions as a ligand and activator of the aryl hydrocarbon receptor leading to innate immunity suppression, and activation of Tregs, and promotes the expression of PD1 in CD8 T-cells facilitating an immune-tolerant TME (Hagiwara *et al*. 2020). The other TRP metabolite serotonin production is initiated by the enzyme TPH which exists in 2 isoforms, TPH1 – mainly expressed in the gut- and TPH2 – mainly expressed in neurons. The overexpression of TPH1 upregulates the TRP hydroxylation and mediates the production of 5-hydroxytryptamine (5-HT), a neurotransmitter involved in various activities, including vasoconstriction, gastrointestinal homeostasis, behaviour, mood, and memory. Moreover,

Chapter 6: IMMUNOPHENOTYPING OF PCa PATIENTS' BLOOD

TPH is a stimulatory factor for tumour proliferation and poor prognosis in PCa. In PCa–bearing mouse models, TPH1 was found to promote PCa by inducing TRP hydroxylation (Ge *et al*. 2022).

Moreover, immunosuppression is a major tumour invasion mechanism and MDSCs are one of the most immunosuppressive cells type present in the TME. MDSCs induce oxidative stress and deprive T-cells of essential amino acids such as arginine, tryptophan, and cysteine (Veglia *et al*. 2021). Arginine is essential for lymphocyte function and can be degraded by MDSCs induced Arginase (Li *et al*. 2022). MDSCs also promote tumour angiogenesis and epithelial-mesenchymal transition that can lead to tumour metastasis (Li *et al*. 2017). MDSC-mediated downregulation of T-cell receptor zeta (ζ) leads to T-cell dysfunction (Ezernitchi *et al*. 2006). MDSCs are generally absent in healthy homeostatic conditions and largely exist in pathological conditions with potent immunosuppressive capacity against NK cells and T-cells thereby promoting cancer initiation and progression (Jou, Chaudhury and Nasim, 2024).

Studying inflammatory, and leaky gut markers together with the presence of immunosuppressive MDSCs in the periphery of PCa patients will give insight into identifying potential therapeutic targets to overcome immunosuppression and improve treatment outcomes.

This chapter aims to characterise the immune cell subsets, immunosuppressive regulators (MDSCs), and inflammatory molecules that circulate in the peripheral blood of PCa patients compared with patients with benign prostatic disease.

Chapter 6: IMMUNOPHENOTYPING OF PCa PATIENTS' BLOOD

6.2. Results

6.2.1. Clinical demographics of patients involved in this study.

Blood samples were collected from 32 participants aged between 47 and 78 years from September 2021 to May 2023. According to the clinical details provided for the participants at the time the blood was taken, 12 subjects had benign, 3 subjects had low, 9 had intermediate and 8 participants had high-grade PCa. PBMCs were isolated from the whole blood by Ficoll- Paque (density 1.077g/mL) density gradient centrifugation. The clinical demographics included serum PSA, prostate volume, Prostate-specific antigen density (PSAD), Gleason grade, pathology stage of the tumour, and D'Amico classification (Table 6.1).

Chapter 6: IMMUNOPHENOTYPING OF PCa PATIENTS' BLOOD

Study No.	Patient's Age	Prostate volume (cc)	PSA (ng/mL)	PSAD (ng/mL/cc)	Grading	Gleason Score	Pathology Stage	D'Amico Classification
LE342	78	58	7.2	0.12	Negative	N/A		
LE344	76	75	9.4	0.13	Negative	N/A		
LE345	67	55	5.3	0.10	Negative	N/A		
LE346	68	80	15	0.19	Negative	N/A		
LE351	53	40.74	4.6	0.11	Negative	N/A		
LE353	74	42	2.7	0.06	Negative	N/A		
LE355	47	85	3.8	0.04	Negative	N/A		
LE356	52	32.51	11	0.34	Negative	N/A		
LE357	73	128.47	10.6	0.08	Negative	N/A		
LE365	63	21	117	0.18	Negative	N/A		
LE372	74	7.8	35	0.22	Negative	N/A		
LE376	55	4.2	32	0.13	Negative	N/A		
LE362	65	76.07	6.4	0.08	3+3=6	6	T2	Low
LE368	73	20	44	0.45	3+3=6	6	T2	Low
LE374	76	4.5	38	0.12	3+3=6	6	T2	Low
LE343	69	48	7.7	0.16	3+4=7	7	T1c	Intermediate
LE352	67	15	0.49	0.03	3+4=7	7	T2	Intermediate
LE358	64	33.26	11	0.33	3+4=7	7	T2	Intermediate
LE360	63	98.75	5.2	0.05	3+4=7	7	T2	Intermediate
LE361	65	33.81	5.7	0.17	3+4=7	7	T2	Intermediate
LE363	72	197	12	0.06	3+4=7	7	T2	Intermediate
LE366	77	10	35	0.29	3+4=7	7	T2	Intermediate
LE370	69	6.2	31	0.2	3+4=7	7	T2	Intermediate
LE375	68	6.4	43	0.15	3+4=7	7	T2	Intermediate
LE354	55	46	7.2	0.16	4+5=9	9	T2	HIGH
LE359	73	38.56	4.6	0.12	4+5=9	9	T3a	HIGH
LE364	55	3.8	44	0.09	4+3=7	7	T2	HIGH
LE367	77	14	37	0.38	4+3=7	7	T2	HIGH
LE369	77	6.2	10	0.62	5+4=9	9	T2	HIGH
LE371	75	11	76	0.14	4+3=7	7	T2	HIGH
LE373	76	6.2	28	0.22	4+5=9	9	T2	HIGH
LE377	61	8.6	33	0.26	4+5=9	9	T2	HIGH

Table: 6.1*. Clinical information of benign vs PCa patients' samples obtained for this study. Abbreviation: PSA- prostate-specific antigen. PSAD- PSA density.*

Chapter 6: IMMUNOPHENOTYPING OF PCa PATIENTS' BLOOD

Serum PSA levels, measured in ng/mL, can vary among individuals, and tend to increase slightly with age. In men aged 70-79, a PSA level of 2.5 to 6.5 ng/mL is generally considered normal (Bratt *et al*. 2023). The PSA levels in benign cases ranged from 2.7 to 35 ng/mL, with one exceptional case measuring 117 ng/mL, where the patient was 63 years old and had a prostate volume of 21cc. Among the cancer patients, PSA levels varied from 5.2 to 76 ng/mL, with one markedly elevated case of 183 ng/mL observed in a patient with high-risk prostate cancer, characterized by a Gleason grade of 5+4=9. Notably, a deficient PSA level of 0.49 ng/mL was observed in an intermediate-risk patient aged 69 years, who had a prostate volume of 15 cc.

Although PSA levels often rise with age and can be influenced by prostate inflammation, in this study, the clinical demographics of the patient analysis in this study revealed no clear correlation (Figure 6.1(A)) between PSA levels and age. Interestingly, a significant negative correlation was observed between PSA levels and prostate volume (PSA vs prostate volume * P= 0.0187), suggesting that elevated serum PSA levels are more closely associated with benign and cancerous conditions rather than with age or prostate size. The comparison of PSA levels between benign and PCa revealed that PSA levels were higher in the PCa group, though the difference was not statistically significant (Figure 6.1 (B)).

Chapter 6: IMMUNOPHENOTYPING OF PCa PATIENTS' BLOOD

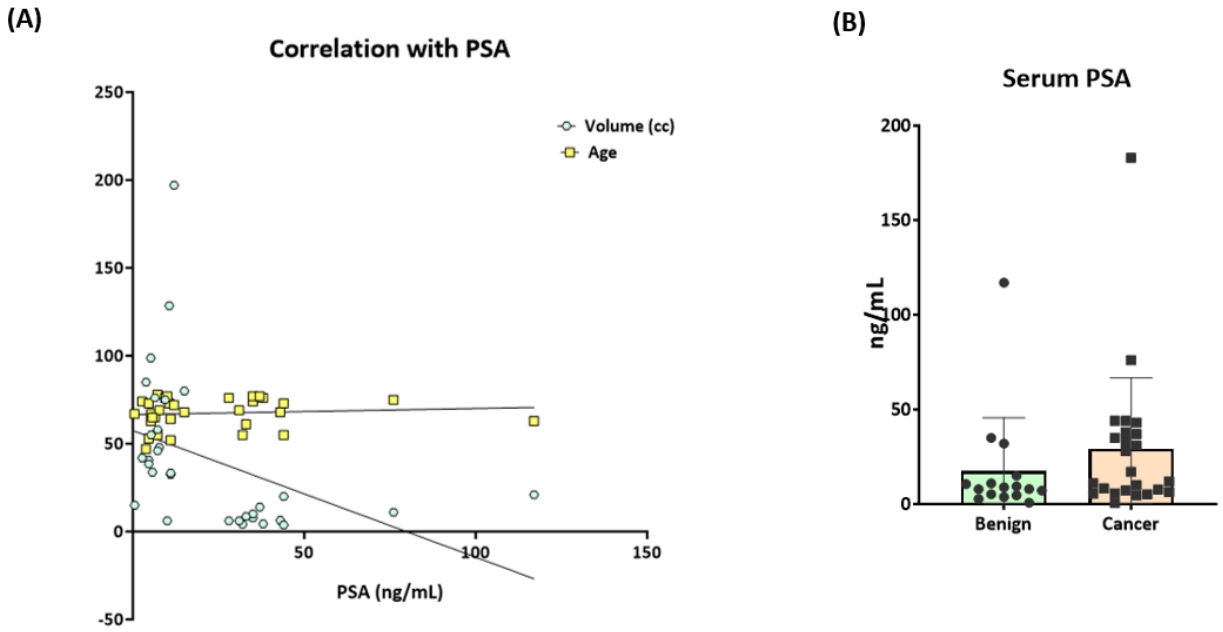

Figure 6.1. (A) Correlation of PSA with prostate volume and age*. Linear regression analysis of given patient data reveals no correlation between age and PSA and a negative correlation between PSA and prostate volume *p=0.0187.* ***(B) Comparative study of PSA level Benign vs PCa****. The PSA levels were comparatively higher in PCa patients than in the subjects who had benign prostatic hyperplasia.*

PSA density (PSAD) is a clinical metric calculated by dividing the serum PSA level (ng/mL) by the prostate volume (cc) and is used as a diagnostic tool to differentiate between benign prostatic hyperplasia (BPH) and PCa, as well as to assess the aggressiveness of malignancy. A higher PSAD indicates a greater likelihood of cancer. Men having a PSAD of less than 0.09 ng/mL^2 indicate a 4% chance of clinically significant disease. PSAD values between 0.09–0.19 are considered a grey zone when combined with a prostate volume below 33 mL (Yusim *et al*. 2020). Clinical data provided in this study revealed that most BPH patients had PSAD values between 0.09 and 0.19, with one patient showing a PSAD of 0.22 and a PSA level of 35 ng/mL, indicating an elevated risk of developing PCa. Among the prostate cancer patients, PSAD values ranged from 0.3 to 0.62, with seven patients having PSAD levels above 0.2. Among the PCa subjects, the cancers were graded using the Gleason score, which was calculated by adding together the most two common grades of cancer cells which refers to how abnormal / differentiated the cancer cells look compared to the normal cells under the

microscope (Murray, 2021). A lower grade means the cancer is less aggressive. As the clinical data (Table 6.1) provided implicated, a score more than or equal to 6 is considered cancer. The pathology stage indicates the extent of the primary tumour, which is usually described as T-stage (T 1-4, T4 being the most advanced) (Frederik, 2015). The data shows that most had developed to a T2 stage, meaning the cancer was still confined to the prostate. None of the patients tested were T4 where the cancer had spread into the nearby organs such as the bladder or lymph nodes. The cancers were classified according to the D'Amico classification (Frederik, 2015) which is based on the tumour size, Gleason grade, and PSA level as 'low-risk', 'intermediate-risk', and 'high-risk' PCa.

In addition to analysing the clinical demographics of the patients, this study evaluated the presence of immune cells, MDSC, as well as biomarkers related to inflammation and leaky gut in the periphery of PCa patients and compared the findings against the BPH cohorts. PCa patients were initially categorized into low, intermediate, and high-risk groups according to the D'Amico classification. The data were initially analysed across different cancer subgroups - but no significant differences between the concentrations of the different molecules were observed (data not shown). Moreover, due to the small sample size within each group -particularly the 'low risk' group that included only 3 patients – these patients were combined with benign for analysis to ensure more representative results. The results obtained are explained in the next section.

6.2.2. Whole blood immunophenotyping

Whole blood immunophenotyping was used to determine the proportion of NK, T, and B-cell present in the periphery of the patients and assess whether these could distinguish between benign and PCa disease.

Flow cytometry panel and gating strategy were applied as was described in a previous study from our lab (Cosma *et al*. 2021). This study had been conducted to predict the presence of PCa and the clinical risk of PCa in asymptomatic men with PSA levels elevated above the normal, without the need for invasive biopsies, by utilising machine learning models.

Chapter 6: IMMUNOPHENOTYPING OF PCa PATIENTS' BLOOD

100µL of whole blood and appropriate antibodies (Table 2.11) were added to Trucount tubes, and the lyophilized pellet inside the tube dissolves, releasing a known number of fluorescent beads. Absolute cell count was then calculated by gating the bead population and comparison with cellular events to bead events and was then analysed using GraphPad prism. The gating strategy used is illustrated in the Figure 6.2. The panel confirmed the CD45 expression and identified the population including lymphocytes, monocytes, and granulocytes. $CD3^{+}$ T-cells were further gated and expression of CD4 and CD8 T-cells were identified, while $CD3^{neg}$ $CD19^{+}$ B cells were also identified. CD45RA, CD27, and CD28 were used to identify effector memory ($CD45RA^{neg}$ $CD27^{neg}$ $CD28^{neg}$) cells, central memory ($CD45RA^{neg}CD27^{+}CD28^{+}$) cells, naïve ($CD45RA^{+}CD27^{+}CD28^{+}$) cells, and TEMRA ($CD45RA^{+}CD27^{neg}CD28^{neg}$) for both CD4 and CD8 populations. To identify NK cells, cells were gated from $CD45^{+}$ and further gated to $CD56^{+}$, which is an NK cell marker. To further identify NK cell subsets that co-express T-cell receptor and NK-cell markers, $CD56^{+}$ cells were gated for $CD4^{+}$ NKT cells ($CD3^{+}CD56^{+}CD4^{+}$) and $CD8^{+}$ NKT cells ($CD3^{+}CD56^{+}CD8^{+}$).

Chapter 6: IMMUNOPHENOTYPING OF PCa PATIENTS' BLOOD

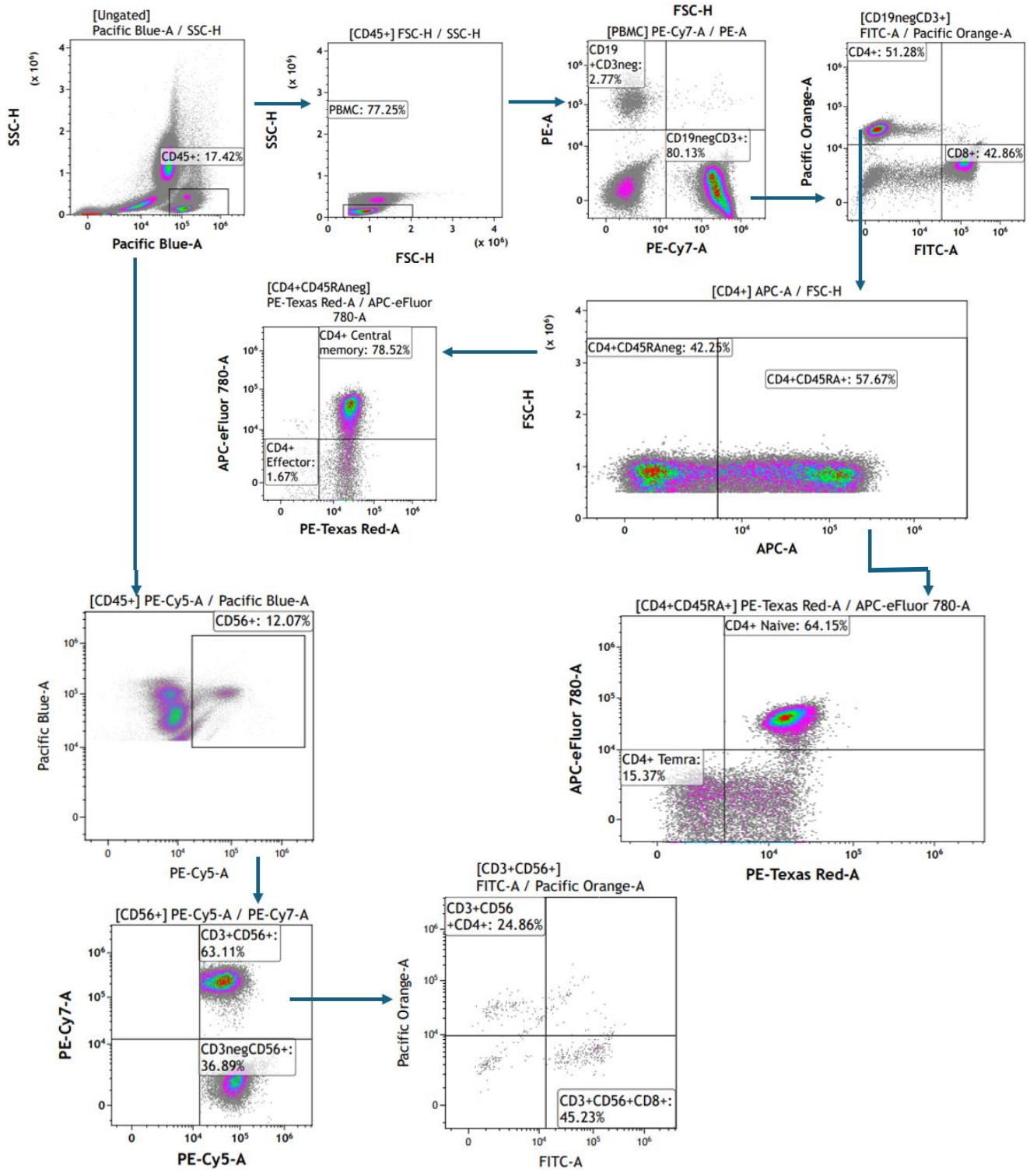

Figure 6.2. The gating strategy of whole blood immunophenotyping. *The Figure shown here describes the dating strategy used to identify B cells, CD8 population of NKT cells, and CD8⁺ T-cells subsets: naïve, effector memory, central memory and TERMA cells. Similarly, CD4+ NKT cells and CD4⁺ T-cell subsets were also*

identified from CD4⁺ cells using the same gating strategy. Fluorochrome APC eFluor 780 is for CD27 and PE-texas Red is for CD28 staining shown in the gating strategy.

Cosma *et al.* 2021 built a bidirectional Long Short-Term Memory Deep Neural Network (biLSTM) model for detecting the presence of PCa in men having PSA levels < 20 ng/mL. Five phenotypic features $CD8^{+}CD45RA^{neg}$ ($CD8^{+}$ Effector Memory cells), $CD4^{+}CD45RA^{neg}$ ($CD4^{+}$ Effector Memory cells), $CD4^{+}CD45RA^{+}$ ($CD4^{+}$ Terminally Differentiated Effector Memory Cells re-expressing CD45RA), $CD3^{-}CD19^{+}$ (B cells), $CD8^{+}/CD4^{+}$ $CD3^{+}CD56^{+}$ (NKT cells) which when taken together with age could differentiate between prostate cancer and benign cancer in men with PSA < 20 ng/mL. An identical analysis could not be performed with these data as the person with the computational skills had, by then, left the University and was not able to analyse these data.

Nonetheless, the analysis performed here revealed a significantly higher proportion of $CD4^{+}$ effector memory T cells in prostate cancer (PCa) patient samples compared to benign controls. Additionally, $CD19^{+}$ B cells, and $CD8^{+}$ NK T cells were more prevalent in the PCa samples, though these differences did not reach statistical significance. On the other hand, the NK cell subset co-expressing $CD4^{+}$ T-cell receptors, and $CD8^{+}$ effector cells, showed no differences between the PCa and benign groups. Terminal effector memory T-cells (TEMRA cells) are associated with immune senescence and are characterised by a decrease in proliferation potential but exhibit strong cytotoxicity and proinflammatory activity (Guo, Liu, and Su, 2023). $CD4^{+}$ TEMRA cells were also elevated in the PCa group, this increase was not statistically significant when compared to the benign group.

Chapter 6: IMMUNOPHENOTYPING OF PCa PATIENTS' BLOOD

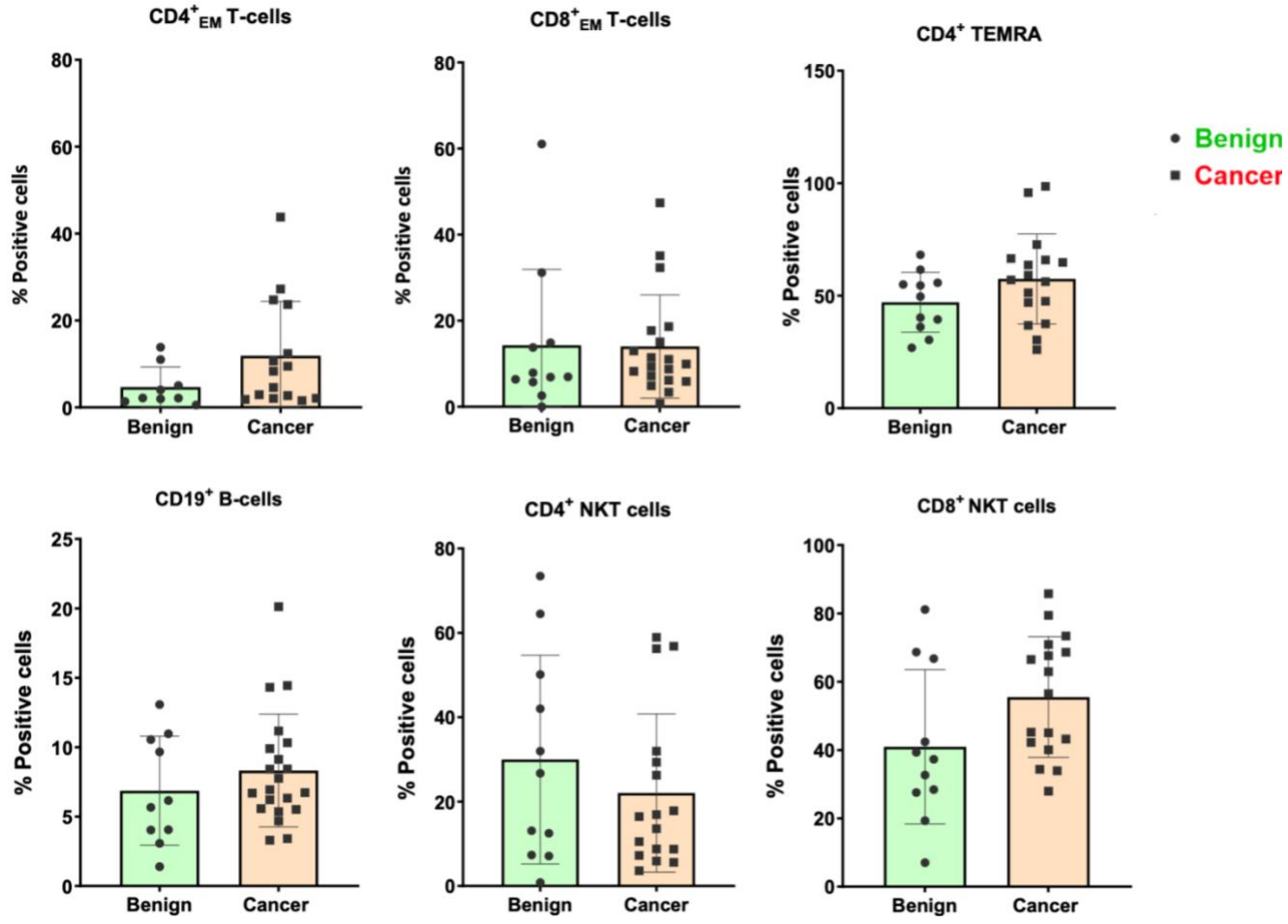

Figure 6.3. NKT, T effector, CD4⁺ TEMRA and B-cell phenotypic features present in the periphery of the patients; benign vs cancer. *The results obtained revealed a higher presence of CD4⁺ effector memory (*p= 0.0424), CD19⁺ B-cells, and CD8⁺ NKT cells in PCa samples. The statistical significance was calculated using an unpaired t-test.*

Since biLSTM model was built to detect the presence of PCa in men having PSA levels < 20 ng/mL (Cosma *et al*. 2021), the benign (n=5) and PCa (n=7) samples with PSA < 20 ng/mL were compared. The results obtained are shown in Figure 6.4. An increased expression of CD8⁺ effector memory cells, CD4⁺ TEMRA, CD19⁺ B-cells, and CD8⁺NKT cells was observed with a decreased expression of CD4⁺ NKT cells.

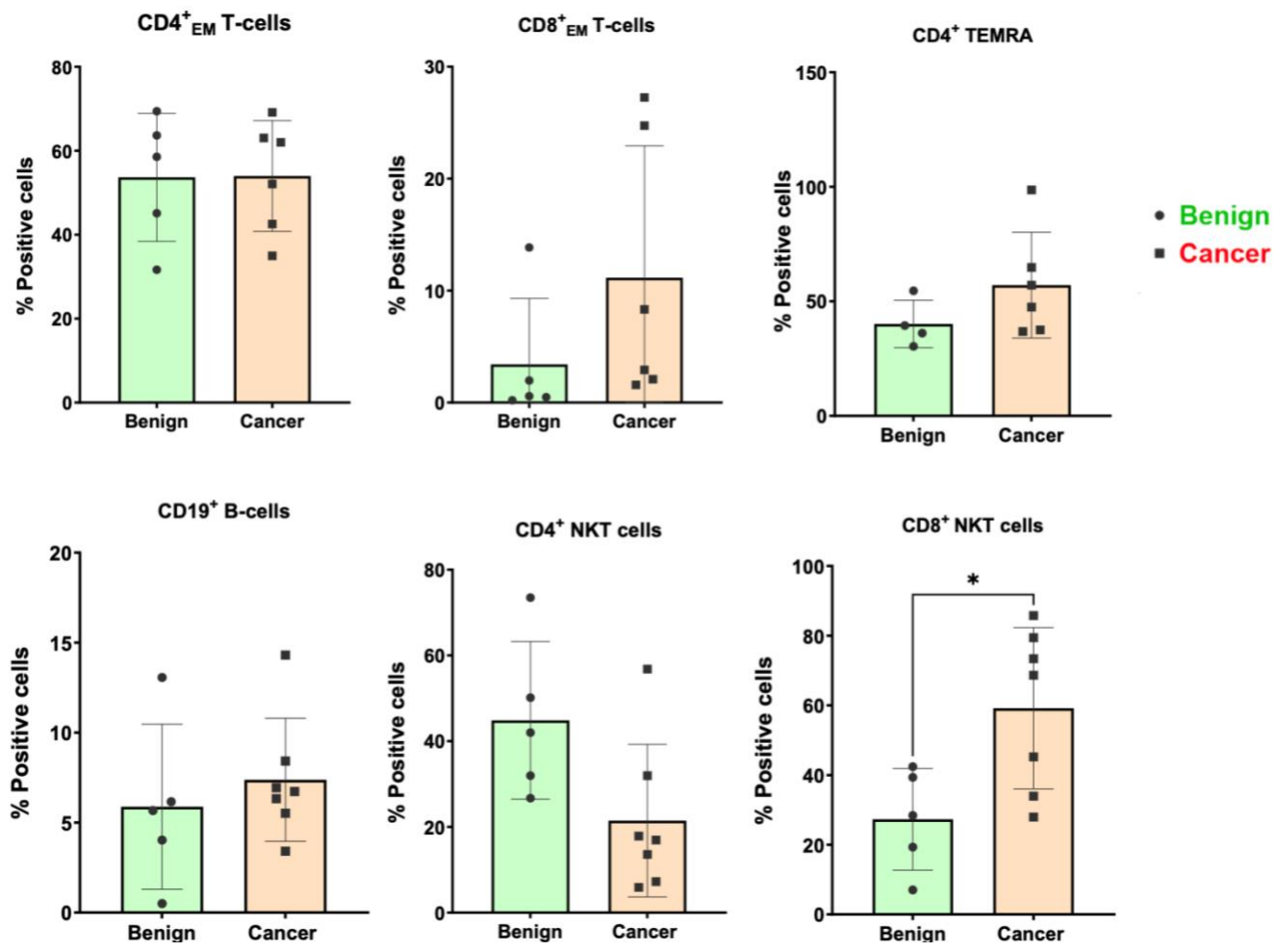

***Figure 6.4**. NKT, T effector, CD4⁺ TEMRA and B cell phenotypic features of Benign vs PCa patients with PSA < 20 ng/mL. The statistical significance was determined using an unpaired t-test.*

6.2.3. Identification of distinct populations of MDSCs in benign vs PCa patients

A million PBMCs were stained using the panel as described in Table 2.10 to identify the presence of monocytes, M-MDSCs, and G-MDSCs population in the periphery of patients with intermediate/high-risk PCa and benign prostatic disease. Percentage positive cells were determined using Kaluza software and analysed using GraphPad Prism. Figure 6.5 shows the representative flow cytometry gating strategy used for one of the patients in the study; all other samples were gated similarly.

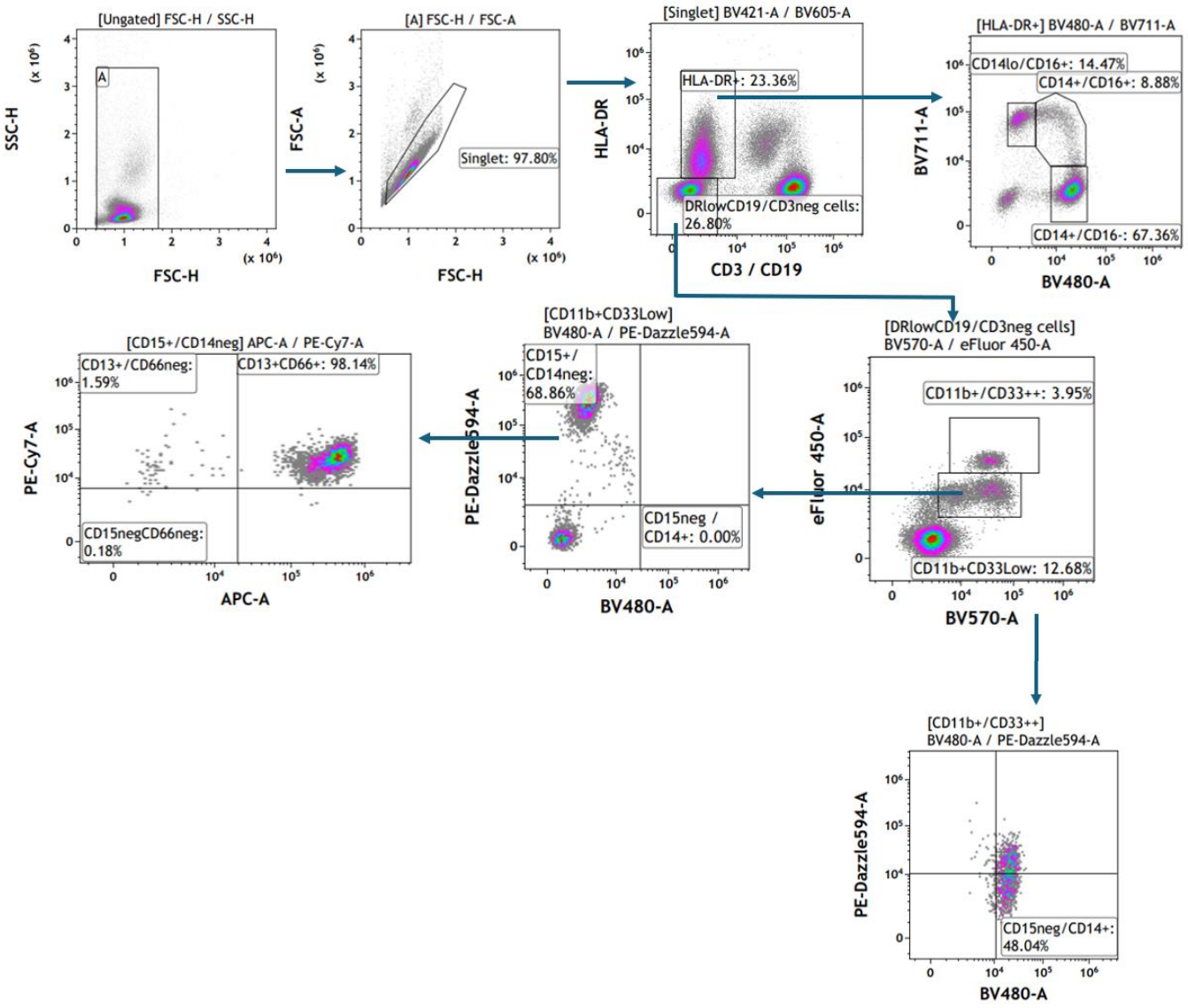

Figure 6.5. An illustration of the gating strategy (patient sample LE356) used for immunophenotyping of monocytes and MDSCs*. Debris and doublets were removed from FSC-H and FSC-A density plots. Singlets were selected based on HLA-DR and CD3/CD19 markers to exclude T-cell/B-cell negative populations, identifying HLA-DR^{+} and HLA-DR^{low} groups. HLA-DR^{+} cells were further sorted by CD14 and CD16 to categorise monocyte subsets (CD14^{+}/CD16^{neg}, CD14^{+}/CD16^{+}, CD14^{neg}/CD16^{+}). HLA-DR^{low} cells were sorted to identify CD11b^{+} CD33^{++}/CD33^{low} cells. CD11b^{+}CD33^{++} cells were analysed for CD15^{neg} CD14^{+} M-MDSCs, and CD11b^{+}CD33^{low} cells were analysed for CD15^{+}CD14^{neg} and then CD13^{+}CD66^{+} G-MDSCs.*

Chapter 6: IMMUNOPHENOTYPING OF PCa PATIENTS' BLOOD

Debris and doublets were excluded on FSC-H and FSC-A density plots. CD3/CD19 dump channel was used to select out the T-cell/B-cell negative population. The singlets were gated on HLA-DR^{+} and CD3/CD19^{neg} and identified HLA-DR^{+} and HLA-DR^{low} populations. HLADR^{+} cells were further gated on CD14 and CD16 to identify the monocyte subsets (CD14^{+}/CD16^{neg}, CD14^{+}/CD16^{+} and CD14^{neg}/CD16^{+}).

The results (Figure 6.6) obtained showed that the percentage of HLA-DR^{+} cells between benign and malignant conditions was similar which is roughly 20%. Among the three subsets of HLA-DR^{+} cells, less than 10 % of cells were found to be CD16^{+} and CD14^{+}. Interestingly 2 clear sub-populations were visible within each of the patients group. 3 benign patients had the same level of intermediate monocytes as the cancer group (A) while 5 of the cancer group had low level of intermediate monocytes like the benign group (B) which resemble the majority of benign. Intermediate monocytes have been shown to produce abundant level of proinflammatory cytokines. It would have been of interest to follow these patients to find how they progress. About 15% were CD14^{low} and CD16^{+}; and the majority (nearly 80%) of cells were CD14^{+} and CD16^{neg}. No significant differences in any subset of monocytes were found between the two groups.

Chapter 6: IMMUNOPHENOTYPING OF PCa PATIENTS' BLOOD

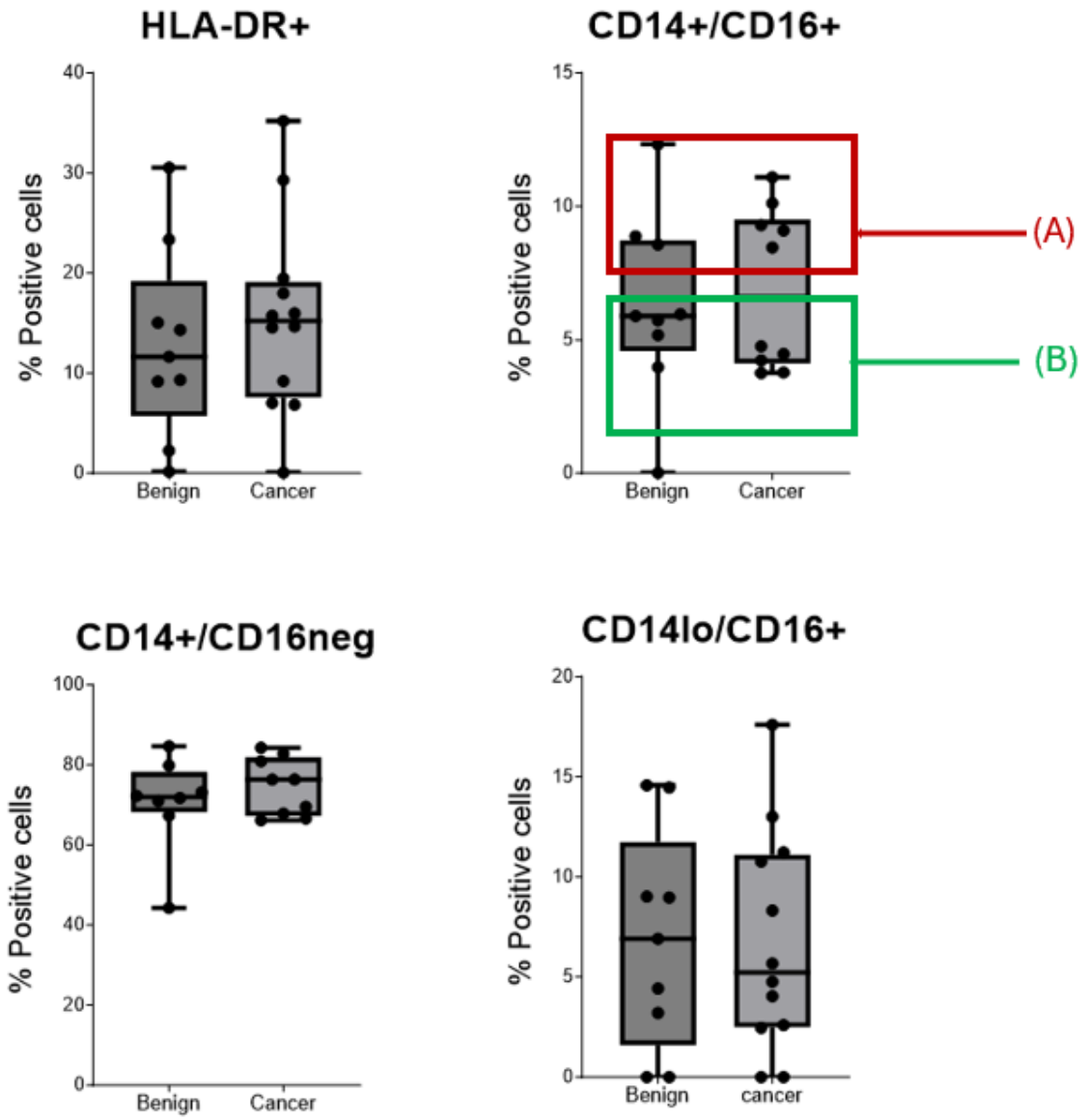

Figure 6.6. Percentage of monocytes identified in the PBMCs isolated from patient blood samples. *Monocytes were recognised as HLA-DR⁺, and three different subtypes of HLA-DR⁺ monocytes were gated on CD14 and CD16. Benign n=9 and Cancer n=12.*

MDSCs were gated on HLA-DR ^{low} CD19^{neg}/CD3^{neg} cell populations. Among the two subtypes, M-MDSCs displayed a phenotype of CD11b^{+}CD33^{++}, whereas G-MDSCs were CD11b^{+}CD33^{low}, hence CD15^{+}CD14^{neg} cells were identified from CD11b^{+}CD33^{low} and CD15^{neg}CD14^{+} cells were gated from CD11b^{+}CD33^{++}. CD66 is a marker that is expressed only

by G-MDSCs. $CD15^{+}$ $CD14^{neg}$ cells were further gated to identify the expression of CD13 and CD66.

To identify the monocytic MDSC population, $CD15^{neg}/CD14^{+}$ cells were gated from $CD11b^{+}CD33^{++}$ cells. Percentage positive cells were determined using Kaluza software and analysed using GraphPad Prism.

The results obtained by the flow cytometric analysis identified the presence of a higher population of (M-MDSC) $CD11b^{+}CD33^{++}$ cells in cancer group compared to the benign group. The $CD15^{neg}CD14^{+}$ population gated from $CD11b^{+}CD33^{++}$ also were found to be significantly higher in the cancer group compared to the benign group. Like the results obtained for M-MDSC, flow cytometric analysis identified a lower percentage of CD11+CD33 ^{low} phenotype G-MDSCs population in benign compared to the cancer group, though there was no significant difference. $CD15^{+}$ $CD14^{neg}$ phenotypes further gated from $CD11^{+}CD33^{low}$ cells were also found to be lower in the benign group. The special marker for G-MDSCs like Arg-1 and CD13/CD66 further confirmed the presence of higher G-MDSCs (Arg+/ $CD13^{+}CD66^{+}/CD63^{+}PD\text{-}L1^{neg}$) in cancer compared to benign with a significant difference shown in the CD13/CD66 gated populations. However, there wasn't any difference in the expression of CD63 and PD-L1 was noticed between the groups. No significant difference between the groups observed may be due to the lesser number of subjects involved in the study.

Chapter 6: IMMUNOPHENOTYPING OF PCa PATIENTS' BLOOD

(A)

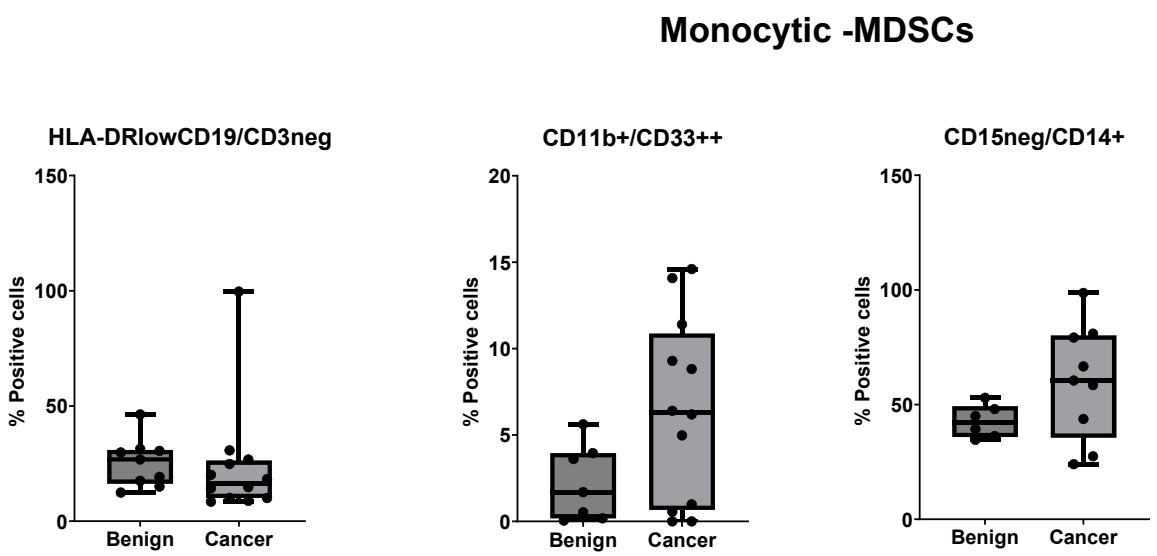

(B)

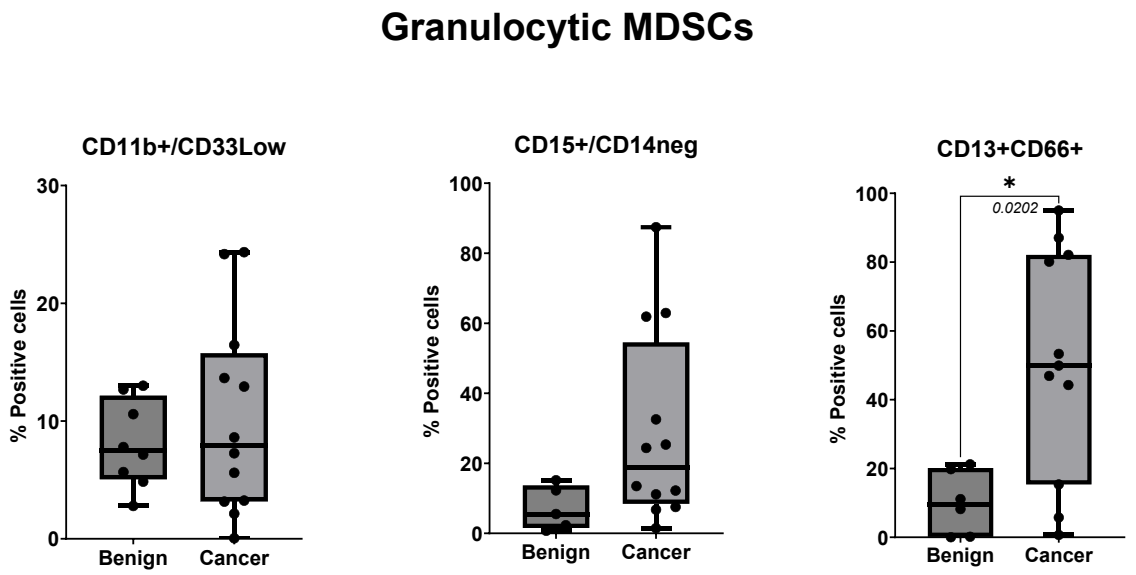

Figure 6.7. Comparison of phenotypic features of MDSCs. *MDSCs were identified as HLA-DR low/CD19 neg/CD3neg cells. (A) M-MDSCs and (B) G-MDSCs were further differentiated from HLA DR^{low} (CD19/CD3 ^{neg}) cell population by gating as CD11b^{+}CD33^{++} CD15negCD14^{+} and CD11b^{+}CD33^{low}, CD15^{+}CD14^{neg}, CD13^{+} CD66^{+}/ CD16^{+} CD10^{+}/ Arg^{+}/CD63^{+}PD-L1^{+} respectively. Mann-Whitney test was used for analysis and P-value was calculated as * p < 0.05, ** p < 0.01, *** p< 0.001, *** p< 0.0001 and not significant p <0.05. Both sub-types of MDSCs were found to be expressed higher in the cancer group compared to the benign group. Benign (n=9) and Cancer (n=12).*

Chapter 6: IMMUNOPHENOTYPING OF PCa PATIENTS' BLOOD

6.2.4. Identification of biomarkers related to inflammation, and leaky gut in benign vs PCa patients.

Plasma was isolated by centrifuging 2mL whole blood at 14000 rpm, for 30 minutes at 4°C and ELISA tests were performed. The following molecules were tested: hemolysis marker haptoglobin (Vanuytsel, Vermeire, and Cleynen, 2013), IL-6, TNF-a, CRP, IL-1b (markers of inflammation), iFABP (or FABP2), LPS (markers of leaky gut) and TPH1 (marker of immunological stress) (Xu *et al*. 2022; Mao, Ding, and Xu, 2021; Fujita *et al*. 2023). Haptoglobin (Hp) is a glycoprotein that binds to free haemoglobin in the blood; free haemoglobin is highly toxic because of the oxidative nature of heme. Hp functions as an antioxidant by binding to free haemoglobin thereby preventing tissue oxidative damage (Vanuytsel, Vermeire and Cleynen, 2013).

The inflammation markers such as CRP was found to be elevated in PCa samples compared to benign, though the differences were not statistically significant but other markers, IL-1b, markers associated with leaky gut (LPS and FABP2), TPH1 and the haemolysis marker haptoglobin showed no difference between benign and PCa samples.

Chapter 6: IMMUNOPHENOTYPING OF PCa PATIENTS' BLOOD

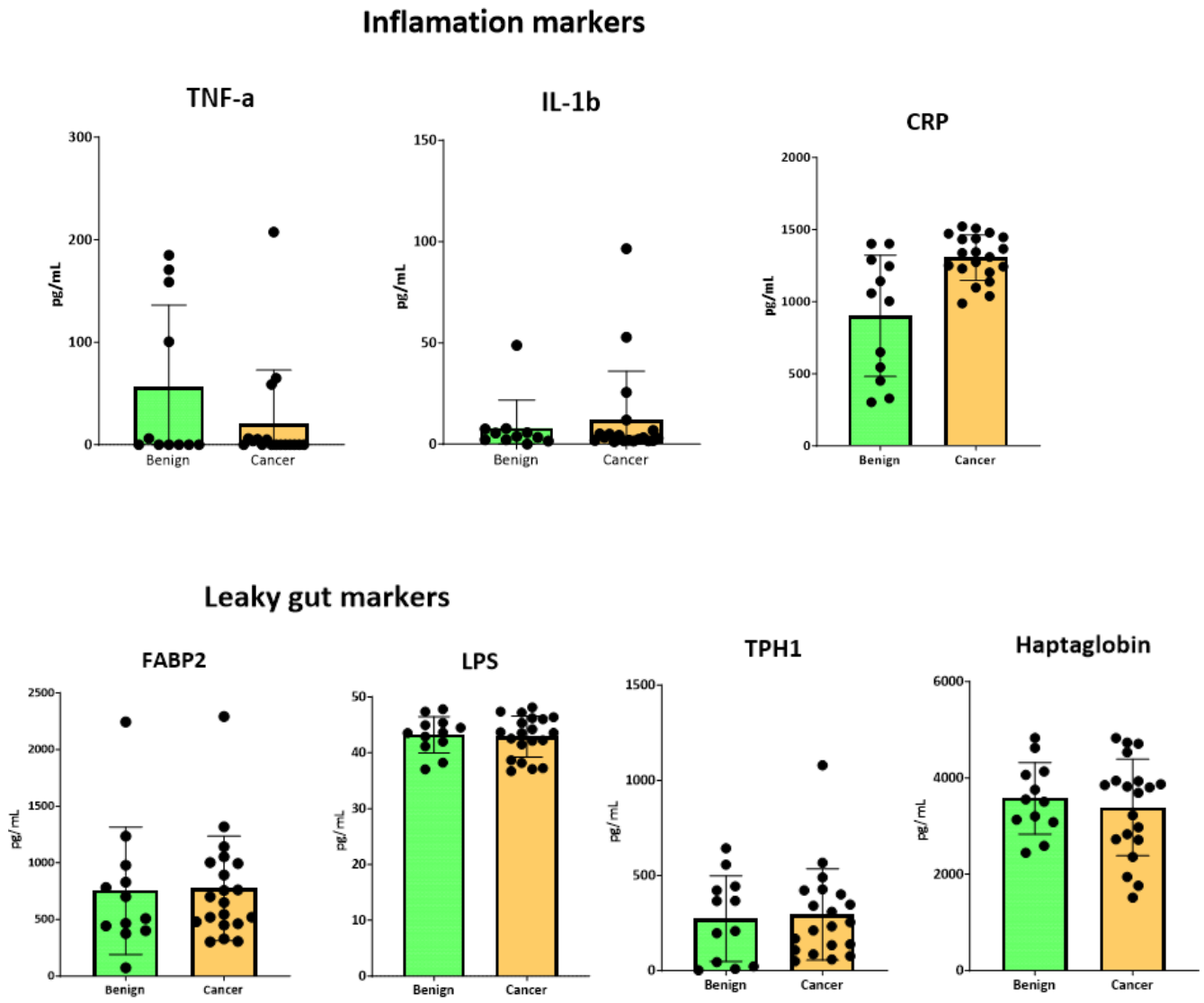

Figure 6.8. Evaluation of inflammation, stress, and leaky gut biomarkers benign vs PCa patients. *Analysis reveals an increase -but not significant- in the circulating inflammatory markers CRP, however there was no difference in the presence of other markers were found between benign and PCa group.*

These biomarkers were further evaluated to determine whether they demonstrated any co-relation with the patients age, Gleason grade, and circulating total PSA levels (Figure 6.9). The linear regression plots reveal that while some biomarkers like haptoglobin and TPH1 show a modest increase with age these did not reach statistics significant). An insignificant positive correlation was noticed between Gleason grade and TPH1, while haptoglobin levels

were shown to marginally decrease as Gleason grade increased. Most of the biomarkers, including CRP, IL-1b, IL-6, TNF-α, LPS, and FABP2, did not shown any correlations with age and Gleason grade. The PSA level correlation analysis showed a negative correlation between haptoglobin and FABP2 with blood PSA levels. Other biomarkers, CRP, TPH1, IL-1b, IL-6, TNF-α, and LPS, were observed to have no correlations with PSA levels.

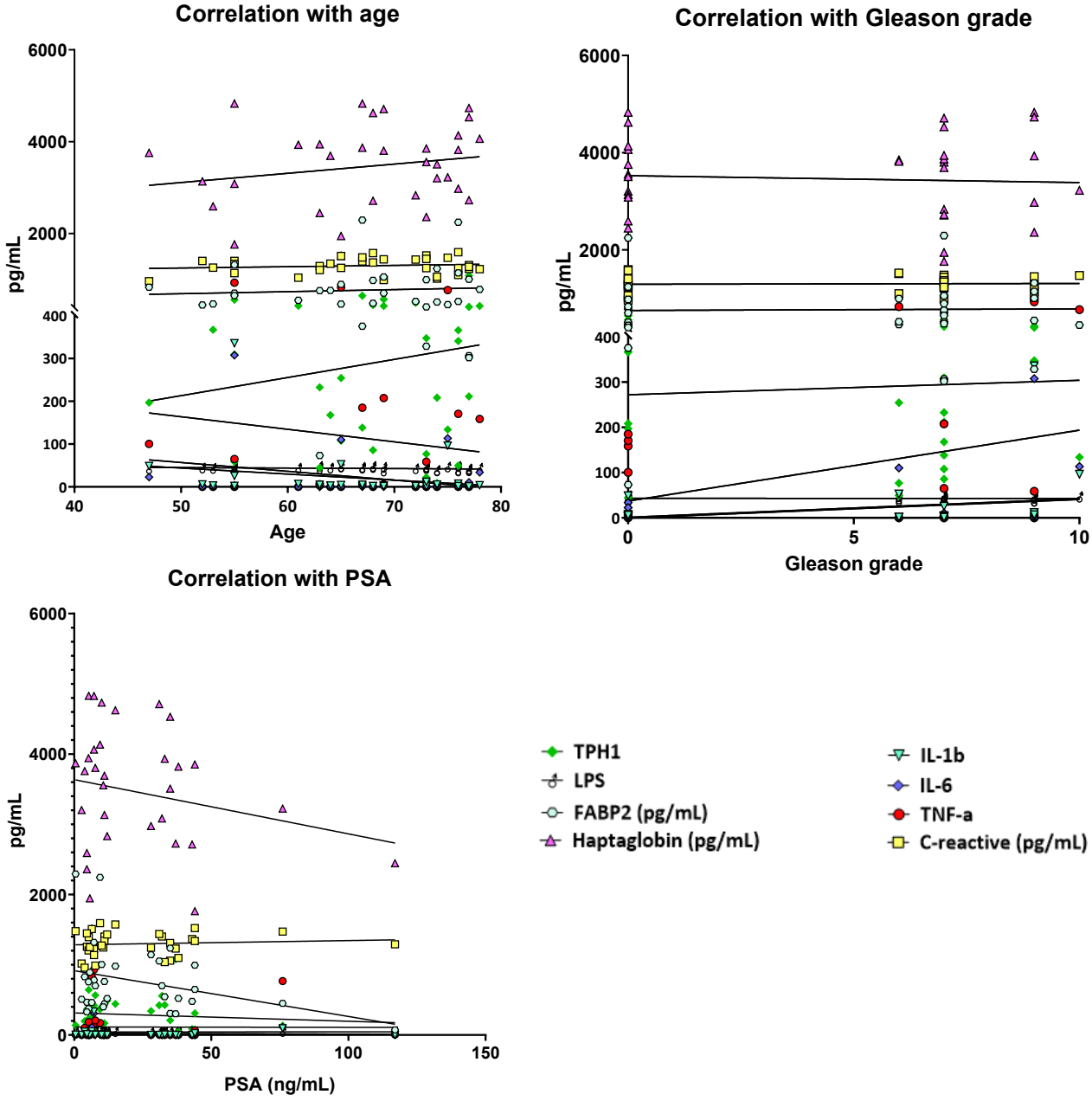

Figure 6.9. Expression of biomarkers in correlation with age, Gleason grade and PSA. *Linear regression plots analysis reveals a positive correlation between Gleason grade and TPH1, and a negative correlation between haptoglobin and FABP2 with PSA levels, however, none of the analysis were statistically significant.*

Chapter 6: IMMUNOPHENOTYPING OF PCa PATIENTS' BLOOD

Using Spearman's rho, the correlation between each biomarker was further performed, revealing several positive correlations among the expression of biomarkers in the periphery (Figure 6.10). The significance values for these correlations are detailed in Table 6.2. Specifically, the leaky gut marker LPS showed a positive correlation with inflammatory markers IL-1b, TNF- α, and CRP. Additionally, a positive correlation was observed between IL-1b and TNF- α. The haemolysis marker haptoglobin was also positively associated with both CRP (inflammation) and FABP2 (leaky gut). These findings suggest a link between leaky gut, inflammation, and haemolysis.

			CRP	FABP2	Hap	IL_1	IL_6	LPS	TNF	Age	PSA	Vol
Spearman's rho	CRP	Correlation Coefficient	1.000	0.010	-0.043	0.051	0.200	.376*	0.156	0.023	0.143	0.007
		Sig. (2-tailed)		0.957	0.817	0.783	0.273	0.034	0.394	0.901	0.435	0.970
		N	32	32	32	32	32	32	32	32	32	32
	FABP2	Correlation Coefficient	0.010	1.000	.424*	0.101	0.002	-0.254	0.114	0.017	-0.184	-0.083
		Sig. (2-tailed)	0.957		0.016	0.584	0.991	0.161	0.536	0.924	0.314	0.653
		N	32	32	32	32	32	32	32	32	32	32
	Hap	Correlation Coefficient	-0.043	.424*	1.000	-0.127	0.018	-0.309	0.324	0.222	-0.129	0.109
		Sig. (2-tailed)	0.817	0.016		0.488	0.922	0.085	0.070	0.222	0.481	0.553
		N	32	32	32	32	32	32	32	32	32	32
	IL_1	Correlation Coefficient	0.051	0.101	-0.127	1.000	0.197	.545**	.568**	-.376*	-0.157	0.295
		Sig. (2-tailed)	0.783	0.584	0.488		0.280	0.001	0.001	0.034	0.390	0.101
		N	32	32	32	32	32	32	32	32	32	32
	IL_6	Correlation Coefficient	0.200	0.002	0.018	0.197	1.000	0.133	0.043	-0.140	0.209	-0.084
		Sig. (2-tailed)	0.273	0.991	0.922	0.280		0.469	0.816	0.444	0.251	0.647
		N	32	32	32	32	32	32	32	32	32	32
	LPS	Correlation Coefficient	.376*	-0.254	-0.309	.545**	0.133	1.000	.477**	-0.309	0.036	0.270
		Sig. (2-tailed)	0.034	0.161	0.085	0.001	0.469		0.006	0.085	0.846	0.134
		N	32	32	32	32	32	32	32	32	32	32
	TNF	Correlation Coefficient	0.156	0.114	0.324	.568**	0.043	.477**	1.000	-0.052	-0.123	0.282
		Sig. (2-tailed)	0.394	0.536	0.070	0.001	0.816	0.006		0.779	0.501	0.118
		N	32	32	32	32	32	32	32	32	32	32
	Age	Correlation Coefficient	0.023	0.017	0.222	-.376*	-0.140	-0.309	-0.052	1.000	0.208	-0.134
		Sig. (2-tailed)	0.901	0.924	0.222	0.034	0.444	0.085	0.779		0.254	0.465
		N	32	32	32	32	32	32	32	32	32	32
	PSA	Correlation Coefficient	0.143	-0.184	-0.129	-0.157	0.209	0.036	-0.123	0.208	1.000	-.592**
		Sig. (2-tailed)	0.435	0.314	0.481	0.390	0.251	0.846	0.501	0.254		0.000
		N	32	32	32	32	32	32	32	32	32	32
	Vol	Correlation Coefficient	0.007	-0.083	0.109	0.295	-0.084	0.270	0.282	-0.134	-.592**	1.000
		Sig. (2-tailed)	0.970	0.653	0.553	0.101	0.647	0.134	0.118	0.465	0.000	
		N	32	32	32	32	32	32	32	32	32	32

Table 6.2. Spearman's rho, the correlation analysis between each biomarker tested. *The significant positive association between the biomarkers is highlighted.*

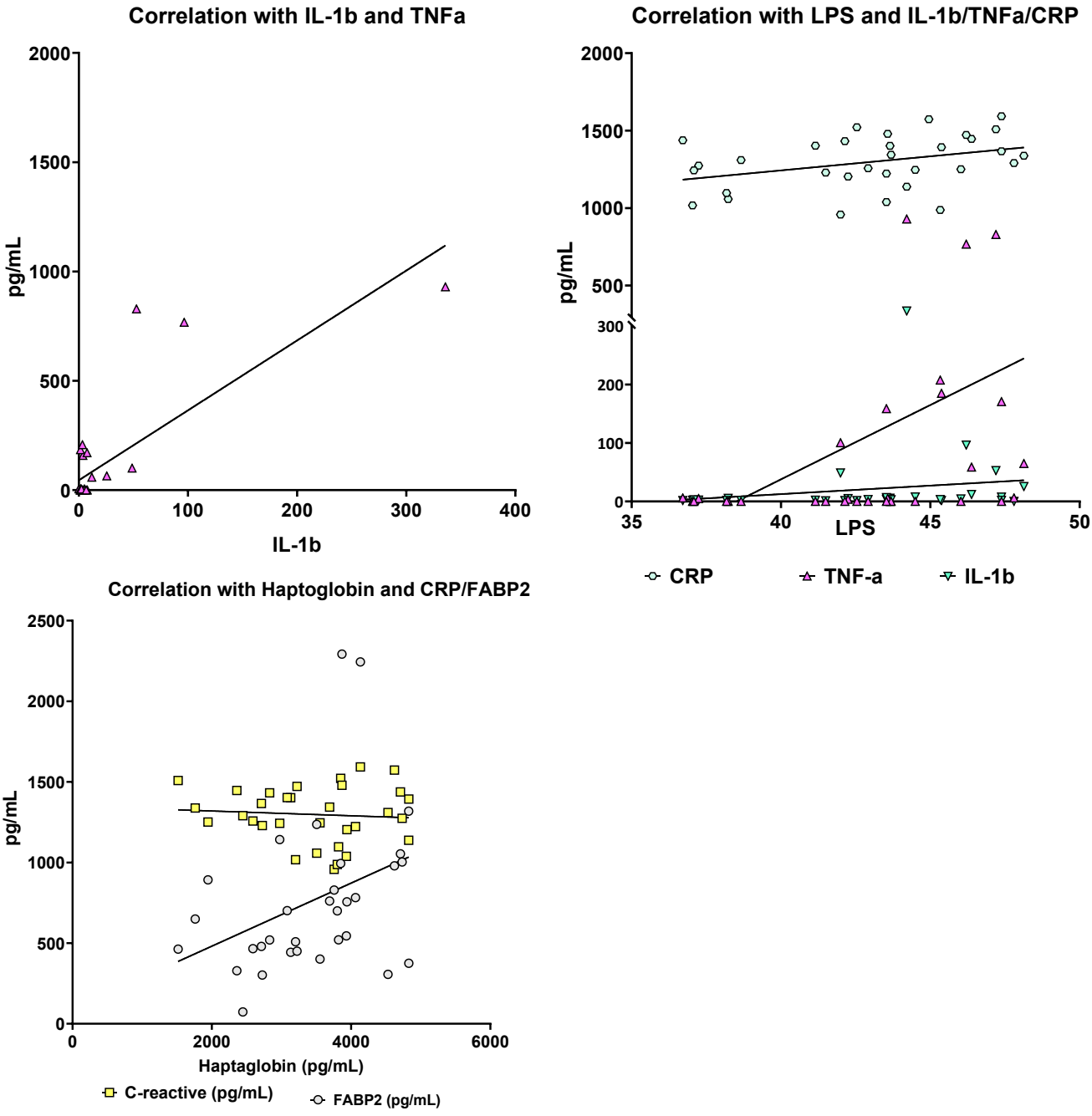

Figure 6.10. The correlation between biomarkers. *The significant positive correlation between leaky gut, inflammation, and haemolysis markers is illustrated in Table 6.2.*

Chapter 6: IMMUNOPHENOTYPING OF PCa PATIENTS' BLOOD

6.3. Discussion

The immune-based therapies have not shown promising results in PCa treatments according to ongoing clinical trials, which is mainly attributed to the immunosuppressive TME of prostate tumours. MDSCs are the main immunosuppressive cells in the TME of PCa which aids the immune escape of tumour cells. Identifying the presence of MDSCs in the peripheral blood of PCa patients will give insight into developing therapeutic strategies to treat tumours more efficiently.

This study analysed the two subsets of MDSCs, monocytic MDSCs (M-MDSC) and granulocytic (polymorphonuclear) MDSCs (PMN or G-MDSC) in detail, since these regulate the immune responses in cancer (Ostrand-Rosenberg, Fenselau 2018). G-MDSCs are found to be highly expressed in cancer when compared to healthy individuals in various cancers (Calcinotto *et al*. 2018).

The results obtained in this study revealed more expression of M-MDSCs and G-MDSCs (but not significantly prevalent) in cancer patients compared to benign subjects. Among the MDSC subtypes, G-MDSCs were found to be prevalent in both benign and cancer patients. The statistically significant difference not obtained between benign and cancer patients could be due to the small sample size. Moreover, being a small number of sample size, the subjects included in the study were heterogeneous, with different stages, grades, and risks of PCa, along with varying PSA levels. This biological heterogeneity could also lead to differences and difficulties in immunophenotyping (Cassetta *et al*. 2019). The stability of G-MDSCs has been a limiting factor in G-MDSC research; the sample needs to be processed within 3 hours of drawing the blood (Tumino *et al*. 2019). A detailed comparison with the MDSC immunophenotyping of healthy individuals would also help in better evaluation of the expression patterns. To better understand the MDSC subsets and their role in cancer progression and immunosuppression, more patient samples need to be acquired and analysed.

The patient demographics obtained for this study included age, prostate volume, PSA levels, Gleason grade and risk levels of PCa. The samples were collected from 32 individuals aged 47-78, among whom 12 were diagnosed with benign conditions. PSA testing, while

commonly used as a diagnostic tool for PCa, is not conclusive on its own since increased PSA levels can also be observed in noncancerous conditions such as prostatitis, benign prostatic hyperplasia, and age-related prostate enlargement. In this study, the correlation between age and PSA levels was assessed and found not to correlate with each other. Additionally, a negative correlation was observed between prostate volume and PSA levels. However, PSA levels tended to be higher in patients with PCa compared to those with benign conditions, suggesting that elevated PSA is more closely associated with the presence of cancer rather than prostate volume or patient age.

PSA levels are being used as the basis for referral for biopsy and people who have a PSA more than 20 ng/ml or higher than age-related normal are referred for biopsy (Liu *et al*. 2020). However, patients whose PSA level range between 4ng/mL and 10ng/mL fall in "Gray-zone" where many will be referred for a biopsy and yet only 1 in 4 will be diagnosed with cancer (Karunasinghe *et al*. 2022). A previous study from our group used an advanced computational data extraction approach combining PSA, age, and flow cytometry predictors to distinguish patients with benign cancer from those with cancer (Cosma *et. al*. 2017). In this study a different flow cytometer but with a similar panel and gating strategy was applied to study a new patient's cohort, to analyse the presence and clinical risk of PCa in asymptomatic men with PSA levels elevated above the normal. While it was not possible to analyse the current samples using the same computational approach, the presence of PCa in men having PSA levels < 20 ng/mL were compared to benign samples also with a PSA < 20 ng/mL. The results obtained showed a significant increase in the proportion of $CD8^+$NKT cells and an increase in the proportion of $CD8^+$ effector memory cells in the cancer cohort as well as an increase in $CD4^+$TEMRA, $CD19^+$ B cells albeit not significant, and a decreased in the proportion of $CD4^+$ NKT cells.

A total of 32 patient samples were analysed and the absolute cell count of several cell types in the whole blood sample was determined. Although a PSA < 4 ng/ml is normal and a PSA above 20ng/mL is suspected to be associated with PCa (Gao *et al*. 2019), exceptional PSA levels were noticed, either much higher or lower than these values. An elevated PSA (117 ng/mL) without having cancer (false positive) and men with low PSA (0.49 ng/mL), were

diagnosed with intermediate-risk PCa (false negative). More patient samples and collecting more factors like DRE, prostate health index, and PSA velocity along with characterization of whole blood immunome would help in predicting PCa risk and prevent unnecessary biopsies.

Another objective was the evaluation of inflammation and leaky gut-associated biomarkers in the plasma samples. Serum levels of various inflammatory cytokines including IL-1 (Xu *et al*. 2022), IL-6, IL-8, and TNF-α (Mao, Ding, and Xu, 2021), are elevated in patients with mCRPC and are recognised as a potential biomarker for PCa progression. This study also found similar results, showing that inflammatory markers IL-6, TNF-α, C-reactive protein, and IL-1β were elevated (though it was not statistically significant) in PCa patients compared to those with benign conditions. This study also observed a positive correlation with leaky gut marker LPS with inflammatory markers IL-1b, TNF-a, and CRP as well as between FABP2 and CRP. These findings align with the conclusions of Fujita *et al* (2023), that Leaky gut plays a crucial role in inflammation, leaked LPS into the systemic circulation can trigger inflammatory responses and increased risk of cancer. However, the correlation between these molecules was shown to be not linked to the presence of cancer. The factors contributing to the elevated inflammation and leaky gut may linked to the diet and mental status of patients. Studies conducted by Osimo *et al* (2020) and Kennedy and Niedzwiedz, (2022) have observed that elevated levels of inflammatory markers were associated with depression or stress-related disorders. Therefore, a new study was planned to include an evaluation of the diet and psychological status of PCa patients as overall inflammation is more closely linked to these factors and may influence PCa progression.

TPH is a stimulatory factor for cancer proliferation and poor prognosis in PCa. Ge *et al* (2022) reported in their study that, TPH1 was found to contribute to tumour growth and poor prognosis in patients with prostate cancer inducing TRP hydroxylation and production of 5-hydroxytryptamine. In this study, the comparative expression of TPH1 between benign and PCa patients revealed no difference. However, TPH1 displayed a positive, albeit statistically insignificant, correlation with both age and Gleason grade.

In summary, as a future direction while developing immunotherapies for PCa, combinatorial strategies to inhibit the accumulation and expansion of MDSCs could enhance vaccination responses. Additionally, the crucial role of inflammation in PCa progression further emphasizes the need to consider inflammatory pathways when designing therapeutic strategies. It is also important to recognize that the impact of stress on prostate cancer is complex and cannot be easily mitigated.

Chapter 7: DISCUSSION

7. Discussion

7.1. Discussion

Localized PCa is a relatively slow progressing disease however, there is no curative treatment for the disease if the patient becomes resistant to androgen deprivation therapy and develops mCRPC (Desai, McManus, and Sharifi, 2021). Various immunotherapies developed including checkpoint inhibitors, and adoptive cell transfer therapies to treat advanced PCa, have undergone clinical trials, yet none have achieved significant success except the Sipuleucel-T vaccine. Despite promising preclinical results, clinical trials were not satisfactory due to the heterogenicity, complex TME, and immune evasion mechanisms in PCa. Sipuleucel-T the currently FDA-approved treatment option for mCRPC, only improved the OS of patients by a few months in men with mCRPC in the phase III clinical trial, nonetheless, none of the patients who received this vaccine showed a significant difference in time to disease progression. Moreover, this is an autologous cellular immunotherapy, requiring autologous $CD45^+$ cells to be taken out for *ex vivo* stimulation with PAP-GM-CSF before being reinfused back into the patients (Elsheikh, Makram and Nguyen Tien Huy, 2023). The advised course of Sipuleucel-T therapy includes three complete doses given at two-week intervals (Madan and Gulley, 2011). In addition to the production's complexity, the Sipuleucel-T vaccine's cost limits its worldwide accessibility.

While several immunotherapies have been tested in clinical trials, their success has been hindered by the highly immunosuppressive PCa TME which includes Tregs, M2 macrophages, and MDSCs, causing challenges to the efficacy of immunotherapies; particularly immune checkpoint therapies, which were less effective due to the low infiltration of T-cells into the tumour. Given these challenges, developing a therapeutic vaccine represents a promising approach, unlike other immunotherapies like monoclonal antibodies and immune checkpoint inhibitor therapies, vaccines can enhance the immune system's ability to target and destroy malignant cells. The target cancer cell recognition and lysis can be improved through both cell-mediated and humoral immune responses. In addition, vaccines have the potential to induce long-lasting immune responses by creating a memory that can hypothetically lead to ongoing immune surveillance and the possible

elimination of disseminated cancer cells, ultimately reducing the risk of recurrence and disease progression.

The FDA-approved therapeutic vaccine Sipuleucel-T was reported to be well tolerated with manageable side effects demonstrating the safety and immunogenicity of targeting tumour-associated antigen PAP for developing immunotherapy that could enhance the treatment efficacy and patient outcomes in PCa (Elsheikh, Makram and Nguyen Tien Huy, 2023). Nonetheless, using a whole protein for vaccine development presents several challenges including uncontrolled anti-drug antibody response, which can lead to rapid systemic effects, hypersensitivity reactions, or immune-complex-mediated inflammatory responses (Liu *et al*. 2022). Long peptides containing MHC class I and class II epitopes are immunodominant and can be synthesized at a low cost, making them a more effective means of producing targeted immune responses than whole protein sequences (Nelde, Rammensee, and Walz, 2021).

Previous research conducted in our lab using PAP 114-128 -MSAMTNLAALFPPEG, 15 AA long PAP sequence shown to be effective in eliciting peptide-specific T-cell responses in HHDII/DR1 mice when administrated as a DNA ImmunoBody® vaccine (Saif *et al*. 2014). However, this small peptide limited its obtainability to HLA- $A2^{+}$ haplotype patients. Therefore, this 15 AA long peptide was elongated to 42 AA long [PAP 103- 144] and one amino acid was changed at position 116 to increase the immunogenicity of the sequence. This new sequence included additional peptides predicted to bind to more HLA haplotypes (Le Vu *et al*. 2022). The longer sequence of PAP was no longer possible to use ImmunoBody® because adding 42AA long peptides within the complementarity-determining region of an antibody disrupted the conformation and an initial study with the ImmunoBody® PAP and CAF®09 found that using CAF®09 adjuvanted vaccine was better. PAP42mer + CAF®09 vaccine has improved secretory IFN-γ and PAP-specific splenic T-cells in HHDII/DR1 mouse models, however, no CD4+ T-lymphocyte mediated responses were demonstrated (Le Vu *et al*. 2022).

To optimise the immunogenic potential of the hPAP42mer vaccine, the previously obtained results were initially validated by conducting an immunisation study under the same

experimental conditions. The involvement of CD8 and CD4 types of T-cells is crucial for an effective immune response, thus optimal vaccination strategies should induce CD8 and CD4 antigen-specific immune responses. $CD8^+$ T-cells mediate direct tumour cell lysis by recognizing tumour antigens presented on MHC class-I molecules; however, the tumour lysis is also dependent on activated $CD4^+$ T-cells. $CD4^+$ cells enhance the cross-priming of $CD8^+$ cells through APC interaction and are essential for the generation of memory T-cells including $CD8^+$ memory T-cells. Furthermore, $CD4^+$ T-cells exhibit cytolytic functions towards cancer cells expressing MHC class II- antigen complex (Riazi Rad *et al*. 2015).

Therefore, to improve the anti-tumor efficacy of MutPAP42mer by improving $CD4^+$ T-lymphocyte mediated responses, two novel 15-mer PAP peptides (PQG and CPR) were identified and tested for their immunogenicity. hPAP 15mer CPR was shown to be more immunogenic than hPAP 15mer PQG and thus was incorporated with the MutPAP42mer vaccine formulation. The immunogenicity of the 15mer CPR peptide and the MutPAP42mer sequence was tested using different adjuvants - CAF®09b, CpG 2935+IFA, and CpG1826+IFA - and was found that when the peptides were administered with CAF®09b adjuvant, induced a greater number of IFNg compared to the CpG and IFA adjuvants. Adjuvants are used in the peptide vaccine formulation to enhance the immune response by antigen localisation and enhance antigen uptake by APCs. Different adjuvants stimulate an immune response in different ways, thereby testing different adjuvants with the peptide vaccine formulation will help to identify the optimal adjuvant that maximises the peptide efficiency. CpG adjuvant is a TLR-9 agonist, induces both humoral and cellular responses and has been used in clinical trials of cancer vaccines (Guillem Montamat *et al*. 2021). IFA is an oil-in-water emulsion that creates a depot effect, providing sustained release of antigen and prolonged exposure to the immune system thereby inducing a robust and durable immune response (Apostólico *et al*. 2016). IFA has been shown to increase immunogenicity, by prolonged antigen presentation in preclinical studies (Melssen *et al*. 2022). CAF®09b is a TLR-3 agonist, that increases antigen intake by APCs and proinflammatory signalling for the stimulation of vaccine-specific $CD4^+$ and $CD8^+$ T-cells (Sofie Kirial Mork *et al*. 2023).

Chapter 7: DISCUSSION

It is also interesting to note that, each vaccine strategy had a different route of administration. The CpG+ IFA vaccine was administered subcutaneously while the CAF®09b vaccine was injected through the intraperitoneal route as recommended by collaborators providing the CAF®09b adjuvant. Intraperitoneal administration allows rapid diffusion of the vaccine throughout the peritoneal cavity, where the antigen-presenting cells, such as DCs and macrophages, can take up the antigen-adjuvant complex and initiate a robust immune response. CAF®09b was shown to be efficient in generating $CD4^+$ and $CD8^+$ T-cell responses in clinical settings when administered through the intraperitoneal or intramuscular route (Sofie Kirial Mork *et al*. 2023). There is evidence suggesting that the route of vaccination can influence the immune responses elicited in the spleen. A study comparing the protective efficacy of subcutaneous and intranasal immunization routes in mice found that while both routes provided protection against disseminated infection of the spleen and liver, subcutaneous immunization conferred significant protection against infection of the spleen, liver, and lungs. This indicates that subcutaneous vaccination can effectively induce immune responses in the spleen, though the extent and nature of these responses may vary depending on the specific vaccine and pathogen involved (Bhattacharjee *et al*. 2006).

After the optimization of the vaccination strategy, the CAF®09b adjuvanted vaccine was further assessed. Beyond the generation of IFN-γ response, the functional phenotype of vaccine-induced T-cells was evaluated. The long MuthPAP42mer sequence which contained both MHC class-I and class-II epitopes, and the hPAP15mer CPR which is predicted to bind to HLA-DR1, were able to generate a $CD4^+$/$CD8^+$-driven immune response in HHDII-DR1 mice. $CD8^+$/$CD4^+$ specific responses were proven by co-culture ELISpot assay, in which the splenocytes of immunised mice were co-cultured with MHC class I and class II epitopes of PAP42mer and PAP 15mer CPR with and without the addition of anti-CD8/CD4 antibody. Adding anti- CD4/ CD8 antibody serves to block the CD4 and CD8 T-cell receptors, effectively inhibiting their responses. Additionally, vaccine-induced $CD8^+$ specific responses also were confirmed by vaccine-specific MHC class I pentamer analysis.

Chapter 7: DISCUSSION

Interestingly, out of the class I and Class II epitopes tested for immunogenicity, ILL (Class-I) LAAL and CPR (Class II) were found to be inducing the highest IFN-γ responses.

Following the assessment of the immunogenicity of the vaccine, the efficacy of vaccine-induced T-cells to recognize and lyse target cells expressing the PAP and HHDIH genes was evaluated. Given that the vaccine is made of hPAP peptides, tumour cell lysis by vaccine-induced CTLs is mediated by the presentation of PAP-derived antigen via the MHC molecule followed by its recognition by CTLs. Therefore, target cells that do not naturally express PAP protein were modified to express PAP antigen and suitable controls for cells that naturally express PAP antigen were prepared by knocking down the expression of PAP. PAP expression and PAP knockdown were confirmed by qPCR and western blot analysis. In addition, all human target cells were transfected with chimeric HLA A2 molecules to enhance their target recognition and lysis by T-cells generated in the HHDII mice. The stability of HHDII and PAP transfections performed in this study was assessed through the cloning of Du145 HHDII PAP cells, which confirmed the highest expression levels of both PAP and HHDII. In HEK293t cells, PAP expression was successfully confirmed for the HHDII PAP construct. Similarly, in LNCap HHDII shRNA cells, PAP knockdown was confirmed over three consecutive passages. A comparable confirmation of mPAP knockdown was achieved in TRAMP C1 and TRAMP C2 shRNA cells, which was also observed across three consecutive passages. For the cytotoxicity experiment, cells from the same early passages were utilized.

The vaccine induced CTLs were able to recognize and lyse target cell lines (both PCa and non-cancerous), however, there were lysis of control cells that don't express PAP antigen also was noticed. The non-specific killing demonstrated *in vitro* could be explained as a cytokine-mediated response, where the cytokines such as IFN-γ and TNF-α, released by activated T-cells can induce direct cytotoxic effects on cancer cells independent of antigen specificity. In addition to the cytokine release**,** activated T-cells may release cytotoxic granules containing perforin and granzymes and cause apoptosis in the neighbouring cancer cells (Yu *et al*. 2023). Non-specific responses can also be referred to as adjuvant-

induced responses, as CAF®09b has been demonstrated to be effective in generating robust $CD4^+$ and CD8+ T-cell responses (Sofie Kirial Mork *et al*. 2023).

While it might have been better to use the radioactive chromium-releasing method a highly sensitive assay used to determine low levels of cytotoxicity (Karimi *et al*. 2014). However, the use of standard radioactive chromium was not accessible due to problems in the handling, storage, and disposal of the material. The CCK- 8 assay used to assess the cytotoxicity towards PCa cell lines is that CCK-8 assay which indirectly measures the percentage of cytotoxicity. The tetrazolium-based assay is also highly sensitive to environmental factors and culture conditions such as the pH of the medium and interference of chemicals like magnesium or carbon particles (Scarcello *et al*. 2020).

In addition, the MutPAP42mer +PAP15mer CPR +CAF®09b vaccine tested in HHDII DP4 models also confirmed the immunogenicity of the vaccine, and vaccine-specific $CD3^+$ T-cells were able to recognize the target cells invitro in HLA and PAP restricted manner. The ability of the vaccine to produce $CD8^+$ CTLs was demonstrated by a specific reduction in IFN-γ production when $CD8^+$ co-receptor blocking with anti-$CD8^+$ antibody was applied to T-cells. Although the results obtained were promising, an *in vitro* target-killing assay could not be carried out as a next step because there was insufficient HHDII DP4 availability and time constraints.

HHDII/DR1 and HHDII/DP4 are double transgenic mice that lack the murine H-2 genes, instead, they express an MHC class I molecule consisting of α1 and α2 chains of human HLA A*0201 chimeric with murine H-2Dd α3 called (HHDII) which is covalently linked to human β2M and an MHC class II molecule comprising of human HLA-DRB*0101 for HHDII DR1 (Pajot *et al*. 2004) or human HLA DP*0401 and human CD4 for HHDII DP4 mice (Victoria Anne Brentville *et al*. 2022). These transgenic models allow studying immune responses to various vaccines that encode multiple epitopes for HLA class I and class II peptides within the murine host system, and the results obtained can be applied to clinical settings.

Therefore, the next step of the study requirement was to evaluate the *in vivo* efficacy of the vaccine by developing HHDII DR1 tumour models. Given that these models are double transgenic, murine cell lines can be recognized as foreign by the host, leading to immune

rejection. Human cell lines typically do not grow in murine host systems for similar reasons, resulting in immune-mediated rejection. To overcome these challenges, a murine cell line that is genetically modified to be devoid of murine β2M gene and transfected with chimeric HLA A2 gene can be used. For that, TRAMP C1, a murine PCa cell line expressing murine PAP, was engineered for compatibility with the HHDII mice. This was achieved by employing CRISPR-Cas9 technology to knock out the murine β2M gene, which is essential for the presentation of murine MHC molecules. Additionally, the murine PAP gene was knocked down and transfected with the human PAP gene. The cells were then further transfected to express the HHDII gene. The genetic modification of the TRAMP C1 cell line was successfully achieved; however, the entire process of preparing this target cell line for the HHDII tumour model took unexpectedly longer than a year. While the TRAMP C1 cell line was being modified, the vaccine's efficacy was evaluated using C57BL/6J mice, which served as a proof of concept. Since PAP is a self-antigen also expressed in normal prostate tissue, the C57BL/6J model was suitable for determining whether the PAP-derived vaccine could elicit an appropriate immune response and break tolerance to the PAP protein.

However, C57BL/6J models are not double transgenic, thus, the wild-type form of the human PAP42mer peptide was used for immunisation. Initial results showed that the group of animals receiving the hPAP42mer +15mer CPR +CAF®09b immunization exhibited the highest IFN- γ responses, indicating the immunostimulatory properties of the adjuvant in conjunction with the peptides. Despite the expectation that the human WT PAP15-mer CPR would bind more effectively to H-2IAb compared to its murine counterparts with three amino acid alterations, no significant immunogenicity was observed when vaccine-induced splenocytes were co-cultured *in vitro* with the CPR peptide. The hPAP42mer WT peptide, which includes both MHC class I and class II epitopes, was found to be immunogenic in C57BL/6J mice, generating a vaccine-specific $CD8^+$ and $CD4^+$ T-cell response. Furthermore, the vaccine-induced T-cells demonstrated the ability to recognise and lyse murine PCa cells TRAMP C1 and TRAMP C2 *in vitro*, attaining 65% lysis of TRAMP C1 cells and 76% lysis of TRAMP C2 cells. These results were significantly higher than the cytotoxicity observed in control cell lines TRAMP C1/TRAMP C2+ shRNA. TRAMP C2 expresses more PAP compared

to TRAMP C1 cell lines (section 3.2.1.2.2) and demonstrated more killing *in vitro*. Therefore, to assess the vaccine efficacy, TRAMP C2 cells were used to generate C57BL/6J PCa tumour models. These cell lines also were confirmed for their MHC class I expression (section 3.2.1.2.1).

TRAMP C2 cells were subcutaneously injected into the right flank of C57BL/6J mice to establish a transplantable tumour model for the study. The *in vivo* assessment aimed to evaluate the vaccine's efficacy in reducing tumour growth, improving survival rates. Additionally, the effect of the vaccine to stimulate the immune system was evaluated by immunophenotyping of tumour-infiltrating cells. In the initial tumour study, $5x10^6$ TRAMP C2 cells were used for tumour implantation. Vaccine efficacy was tested in a prophylactic setting, where animals received three doses of immunisation and were subsequently challenged with TRAMP C2 cells two weeks later. The results indicated a reduction in tumour growth on day 23. However, the tumour grew rapidly thereafter, suggesting the lack of long-term efficacy of the vaccine in controlling the tumour progression. Immunophenotyping of TILs revealed activation of $CD4^+$ T helper cells and an increase in IFN-γ producing $CD4^+$ cells following immunization. Besides, the immunization had led to a reduction in PD-1 expression on $CD4^+$ T-cells.

However, the study also revealed a higher expression of immunosuppressive G-MDSCs and $FoxP3^+$ regulatory T-cells, which contributed to a suppressive TME. Elevated levels of immune checkpoint molecules, such as CTLA-4, PD-1, and TIM-3 on $CD8^+$ T -cells, as well as CTLA-4 and LAG-3 on $CD4^+$ T-cells, further indicated significant T-cell exhaustion within the TME. It was hypothesized that continuing immunisations even after tumour implantation could potentially reduce the factors affecting immunosuppressive TME in reducing the tumour growth.

The subsequent tumour study aimed to analyse the effects of vaccine in castrated mice. PCa cell growth is dependent on androgen receptors and androgen depletion inhibits the growth of PCa, making ADT a universally accepted treatment for men with advanced PCa (Sekhoacha *et al*. 2022). Patients with advanced PCa are likely to undergo some form of ADT, as it is the standard treatment. Therefore, this study evaluated how castration might impact

the efficacy of the PAP42mer vaccine in prostate tumour-bearing C57Bl/6J mice. Given that TRAMP C2 cells grow in an androgen-independent manner (Philippou *et al*. 2020), TRAMP C2 tumours implanted in castrated mice would effectively model the clinical scenario of castration-resistant PCa.

Due to the limited effectiveness of the vaccine observed in the previous tumour growth study, a few modifications were implemented prior to the next study. First, a lower number of TRAMP C2 cells ($2x10^6$) were used for tumour implantation, compared to the $5x10^6$ cells used previously. This adjustment was made based on the hypothesis that the higher dose of TRAMP C2 cells may have contributed to the rapid tumour growth observed in the earlier study. Second, the immunisation protocol was altered, with immunisations being administered at one-week intervals instead of two-week intervals. This change was made with the hypothesis that a stronger immune response could be achieved by more frequent dosing. Additionally, it was decided to continue immunisations after the tumour challenge. However, signs of toxicity were observed in one of the test groups following the second dose of immunisation after the tumour challenge, leading to the loss of 50% of the animals in that group. It was strongly suspected that a modification in the CAF®09b formulation was the contributing factor to the toxicity developed. As a result, all animals in both test groups stopped receiving further immunisations, and it was too late in the study to attempt a different, more potent adjuvant. Group 2 (immunisation before castration) received a total of five doses of immunisation (three before and two after the tumour implantation) and one dose of degarelix. Group 3 (immunisation after castration) received four doses of immunization (three before and one after the tumour implantation) and two doses of degarelix.

The study confirmed that castration effectively reduced testosterone levels in tumour-bearing mice; however, this reduction did not affect tumour growth. A limitation of the study was the lack of evaluation of how castration might also modulate the immune system, both in naïve mice and in TRAMP C2 tumour-bearing models. Evaluating the immunomodulatory effects of castration in these contexts could have provided more understanding. Instead, the ‘castration alone’ treatment group in this experiment was compared to the ‘tumour

alone' group from the previous experiment. Although these results are comparable, it is important to note that the groups received different tumour doses ($5x10^6$ TRAMP C2 cells in the 'tumour alone' group versus $2x10^6$ TRAMP C2 cells in the castration group), drawing a definite conclusion is still argumentative.

Despite reducing the number of TRAMP C2 cells, the treatment groups that received immunisation either before or after degarelix treatment did not show any reduction in tumour growth compared to the control group, which received degarelix alone.

Immunophenotyping analysis revealed that castration had reduced the expression of effector memory T-cells, IFN-γ releasing $CD4^+$ and $CD8^+$ T-cells, and $CD4^+CD25^+FoxP3^+$ Tregs in TRAMP C2 tumour-bearing mice. And there were increased levels of M-MDSCs, $LAG\text{-}3^+CD4^+/CD8^+$ T-cells, and $CTLA\text{-}4^+$ $CD8^+$ T-cells suggesting that castration induced an immunosuppressive TME in PCa tumour-bearing mice. Interestingly, vaccination appeared to counteract the immunosuppressive effects of castration by enhancing the effector functions of both $CD4^+$ and $CD8^+$ T-cells in the treatment groups. Exhaustion markers such as PD-1, CTLA-4, TIM-3, and LAG-3 were reduced in $CD4^+$ and $CD8^+$ T-cells following immunisation with castration. Moreover, the percentage of IFN-γ releasing $CD8^+$ T-cells was increased in both treatment groups, with a significant increase when the vaccine was given after degarelix treatment. Furthermore, the presence of Tregs was further reduced when the vaccine was administered before castration, contrasting with findings from Tang *et al* (2012), who observed an increased proportion of $CD4^+CD25^+FoxP3^+$ Tregs in castrated and immunised animals in their study. Tang *et al* (2012) also noted that the ability of androgen ablation to enhance immune responses to PCa antigens may vary depending on the antigen and the strength of the T-cell response generated. In this study, however, the PAP42mer WT vaccine, when applied in conjunction with castration, effectively reduced the levels of $CD4^+CD25^+FoxP3^+$ Tregs in tumour-bearing mice. Although Fc blocking was performed at the initial step of staining, this study did not include isotype controls. Instead, cells without staining were used as the experimental control. Incorporating isotype controls—antibodies of the same isotype but specific to irrelevant antigens—would have been a better approach for distinguishing specific antigen-antibody interactions from non-specific binding

(Andersen *et al*. 2016). This inclusion would have enhanced the accuracy of flow cytometry analyses.

These findings indicate that the hPAP42mer WT +CAF®09b vaccine was able to successfully stimulate the immune system in PCa tumour-bearing mice with the effect being further enhanced when the vaccine was administered with androgen ablation. Moreover, this study reveals that immunisation administered before and after castration had positive effects, corroborating to some extend with what, Drake *et al* (2005) and Yi Ting Koh *et al* (2009) observed. The study by Drake *et al* (2005), which used adoptive transfer of prostate-specific $CD4^+$ T-cells in transgenic mice expressing the model antigen influenza haemagglutinin. Their results suggested that immunotherapy for PCa was most effective when administered after androgen ablation. Also, Yi Ting Koh *et al* (2009) found that androgen deprivation enhanced immune responses to vaccination but only when applied after immunisation. However, the presence of MDSC especially G-MDSCs was higher in both castrated and castrated +immunized groups, indicating the cause of the lack of efficient tumour reduction noticed.

While assessing the efficacy of the vaccine in preclinical models, the presence of immune cell subsets, immunosuppressive regulators, and inflammatory molecules in the periphery of PCa patients, were also studied. Evaluating these factors are crucial while developing an immunotherapy for PCa and translating them into clinical practice. This study contained blood samples from 12 benign and 20 PCa patients.

The patient demographics collected for this study included the patient's age, prostate volume, PSA levels, Gleason grade, and D'Amico classification of PCa. PSA levels are common diagnostic measures for PCa and individuals having PSA levels below 4 ng/mL are generally considered normal, and a level above 20 ng/mL is often associated with PCa (Xu *et al*. 2022). Patients with susceptible PSA higher than age-related normal level are being referred for further diagnosis by prostate biopsy (Liu *et al*. 2020). Nonetheless, PSA levels alone should not be the sole criterion for directing patients toward invasive biopsies as PSA levels can fluctuate due to various factors, including age, lifestyle, and ethnicity (Karunasinghe *et al*. 2022).

Chapter 7: DISCUSSION

The study specifically analysed both monocytic and granulocytic MDSCs given their role in regulating immune responses in cancer. The results of this study revealed higher levels of M-MDSCs and G-MDSCs in cancer patients compared to those with benign prostatic disease, although the difference was not statistically significant. G-MDSCs are highly expressed in cancer compared to healthy individuals across various cancer types (Calcinotto *et al*. 2018; Wen *et al*. 2020).

Another objective of this study was to evaluate biomarkers associated with inflammation and leaky gut in plasma isolated from these participants. The findings showed that inflammatory markers IL-6, TNF-α, C-reactive protein, and IL-1β were elevated in PCa patients compared to those with benign conditions, although these differences were not statistically significant. Additionally, the study observed a positive correlation between the leaky gut marker LPS and inflammatory markers IL-1β, TNF-α, and CRP, as well as between FABP2 and CRP. These findings are like the results Fujita et al (2023) who noted that a leaky gut plays a crucial role in inflammation, as leaked LPS into systemic circulation can trigger inflammatory responses and increase the risk of cancer.

The mental status and the diet may be at the origin of the elevated inflammation and leaky gut observed rather than being due to the presence of cancer. Chronic infections or pathogen carriage can contribute to persistent inflammatory responses, which may, in turn, influence the development and progression of PCa (Sfanos, Isaacs and De, 2013). A meta-analysis conducted by (Osimo *et al*. 2020) to find the differences of immune markers in depression, including a total of 107 studies that reported measurements from 5,166 patients with depression and 5,083 controls reported that CRP, IL-6 IL-3 IL-12 and TNFα markers were significantly higher in patients with depression. The findings of Kennedy and Niedzwiedz, (2022) including 353,136 participants of which 12,759 had a history of anxiety or stress-related disorder also support the evidence of increased circulating inflammatory markers associated with anxiety and stress-related disorders. Therefore, an intervention study which would restore a diet and mental status that would reduce inflammation is beneficial before immunising the patients as inflammation is more closely link to these factors and might then influence the progression of the cancer.

Chapter 7: DISCUSSION

Though the analysis MDSCs, and circulating biomarkers showed a difference between benign and PCa patients, statistically significant differences were not observed, this could be attributed to the small sample size. Furthermore, the subjects included in the study were heterogeneous, with variations in PCa stages, grades, risk levels, and PSA levels. This biological heterogeneity may have contributed to the observed differences and challenges in immunophenotyping as Cassetta *et al* (2019) supported. To gain a deeper understanding of inflammatory, leaky gut biomarkers as well as MDSC subsets and their role in cancer progression a larger cohort patient sample is necessary for the analysis. The stability of G-MDSCs is also a limiting factor in this research, as the blood samples need to be processed within three hours of blood collection to ensure the accuracy of the results (Tumino et al. 2019). A detailed comparison with immunophenotyping in healthy individuals would provide a more comprehensive evaluation of expression patterns of MDSCs and immune cell distribution in cancerous and non-cancerous conditions.

Evidence from tumour studies demonstrating increased tumour-infiltrating MDSCs, coupled with blood analyses of PCa patients showing elevated circulating MDSCs, underlines the critical importance of developing strategies to target MDSC-mediated immunosuppressive mechanisms while developing immunotherapy for PCa. MDSCs suppress anti-tumour immunity through mechanisms mainly including inducible nitric oxide synthase (iNOS), arginase 1, reactive oxygen species (ROS)-mediated pathways and secretion of immunosuppressive cytokines such as IL-10. Currently, there are no clinically approved drugs available that specifically target MDSCs. Yet preclinical studies, directly targeting the MDSC suppressive mechanism have shown success in overcoming the therapeutic resistance in cancer models (Jou, Chaudhury, and Nasim, 2024). $Arg1^+$ MDSCs can also be targeted via chemotherapy; Doxorubicin is a chemotherapeutic agent used for breast cancer treatment found to reduce expression of MDSC-associated genes including Arg1, and iNOS, in breast tumour mouse models (Zamani et al. 202Likewise, chemotherapy can also reduce MDSC iNOS expression, docetaxel has been shown to reduce MDSC Arg1

and iNOS activity allowing anti-tumour effector function in colon cancer tumour models (Hu *et al*. 2020).

7.2 Conclusion and future perspectives

In conclusion, a PAP peptide-based vaccine was developed for the treatment of advanced PCa that had demonstrated efficacy in stimulating the immune response in PCa-bearing mice. Moreover, the therapeutic effect was further enhanced when the immunisation was combined with ADT. However, the immunosuppressive impact of MDSCs, particularly G-MDSCs, was associated with poor vaccine effectiveness in reducing tumour growth in preclinical models. Notably, elevated levels of G-MDSCs were also detected in the peripheral blood of PCa patients compared to benign prostatic hyperplasia, highlighting their potential role in the immunosuppressive TME of PCa. Thus, administering the vaccine in conjunction with androgen ablation—a standardized treatment for PCa—while employing strategies to reduce MDSC-mediated suppression, will enhance the therapeutic efficacy of the vaccination.

Given these considerations, the next step involves assessing the efficacy of the mutPAP42mer + PAP15mer CPR vaccine in HHDII humanized models – which was proposed to be done as part of this research but was not able to be carried out due to time restraints and funding issues. Besides, the adjuvant CAF®09b, which was associated with toxicity towards the end of the *in vivo* evaluation of the hPAP42mer WT vaccine, raises concerns about its continued use. Taking this limitation into consideration, utilizing an mRNA form of the vaccine might be beneficial. mRNA vaccines offer several advantages, including the ability to deliver multiple antigens within a single formulation, relatively low production costs, safety in administration, and a targeted ability to elicit both humoral and cellular immune responses against specific antigens (Elsheikh, Makram, and Nguyen Tien Huy, 2023; Liu *et al*. 2022). In addition, the importance of mRNA vaccines has been particularly highlighted by the recent success in developing COVID-19 vaccines against the SARS-CoV-2 virus. mRNA vaccines function by delivering mRNA molecules directly into the cytoplasm, where they are translated to produce antigens, thereby generating efficient immune

responses due to immediate antigen production. However, the efficacy of mRNA vaccines can be compromised by challenges such as the difficulty of delivering synthesized RNA across the cell membrane without being degraded by the endosomes. To address these issues, it is crucial to encapsulate the RNA of the mutPAP42mer + PAP15mer CPR vaccine in lipid nanoparticles, like the approach used in the FDA-approved SARS-CoV-2 mRNA vaccines BNT162b2 (Pfizer) and mRNA-1273 (Moderna) (Wang Bolin *et al*. 2023).

REFERENCE LIST

1. A, C., Travers, P., Walport, M. and Shlomchik, M.J. (2018). *Principles of innate and adaptive immunity*. [online] Nih.gov. Available at: https://www.ncbi.nlm.nih.gov/books/NBK27090/.
2. Abd-Aziz, N. and Poh, C.L. (2022). Development of Peptide-Based Vaccines for Cancer. *Journal of Oncology*, 2022, pp.1–17. doi: https://doi.org/10.1155/2022/9749363.
3. Abeles, R.D., McPhail, M.J., Sowter, D., Antoniades, C.G., Vergis, N., Vijay, G.K.M., Xystrakis, E., Khamri, W., Shawcross, D.L., Ma, Y., Wendon, J.A. and Vergani, D. (2012). CD14, CD16 and HLA-DR reliably identifies human monocytes and their subsets in the context of pathologically reduced HLA-DR expression by CD14hi/CD16neg monocytes: Expansion of CD14hi/CD16pos and contraction of CD14lo/CD16pos monocytes in acute liver fail. *Cytometry Part A*, 81A(10), pp.823–834. doi:https://doi.org/10.1002/cyto.a.22104.
4. Abusalem, M., Martiniova, L., Soebianto, S., DePalatis, L. and Ravizzini, G. (2023). Current Status of Radiolabeled Monoclonal Antibodies Targeting PSMA for Imaging and Therapy. *Cancers*, 15(18), pp.4537–4537. doi:https://doi.org/10.3390/cancers15184537.
5. Al-Fayez, S. and El-Metwally, A. (2023). Cigarette smoking and prostate cancer: A systematic review and meta-analysis of prospective cohort studies. *Tobacco Induced Diseases*, 21(February), pp.1–12. doi:https://doi.org/10.18332/tid/157231.
6. Al-Ghazawi, M., Salameh, H., Amo-Afful, S., Khasawneh, S., Ghanem, R., Al-Ghazawi, M., Salameh, H., Amo-Afful, S., Khasawneh, S. and Ghanem, R. (2023). An In-Depth Look Into the Epidemiological and Etiological Aspects of Prostate Cancer: A Literature Review. *Cureus*, [online] 15(11). doi: https://doi.org/10.7759/cureus.48252.
7. Anassi, E. and Ndefo, U.A. (2011). Sipuleucel-T (Provenge) Injection. *Pharmacy and Therapeutics*, [online] 36(4), pp.197–202.
8. Andersen, M.N., Al-Karradi, S.N.H., Kragstrup, T.W. and Hokland, M. (2016). Elimination of erroneous results in flow cytometry caused by antibody binding to Fc receptors on human monocytes and macrophages. *Cytometry. Part A: The Journal of the International Society for Analytical Cytology*, 89(11), pp.1001–1009. doi: https://doi.org/10.1002/cyto.a.22995.
9. Apostólico, J. de S., Lunardelli, V.A.S., Coirada, F.C., Boscardin, S.B. and Rosa, D.S. (2016). Adjuvants: Classification,Modus Operandi, and Licensing. *Journal of Immunology Research*, 2016, pp.1–16. doi:https://doi.org/10.1155/2016/1459394.

REFERENCE LIST

10. Archer, M., Dogra, N. and Kyprianou, N. (2020). Inflammation as a Driver of Prostate Cancer Metastasis and Therapeutic Resistance. *Cancers*, 12(10), p.2984. doi:https://doi.org/10.3390/cancers12102984.
11. Arthur, R., Williams, R., Garmo, H., Holmberg, L., Stattin, P., Malmström, H., Lambe, M., Hammar, N., Walldius, G., Robinsson, D., Jungner, I. and Van Hemelrijck, M. (2018). Serum inflammatory markers in relation to prostate cancer severity and death in the Swedish AMORIS study. *International Journal of Cancer*, 142(11), pp.2254–2262. doi:https://doi.org/10.1002/ijc.31256.
12. Bachmann, M.F. and Oxenius, A. (2007). Interleukin 2: from immunostimulation to immunoregulation and back again. *EMBO reports*, 8(12), pp.1142–1148. doi:https://doi.org/10.1038/sj.embor.7401099.
13. Balk, S.P., Ko, Y.-J. and Bubley, G.J. (2003). Biology of Prostate-Specific Antigen. *Journal of Clinical Oncology*, 21(2), pp.383–391. doi:https://doi.org/10.1200/jco.2003.02.083.
14. Bausart, M., Bozzato, E., Joudiou, N., Xanthippi Koutsoumpou, Manshian, B., Véronique Préat and Gallez, B. (2023). Mismatch between Bioluminescence Imaging (BLI) and MRI When Evaluating Glioblastoma Growth: Lessons from a Study Where BLI Suggested 'Regression' while MRI Showed 'Progression'. *Cancers*, 15(6), pp.1919–1919. doi:https://doi.org/10.3390/cancers15061919.
15. Beer, T.M., Kwon, E.D., Drake, C.G., Fizazi, K., Logothetis, C., Gravis, G., Ganju, V., Polikoff, J., Saad, F., Humanski, P., Piulats, J.M., Gonzalez Mella, P., Ng, S.S., Jaeger, D., Parnis, F.X., Franke, F.A., Puente, J., Carvajal, R., Sengeløv, L. and McHenry, M.B. (2017). Randomized, Double-Blind, Phase III Trial of Ipilimumab Versus Placebo in Asymptomatic or Minimally Symptomatic Patients With Metastatic Chemotherapy-Naive Castration-Resistant Prostate Cancer. *Journal of Clinical Oncology*, 35(1), pp.40–47. doi:https://doi.org/10.1200/jco.2016.69.1584.
16. Belkahla, S., Nahvi, I., Biswas, S., Nahvi, I. and Ben Amor, N. (2022). Advances and development of prostate cancer, treatment, and strategies: A systemic review. *Frontiers in Cell and Developmental Biology*, 10(1). doi:https://doi.org/10.3389/fcell.2022.991330.
17. Berraondo, P., Sanmamed, M.F., Ochoa, M.C., Etxeberria, I., Aznar, M.A., Pérez-Gracia, J.L., Rodríguez-Ruiz, M.E., Ponz-Sarvise, M., Castañón, E. and Melero, I. (2019). Cytokines in

REFERENCE LIST

clinical cancer immunotherapy. *British Journal of Cancer*, [online] 120(1), pp.6–15. doi:https://doi.org/10.1038/s41416-018-0328-y.

18. Bhattacharjee, A.K., Izadjoo, M.J., Zollinger, W.D., Nikolich, M.P. and Hoover, D.L. (2006). Comparison of Protective Efficacy of Subcutaneous versus Intranasal Immunization of Mice with a*Brucella melitensis*Lipopolysaccharide Subunit Vaccine. *Infection and Immunity*, 74(10), pp.5820–5825. doi:https://doi.org/10.1128/iai.00331-06.

19. Blum, J.S., Wearsch, P.A. and Cresswell, P. (2013). Pathways of Antigen Processing. *Annual Review of Immunology*, 31(1), pp.443–473. doi:https://doi.org/10.1146/annurev-immunol-032712-095910.
20. Bonollo, F., Thalmann, G.N., Kruithof-de Julio, M. and Karkampouna, S. (2020). The Role of Cancer-Associated Fibroblasts in Prostate Cancer Tumorigenesis. *Cancers*, 12(7), p.1887. doi:https://doi.org/10.3390/cancers12071887.
21. Bou-Dargham, M.J., Sha, L., Sang, Q.-X.A. and Zhang, J. (2020). Immune landscape of human prostate cancer: immune evasion mechanisms and biomarkers for personalized immunotherapy. *BMC Cancer*, 20(1). doi:https://doi.org/10.1186/s12885-020-07058-y.
22. Bratt, O., Auvinen, A., Godtman, R.A., Hellström, M., Hugosson, J., Lilja, H., Wallström, J. and Roobol, M.J. (2023). Screening for prostate cancer: evidence, ongoing trials, policies and knowledge gaps. *BMJ Oncology*, [online] 2(1). doi:https://doi.org/10.1136/bmjonc-2023-000039.
23. Brawer, M.K. (2005). Prostatic Intraepithelial Neoplasia: An Overview. *Reviews in Urology*, [online] 7(Suppl 3), pp.S11–S18.
24. Bray, F., Mathieu Laversanne, Sung, H., Ferlay, J., Siegel, R.L., Soerjomataram, I. and Jemal, A. (2024). Global cancer statistics 2022: GLOBOCAN estimates of incidence and mortality worldwide for 36 cancers in 185 countries. *Ca (Print)*. doi:https://doi.org/10.3322/caac.21834.
25. Bryant, C.D. (2011). The blessings and curses of C57BL/6 substrains in mouse genetic studies. *Annals of the New York Academy of Sciences*, [online] 1245(1), pp.31–33. doi:https://doi.org/10.1111/j.1749-6632.2011.06325.x.
26. Buhrman, J.D. and Slansky, J.E. (2013). Improving T cell responses to modified peptides in tumor vaccines. *Immunologic research*, [online] 55(1-3), pp.34–47. doi:https://doi.org/10.1007/s12026-012-8348-9.

REFERENCE LIST

27. Burch, P.A., Croghan, G.A., Gastineau, D.A., Jones, L.A., Kaur, J.S., Kylstra, J.W., Richardson, R.L., Valone, F.H. and Vuk-Pavlović, S. (2004). Immunotherapy (APC8015, Provenge®) targeting prostatic acid phosphatase can induce durable remission of metastatic androgen-independent prostate cancer: A phase 2 trial. *The Prostate*, 60(3), pp.197–204. doi:https://doi.org/10.1002/pros.20040.
28. Calcinotto, A., Spataro, C., Zagato, E., Di Mitri, D., Gil, V., Crespo, M., De Bernardis, G., Losa, M., Mirenda, M., Pasquini, E., Rinaldi, A., Sumanasuriya, S., Lambros, M.B., Neeb, A., Lucianò, R., Bravi, C.A., Nava-Rodrigues, D., Dolling, D., Prayer-Galetti, T. and Ferreira, A. (2018). IL-23 secreted by myeloid cells drives castration-resistant prostate cancer. *Nature*, 559(7714), pp.363–369. doi:https://doi.org/10.1038/s41586-018-0266-0.
29. Caram, M.E.V., Ross, R., Lin, P. and Mukherjee, B. (2019). Factors Associated With Use of Sipuleucel-T to Treat Patients With Advanced Prostate Cancer. *JAMA Network Open*, 2(4), p.e192589. doi:https://doi.org/10.1001/jamanetworkopen.2019.2589.
30. Carlsson, B., Forsberg, O., Bengtsson, M., Tötterman, T.H. and Essand, M. (2007). Characterization of human prostate and breast cancer cell lines for experimental T cell-based immunotherapy. *The Prostate*, 67(4), pp.389–395. doi:https://doi.org/10.1002/pros.20498.
31. Carneiro, A., Racy, D., Carlos Eduardo Bacchi, Ramos, K., Renee Zon Filippi, Fernandes, A., Joao Victor Salvajoli, Rodrigo, Ronaldo Hueb Baroni, Alvaro Sadek Sarkis, Carlos, A., Bruno Santos Benigno, Gustavo Cardoso Guimarães, Saad Aldousari, Aguinaldo Cesar Nardi, Alexandre, Amr Nowier, Nardozza, A., Adamy, A. and Celso (2021). Consensus on Screening, Diagnosis, and Staging Tools for Prostate Cancer in Developing Countries: A Report From the First Prostate Cancer Consensus Conference for Developing Countries (PCCCDC). *JCO global oncology*, [online] 44(7), pp.516–522. doi:https://doi.org/10.1200/go.20.00527.
32. Cassetta, L., Baekkevold, E.S., Brandau, S., Bujko, A., Cassatella, M.A., Dorhoi, A., Krieg, C., Lin, A., Loré, K., Marini, O., Pollard, J.W., Roussel, M., Scapini, P., Umansky, V. and Adema, G.J. (2019). Deciphering myeloid-derived suppressor cells: isolation and markers in humans, mice and non-human primates. *Cancer Immunology, Immunotherapy*, [online] 68(4), pp.687–697. doi:https://doi.org/10.1007/s00262-019-02302-2.
33. Castelli, F.A., BuhotC., Sanson, A., Zarour, H., Pouvelle-Moratille, S., NonnC., Gahery-SégardH., GuilletJ.-G., MénezA., Georges, B. and MaillèreB. (2002). HLA-DP4, the Most

REFERENCE LIST

Frequent HLA II Molecule, Defines a New Supertype of Peptide-Binding Specificity. *The Journal of Immunology*, 169(12), pp.6928–6934. doi:https://doi.org/10.4049/jimmunol.169.12.6928.

34. Cazzato, G., Colagrande, A., Cimmino, A., Cicco, G., Scarcella, V.S., Tarantino, P., Lospalluti, L., Romita, P., Foti, C., Demarco, A., Sablone, S., Candance, P.M.V., Cicco, S., Lettini, T., Ingravallo, G. and Resta, L. (2021). HMGB1-TIM3-HO1: A New Pathway of Inflammation in Skin of SARS-CoV-2 Patients? A Retrospective Pilot Study. *Biomolecules*, [online] 11(8), p.1219. doi:https://doi.org/10.3390/biom11081219.
35. Celma, P. Servián, Planas, J., Placer, J., Quilez, M.T., M.A. Arbós, I. de Torres and J. Morote (2014). Clinical significance of proliferative inflammatory atrophy in prostate biopsy. *Actas urológicas españolas*, 38(2), pp.122–126. doi: https://doi.org/10.1016/j.acuroe.2013.10.011.
36. Cenerenti, M., Saillard, M., Romero, P. and Jandus, C. (2022). The Era of Cytotoxic CD4 T Cells. *Frontiers in Immunology*, 13. doi:https://doi.org/10.3389/fimmu.2022.867189.
37. Chakrabarti, R. and Kang, Y. (2015). Transplantable Mouse Tumor Models of Breast Cancer Metastasis. *Methods in molecular biology*, pp.367–380. doi:https://doi.org/10.1007/978-1-4939-2297-0_18.
38. Chandran, S.S., Somerville, R.P.T., Yang, J.C., Sherry, R.M., Klebanoff, C.A., Goff, S.L., Wunderlich, J.R., Danforth, D.N., Zlott, D., Paria, B.C., Sabesan, A.C., Srivastava, A.K., Xi, L., Pham, T.H., Raffeld, M., White, D.E., Toomey, M.A., Rosenberg, S.A. and Kammula, U.S. (2017). Treatment of metastatic uveal melanoma with adoptive transfer of tumour-infiltrating lymphocytes: a single-centre, two-stage, single-arm, phase 2 study. *The Lancet Oncology*, 18(6), pp.792–802. doi:https://doi.org/10.1016/s1470-2045(17)30251-6.
39. Chang, J. (2021). MHC multimer: A Molecular Toolbox for Immunologists. *Molecules and Cells*, 44(5), pp.328–334. doi:https://doi.org/10.14348/molcells.2021.0052.
40. Chen, C.-H., Tsai, C.-Y. and Pu, Y.-S. (2023). Primary Total Prostate Cryoablation for Localized High-Risk Prostate Cancer: 10-Year Outcomes and Nomograms. *Cancers*, [online] 15(15), pp.3873–3873. doi:https://doi.org/10.3390/cancers15153873.
41. Chinen, T., Kannan, A.K., Levine, A.G., Fan, X., Klein, U., Zheng, Y., Gasteiger, G., Feng, Y., Fontenot, J.D. and Rudensky, A.Y. (2016). An essential role for the IL-2 receptor in Treg cell function. *Nature Immunology*, 17(11), pp.1322–1333. doi:https://doi.org/10.1038/ni.3540.

REFERENCE LIST

42. Chong, Z.X., Yeap, S.K. and Ho, W.Y. (2021). Transfection types, methods and strategies: a technical review. *PeerJ*, 9(11165). doi:https://doi.org/10.7717/peerj.11165.
43. Chudley, L., McCann, K., Mander, A., Tjelle, T., Campos-Perez, J., Godeseth, R., Creak, A., Dobbyn, J., Johnson, B., Bass, P., Heath, C., Kerr, P., Mathiesen, I., Dearnaley, D., Stevenson, F. and Ottensmeier, C. (2012). DNA fusion-gene vaccination in patients with prostate cancer induces high-frequency CD8+ T-cell responses and increases PSA doubling time. *Cancer Immunology, Immunotherapy*, 61(11), pp.2161–2170. doi:https://doi.org/10.1007/s00262-012-1270-0.
44. Chulpanova, D.S., Kitaeva, K.V., Rutland, C.S., Rizvanov, A.A. and Solovyeva, V.V. (2020). Mouse Tumor Models for Advanced Cancer Immunotherapy. *International Journal of Molecular Sciences*, 21(11). doi:https://doi.org/10.3390/ijms21114118.
45. Cibrián, D. and Sánchez-Madrid, F. (2017). CD69: from activation marker to metabolic gatekeeper. *European Journal of Immunology*, [online] 47(6), pp.946–953. doi:https://doi.org/10.1002/eji.201646837.
46. Cogels, M.M., Rouas, R., Ghanem, G.E., Martinive, P., Awada, A., Van Gestel, D. and Krayem, M. (2021). Humanized Mice as a Valuable Pre-Clinical Model for Cancer Immunotherapy Research. *Frontiers in Oncology*, 11. doi:https://doi.org/10.3389/fonc.2021.784947.
47. Cooper, G.M. (2020). *The Development and Causes of Cancer*. [online] Nih.gov. Available at: https://www.ncbi.nlm.nih.gov/books/NBK9963/.
48. Cosma, G., McArdle, S.E., Foulds, G.A., Hood, S.P., Reeder, S., Johnson, C., Khan, M.A. and Pockley, A.G. (2021). Prostate Cancer: Early Detection and Assessing Clinical Risk Using Deep Machine Learning of High Dimensional Peripheral Blood Flow Cytometric Phenotyping Data. *Frontiers in Immunology*, 12(1). doi:https://doi.org/10.3389/fimmu.2021.786828.
49. Cosma, G., McArdle, S.E., Reeder, S., Foulds, G.A., Hood, S., Khan, M. and Pockley, A.G. (2017). Identifying the Presence of Prostate Cancer in Individuals with PSA Levels <20 ng ml−1 Using Computational Data Extraction Analysis of High Dimensional Peripheral Blood Flow Cytometric Phenotyping Data. *Frontiers in Immunology*, 8(1). doi:https://doi.org/10.3389/fimmu.2017.01771
50. Dai, S., Mo, Y., Wang, Y., Xiang, B., Liao, Q., Zhou, M., Li, X., Li, Y., Xiong, W., Li, G., Guo, C. and Zeng, Z. (2020). Chronic Stress Promotes Cancer Development. *Frontiers in Oncology*, 10(1492). doi:https://doi.org/10.3389/fonc.2020.01492.

REFERENCE LIST

51. de Winde, C.M., Munday, C. and Acton, S.E. (2020). Molecular mechanisms of dendritic cell migration in immunity and cancer. *Medical Microbiology and Immunology*, 209(4), pp.515–529. doi:https://doi.org/10.1007/s00430-020-00680-4.
52. Desai, K., McManus, J.M. and Sharifi, N. (2021). Hormonal Therapy for Prostate Cancer. *Endocrine Reviews*, 42(3). doi:https://doi.org/10.1210/endrev/bnab002.
53. dos, D., Jerónimo, C. and Correia, M.P. (2023). Epigenetic modulation and prostate cancer: Paving the way for NK cell anti-tumor immunity. *Frontiers in immunology*, 14(14). doi:https://doi.org/10.3389/fimmu.2023.1152572.
54. Dowling, C.E., Berthon Eliche and Bagasra, O. (2022). Effects of Amygdalin on prostate cancer. *Elsevier eBooks*, pp.591–609. doi:https://doi.org/10.1016/b978-0-323-90572-5.00022-6.
55. Drake, C.G., Amy, Mihalyo, M.A., Huang, C.-G., Kelleher, E.S., Ravi, S., Hipkiss, E.L., Flies, D.B., Kennedy, E.P., Long, M., McGary, P.D., Coryell, L., Nelson, W.G., Pardoll, D.M. and Adler, A.C. (2005). Androgen ablation mitigates tolerance to a prostate/prostate cancer-restricted antigen. *Cancer Cell*, 7(3), pp.239–249. doi:https://doi.org/10.1016/j.ccr.2005.01.027.
56. Einwallner, E., Subasic, A., Strasser, A., Augustin, D., Thalhammer, R., Steiner, I. and Schwarzinger, I. (2013). Lysis matters: Red cell lysis with FACS Lyse affects the flow cytometric enumeration of circulating leukemic blasts. *Journal of Immunological Methods*, 390(1-2), pp.127–132. doi:https://doi.org/10.1016/j.jim.2013.01.013.
57. Elsheikh, R., Makram, A.M. and Nguyen Tien Huy (2023). Therapeutic Cancer Vaccines and Their Future Implications. *Vaccines*, 11(3), pp.660–660. doi:https://doi.org/10.3390/vaccines11030660.
58. Enokida, T., Moreira, A. and Bhardwaj, N. (2021). Vaccines for immunoprevention of cancer. *Journal of Clinical Investigation*, 131(9). doi:https://doi.org/10.1172/jci146956.
59. Epstein, J.I., Zelefsky, M.J., Sjoberg, D.D., Nelson, J.B., Egevad, L., Magi-Galluzzi, C., Vickers, A.J., Parwani, A.V., Reuter, V.E., Fine, S.W., Eastham, J.A., Wiklund, P., Han, M., Reddy, C.A., Ciezki, J.P., Nyberg, T. and Klein, E.A. (2016). A Contemporary Prostate Cancer Grading System: A Validated Alternative to the Gleason Score. *European Urology*, 69(3), pp.428–435. doi:https://doi.org/10.1016/j.eururo.2015.06.046.
60. Esteban-Fabró, R., Willoughby, C.E., Piqué-Gili, M., Montironi, C., Abril-Fornaguera, J., Peix, J., Torrens, L., Mesropian, A., Balaseviciute, U., Miró-Mur, F., Mazzaferro, V., Pinyol, R. and

REFERENCE LIST

Llovet, J.M. (2022). Cabozantinib enhances anti-PD1 activity and elicits a neutrophil-based immune response in hepatocellular carcinoma. *Clinical cancer research : an official journal of the American Association for Cancer Research*, [online] 28(11), pp.2449–2460. doi:https://doi.org/10.1158/1078-0432.CCR-21-2517.

61. Fan, T., Zhang, M., Yang, J., Zhu, Z., Cao, W. and Dong, C. (2023). Therapeutic cancer vaccines: advancements, challenges, and prospects. *Signal Transduction and Targeted Therapy*, 8(1). doi:https://doi.org/10.1038/s41392-023-01674-3.
62. Feola, S., Chiaro, J., Martins, B. and Cerullo, V. (2020). Uncovering the Tumor Antigen Landscape: What to Know about the Discovery Process. *Cancers*, 12(6), p.1660. doi:https://doi.org/10.3390/cancers12061660.
63. Fleri, W., Paul, S., Dhanda, S.K., Mahajan, S., Xu, X., Peters, B. and Sette, A. (2017). The Immune Epitope Database and Analysis Resource in Epitope Discovery and Synthetic Vaccine Design. *Frontiers in Immunology*, 8(8). doi:https://doi.org/10.3389/fimmu.2017.00278.
64. Francesco Saverio Guerra, Eusebi, L., Bartelli, F., Cecchini, S., Paci, E. and Guglielmi, G. (2023). Staging of Prostate Cancer: Role of Multiparametric Magnetic Resonance Imaging in Different Risk Classes. *Urology Research and Practice*, [online] 49(4), pp.216–224. doi:https://doi.org/10.5152/tud.2023.22261.
65. Franklin, M.R., Platero, S., Saini, K.S., Curigliano, G. and Anderson, S. (2022). Immuno-oncology trends: preclinical models, biomarkers, and clinical development. *Journal for ImmunoTherapy of Cancer*, 10(1), p.e003231. doi:https://doi.org/10.1136/jitc-2021-003231.
66. Frederik Birkebæk Thomsen (2015). Active surveillance strategy for patients with localized prostate cancer: criteria for progression. *PubMed*, 62(2).
67. Fu, Y., Lin, Q., Zhang, Z. and Zhang, L. (2020). Therapeutic strategies for the costimulatory molecule OX40 in T-cell-mediated immunity. *Acta Pharmaceutica Sinica B*, 10(3), pp.414–433. doi:https://doi.org/10.1016/j.apsb.2019.08.010.
68. Fujita, K., Matsushita, M., De, M.A., Hatano, K., Minami, T., Norio Nonomura and Uemura, H. (2023). The Gut-Prostate Axis: A New Perspective of Prostate Cancer Biology through the Gut Microbiome. *Cancers*, 15(5), pp.1375–1375. doi:https://doi.org/10.3390/cancers15051375.
69. Galluzzi, L., Vacchelli, E., Pedro, J.-M.B.-S., Buqué, A., Senovilla, L., Baracco, E.E., Bloy, N., Castoldi, F., Abastado, J.-P., Agostinis, P., Apte, R.N., Aranda, F., Ayyoub, M., Beckhove, P.,

REFERENCE LIST

Blay, J.-Y., Bracci, L., Caignard, A., Castelli, C., Cavallo, F. and Celis, E. (2014). Classification of current anticancer immunotherapies. *Oncotarget*, 5(24), pp.12472–12508. doi:https://doi.org/10.18632/oncotarget.2998.

70. Gao, Y., Zhang, M., Li, X., Zeng, P., Wang, P. and Zhang, L. (2019). Serum PSA levels in patients with prostate cancer and other 33 different types of diseases. *Progress in Molecular Biology and Translational Science*, [online] 162(1), pp.377–390. doi:https://doi.org/10.1016/bs.pmbts.2018.12.013.
71. Ge, C., Yan, J., Yuan, X. and Xu, G. (2022). A positive feedback loop between tryptophan hydroxylase 1 and β-Catenin/ZBP-89 signaling promotes prostate cancer progression. *Frontiers in Oncology*, [online] 12(12), p.923307. doi:https://doi.org/10.3389/fonc.2022.923307.
72. Golombos, D.M., Ayangbesan, A., O'Malley, P., Lewicki, P., Barlow, L., Barbieri, C.E., Chan, C., DuLong, C., Abu-Ali, G., Huttenhower, C. and Scherr, D.S. (2018). The Role of Gut Microbiome in the Pathogenesis of Prostate Cancer: A Prospective, Pilot Study. *Urology*, [online] 111(111), pp.122–128. doi:https://doi.org/10.1016/j.urology.2017.08.039.
73. Golubovskaya, V. and Wu, L. (2016). Different Subsets of T Cells, Memory, Effector Functions, and CAR-T Immunotherapy. *Cancers*, 8(3), p.36. doi:https://doi.org/10.3390/cancers8030036.
74. Gong, J., Kim, D.M., Freeman, M.R., Kim, H., Ellis, L., Smith, B., Theodorescu, D., Posadas, E., Figlin, R., Bhowmick, N. and Freedland, S.J. (2023). Genetic and biological drivers of prostate cancer disparities in Black men. *Nature Reviews Urology*, [online] pp.1–16. doi:https://doi.org/10.1038/s41585-023-00828-w.
75. Gubser, C., Pascoe, R.D., Chang, J., Chiu, C., Solomon, A., Cao, R., Rasmussen, T.A. and Lewin, S.R. (2023). GITR activation ex vivo impairs CD8 T cell function in people with HIV on antiretroviral therapy. *iScience*, [online] 26(11), p.108165. doi:https://doi.org/10.1016/j.isci.2023.108165.
76. Guerin, M.V., Finisguerra, V., Van den Eynde, B.J., Bercovici, N. and Trautmann, A. (2020). Preclinical murine tumor models: A structural and functional perspective. *eLife*, [online] 9, p.e50740. doi:https://doi.org/10.7554/eLife.50740.

REFERENCE LIST

77. Guillem Montamat, Leonard, C., Poli, A., Klimek, L. and Ollert, M. (2021). CpG Adjuvant in Allergen-Specific Immunotherapy: Finding the Sweet Spot for the Induction of Immune Tolerance. *Frontiers in Immunology*, 12. doi:https://doi.org/10.3389/fimmu.2021.590054.
78. Gulley, J.L., Borre, M., Vogelzang, N.J., Ng, S., Agarwal, N., Parker, C., Pook, D., Per Rathenborg, Flaig, T.W., Carles, J., Saad, F., Shore, N.D., Chen, L., Heery, C.R., Gerritsen, W.R., Priou, F., Langkilde, N.C., Novikov, A. and Kantoff, P.W. (2019). Phase III Trial of PROSTVAC in Asymptomatic or Minimally Symptomatic Metastatic Castration-Resistant Prostate Cancer. *Journal of Clinical Oncology*, [online] 37(13), pp.1051–1061. doi:https://doi.org/10.1200/jco.18.02031.
79. Guo, L., Liu, X. and Su, X. (2023). The role of TEMRA cell-mediated immune senescence in the development and treatment of HIV disease. *Frontiers in immunology*, 14(1). doi:https://doi.org/10.3389/fimmu.2023.1284293.
80. Gurel, B., Lucia, M.S., Thompson, I.M., Goodman, P.J., Tangen, C.M., Kristal, A.R., Parnes, H.L., Hoque, A., Lippman, S.M., Sutcliffe, S., Peskoe, S.B., Drake, C.G., Nelson, W.G., De Marzo, A.M. and Platz, E.A. (2014). Chronic Inflammation in Benign Prostate Tissue Is Associated with High-Grade Prostate Cancer in the Placebo Arm of the Prostate Cancer Prevention Trial. *Cancer Epidemiology Biomarkers & Prevention*, 23(5), pp.847–856. doi:https://doi.org/10.1158/1055-9965.epi-13-1126.
81. Haffner, M.C., Zwart, W., Roudier, M.P., True, L.D., Nelson, W.G., Epstein, J.I., De Marzo, A.M., Nelson, P.S. and Yegnasubramanian, S. (2020). Genomic and phenotypic heterogeneity in prostate cancer. *Nature Reviews Urology*, [online] 18(2), pp.1–14. doi:https://doi.org/10.1038/s41585-020-00400-w.
82. Hagiwara, A., Nakamura, Y., Nishimoto, R., Ueno, S. and Miyagi, Y. (2020). Induction of tryptophan hydroxylase in the liver of s.c. tumor model of prostate cancer. *Cancer Science*, [online] 111(4), pp.1218–1227. doi:https://doi.org/10.1111/cas.14333.
83. Han, H. (2018). RNA Interference to Knock Down Gene Expression. *Methods in Molecular Biology*, 1706, pp.293–302. doi:https://doi.org/10.1007/978-1-4939-7471-9_16.
84. Hanley, P.J. (2023). Elusive physiological role of prostatic acid phosphatase (PAP): generation of choline for sperm motility via auto-and paracrine cholinergic signaling. *Frontiers in Physiology*, [online] 14. doi:https://doi.org/10.3389/fphys.2023.1327769.

REFERENCE LIST

85. Hay, Z.L.Z. and Slansky, J.E. (2022). Granzymes: The Molecular Executors of Immune-Mediated Cytotoxicity. *International Journal of Molecular Sciences*, 23(3), p.1833. doi:https://doi.org/10.3390/ijms23031833.
86. Hegde, S., Leader, A.M. and Mérad, M. (2021). MDSC: Markers, development, states, and unaddressed complexity. *Immunity*, 54(5), pp.875–884. doi:https://doi.org/10.1016/j.immuni.2021.04.004.
87. Heimberger, A., Brat, D. and Lesniak, M. (2023). Next-generation antigen-presenting cell immune therapeutics for gliomas. *Journal of Clinical Investigation*, 1(1). doi:https://doi.org/10.1172/JCI163449.
88. Helene Hartvedt Grytli, Fagerland, M.W., Fosså, S.D. and Kristin Austlid Taskén (2014). Association Between Use of β-Blockers and Prostate Cancer–Specific Survival: A Cohort Study of 3561 Prostate Cancer Patients with High-Risk or Metastatic Disease. *European Urology*, 65(3), pp.635–641. doi:https://doi.org/10.1016/j.eururo.2013.01.007.
89. Henrik Ugge, Downer, M.K., Carlsson, J., Bowden, M., Davidsson, S., Mucci, L.A., Fall, K., Andersson, S. and Ove Andrén (2019). Circulating inflammation markers and prostate cancer. *The prostate*, 79(11), pp.1338–1346. doi:https://doi.org/10.1002/pros.23842.
90. Henry, G.H., Malewska, A., Joseph, D.B., Malladi, V.S., Lee, J., Torrealba, J., Mauck, R.J., Gahan, J.C., Raj, G.V., Roehrborn, C.G., Hon, G.C., MacConmara, M.P., Reese, J.C., Hutchinson, R.C., Vezina, C.M. and Strand, D.W. (2018). A Cellular Anatomy of the Normal Adult Human Prostate and Prostatic Urethra. *Cell Reports*, [online] 25(12), pp.3530-3542.e5. doi:https://doi.org/10.1016/j.celrep.2018.11.086.
91. Hensel, J.A., Khattar, V., Ashton, R. and Ponnazhagan, S. (2018). Characterization of immune cell subtypes in three commonly used mouse strains reveals gender and strain-specific variations. *Laboratory Investigation*, 99(1), pp.93–106. doi:https://doi.org/10.1038/s41374-018-0137-1.
92. Higano, C.S., Schellhammer, P.F., Small, E.J., Burch, P.A., Nemunaitis, J., Yuh, L., Provost, N. and Frohlich, M.W. (2009). Integrated data from 2 randomized, double-blind, placebo-controlled, phase 3 trials of active cellular immunotherapy with sipuleucel-T in advanced prostate cancer. *Cancer*, 115(16), pp.3670–3679. doi:https://doi.org/10.1002/cncr.24429.

REFERENCE LIST

93. Hinata, N. and Fujisawa, M. (2022). Racial Differences in Prostate Cancer Characteristics and Cancer-Specific Mortality: An Overview. *The World Journal of Men's Health*, 40(2), p.217. doi:https://doi.org/10.5534/wjmh.210070.

94. Höfer, T., Krichevsky, O. and Altan-Bonnet, G. (2012). Competition for IL-2 between Regulatory and Effector T Cells to Chisel Immune Responses. *Frontiers in Immunology*, [online] 3(1). doi:https://doi.org/10.3389/fimmu.2012.00268.

95. Hu, Y., Liu, J., Cui, P., Liu, T., Piao, C., Xu, X., Zhang, Q., Xiao, M., Lu, Y., Liu, X., Wang, Y. and Lu, X. (2020). Synergistic effect of adoptive immunotherapy and docetaxel inhibits tumor growth in a mouse model. *Cellular Immunology*, 348(1), pp.104036–104036. doi https://doi.org/10.1016/j.cellimm.2019.104036.

96. Huang, C., Shao, N., Huang, Y., Chen, J., Wang, D., Hu, G., Zhang, H., Luo, L. and Xiao, Z. (2023). Overcoming challenges in the delivery of STING agonists for cancer immunotherapy: A comprehensive review of strategies and future perspectives. *Materials Today Bio*, 23, pp.100839–100839. doi:https://doi.org/10.1016/j.mtbio.2023.100839.

97. Irshad, S. and Abate-Shen, C. (2012). Modeling prostate cancer in mice: something old, something new, something premalignant, something metastatic. *Cancer and Metastasis Reviews*, 32(1-2), pp.109–122. doi:https://doi.org/10.1007/s10555-012-9409-1.

98. Ishibashi, A., Saga, K., Hisatomi, Y., Li, Y., Kaneda, Y. and Nimura, K. (2020). A simple method using CRISPR-Cas9 to knock-out genes in murine cancerous cell lines. *Scientific Reports*, 10(1), p.22345. doi:https://doi.org/10.1038/s41598-020-79303-0.

99. Iuchi, K., Oya, K., Hosoya, K., Sasaki, K., Sakurada, Y., Nakano, T. and Hisatomi, H. (2019). Different morphologies of human embryonic kidney 293T cells in various types of culture dishes. *Cytotechnology*, 72(1), pp.131–140. doi:https://doi.org/10.1007/s10616-019-00363-w.

100. Jachetti, E., Mazzoleni, S., Grioni, M., Ricupito, A., Brambillasca, C., Generoso, L., Calcinotto, A., Freschi, M., Mondino, A., Galli, R. and Bellone, M. (2013). Prostate cancer stem cells are targets of both innate and adaptive immunity and elicit tumor-specific immune responses. *OncoImmunology*, 2(5), p.e24520. doi:https://doi.org/10.4161/onci.24520.

101. Jain, M. and Sapra, A. (2020). Cancer Prostate Screening. *Prostate Cancer Screening*. [online] Available at: https://www.ncbi.nlm.nih.gov/books/NBK556081/.

REFERENCE LIST

102. Jain, S., Dash, P., Minz, A.P., Satpathi, S., Samal, A.G., Behera, P.K., Satpathi, P.S. and Senapati, S. (2018). Lipopolysaccharide (LPS) enhances prostate cancer metastasis potentially through NF-κB activation and recurrent dexamethasone administration fails to suppress it in vivo. *The Prostate*, 79(2), pp.168–182. doi:https://doi.org/10.1002/pros.23722.

103. Jameson, S.C. and Masopust, D. (2018). Understanding Subset Diversity in T Cell Memory. *Immunity*, 48(2), pp.214–226. doi:https://doi.org/10.1016/j.immuni.2018.02.010.

104. Jayusman, P.A., Mohamed, I.N. and Shuid, A.N. (2018). The Effects of Chemical Castration with Degarelix on Bone Turnover: Densitometric and Biomechanics Bone Properties of Male Rats. *International Journal of Endocrinology and Metabolism*, 16(3). doi:https://doi.org/10.5812/ijem.64038.

105. Jiang, Y., Li, Y. and Zhu, B. (2015). T-cell exhaustion in the tumor microenvironment. *Cell Death & Disease*, 6(6), pp.e1792–e1792. doi:https://doi.org/10.1038/cddis.2015.162.

106. Jie, J., Zhang, Y., Zhou, H., Zhai, X., Zhang, N., Yuan, H., Ni, W. and Tai, G. (2018). CpG ODN1826 as a Promising Mucin1-Maltose-Binding Protein Vaccine Adjuvant Induced DC Maturation and Enhanced Antitumor Immunity. *International Journal of Molecular Sciences*, [online] 19(3), p.920. doi:https://doi.org/10.3390/ijms19030920.

107. Jou, E., Chaudhury, N. and Nasim, F. (2024). Novel therapeutic strategies targeting myeloid-derived suppressor cell immunosuppressive mechanisms for cancer treatment. *Exploration of Targeted Anti-tumor Therapy*, [online] 5(1), pp.187–207. doi:https://doi.org/10.37349/etat.2024.00212.

108. Jubelin, C., Muñoz-Garcia, J., Griscom, L., Cochonneau, D., Ollivier, E., Heymann, M.-F., Vallette, F.M., Oliver, L. and Heymann, D. (2022). Three-dimensional in vitro culture models in oncology research. *Cell & Bioscience*, 12(1). doi:https://doi.org/10.1186/s13578-022-00887-3.

109. Kaczmarek, M., Poznańska, J., Fechner, F., Michalska, N., Paszkowska, S., Napierała, A. and Mackiewicz, A. (2023). Cancer Vaccine Therapeutics: Limitations and Effectiveness—A Literature Review. *Cells*, 12(17), p.2159. doi:https://doi.org/10.3390/cells12172159.

110. Kantoff, P.W., Gulley, J.L. and Pico-Navarro, C. (2017). Revised Overall Survival Analysis of a Phase II, Randomized, Double-Blind, Controlled Study of PROSTVAC in Men

REFERENCE LIST

With Metastatic Castration-Resistant Prostate Cancer. *Journal of Clinical Oncology*, 35(1), pp.124–125. doi:https://doi.org/10.1200/jco.2016.69.7748.

111. Kantoff, P.W., Higano, C.S., Shore, N.D., Berger, E.R., Small, E.J., Penson, D.F., Redfern, C.H., Ferrari, A.C., Dreicer, R., Sims, R.B., Xu, Y., Frohlich, M.W. and Schellhammer, P.F. (2010). Sipuleucel-T Immunotherapy for Castration-Resistant Prostate Cancer. *New England Journal of Medicine*, 363(5), pp.411–422. doi:https://doi.org/10.1056/nejmoa1001294.

112. Kapałczyńska, M., Kolenda, T., Przybyła, W., Zajączkowska, M., Teresiak, A., Filas, V., Ibbs, M., Bliźniak, R., Łuczewski, Ł. and Lamperska, K. (2016). 2D and 3D cell cultures – a comparison of different types of cancer cell cultures. *Archives of Medical Science*, 14(4). doi:https://doi.org/10.5114/aoms.2016.63743.

113. Karimi, M.A., Lee, E., Bachmann, M.H., Salicioni, A.M., Behrens, E.M., Kambayashi, T. and Baldwin, C.L. (2014). Measuring Cytotoxicity by Bioluminescence Imaging Outperforms the Standard Chromium-51 Release Assay. *PLoS ONE*, 9(2), p.e89357. doi:https://doi.org/10.1371/journal.pone.0089357.

114. Kazuyuki Numakura, Kobayashi, M., Muto, Y., Sato, H., Sekine, Y., Ryuta Sobu, Aoyama, Y., Takahashi, Y., Okada, S., Hajime Sasagawa, Narita, S., Kumagai, S., Wada, Y., Mori, N. and Tomonori Habuchi (2023). The Current Trend of Radiation Therapy for Patients with Localized Prostate Cancer. *Current Oncology*, 30(9), pp.8092–8110. doi:https://doi.org/10.3390/curroncol30090587.

115. Kennedy, E. and Niedzwiedz, C.L. (2022). The association of anxiety and stress-related disorders with C-reactive protein (CRP) within UK Biobank. *Brain, Behavior, & Immunity - Health*, 19(1), p.100410. doi:https://doi.org/10.1016/j.bbih.2021.100410.

116. Khong, H. and Overwijk, W.W. (2016). Adjuvants for peptide-based cancer vaccines. *Journal for ImmunoTherapy of Cancer*, 4(1). doi:https://doi.org/10.1186/s40425-016-0160-y.

117. Koh, C., Lee, S., Kwak, M., Kim, I. and Chung, Y. (2023). CD8 T-cell subsets: heterogeneity, functions, and therapeutic potential. *Experimental & Molecular Medicine*, 55(11), pp.2287–2299. doi:https://doi.org/10.1038/s12276-023-01105-x.

118. Koinis, F., Xagara, A., Chantzara, E., Leontopoulou, V., Aidarinis, C. and Kotsakis, A. (2022). Myeloid-Derived Suppressor Cells in Prostate Cancer: Present Knowledge and Future Perspectives. *Cells*, 11(1), p.20. doi:https://doi.org/10.3390/cells11010020.

REFERENCE LIST

119. Komori, T., Hata, S., Akira Mabuchi, Genova, M., Harada, T., Fukuyama, M., Chinen, T. and Kitagawa, D. (2023). A CRISPR-del-based pipeline for complete gene knockout in human diploid cells. *Journal of Cell Science*, 136(6). doi:https://doi.org/10.1242/jcs.260000.

120. Kong, H.Y. and Byun, J. (2013). Emerging Roles of Human Prostatic Acid Phosphatase. *Biomolecules and Therapeutics*, [online] 21(1), pp.10–20. doi:https://doi.org/10.4062/biomolther.2012.095.

121. Kumar, B.V., Connors, T. and Farber, D.L. (2018). Human T cell development, localization, and function throughout life. *Immunity*, 48(2), pp.202–213. doi:https://doi.org/10.1016/j.immuni.2018.01.007.

122. Kwon, E.D., Drake, C.G., Scher, H.I., Fizazi, K., Bossi, A., van den Eertwegh, A.J.M., Krainer, M., Houede, N., Santos, R., Mahammedi, H., Ng, S., Maio, M., Franke, F.A., Sundar, S., Agarwal, N., Bergman, A.M., Ciuleanu, T.E., Korbenfeld, E., Sengelov, L. and Hansen, S. (2014). Ipilimumab versus placebo after radiotherapy in patients with metastatic castration-resistant prostate cancer that had progressed after docetaxel chemotherapy (CA184-043): a multicentre, randomised, double-blind, phase 3 trial. *The Lancet Oncology*, 15(7), pp.700–712. doi:https://doi.org/10.1016/s1470-2045(14)70189-5.

123. Lampreht Tratar, U., Horvat, S. and Cemazar, M. (2018). Transgenic Mouse Models in Cancer Research. *Frontiers in Oncology*, 8(268). doi:https://doi.org/10.3389/fonc.2018.00268.

124. Le Vu, P., Vadakekolathu, J., Idri, S., Nicholls, H., Cavaignac, M., Reeder, S., Khan, M.A., Christensen, D., Pockley, A.G. and McArdle, S.E. (2022). A Mutated Prostatic Acid Phosphatase (PAP) Peptide-Based Vaccine Induces PAP-Specific CD8+ T Cells with Ex Vivo Cytotoxic Capacities in HHDII/DR1 Transgenic Mice. *Cancers*, 14(8), p.1970. doi:https://doi.org/10.3390/cancers14081970.

125. Lechner, M.G., Karimi, S.S., Keegan Barry-Holson, Angell, T.E., Murphy, K.A., Church, C.H., Ohlfest, J.R., Hu, P. and Epstein, A.L. (2013). Immunogenicity of Murine Solid Tumor Models as a Defining Feature of In Vivo Behavior and Response to Immunotherapy. *Journal of Immunotherapy*,36(9),pp.477–489. doi:https://doi.org/10.1097/01.cji.0000436722.46675.4a.

126. Lee, J.W. and Chung, M.J. (2022). Prostate only radiotherapy using external beam radiotherapy: A clinician's perspective. *World Journal of Clinical Cases*, 10(29), pp.10428–10434. doi:https://doi.org/10.12998/wjcc.v10.i29.10428.

REFERENCE LIST

127. Lerner, E.C., Woroniecka, K.I., D'Anniballe, V.M., Wilkinson, D.S., Mohan, A.A., Lorrey, S.J., Waibl-Polania, J., Wachsmuth, L.P., Miggelbrink, A.M., Jackson, J.D., Cui, X., Raj, J.A., Tomaszewski, W.H., Cook, S.L., Sampson, J.H., Patel, A.P., Khasraw, M., Gunn, M.D. and Fecci, P.E. (2023). CD8+ T cells maintain killing of MHC-I-negative tumor cells through the NKG2D–NKG2DL axis. *Nature Cancer*, [online] 4(9), pp.1258–1272. doi:https://doi.org/10.1038/s43018-023-00600-4.

128. Li, D., Xu, W., Chang, Y., Xiao, Y., He, Y. and Ren, S. (2023). Advances in landscape and related therapeutic targets of the prostate tumor microenvironment. *Acta Biochimica et Biophysica Sinica*, [online] 55(6), pp.956–973. doi:https://doi.org/10.3724/abbs.2023092.

129. Li, X., Wang, Y., Li, J., Xinyue, M., Liu, Y. and Huang, H. (2022). qPCRtools: An R package for qPCR data processing and visualization. *Frontiers in Genetics*, 13. doi:https://doi.org/10.3389/fgene.2022.1002704.

130. Li, Y., Wang, W., Yang, F., Xu, Y., Feng, C. and Zhao, Y. (2019). The regulatory roles of neutrophils in adaptive immunity. *Cell Communication and Signaling*, 17(1). doi:https://doi.org/10.1186/s12964-019-0471-y.

131. Lin, M.J., Svensson-Arvelund, J., Lubitz, G.S., Marabelle, A., Melero, I., Brown, B.D. and Brody, J.D. (2022). Cancer vaccines: the next immunotherapy frontier. *Nature Cancer*, 3(8), pp.911–926. doi:https://doi.org/10.1038/s43018-022-00418-6.

132. Lin, Y., Xu, J. and Lan, H. (2019). Tumor-associated macrophages in tumor metastasis: biological roles and clinical therapeutic applications. *Journal of Hematology & Oncology*, 12(1). doi:https://doi.org/10.1186/s13045-019-0760-3.

133. Liu, J., Dong, B., Qu, W., Wang, J., Xu, Y., Yu, S. and Zhang, X. (2020). Using clinical parameters to predict prostate cancer and reduce the unnecessary biopsy among patients with PSA in the gray zone. *Scientific Reports*, [online] 10(1), p.5157. doi:https://doi.org/10.1038/s41598-020-62015-w.

134. Liu, J., Fu, M., Wang, M., Wan, D., Wei, Y. and Wei, X. (2022). Cancer vaccines as promising immuno-therapeutics: platforms and current progress. *Journal of Hematology & Oncology*, 15(1). doi:https://doi.org/10.1186/s13045-022-01247-x.

135. Liu, Y., Wu, W., Cai, C., Zhang, H., Shen, H. and Han, Y. (2023). Patient-derived xenograft models in cancer therapy: technologies and applications. *Signal Transduction and Targeted Therapy*, 8(1), pp.1–24. doi:https://doi.org/10.1038/s41392-023-01419-2.

REFERENCE LIST

136. Long, L., Zhang, X., Chen, F., Pan, Q., Phiphatwatchara, P., Zeng, Y. and Chen, H. (2018). The promising immune checkpoint LAG-3: from tumor microenvironment to cancer immunotherapy. *Genes & Cancer*, 9(5). doi:https://doi.org/10.18632/genesandcancer.180.

137. Look, T., Meister, H., Weller, M. and Weiss, T. (2023). Protocol for the expansion of mouse immune effector cells for in vitro and in vivo studies. *STAR Protocols*, [online] 4(4), p.102700. doi:https://doi.org/10.1016/j.xpro.2023.102700.

138. LUO, Z., SHI, H., ZHANG, H., LI, M., ZHAO, Y., ZHANG, J., GUO, F., LUO, S., SUN, P., ZHANG, D., QIAN, Z. and YANG, L. (2012). Plasmid DNA containing multiple CpG motifs triggers a strong immune response to hepatitis B surface antigen when combined with incomplete Freund's adjuvant but not aluminum hydroxide. *Molecular Medicine Reports*, 6(6), pp.1309–1314. doi:https://doi.org/10.3892/mmr.2012.1079.

139. Madan, R.A. and Gulley, J.L. (2011). Sipuleucel-T: harbinger of a new age of therapeutics for prostate cancer. *Expert review of vaccines*, [online] 10(2), pp.141–150. doi:https://doi.org/10.1586/erv.10.173.

140. Magi-Galluzzi, C. (2018). Prostate cancer: diagnostic criteria and role of immunohistochemistry. *Modern Pathology*, 31(S1), pp.12–21. doi:https://doi.org/10.1038/modpathol.2017.139.

141. Magnon, C., Hall, S.J., Lin, J., Xue, X., Gerber, L., Freedland, S.J. and Frenette, P.S. (2013). Autonomic Nerve Development Contributes to Prostate Cancer Progression. *Science*, 341(6142), pp.1236361–1236361. doi:https://doi.org/10.1126/science.1236361.

142. Mandel, P., Wenzel, M., Hoeh, B., Welte, M.N., Preisser, F., Inam, T., Wittler, C., Humke, C., Köllermann, J., Wild, P., Würnschimmel, C., Tilki, D., Graefen, M., Kluth, L.A., Karakiewicz, P.I., Chun, F.K.-H. . and Becker, A. (2021). Immunohistochemistry for Prostate Biopsy—Impact on Histological Prostate Cancer Diagnoses and Clinical Decision Making. *Current Oncology*, [online] 28(3), pp.2123–2133. doi:https://doi.org/10.3390/curroncol28030197.

143. Mangalam, A.K., Rodriguez, M. and David, C.S. (2006). Role of MHC class II expressing CD4+ T cells in proteolipid protein91–110-induced EAE in HLA-DR3 transgenic mice. *European Journal of Immunology*, 36(12), pp.3356–3370. doi:https://doi.org/10.1002/eji.200636217.

REFERENCE LIST

144. Mao, C., Ding, Y. and Xu, N. (2021). A Double-Edged Sword Role of Cytokines in Prostate Cancer Immunotherapy. *Frontiers in Oncology*, 11(1). doi:https://doi.org/10.3389/fonc.2021.688489.

145. Martini, M., Testi, M.G., Pasetto, M., Picchio, M.C., Innamorati, G., Mazzocco, M., Ugel, S., Cingarlini, S., Bronte, V., Zanovello, P., Krampera, M., Mosna, F., Cestari, T., Riviera, A.P., Brutti, N., Barbieri, O., Matera, L., Tridente, G., Colombatti, M. and Sartoris, S. (2010). IFN-γ-mediated upmodulation of MHC class I expression activates tumor-specific immune response in a mouse model of prostate cancer. *Vaccine*, 28(20), pp.3548–3557. doi:https://doi.org/10.1016/j.vaccine.2010.03.007.

146. Maruhashi, T., Sugiura, D., Okazaki, I. and Okazaki, T. (2020). LAG-3: from molecular functions to clinical applications. *Journal for ImmunoTherapy of Cancer*, 8(2), p.e001014. doi:https://doi.org/10.1136/jitc-2020-001014.

147. Mastelic-Gavillet, B., Navarro Rodrigo, B., Décombaz, L., Wang, H., Ercolano, G., Ahmed, R., Lozano, L.E., Ianaro, A., Derré, L., Valerio, M., Tawadros, T., Jichlinski, P., Nguyen-Ngoc, T., Speiser, D.E., Verdeil, G., Gestermann, N., Dormond, O., Kandalaft, L., Coukos, G. and Jandus, C. (2019). Adenosine mediates functional and metabolic suppression of peripheral and tumor-infiltrating CD8+ T cells. *Journal for ImmunoTherapy of Cancer*, 7(1). doi:https://doi.org/10.1186/s40425-019-0719-5.

148. Mateusz Kciuk, Esam Bashir Yahya, Ibrahim, M., Rashid, S., Muhammad Omer Iqbal, Kontek, R., Abdulsamad, M.A. and Allaq, A.A. (2023). Recent Advances in Molecular Mechanisms of Cancer Immunotherapy. *Cancers*, 15(10), pp.2721–2721. doi:https://doi.org/10.3390/cancers15102721.

149. McArdle, S. (2009). Cancer vaccines: Uses of HLA transgenic mice compared to genetically modified mice. *Frontiers in Bioscience*, Volume(14), p.4640. doi:https://doi.org/10.2741/3556.

150. McArdle, S.E., Pockley, A.G., Gibson, G.R. and Rees, R.C. (2014). Prostate cancer. *OncoImmunology*, 3(3), p.e28049. doi:https://doi.org/10.4161/onci.28049.

151. McNeel, D.G., Dunphy, E.J., Davies, J.G., Frye, T., Johnson, L.E., Mary Jane Staab, Horvath, D., Straus, J., Alberti, D., Marnocha, R., Liu, G., Eickhoff, J. and Wilding, G. (2009). Safety and Immunological Efficacy of a DNA Vaccine Encoding Prostatic Acid Phosphatase

REFERENCE LIST

in Patients With Stage D0 Prostate Cancer. *Journal of Clinical Oncology*, 27(25), pp.4047–4054. doi:https://doi.org/10.1200/jco.2008.19.9968.

152. McNeel, D.G., Eickhoff, J.C., Johnson, L.E., Roth, A.R., Perk, T.G., Fong, L., Antonarakis, E.S., Wargowski, E., Jeraj, R. and Liu, G. (2019). Phase II Trial of a DNA Vaccine Encoding Prostatic Acid Phosphatase (pTVG-HP [MVI-816]) in Patients With Progressive, Nonmetastatic, Castration-Sensitive Prostate Cancer. *Journal of Clinical Oncology*, [online] 37(36), pp.3507–3517. doi:https://doi.org/10.1200/jco.19.01701.

153. McNeel, D.G., Emamekhoo, H., Eickhoff, J.C., Kyriakopoulos, C.E., Wargowski, E., Tonelli, T.P., Johnson, L.E. and Liu, G. (2023). Phase 2 trial of a DNA vaccine (pTVG-HP) and nivolumab in patients with castration-sensitive non-metastatic (M0) prostate cancer. *Journal for Immunotherapy of Cancer*, [online] 11(12), p.e008067. doi:https://doi.org/10.1136/jitc-2023-008067.

154. Melief, C.J.M. and van der Burg, S.H. (2008). Immunotherapy of established (pre)malignant disease by synthetic long peptide vaccines. *Nature Reviews Cancer*, 8(5), pp.351–360. doi:https://doi.org/10.1038/nrc2373.

155. Melief, C.J.M., van Hall, T., Arens, R., Ossendorp, F. and van der Burg, S.H. (2015). Therapeutic cancer vaccines. *Journal of Clinical Investigation*, 125(9), pp.3401–3412. doi:https://doi.org/10.1172/jci80009.

156. Melssen, M.M., Fisher, C.T., Slingluff, C.L. and Cornelis J.M. Melief (2022). Peptide emulsions in incomplete Freund's adjuvant create effective nurseries promoting egress of systemic $CD4^{+}$and $CD8^{+}$T cells for immunotherapy of cancer. *Journal for ImmunoTherapy of Cancer*, 10(9), pp.e004709–e004709. doi:https://doi.org/10.1136/jitc-2022-004709.

157. Messex, J.K. and Liou, G.-Y. (2023). Impact of Immune Cells in the Tumor Microenvironment of Prostate Cancer Metastasis. *Life*, 13(2), p.333. doi:https://doi.org/10.3390/life13020333.

158. Michalaki, V., Syrigos, K., Charles, P. and Waxman, J. (2004). Serum levels of IL-6 and TNF-α correlate with clinicopathological features and patient survival in patients with prostate cancer. *British Journal of Cancer*, 90(12), pp.2312–2316. doi:https://doi.org/10.1038/sj.bjc.6601814.

159. Millrud, C.R., Bergenfelz, C. and Leandersson, K. (2017). On the origin of myeloid-derived suppressor cells. *Oncotarget*, 8(2). doi:https://doi.org/10.18632/oncotarget.12278.

REFERENCE LIST

160. Mirabelli, P., Coppola, L. and Salvatore, M. (2019). Cancer Cell Lines Are Useful Model Systems for Medical Research. *Cancers*, 11(8). doi:https://doi.org/10.3390/cancers11081098.

161. Mo, R., Han, Z., Liang, Y., Ye, J., Wu, S., Lin, S.X., Zhang, Y., Song, S., Jiang, F., Zhong, W. and Wu, C. (2019). Expression of PD-L1 in tumor-associated nerves correlates with reduced $CD8^{+}$tumor-associated lymphocytes and poor prognosis in prostate cancer. *International Journal of Cancer*, 144(12), pp.3099–3110. doi:https://doi.org/10.1002/ijc.32061.

162. Morath, A. and Schamel, W.W. (2020). αβ and γδ T cell receptors: Similar but different. *Journal of Leukocyte Biology*, 107(6), pp.1045–1055. doi:https://doi.org/10.1002/jlb.2mr1219-233r.

163. Mori, K., Kimura, S., Parizi, M.K., Enikeev, D.V., Glybochko, P.V., Seebacher, V., Fajkovic, H., Mostafaei, H., Lysenko, I., Janisch, F., Egawa, S. and Shariat, S.F. (2019). Prognostic Value of Lactate Dehydrogenase in Metastatic Prostate Cancer: A Systematic Review and Meta-analysis. *Clinical Genitourinary Cancer*, 17(6). doi:https://doi.org/10.1016/j.clgc.2019.07.009.

164. Moya, L., Walpole, C., Rae, F., Srinivasan, S., Seim, I., Lai, J., Nicol, D., Williams, E.D., Clements, J.A. and Batra, J. (2023). Characterisation of cell lines derived from prostate cancer patients with localised disease. *Prostate Cancer and Prostatic Diseases*, [online] 26(3), pp.614–624. doi:https://doi.org/10.1038/s41391-023-00679-x.

165. Muniyan, S., Chaturvedi, N., Dwyer, J., LaGrange, C., Chaney, W. and Lin, M.-F. (2013). Human Prostatic Acid Phosphatase: Structure, Function and Regulation. *International Journal of Molecular Sciences*, [online] 14(5), pp.10438–10464. doi:https://doi.org/10.3390/ijms140510438.

166. Murray, T.B.J. (2021). *The Pathogenesis of Prostate Cancer*. [online] PubMed. Available at: https://www.ncbi.nlm.nih.gov/books/NBK571321/.

167. Nanda, N.K., Birch, L., Greenberg, N.M. and Prins, G.S. (2006). MHC class I and class II molecules are expressed in both human and mouse prostate tumor microenvironment. *The Prostate*, 66(12), pp.1275–1284. doi:https://doi.org/10.1002/pros.20432.

168. Nelde, A., Rammensee, H.-G. and Walz, J.S. (2021). The Peptide Vaccine of the Future. *Molecular &Cellular Proteomics*,20,p.100022. doi:https://doi.org/10.1074/mcp.r120.002309.

REFERENCE LIST

169. Ness, N., Andersen, S., Valkov, A., Nordby, Y., Donnem, T., Al-Saad, S., Busund, L.-T., Bremnes, R.M. and Richardsen, E. (2014). Infiltration of CD8+ lymphocytes is an independent prognostic factor of biochemical failure-free survival in prostate cancer. *The Prostate*, 74(14), pp.1452–1461. doi:https://doi.org/10.1002/pros.22862.

170. Ng, K.L. (2021). *The Etiology of Prostate Cancer*. [online] PubMed. Available at: https://www.ncbi.nlm.nih.gov/books/NBK571322/.

171. Nguyen, H., Hird, K., Cardaci, J., Smith, S. and Lenzo, N.P. (2024). Lutetium-177 Labelled Anti-PSMA Monoclonal Antibody (Lu-TLX591) Therapy for Metastatic Prostate Cancer: Treatment Toxicity and Outcomes. *Molecular diagnosis & therapy*, 28(1). doi:https://doi.org/10.1007/s40291-024-00699-w.

172. Nishana, M. and Raghavan, S.C. (2012). Role of recombination activating genes in the generation of antigen receptor diversity and beyond. *Immunology*, 137(4), pp.271–281. doi:https://doi.org/10.1111/imm.12009.

173. Niu, Y., Förster, S. and Muders, M. (2022). The Role of Perineural Invasion in Prostate Cancer and Its Prognostic Significance. *Cancers*, 14(17), p.4065. doi:https://doi.org/10.3390/cancers14174065.

174. Noguchi, M., Fujimoto, K., Arai, G., Uemura, H., Hashine, K., Matsumoto, H., Fukasawa, S., Kohjimoto, Y., Nakatsu, H., Takenaka, A., Fujisawa, M., Uemura, H., Naito, S., Egawa, S., Fujimoto, H., Hinotsu, S. and Itoh, K. (2021). A randomized phase III trial of personalized peptide vaccination for castration-resistant prostate cancer progressing after docetaxel. *Oncology Reports*, [online] 45(1), pp.159–168. doi:https://doi.org/10.3892/or.2020.7847.

175. Ntala, C., Salji, M., Salmond, J., Officer, L., Ana Vieira Teodosio, Blomme, A., McGhee, E.J., Powley, I., Ahmad, I., Marianna Kruithof-de Julio, Thalmann, G., Roberts, E., Goodyear, C.S., Jamaspishvili, T., Berman, D.M., Carlin, L.M., John Le Quesne and Leung, H.Y. (2021). Analysis of Prostate Cancer Tumor Microenvironment Identifies Reduced Stromal CD4 Effector T-cell Infiltration in Tumors with Pelvic Nodal Metastasis. *European urology open science*, [online] 29(5), pp.19–29. doi:https://doi.org/10.1016/j.euros.2021.05.001.

176. Nurieva, R., Wang, J. and Sahoo, A. (2013). T-cell tolerance in cancer. *Immunotherapy*, 5(5), pp.513–531. doi:https://doi.org/10.2217/imt.13.33.

REFERENCE LIST

177. Oh, D.Y. and Fong, L. (2021). Cytotoxic CD4+ T cells in cancer: Expanding the immune effector toolbox. *Immunity*, 54(12), pp.2701–2711. doi:https://doi.org/10.1016/j.immuni.2021.11.015.

178. Osimo, E.F., Pillinger, T., Rodriguez, I.M., Khandaker, G.M., Pariante, C.M. and Howes, O.D. (2020). Inflammatory markers in depression: A meta-analysis of mean differences and variability in 5,166 patients and 5,083 controls. *Brain, Behavior, and Immunity*, [online] 87(2). doi:https://doi.org/10.1016/j.bbi.2020.02.010.

179. Ostrand-Rosenberg, S. and Fenselau, C. (2018). Myeloid-Derived Suppressor Cells: Immune-Suppressive Cells That Impair Antitumor Immunity and Are Sculpted by Their Environment. *The Journal of Immunology*, 200(2), pp.422–431. doi:https://doi.org/10.4049/jimmunol.1701019.

180. Packer, J.R. and Maitland, N.J. (2016). The molecular and cellular origin of human prostate cancer. *Biochimica et Biophysica Acta (BBA) - Molecular Cell Research*, 1863(6), pp.1238–1260. doi:https://doi.org/10.1016/j.bbamcr.2016.02.016.

181. Pajot, A., Michel, M.-L., Fazilleau, N., Pancré, V., Auriault, C., Ojcius, David M., Lemonnier, F.A. and Lone, Y.-C. (2004). A mouse model of human adaptive immune functions:*HLA-A2.1-/HLA-DR1*-transgenic*H-2 class I-/class II*-knockout mice. *European Journal of Immunology*, 34(11), pp.3060–3069. doi:https://doi.org/10.1002/eji.200425463.

182. Palaniyandi Muthukutty, Hyun Young Woo, Murali Ragothaman and So Young Yoo (2023). Recent Advances in Cancer Immunotherapy Delivery Modalities. *Pharmaceutics*, 15(2), pp.504–504. doi:https://doi.org/10.3390/pharmaceutics15020504.

183. Palano, M.T., Gallazzi, M., Cucchiara, M., Dehò, F., Capogrosso, P., Bruno, A. and Mortara, L. (2022). The tumor innate immune microenvironment in prostate cancer: an overview of soluble factors and cellular effectors. *Exploration of Targeted Anti-tumor Therapy*, 3(5), pp.694–718. doi:https://doi.org/10.37349/etat.2022.00108.

184. Parisotto, M. and Metzger, D. (2013). Genetically engineered mouse models of prostate cancer. *Molecular Oncology*, 7(2), pp.190–205. doi:https://doi.org/10.1016/j.molonc.2013.02.005.

185. Pasero, C., Gravis, G., Granjeaud, S., Guerin, M., Thomassin-Piana, J., Rocchi, P., Salem, N., Walz, J., Moretta, A. and Olive, D. (2015). Highly effective NK cells are associated

REFERENCE LIST

with good prognosis in patients with metastatic prostate cancer. *Oncotarget*, 6(16), pp.14360–14373. doi:https://doi.org/10.18632/oncotarget.3965.

186. Pedersen, G.K., Christensen, D. and Andersen, P. (2018). Immunocorrelates of CAF familyadjuvants.*SeminarsinImmunology*,39,pp.4–13. doi:https://doi.org/10.1016/j.smim.2018.10.003.

187. Pennock, N.D., White, J.T., Cross, E.W., Cheney, E.E., Tamburini, B.A. and Kedl, R.M. (2013). T cell responses: naïve to memory and everything in between. *Advances in Physiology Education*, 37(4), pp.273–283. doi:https://doi.org/10.1152/advan.00066.2013.

188. Petitprez, F., Fossati, N., Vano, Y., Freschi, M., Becht, E., Lucianò, R., Calderaro, J., Guédet, T., Lacroix, L., Rancoita, P.M.V., Montorsi, F., Fridman, W.H., Sautès-Fridman, C., Briganti, A., Doglioni, C. and Bellone, M. (2019). PD-L1 Expression and CD8+ T-cell Infiltrate are Associated with Clinical Progression in Patients with Node-positive Prostate Cancer. *European Urology Focus*, 5(2), pp.192–196. doi:https://doi.org/10.1016/j.euf.2017.05.013.

189. Philippou, Y., Sjoberg, H., Murphy, E.A., Said Alyacoubi, Jones, K., Gordon-Weeks, A., Su Myat Phyu, Parkes, E.E., W. Gillies McKenna, Lamb, A., Uzi Gileadi, Cerundolo, V., Scheiblin, D.A., Lockett, S., Wink, D.A., Mills, I.G., Hamdy, F.C., Muschel, R.J. and Bryant, R.J. (2020). Impacts of combining anti-PD-L1 immunotherapy and radiotherapy on the tumour immune microenvironment in a murine prostate cancer model. *British Journal of Cancer*, 123(7), pp.1089–1100. doi:https://doi.org/10.1038/s41416-020-0956-x.

190. Poncette, L., Bluhm, J. and Blankenstein, T. (2022). The role of CD4 T cells in rejection of solid tumors. *Current Opinion in Immunology*, 74(1), pp.18–24. doi:https://doi.org/10.1016/j.coi.2021.09.005.

191. Pulendran, B., S. Arunachalam, P. and O'Hagan, D.T. (2021). Emerging concepts in the science of vaccine adjuvants. *Nature Reviews Drug Discovery*, 20(6), pp.454–475. doi:https://doi.org/10.1038/s41573-021-00163-y.

192. Qin, T., Barron, L., Xia, L., Huang, H., Villarreal, M.M., Zwaagstra, J., Collins, C., Yang, J., Zwieb, C., Kodali, R., Hinck, C.S., Kim, S.K., Reddick, R.L., Shu, C., O'Connor-McCourt, M.D., Hinck, A.P. and Sun, L.-Z. (2016). A novel highly potent trivalent TGF-β receptor trap inhibits early-stage tumorigenesis and tumor cell invasion in murine Pten-deficient prostate glands. *Oncotarget*, [online] 7(52), pp.86087–86102. doi:https://doi.org/10.18632/oncotarget.13343.

REFERENCE LIST

193. Quandt, J., Schlude, C., Bartoschek, M., Will, R., Cid-Arregui, A., Schölch, S., Reissfelder, C., Weitz, J., Schneider, M., Wiemann, S., Momburg, F. and Beckhove, P. (2018). Long-peptide vaccination with driver gene mutations in p53 and Kras induces cancer mutation-specific effector as well as regulatory T cell responses. *OncoImmunology*, 7(12), p.e1500671. doi:https://doi.org/10.1080/2162402x.2018.1500671.

194. Quinn, D.I., Sandler, H.M., Horvath, L.G., Goldkorn, A. and Eastham, J.A. (2017). The evolution of chemotherapy for the treatment of prostate cancer. *Annals of Oncology*, [online] 28(11), pp.2658–2669. doi:https://doi.org/10.1093/annonc/mdx348.

195. Rameshbabu, S., Labadie, B.W., Argulian, A. and Patnaik, A. (2021). Targeting Innate Immunity in Cancer Therapy. *Vaccines*, 9(2), p.138. doi:https://doi.org/10.3390/vaccines9020138.

196. Rastogi, I., Jeon, D., Moseman, J.E., Muralidhar, A., Potluri, H.K. and McNeel, D.G. (2022). Role of B cells as antigen presenting cells. *Frontiers in Immunology*, 13(13), p.954936. doi:https://doi.org/10.3389/fimmu.2022.954936.

197. Rastogi, I., Muralidhar, A. and McNeel, D.G. (2023). Vaccines as treatments for prostate cancer. *Nature Reviews. Urology*, [online] 20(9), pp.544–559. doi:https://doi.org/10.1038/s41585-023-00739-w.

198. Rawla, P. (2019). Epidemiology of Prostate Cancer. *World Journal of Oncology*, 10(2), pp.63–89. doi:https://doi.org/10.14740/wjon1191.

199. Rebello, R.J., Oing, C., Knudsen, K.E., Loeb, S., Johnson, D.C., Reiter, R.E., Gillessen, S., Van der Kwast, T. and Bristow, R.G. (2021). Prostate cancer. *Nature Reviews Disease Primers*, 7(1). doi:https://doi.org/10.1038/s41572-020-00243-0.

200. Riazi Rad, F., Ajdary, S., Omranipour, R., Alimohammadian, M.H. and Hassan, Z.M. (2015). Comparative analysis of CD4+ and CD8+ T cells in tumor tissues, lymph nodes and the peripheral blood from patients with breast cancer. *Iranian biomedical journal*, 19(1), pp.35–44. doi:https://doi.org/10.6091/ibj.1289.2014.

201. Roche, P.A. and Furuta, K. (2015). The ins and outs of MHC class II-mediated antigen processing and presentation. *Nature Reviews Immunology*, [online] 15(4), pp.203–216. doi:https://doi.org/10.1038/nri3818.

202. Rommasi, F. (2021). Bacterial-Based Methods for Cancer Treatment: What We Know and Where We Are. *Oncology and Therapy*. doi:https://doi.org/10.1007/s40487-021-00177-x.

REFERENCE LIST

203. Ross, S.H. and Cantrell, D.A. (2018). Signaling and Function of Interleukin-2 in T Lymphocytes. *Annual review of immunology*, [online] 36(1), pp.411–433. doi:https://doi.org/10.1146/annurev-immunol-042617-053352.

204. Rukaia Almshayakhchi, Nagarajan, D., Jayakumar Vadakekolathu, Barbara Ann Guinn, Reeder, S., Brentville, V., Metheringham, R., A. Graham Pockley, Durrant, L. and McArdle, S. (2021). A Novel HAGE/WT1-ImmunoBody® Vaccine Combination Enhances Anti-Tumour Responses When Compared to Either Vaccine Alone. *Frontiers in Oncology*, 11. doi:https://doi.org/10.3389/fonc.2021.636977.

205. Saha, A., Kolonin, M.G. and DiGiovanni, J. (2023). Obesity and prostate cancer — microenvironmental roles of adipose tissue. doi:https://doi.org/10.1038/s41585-023-00764-9.

206. Saranyutanon, S., Deshmukh, S.K., Dasgupta, S., Pai, S., Singh, S. and Singh, A.P. (2020). Cellular and Molecular Progression of Prostate Cancer: Models for Basic and Preclinical Research. *Cancers*, [online] 12(9), p.2651. doi:https://doi.org/10.3390/cancers12092651.

207. Sarkizova, S., Klaeger, S., Le, P.M., Li, L.W., Oliveira, G., Keshishian, H., Hartigan, C.R., Zhang, W., Braun, D.A., Ligon, K.L., Bachireddy, P., Zervantonakis, I.K., Rosenbluth, J.M., Ouspenskaia, T., Law, T., Justesen, S., Stevens, J., Lane, W.J., Eisenhaure, T. and Lan Zhang, G. (2019). A large peptidome dataset improves HLA class I epitope prediction across most of the human population. *Nature Biotechnology*, 38(2), pp.199–209. doi:https://doi.org/10.1038/s41587-019-0322-9.

208. Scarcello, E., Lambremont, A., Vanbever, R., Jacques, P.J. and Lison, D. (2020). Mind your assays: Misleading cytotoxicity with the WST-1 assay in the presence of manganese. *PLOS ONE*, 15(4), p.e0231634. doi:https://doi.org/10.1371/journal.pone.0231634.

209. Sejda, A., Sigorski, D., Gulczyński, J., Wesołowski, W., Kitlińska, J. and Iżycka-Świeszewska, E. (2020). Complexity of Neural Component of Tumor Microenvironment in Prostate Cancer. *Pathobiology*, 87(Suppl. 2), pp.87–99. doi:https://doi.org/10.1159/000505437.

210. Sekhoacha, M., Riet, K., Motloung, P., Gumenku, L., Adegoke, A. and Mashele, S. (2022). Prostate Cancer Review: Genetics, Diagnosis, Treatment Options, and Alternative

REFERENCE LIST

Approaches. *Molecules (Basel, Switzerland)*, [online] 27(17), p.5730. doi:https://doi.org/10.3390/molecules27175730.

211. Sfanos, K.S., Isaacs, W.B. and De, A.M. (2013). Infections and inflammation in prostate cancer. *American Journal of Clinical and Experimental Urology*, 1(1), p.3.

212. Shen, Y.-C., Ghasemzadeh, A., Kochel, C.M., Nirschl, T.R., Francica, B.J., Lopez-Bujanda, Z.A., Carrera, M.A., Tam, A., Anders, R.A., Selby, M.J., Korman, A.J. and Drake, C.G. (2017). Combining intratumoral Treg depletion with androgen deprivation therapy (ADT): preclinical activity in the Myc-CaP model. *Prostate Cancer and Prostatic Diseases*, 21(1), pp.113–125. doi:https://doi.org/10.1038/s41391-017-0013-x.

213. Shenderov, E., De Marzo, A.M., Lotan, T.L., Wang, H., Chan, S., Lim, S.J., Ji, H., Allaf, M.E., Chapman, C., Moore, P.A., Chen, F., Sorg, K., White, A.M., Church, S.E., Hudson, B., Fields, P.A., Hu, S., Denmeade, S.R., Pienta, K.J. and Pavlovich, C.P. (2023). Neoadjuvant enoblituzumab in localized prostate cancer: a single-arm, phase 2 trial. *Nature Medicine*, [online] 29(4), pp.1–10. doi:https://doi.org/10.1038/s41591-023-02284-w.

214. Shill, D.K., Roobol, M.J., Ehdaie, B., Vickers, A.J. and Carlsson, S.V. (2021). Active surveillance for prostate cancer. *Translational Andrology and Urology*, 10(6), pp.2809–2819. doi:https://doi.org/10.21037/tau-20-1370.

215. Short, E., Warren, A.Y. and Varma, M. (2019). Gleason grading of prostate cancer: a pragmatic approach. *Diagnostic Histopathology*, 25(10), pp.371–378. doi:https://doi.org/10.1016/j.mpdhp.2019.07.001.

216. Shyam Nyati, Stricker, H., Barton, K., Ли Пин, Elshaikh, M.A., Ali, H., Brown, S.L., Hwang, C., Peabody, J.O., Freytag, S.O., Movsas, B. and Siddiqui, F. (2023). A phase I clinical trial of oncolytic adenovirus mediated suicide and interleukin-12 gene therapy in patients with recurrent localized prostate adenocarcinoma. *PLOS ONE*, 18(9), pp.e0291315–e0291315. doi:https://doi.org/10.1371/journal.pone.0291315.

217. Simon, M.M., Greenaway, S., White, J.K., Fuchs, H., Gailus-Durner, V., Wells, S., Sorg, T., Wong, K., Bedu, E., Cartwright, E.J., Dacquin, R., Djebali, S., Estabel, J., Graw, J., Ingham, N.J., Jackson, I.J., Lengeling, A., Mandillo, S., Marvel, J. and Meziane, H. (2013). A comparative phenotypic and genomic analysis of C57BL/6J and C57BL/6N mouse strains. *Genome Biology*, 14(7), p.R82. doi:https://doi.org/10.1186/gb-2013-14-7-r82.

REFERENCE LIST

218. Singh, O. and Bolla, S.R. (2023). *Anatomy, Abdomen and Pelvis, Prostate*. [online] PubMed. Available at: https://www.ncbi.nlm.nih.gov/books/NBK540987/.

219. Skowronek, J. (2013). Review Brachytherapy in the therapy of prostate cancer – an interesting choice. *Współczesna Onkologia*, 5(17), pp.407–412. doi:https://doi.org/10.5114/wo.2013.38557.

220. Slovin, S.F., Ragupathi, G., Musselli, C., Fernandez, C., Diani, M., Verbel, D., Danishefsky, S., Livingston, P. and Scher, H.I. (2005). Thomsen-Friedenreich (TF) antigen as a target for prostate cancer vaccine: clinical trial results with TF cluster (c)-KLH plus QS21 conjugate vaccine in patients with biochemically relapsed prostate cancer. *Cancer immunology, immunotherapy: CII*, [online] 54(7), pp.694–702. doi:https://doi.org/10.1007/s00262-004-0598-5.

221. Small, E.J., Fratesi, P., Reese, D.M., Strang, G., Laus, R., Peshwa, M.V. and Valone, F.H. (2000). Immunotherapy of Hormone-Refractory Prostate Cancer With Antigen-Loaded Dendritic Cells. *Journal of Clinical Oncology*, 18(23), pp.3894–3903. doi:https://doi.org/10.1200/jco.2000.18.23.3894.

222. Sofie Kirial Mørk, Per Kongsted, Christine, M., Benedetta Albieri, Joachim Stoltenborg Granhøj, Donia, M., Martinenaite, E., Morten Orebo Holmström, Madsen, K., Kverneland, A.H., Julie Westerlin Kjeldsen, Rikke Boedker Holmstroem, Cathrine Lund Lorentzen, Nis Nørgaard, Lars Vibe Andreasen, Grith Krøyer Wood, Christensen, D., Michael Schantz Klausen, Sine Reker Hadrup and Per thor Straten (2023). First in man study: Bcl-Xl_42-CAF®09b vaccines in patients with locally advanced prostate cancer. *Frontiers in Immunology*, [online] 14. doi:https://doi.org/10.3389/fimmu.2023.1122977.

223. Stenzl, A., Feyerabend, S., Syndikus, I., Sarosiek, T., Kübler, H., Heidenreich, A., Cathomas, R., Grüllich, C., Loriot, Y., Perez Gracia, S.L., Gillessen, S., Klinkhardt, U., Schröder, A., Schönborn-Kellenberger, O., Reus, V., Koch, S.D., Hong, H.S., Seibel, T., Fizazi, K. and Gnad-Vogt, U. (2017). Results of the randomized, placebo-controlled phase I/IIB trial of CV9104, an mRNA based cancer immunotherapy, in patients with metastatic castration-resistant prostate cancer (mCRPC). *Annals of Oncology*, 28(28), pp.v408–v409. doi:https://doi.org/10.1093/annonc/mdx376.014.

REFERENCE LIST

224. Streicher, J., Meyerson, B.L., Karivedu, V. and Sidana, A. (2019). A review of optimal prostate biopsy: indications and techniques. *Therapeutic Advances in Urology*, 11, p.175628721987007. doi:https://doi.org/10.1177/1756287219870074.

225. Stultz, J. and Fong, L. (2021). How to turn up the heat on the cold immune microenvironment of metastatic prostate cancer. *Prostate Cancer and Prostatic Diseases*, 24(697–717). doi:https://doi.org/10.1038/s41391-021-00340-5.

226. Sun, X. and Kaufman, P.D. (2018). Ki-67: more than a proliferation marker. *Chromosoma*, [online] 127(2), pp.175–186. doi:https://doi.org/10.1007/s00412-018-0659-8.

227. Tae Joo Shin and Yong Rok Lee (2022). Robot-assisted radical prostatectomy in the treatment of patients with clinically high-risk localized and locally advanced prostate cancer: single surgeons functional and oncologic outcomes. *BMC urology*, 22(1). doi:https://doi.org/10.1186/s12894-022-00998-6.

228. Takahashi, Y., Demachi-Okamura, A., Oya, Y., Nakada, T., Sakakura, N., Kuroda, H. and Matsushita, H. (2021). Research advance in tumor specific antigens. *AME Medical Journal*, 6(0). doi:https://doi.org/10.21037/amj-20-121.

229. Tan, E., Chin, C.S.H., Lim, Z.F.S. and Ng, S.K. (2021). HEK293 Cell Line as a Platform to Produce Recombinant Proteins and Viral Vectors. *Frontiers in Bioengineering and Biotechnology*, 9. doi:https://doi.org/10.3389/fbioe.2021.796991.

230. Tandrup Schmidt, S., Khadke, S., Smith Korsholm, K., Perrie, Y., Rades, T., Andersen, P., Foged, C. and Christensen, D. (2016). The administration route is decisive for the ability of the vaccine adjuvant CAF09 to induce antigen-specific CD8+ T-cell responses: The immunological consequences of the biodistribution profile. *Journal of Controlled Release*, [online] 239(34), pp.107–117. doi:https://doi.org/10.1016/j.jconrel.2016.08.034.

231. Tang, L., Shao, H., Wu, Y., Wang, J., Qian, X., He, L., Huang, H. and Xu, Z. (2023). Dominant negative TGFβ receptor II and truncated TIM3 enhance the antitumor efficacy of CAR-T-cell therapy in prostate cancer. *International Immunopharmacology*, [online] 124(1), p.110807. doi:https://doi.org/10.1016/j.intimp.2023.110807.

232. Tang, S., Moore, M.L., Grayson, J.M. and Dubey, P. (2012). Increased CD8+ T-cell Function following Castration and Immunization Is Countered by Parallel Expansion of Regulatory T Cells. *Cancer Research*, 72(8), pp.1975–1985. doi:https://doi.org/10.1158/0008-5472.can-11-2499.

REFERENCE LIST

233. te Marvelde, L., Milne, R.L., Hornby, C.J., Chapman, A.B., Giles, G.G. and Haines, I.E. (2020). Differences in treatment choices for localised prostate cancer diagnosed in private and public health services. *Medical Journal of Australia*, 213(9), pp.411–417. doi:https://doi.org/10.5694/mja2.50794.

234. Thompson-Elliott, B., Johnson, R. and Khan, S.A. (2021). Alterations in TGFβ signaling during prostate cancer progression. *American journal of clinical and experimental urology*, 9(4), pp.318–328.

235. Tian, T. and Li, Z. (2021). Targeting Tim-3 in Cancer With Resistance to PD-1/PD-L1 Blockade. *Frontiers in Oncology*, 11(1). doi:https://doi.org/10.3389/fonc.2021.731175.

236. Tosi, I., Bureau, F., F. Farnir, J.M. Denoix, P. Lekeux and Art, T. (2018). Effects of a P-class CpG-ODN administered by intramuscular injection on plasma cytokines and on white blood cells of healthy horses. *Veterinary Immunology and Immunopathology*, 201(1), pp.57–61. doi:https://doi.org/10.1016/j.vetimm.2018.05.004.

237. Tsai, A.K., Kagalwalla, S., Langer, J., Le-Kumar, T., Le-Kumar, V. and Antonarakis, E.S. (2024). Pembrolizumab for metastatic castration-resistant prostate cancer: trials and tribulations. *Expert Opinion on Biological Therapy*, 24(1-2), pp.51–62. doi:https://doi.org/10.1080/14712598.2024.2311750.

238. Tumino, N., Besi, F., Di Pace, A.L., Mariotti, F.R., Merli, P., Li Pira, G., Galaverna, F., Pitisci, A., Ingegnere, T., Pelosi, A., Quatrini, L., Munari, E., Locatelli, F., Moretta, L. and Vacca, P. (2019). PMN-MDSC are a new target to rescue graft-versus-leukemia activity of NK cells in haplo-HSC transplantation. *Leukemia*, 34(3), pp.932–937. doi:https://doi.org/10.1038/s41375-019-0585-7.

239. Valkenburg, K.C., Amend, S.R. and Pienta, K.J. (2016). Murine Prostate Micro-dissection and Surgical Castration. *Journal of Visualized Experiments*, 1(111). doi:https://doi.org/10.3791/53984.

240. Vanuytsel, T., Vermeire, S. and Cleynen, I. (2013). The role of Haptoglobin and its related protein, Zonulin, in inflammatory bowel disease. *Tissue Barriers*, [online] 1(5). doi:https://doi.org/10.4161/tisb.27321.

241. Veglia, F., Sanseviero, E. and Gabrilovich, D.I. (2021). Myeloid-derived suppressor cells in the era of increasing myeloid cell diversity. *Nature Reviews Immunology*, 21(1). doi:https://doi.org/10.1038/s41577-020-00490-y.

REFERENCE LIST

242. Vicier, C., Ravi, P., Kwak, L., Werner, L., Huang, Y., Evan, C., Loda, M., Hamid, A.A. and Sweeney, C.J. (2020). Association between CD8 and PD-L1 expression and outcomes after radical prostatectomy for localized prostate cancer. *˜The œProstate/˜The œprostate*, 81(1), pp.50–57. doi:https://doi.org/10.1002/pros.24079.

243. Victoria Anne Brentville, Symonds, P., Chua, J., Skinner, A., Daniels, I., Katherine Wendy Cook, Sasa Koncarevic, Martinez-Pinna, R., Shah, S., Ruhul Hasan Choudhury, Vaghela, P., Weston, D., Abdullah Al-Omari, Davis, J. and Durrant, L.G. (2022). Citrullinated glucose-regulated protein 78 is a candidate target for melanoma immunotherapy. *Frontiers in Immunology*, 13. doi:https://doi.org/10.3389/fimmu.2022.1066185.

244. Vogel, R., Reem Al-Daccak, Drews, O., Jessy Alonzeau, Mester, G., Charron, D., Stevanovic, S. and Mallet, J. (2013). Mass Spectrometry Reveals Changes in MHC I Antigen Presentation After Lentivector Expression of a Gene Regulation System. *Molecular Therapy - Nucleic Acids*, [online] 2(1), pp.e75–e75. doi:https://doi.org/10.1038/mtna.2013.3.

245. Vogelzang, N.J., Beer, T.M., Gerritsen, W., Stéphane Oudard, Pawel Wiechno, Bozena Kukielka-Budny, Vladimir Samal, Hajek, J., Feyerabend, S., Khoo, V., Arnulf Stenzl, Tibor Csöszi, Filipovic, Z., Goncalves, F., Prokhorov, A., Cheung, E., Hussain, A., Sousa, N., Bahl, A. and Hussain, S. (2022). Efficacy and Safety of Autologous Dendritic Cell–Based Immunotherapy, Docetaxel, and Prednisone vs Placebo in Patients With Metastatic Castration-Resistant Prostate Cancer. *JAMA Oncology*, [online] 8(4), pp.546–546. doi:https://doi.org/10.1001/jamaoncol.2021.7298.

246. Wang Bolin, Pei, J., Xu, S., Liu, J. and Yu, J. (2023). Recent advances in mRNA cancer vaccines: meeting challenges and embracing opportunities. *Frontiers in Immunology*, [online] 14(14). doi:https://doi.org/10.3389/fimmu.2023.1246682.

247. Wang, I., Song, L., Wang, B.Y., Rezazadeh Kalebasty, A., Uchio, E. and Zi, X. (2022). Prostate cancer immunotherapy: a review of recent advancements with novel treatment methods and efficacy. *American journal of clinical and experimental urology*, [online] 10(4), pp.210–233.

248. Wang, F., Cheng, F. and Zheng, F. (2022). Stem cell like memory T cells: A new paradigm in cancer immunotherapy. *Clinical Immunology*, [online] 241(1), p.109078. doi:https://doi.org/10.1016/j.clim.2022.109078.

REFERENCE LIST

249. Wang, L., Geng, H., Liu, Y., Liu, L., Chen, Y., Wu, F., Liu, Z., Ling, S., Wang, Y. and Zhou, L. (2023). Hot and cold tumors: Immunological features and the therapeutic strategies. *MedComm*, [online] 4(5). doi:https://doi.org/10.1002/mco2.343.

250. Wang, Y., Qiu, F., Xu, Y., Hou, X., Zhang, Z., Huang, L., Wang, H., Xing, H. and Wu, S. (2021). Stem cell-like memory T cells: The generation and application. *Journal of Leukocyte Biology*, [online] 110(6), pp.1209–1223. doi:https://doi.org/10.1002/JLB.5MR0321-145R.

251. Wani, M. and Madaan, S. (2023). What Is New in the Management of High-Risk Localized Prostate Cancer? *Journal of Clinical Medicine*, 12(2), p.455. doi:https://doi.org/10.3390/jcm12020455.

252. Ward, J.E. and McNeel, D.G. (2007). GVAX: an allogeneic, whole-cell, GM-CSF-secreting cellular immunotherapy for the treatment of prostate cancer. *Expert Opinion on Biological Therapy*, 7(12), pp.1893–1902. doi:https://doi.org/10.1517/14712598.7.12.1893.

253. Wedén, S., Klemp, M., Gladhaug, I.P., Møller, M., Eriksen, J.A., Gaudernack, G. and Buanes, T. (2010). Long-term follow-up of patients with resected pancreatic cancer following vaccination against mutant K-ras. *International Journal of Cancer*, 128(5), pp.1120–1128. doi:https://doi.org/10.1002/ijc.25449.

254. Westdorp, H., Skald, A.E., Snijer, B.A., Franik, S., Mulder, S.F., Major, P.P., Foley, R., Gerritsen, W.R. and de Vries, I.J.M. (2014). Immunotherapy for Prostate Cancer: Lessons from Responses to Tumor-Associated Antigens. *Frontiers in Immunology*, 5. doi:https://doi.org/10.3389/fimmu.2014.00191.

255. Wu, J. (2021). Could Harnessing Natural Killer Cell Activity Be a Promising Therapy for Prostate Cancer? *Critical Reviews in Immunology*, [online] 41(2), pp.101–106. doi:https://doi.org/10.1615/critrevimmunol.2021037614.

256. Wu, X., Gong, S., Roy-Burman, P., Lee, P. and Culig, Z. (2013). Current mouse and cell models in prostate cancer research. *Endocrine-related cancer*, [online] 20(4). doi:https://doi.org/10.1530/ERC-12-0285.

257. Wu, Y., Zhang, N., Hashimoto, K., Xia, C. and Dijkstra, J.M. (2021). Structural Comparison Between MHC Classes I and II; in Evolution, a Class-II-Like Molecule Probably Came First. *Frontiers in Immunology*, 12. doi:https://doi.org/10.3389/fimmu.2021.621153.

258. Xia, S., Liu, M., Wang, C., Xu, W., Lan, Q., Feng, S., Qi, F., Bao, L., Du, L., Liu, S., Qin, C., Sun, F., Shi, Z., Zhu, Y., Jiang, S. and Lu, L. (2020). Inhibition of SARS-CoV-2 (previously

REFERENCE LIST

2019-nCoV) infection by a highly potent pan-coronavirus fusion inhibitor targeting its spike protein that harbors a high capacity to mediate membrane fusion. *Cell Research*, 30(4), pp.343–355. doi:https://doi.org/10.1038/s41422-020-0305-x.

259. Xing, J., Zhang, J. and Wang, J. (2023). The Immune Regulatory Role of Adenosine in the Tumor Microenvironment. *International Journal of Molecular Sciences*, 24(19), p.14928. doi:https://doi.org/10.3390/ijms241914928.

260. Xu, P., Wasielewski, L.J., Yang, J.C., Cai, D., Evans, C.P., Murphy, W.J. and Liu, C. (2022). The Immunotherapy and Immunosuppressive Signaling in Therapy-Resistant Prostate Cancer. *Biomedicines*, 10(8), p.1778. doi:https://doi.org/10.3390/biomedicines10081778.

261. Xue, W., Metheringham, R.L., Brentville, V.A., Gunn, B., Symonds, P., Yagita, H., Ramage, J.M. and Durrant, L.G. (2016). SCIB2, an antibody DNA vaccine encoding NY-ESO-1 epitopes, induces potent antitumor immunity which is further enhanced by checkpoint blockade.*OncoImmunology*5(6),p.e11693. doi:https://doi.org/10.1080/2162402x.2016.1169353.

262. Yang, K., Feng, S. and Luo, Z. (2022). Oncolytic Adenovirus, a New Treatment Strategy for Prostate Cancer. *Biomedicines*, 10(12), p.3262. doi:https://doi.org/10.3390/biomedicines10123262.

263. Ye, N., Cai, J., Dong, Y., Chen, H., Bo, Z., Zhao, X., Xia, M. and Han, M. (2022). A multi-omic approach reveals utility of CD45 expression in prognosis and novel target discovery. *Frontiers in Genetics*, 13(8). doi:https://doi.org/10.3389/fgene.2022.928328.

264. Yi, L. and Li, Y. (2022). Stem-like T cells and niches: Implications in human health and disease. *Frontiers in Immunology*, 13(1). doi:https://doi.org/10.3389/fimmu.2022.907172.

265. Yi Ting Koh, Gray, A., Higgins, S., Hubby, B. and W. Martin Kast (2009). Androgen ablation augments prostate cancer vaccine immunogenicity only when applied after immunization. *The Prostate*, 69(6), pp.571–584. doi:https://doi.org/10.1002/pros.20906.

266. Yin, X., He, L. and Guo, Z. (2023). T-cell exhaustion in CAR-T-cell therapy and strategies to overcome it. *Immunology*, 169(4), pp.400–411. doi:https://doi.org/10.1111/imm.13642.

267. Yu, E., Hwang, M.W. and Aragon-Ching, J.B. (2023). Mechanistic Insights on Localized to Metastatic Prostate Cancer Transition and Therapeutic Opportunities. *Research and Reports in Urology*, 15(15), pp.519–529. doi:https://doi.org/10.2147/RRU.S386517.

REFERENCE LIST

268. Yu, P., Steel, J.C., Zhang, M., Morris, J.C., Waitz, R., Fasso, M., Allison, J.P. and Waldmann, T.A. (2012). Simultaneous inhibition of two regulatory T-cell subsets enhanced Interleukin-15 efficacy in a prostate tumor model. *Proceedings of the National Academy of Sciences*, 109(16), pp.6187–6192. doi:https://doi.org/10.1073/pnas.1203479109.

269. Yu, W., Nga TH Truong, Ruhi Polara, Gargett, T., Tea, M.N., Pitson, S.M., Cockshell, M.P., Bonder, C.S., Ebert, L.M. and Brown, M.P. (2023). Endogenous bystander killing mechanisms enhance the activity of novel FAP-CAR-T cells against glioblastoma. *bioRxiv (Cold Spring Harbor Laboratory)*, 18(1). doi:https://doi.org/10.1101/2023.02.21.529331.

270. Yusim, I., Krenawi, M., Mazor, E., Novack, V. and Mabjeesh, N.J. (2020). The use of prostate specific antigen density to predict clinically significant prostate cancer. *Scientific Reports*, 10(1). doi:https://doi.org/10.1038/s41598-020-76786-9.

271. Zahavi, D. and Weiner, L. (2020). Monoclonal Antibodies in Cancer Therapy. *Antibodies*, 9(3), p.34. doi:https://doi.org/10.3390/antib9030034.

272. Zamani, P., Jamshid Gholizadeh Navashenaq, Manouchehr Teymouri, Karimi, M., Mashreghi, M. and Mahmoud Reza Jaafari (2020). Combination therapy with liposomal doxorubicin and liposomal vaccine containing E75, an HER-2/neu-derived peptide, reduces myeloid-derived suppressor cells and improved tumor therapy. *Life Sciences*, 252(252), pp.117646–117646. doi:https://doi.org/10.1016/j.lfs.2020.117646.

273. Zeng, Z., Wong, C.J., Yang, L., Ouardaoui, N., Li, D., Zhang, W., Gu, S., Zhang, Y., Liu, Y., Wang, X., Fu, J., Zhou, L., Zhang, B., Kim, S., Yates, K., Brown, M., Freeman, G., Uppaluri, R., Manguso, R. and Liu, X. (2021). TISMO: syngeneic mouse tumor database to model tumor immunity and immunotherapy response. *Nucleic Acids Research*, 50(D1), pp.D1391–D1397. doi:https://doi.org/10.1093/nar/gkab804.

274. Zhan, Y., Cao, C., Li, A., Mei, H. and Liu, Y. (2023). Enhanced RNA knockdown efficiency with engineered fusion guide RNAs that function with both CRISPR-CasRx and hammerhead ribozyme. *Genome Biol.*, 24(1). doi:https://doi.org/10.1186/s13059-023-02852-w.

275. Zhan, Y., Carrington, E.M., Zhang, Y., Heinzel, S. and Lew, A.M. (2017). Life and Death of Activated T Cells: How Are They Different from Naïve T Cells? *Frontiers in Immunology*, 8(8). doi:https://doi.org/10.3389/fimmu.2017.01809.

REFERENCE LIST

276. Zhang, E., Ding, C., Li, S., Zhou, X., Aikemu, B., Fan, X., Sun, J., Zheng, M. and Yang, X. (2023). Roles and mechanisms of tumour-infiltrating B cells in human cancer: a new force in immunotherapy. *Biomarker Research*, 11(1). doi:https://doi.org/10.1186/s40364-023-00460-1.

277. Zhang, Y., Campbell, B.K., Stylli, S.S., Corcoran, N.M. and Hovens, C.M. (2022). The Prostate Cancer Immune Microenvironment, Biomarkers and Therapeutic Intervention. *Uro*, [online] 2(2), pp.74–92. doi:https://doi.org/10.3390/uro2020010.

278. Zhang, Y. and Zhang, Z. (2020). The history and advances in cancer immunotherapy: understanding the characteristics of tumor-infiltrating immune cells and their therapeutic implications. *Cellular & Molecular Immunology*, 17(8), pp.1–15. doi:https://doi.org/10.1038/s41423-020-0488-6.

279. Zhang, Z., Jimmy Chun-Tien Kuo, Yao, S., Zhang, C., Khan, H. and Lee, R.J. (2021). CpG Oligodeoxynucleotides for Anticancer Monotherapy from Preclinical Stages to Clinical Trials. *Pharmaceutics*,[online]14(1),pp.73–73. doi:https://doi.org/10.3390/pharmaceutics14010073.

280. Zhao, Y., Deng, J., Rao, S., Guo, S., Shen, J., Du, F., Wu, X., Chen, Y., Li, M., Chen, M., Li, X., Li, W., Gu, L., Sun, Y., Zhang, Z., Wen, Q., Xiao, Z. and Li, J. (2022). Tumor Infiltrating Lymphocyte (TIL) Therapy for Solid Tumor Treatment: Progressions and Challenges. *Cancers*, [online] 14(17), p.4160. doi:https://doi.org/10.3390/cancers14174160.

281. Zhen, J.T., Syed, J., Nguyen, K.A., Leapman, M.S., Agarwal, N., Brierley, K., Llor, X., Hofstatter, E. and Shuch, B. (2018). Genetic testing for hereditary prostate cancer: Current status and limitations. *Cancer*, 124(15), pp.3105–3117. doi:https://doi.org/10.1002/cncr.31316.

282. Zhu, M., Liang, Z., Feng, T., Mai, Z., Jin, S., Wu, L., Zhou, H., Chen, Y. and Yan, W. (2023). Up-to-Date Imaging and Diagnostic Techniques for Prostate Cancer: A Literature Review. *Diagnostics*, [online] 13(13), p.2283. doi:https://doi.org/10.3390/diagnostics13132283.

283. Zilio, S. and Serafini, P. (2016). Neutrophils and Granulocytic MDSC: The Janus God of Cancer Immunotherapy. *Vaccines*, 4(3), p.31. doi:https://doi.org/10.3390/vaccines4030031.

284. Zimmermann, J., Schmidt, S., Trebbien, R., Cox, R., Zhou, F., Follmann, F., Pedersen, G. and Christensen, D. (2022). A Novel Prophylaxis Strategy Using Liposomal Vaccine

REFERENCE LIST

Adjuvant CAF09b Protects against Influenza Virus Disease. *International Journal of Molecular Sciences*, 23(3), p.1850. doi:https://doi.org/10.3390/ijms23031850.

APPENDIX

1. Primer Efficiency

(A) (B)

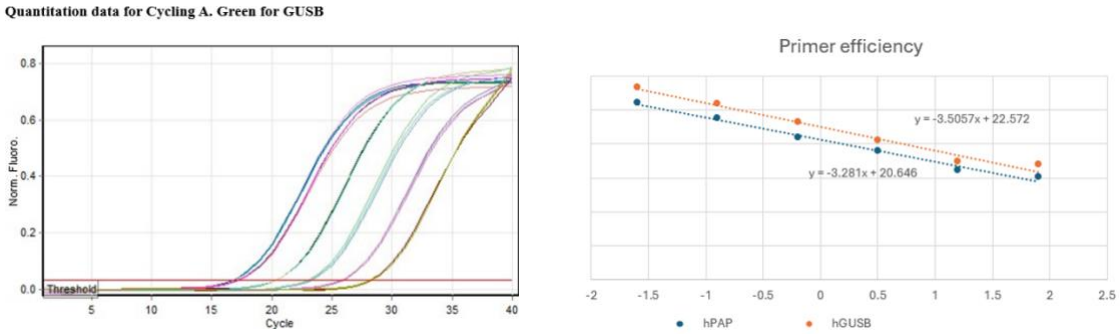

Figure AF.1. (A) An illustration of quantitation data and standard curve generated using Rotor-Gene Q Software 2.3.1.49 for GUSB primer amplification efficiency test. (B) example of primer efficiency calculated. Efficiency of primers hPAP and GUSB are shown in the graph.

2. Genotyping results

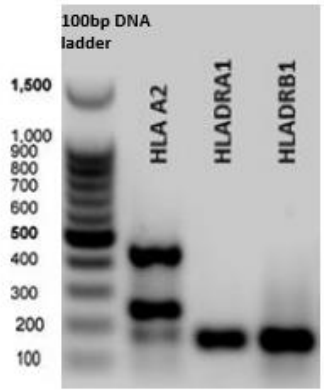

Figure AF.2. An example of agarose gel electrophoresis analysis of genotyping of HHDIIDR1mouse. HLA-A2 transgenic allele band seen at 400bp , HLA-DR-A1 at 153bp and HLA-DR-B1 170bp